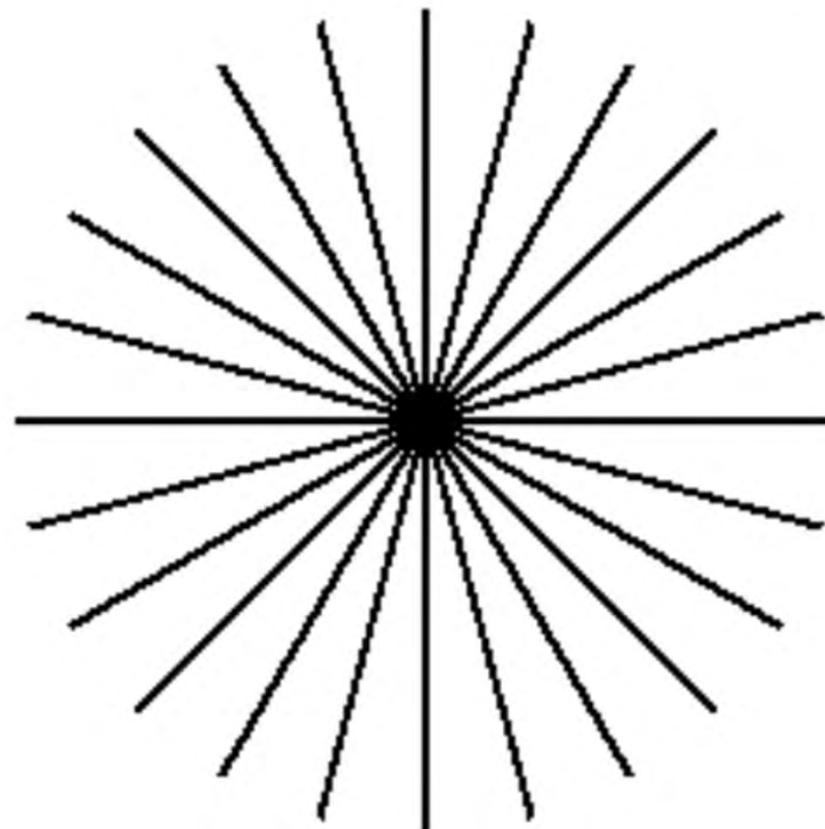
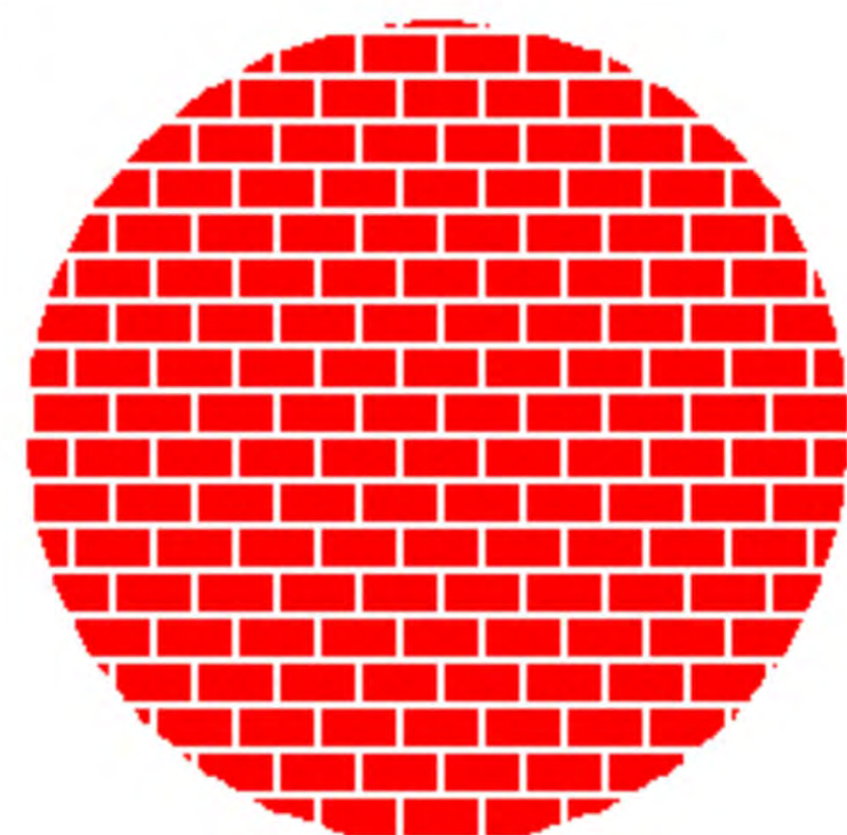
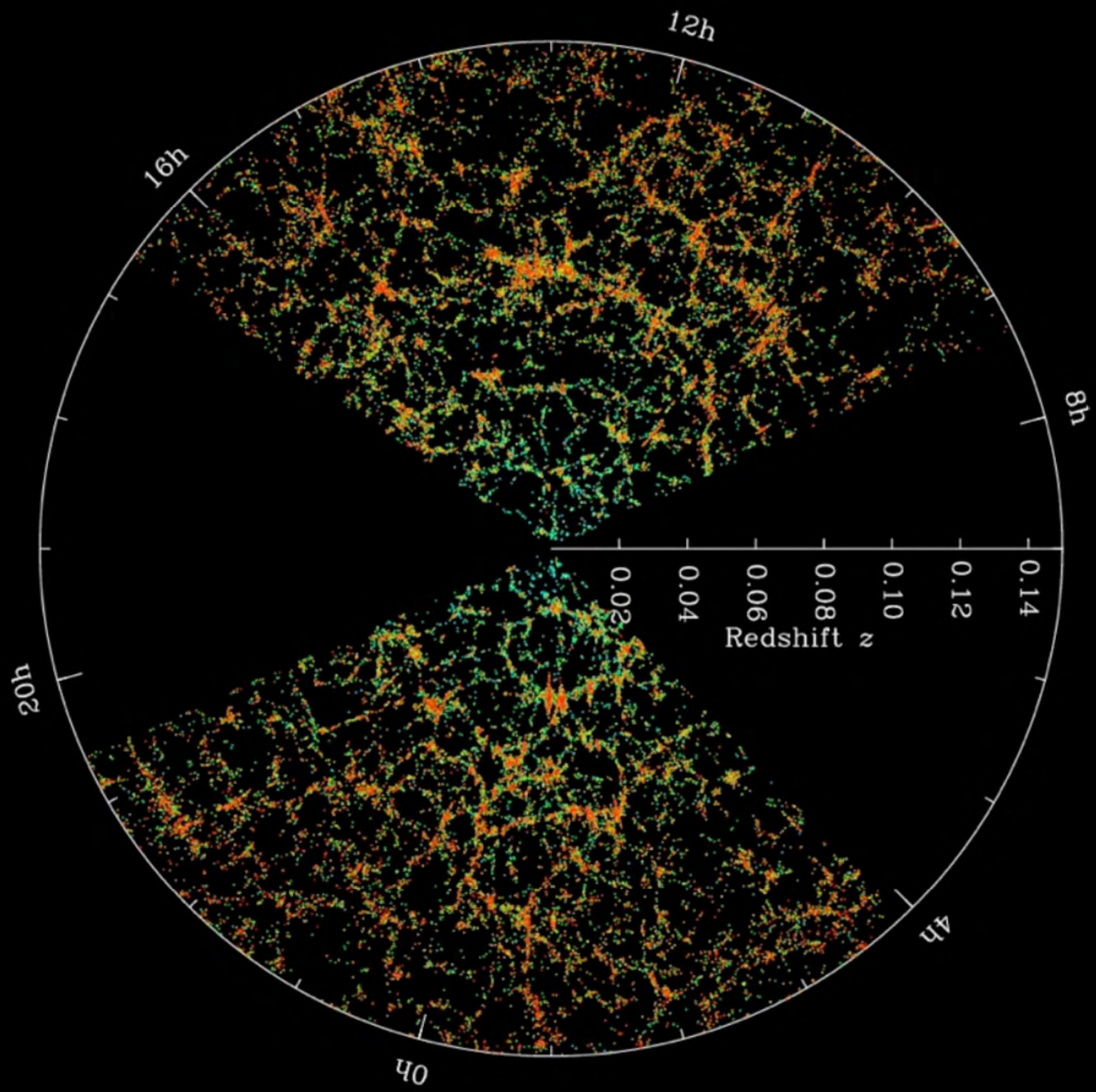


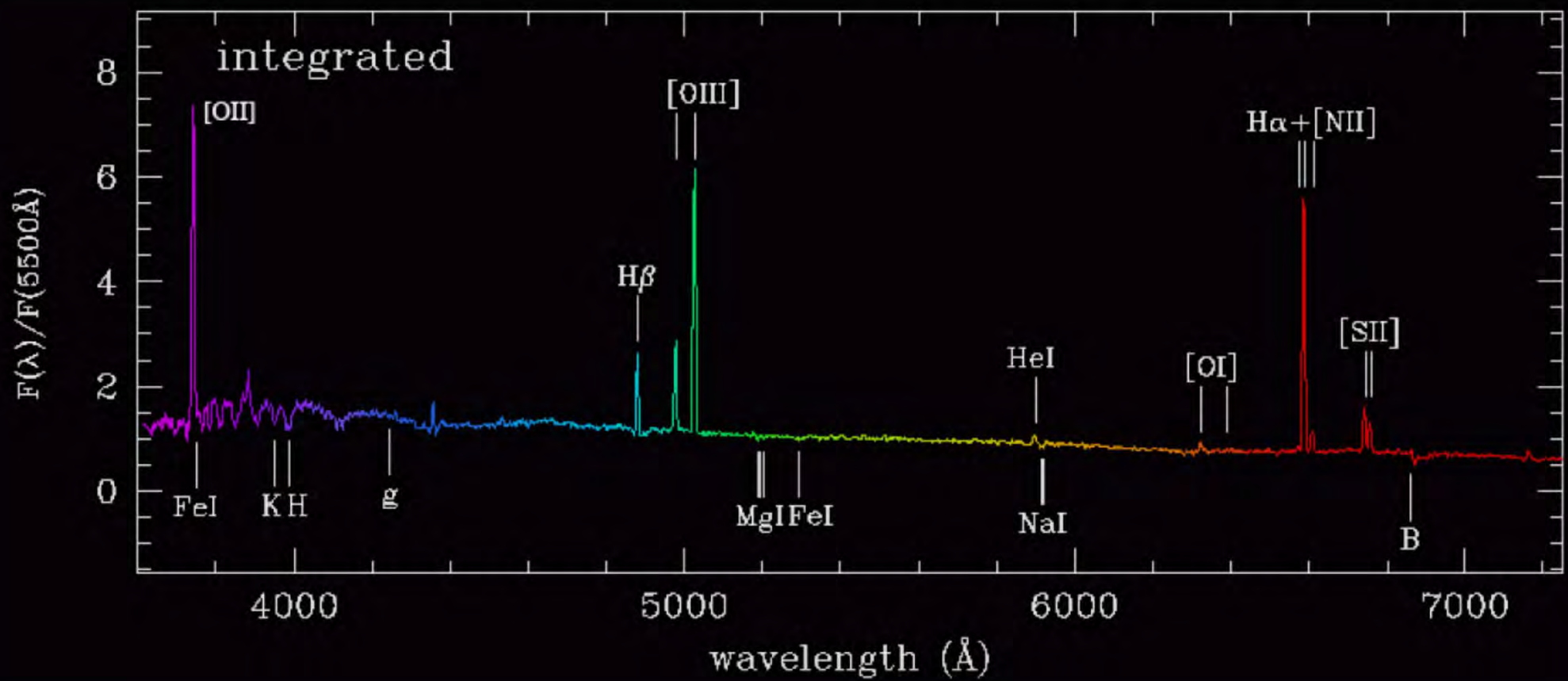
homogeneous



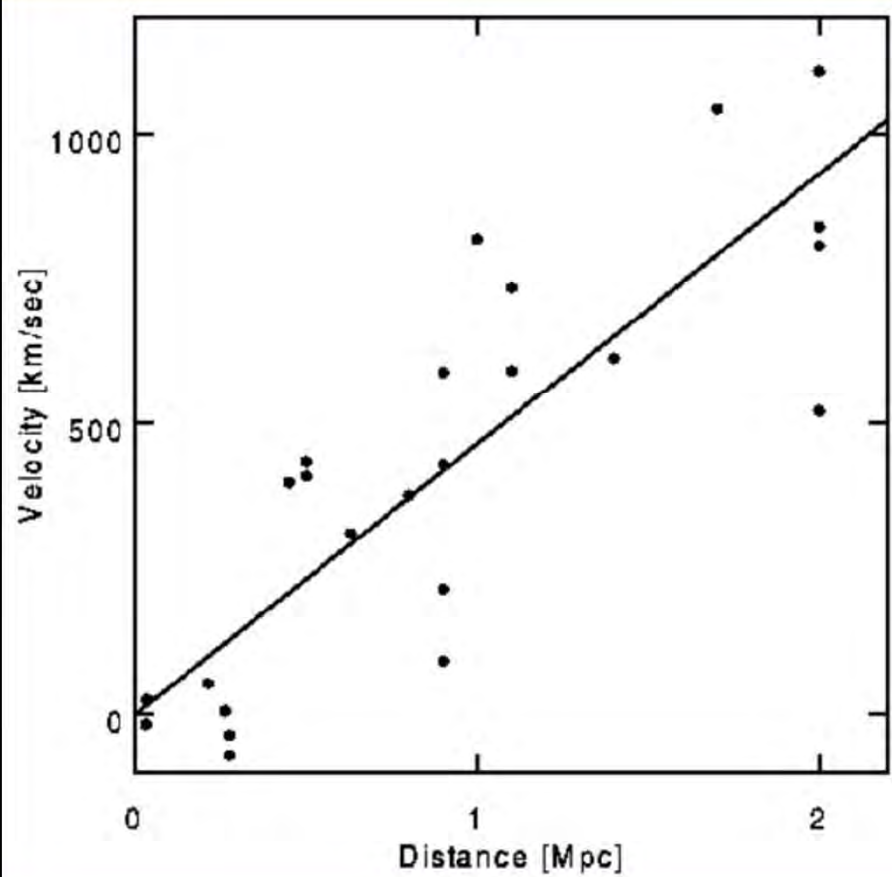
isotropic

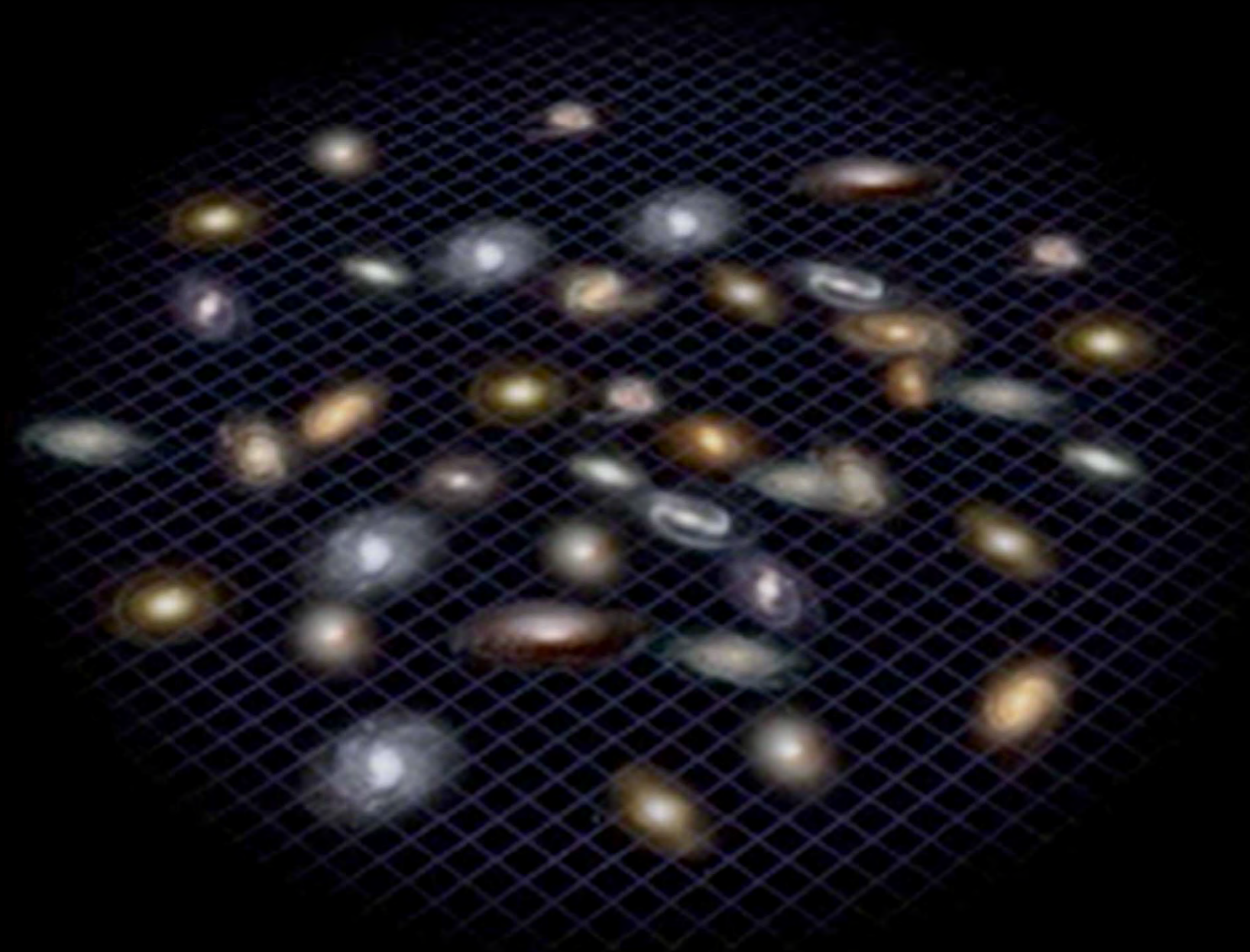


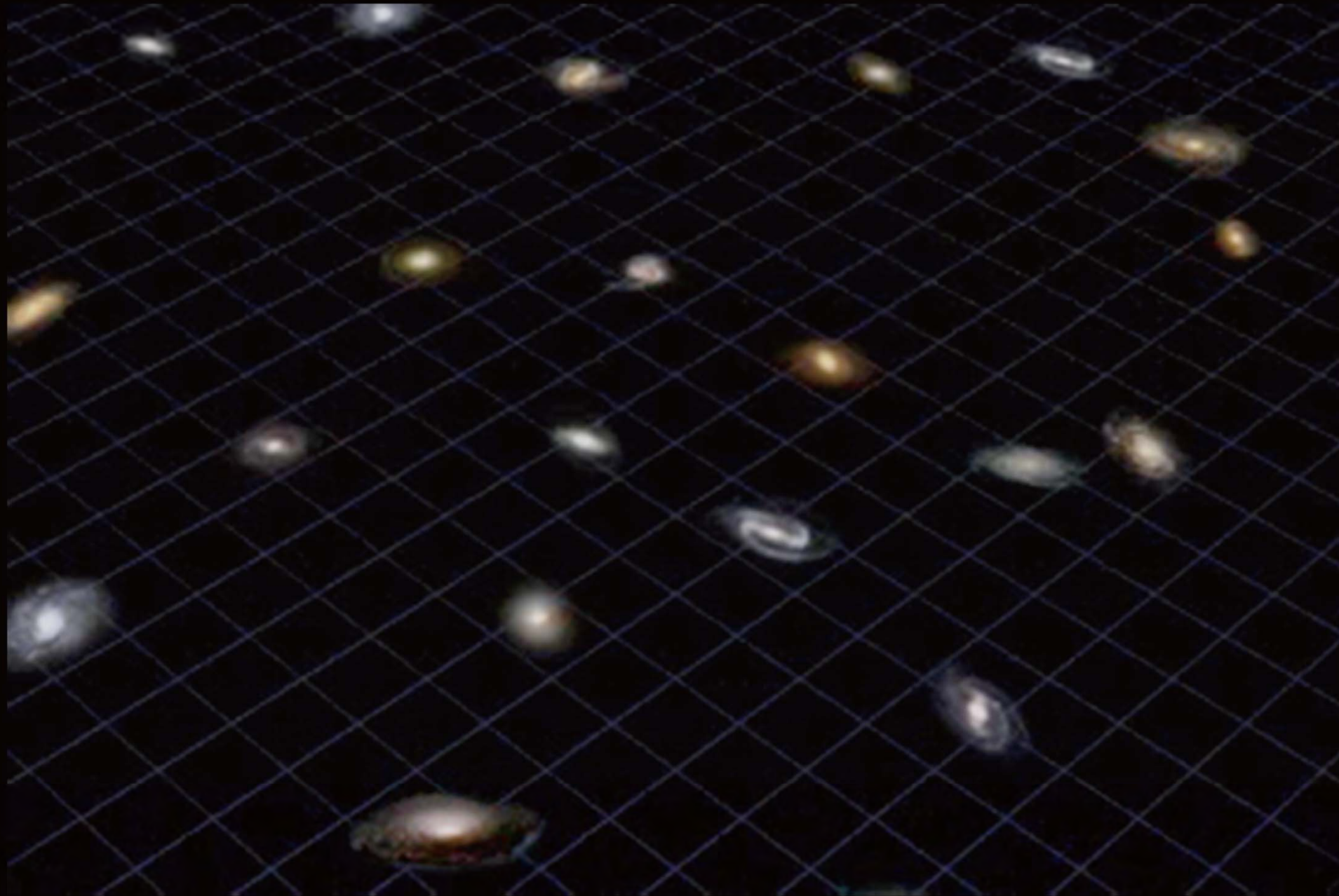


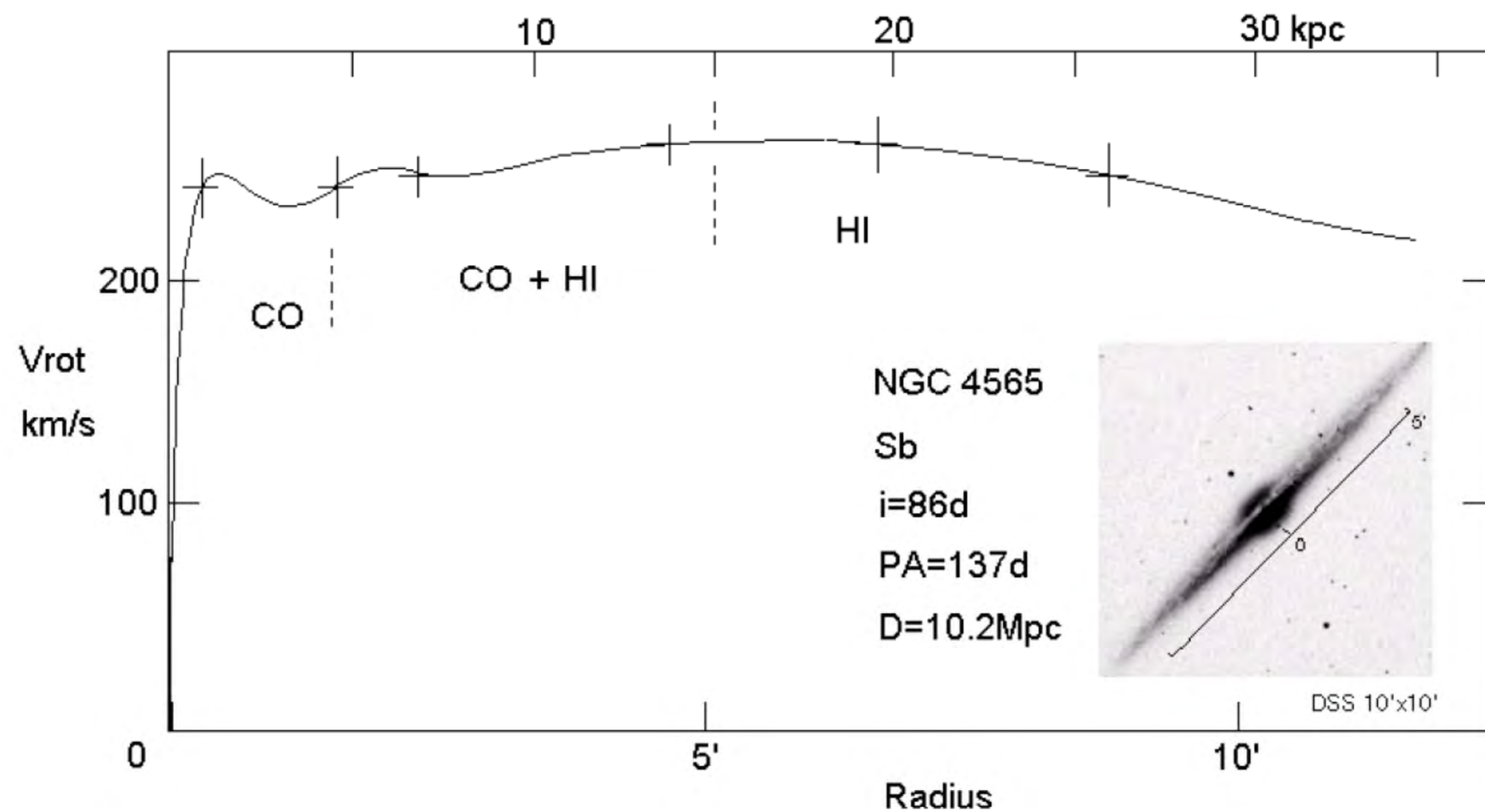


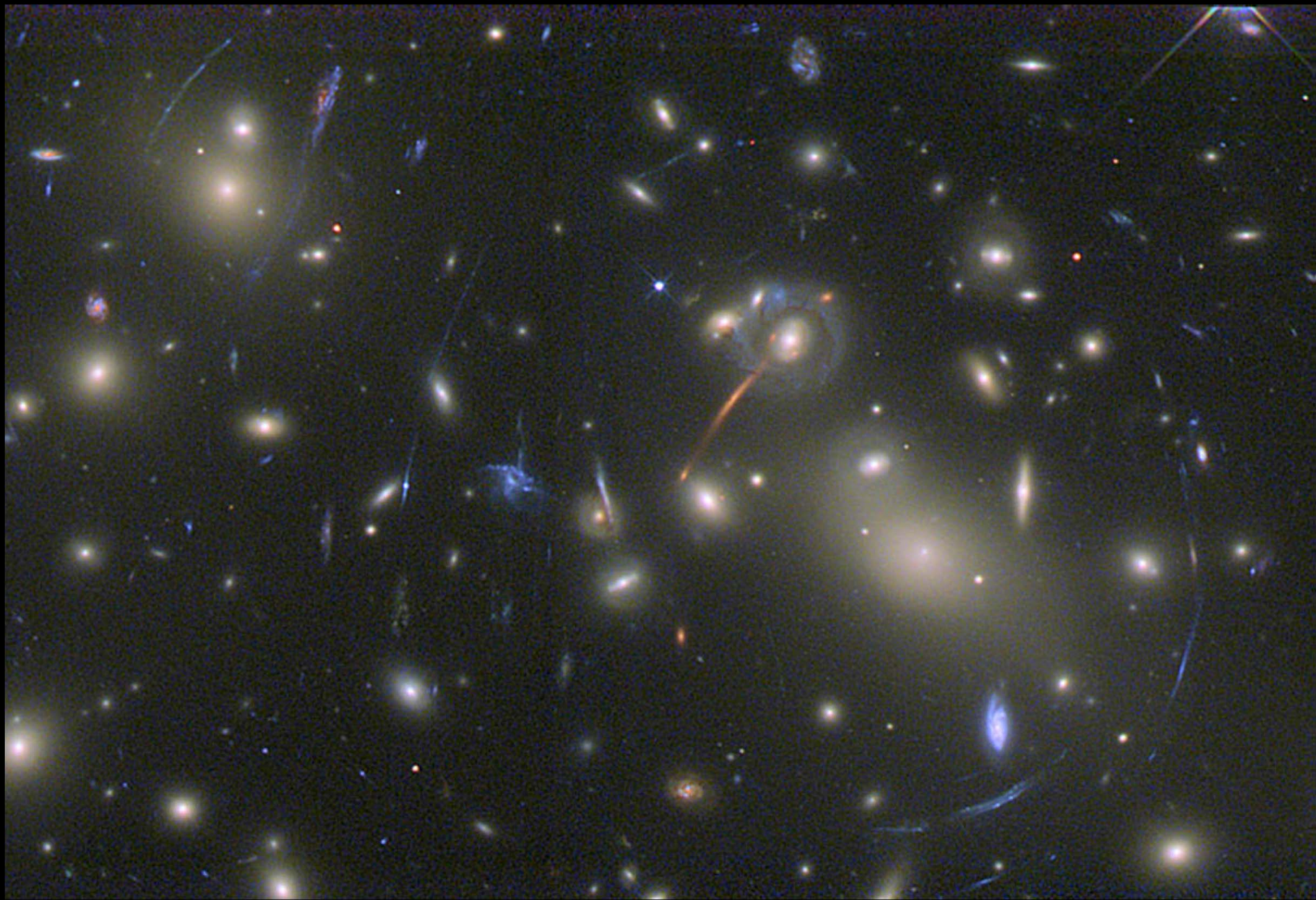
HUBBLE'S ORIGINAL DIAGRAM











What do we know about dark matter? How do we know?



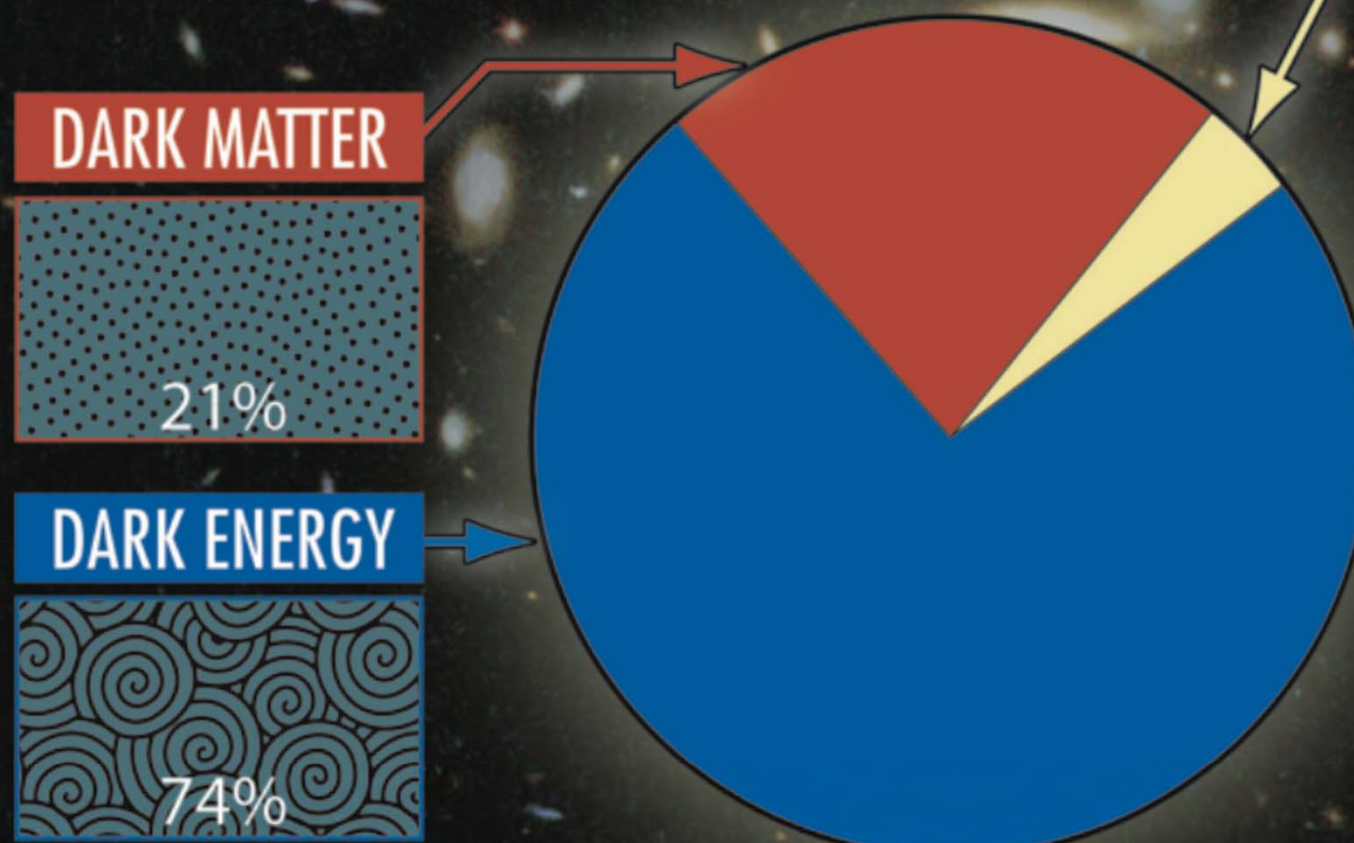
- ✓ Interacts through gravity
- ✓ Interacts rarely via strong, weak, or electromagnetic forces
- ✓ Nearly collision-less
- ✓ Stable on Hubble timescales
- ✓ Mostly non-relativistic
- ✓ 10^{-21} eV (de Broglie wavelength) < mass < $10^9 M_\odot$ (CMB, BBN, LSS)*

To date, all positive measurements of dark matter properties have come from astrophysical observations

* roughly 96 orders of magnitude ; $1 \text{ eV} = 1.7 \times 10^{-36} \text{ kg}$; $1 M_\odot = 2.0 \times 10^{30} \text{ kg}$

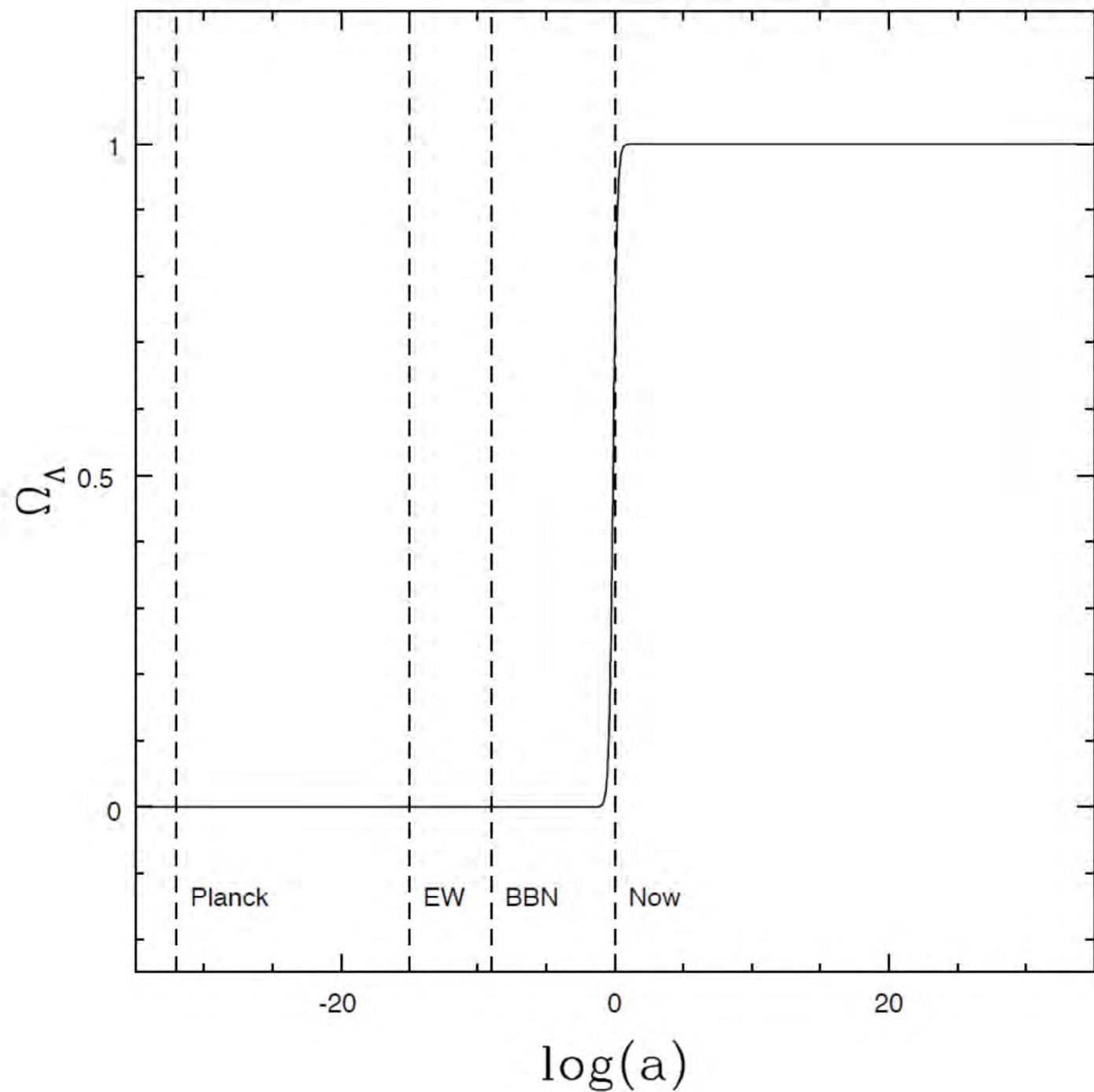


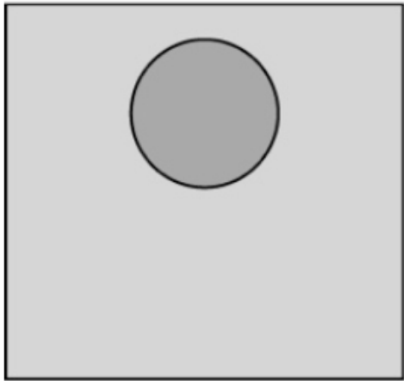
What The Universe Is Made Of



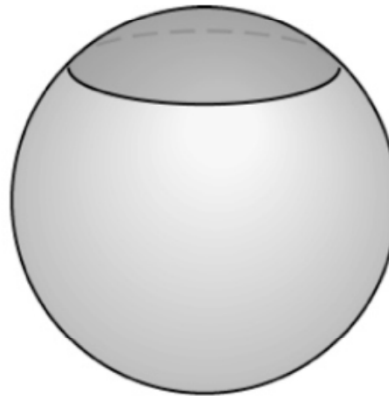
NORMAL MATTER



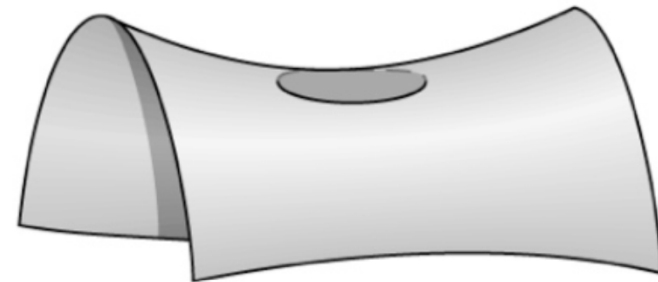




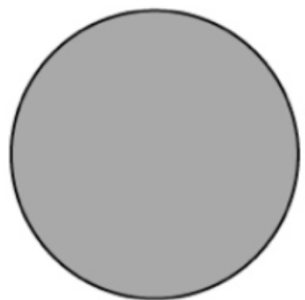
$$C = 2\pi D$$



$$C < 2\pi D$$

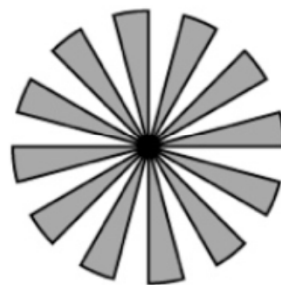


$$C > 2\pi D$$



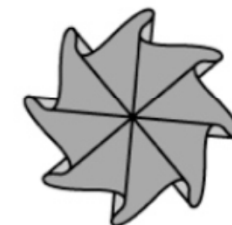
Zero curvature

(a)



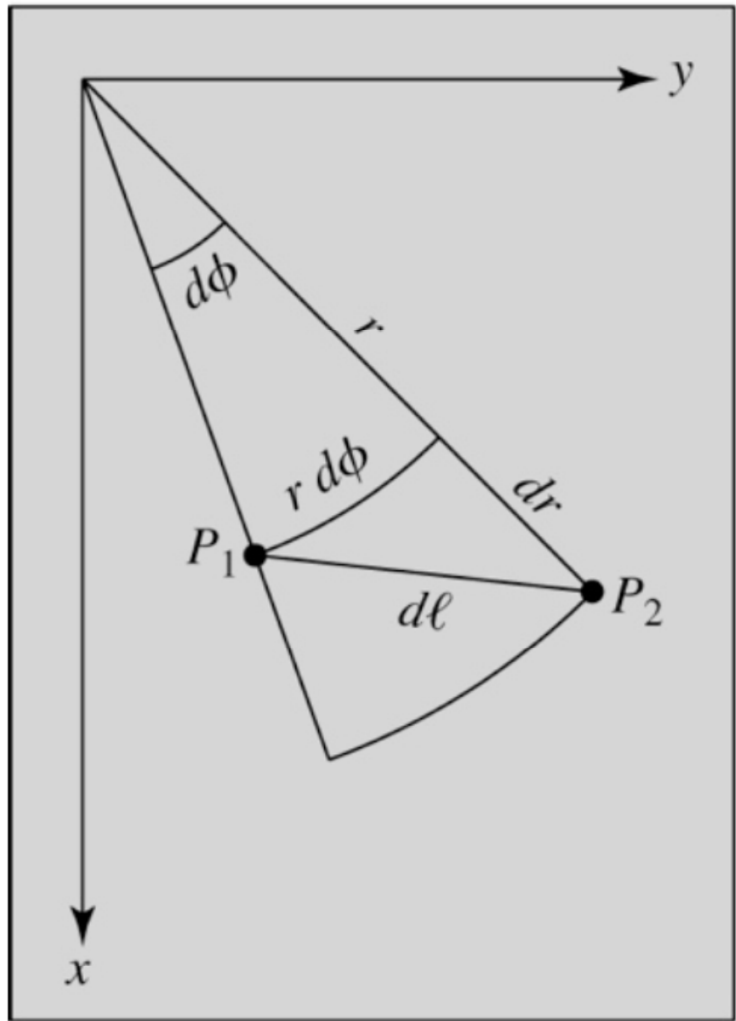
Positive curvature

(b)

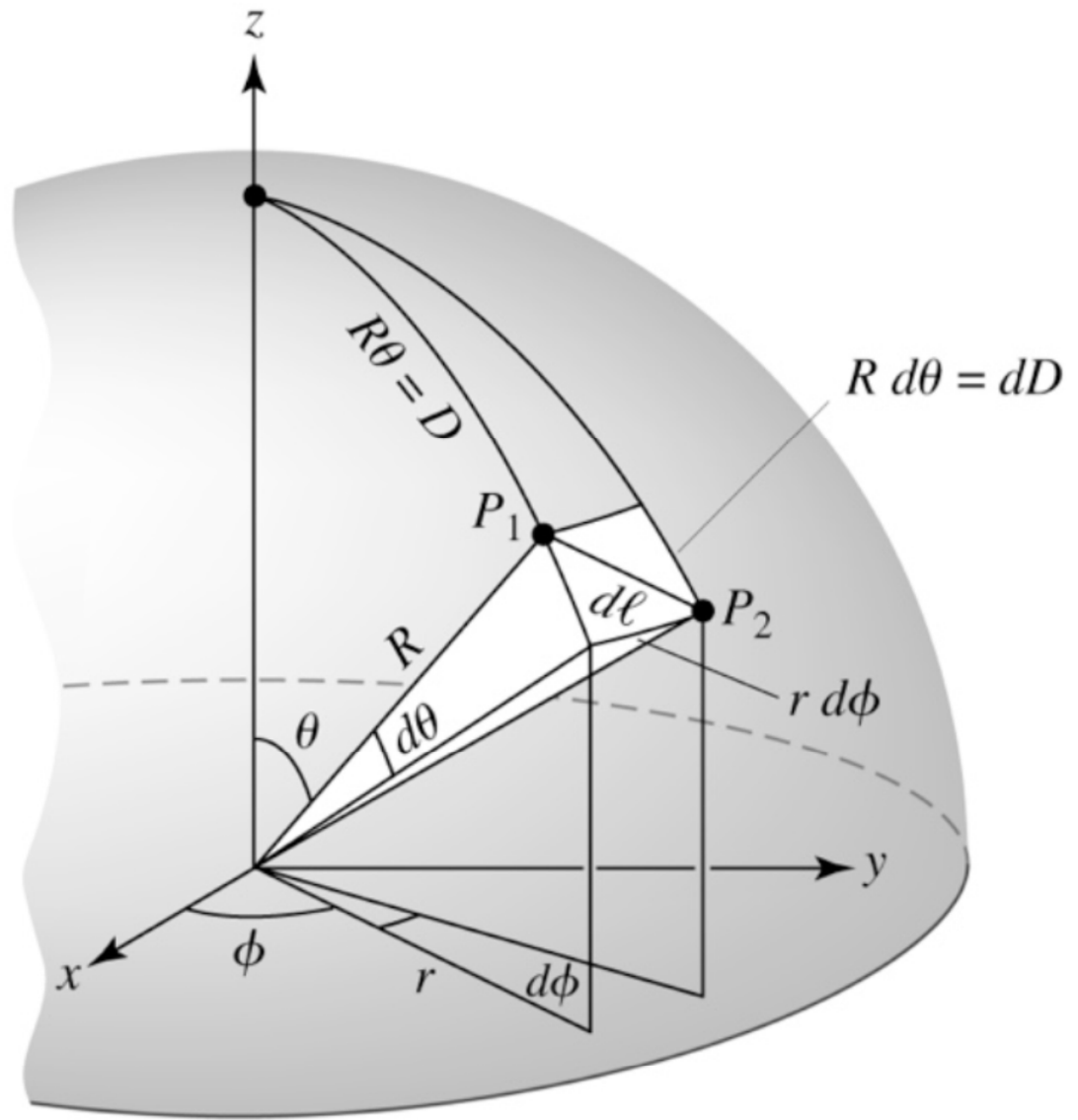


Negative curvature

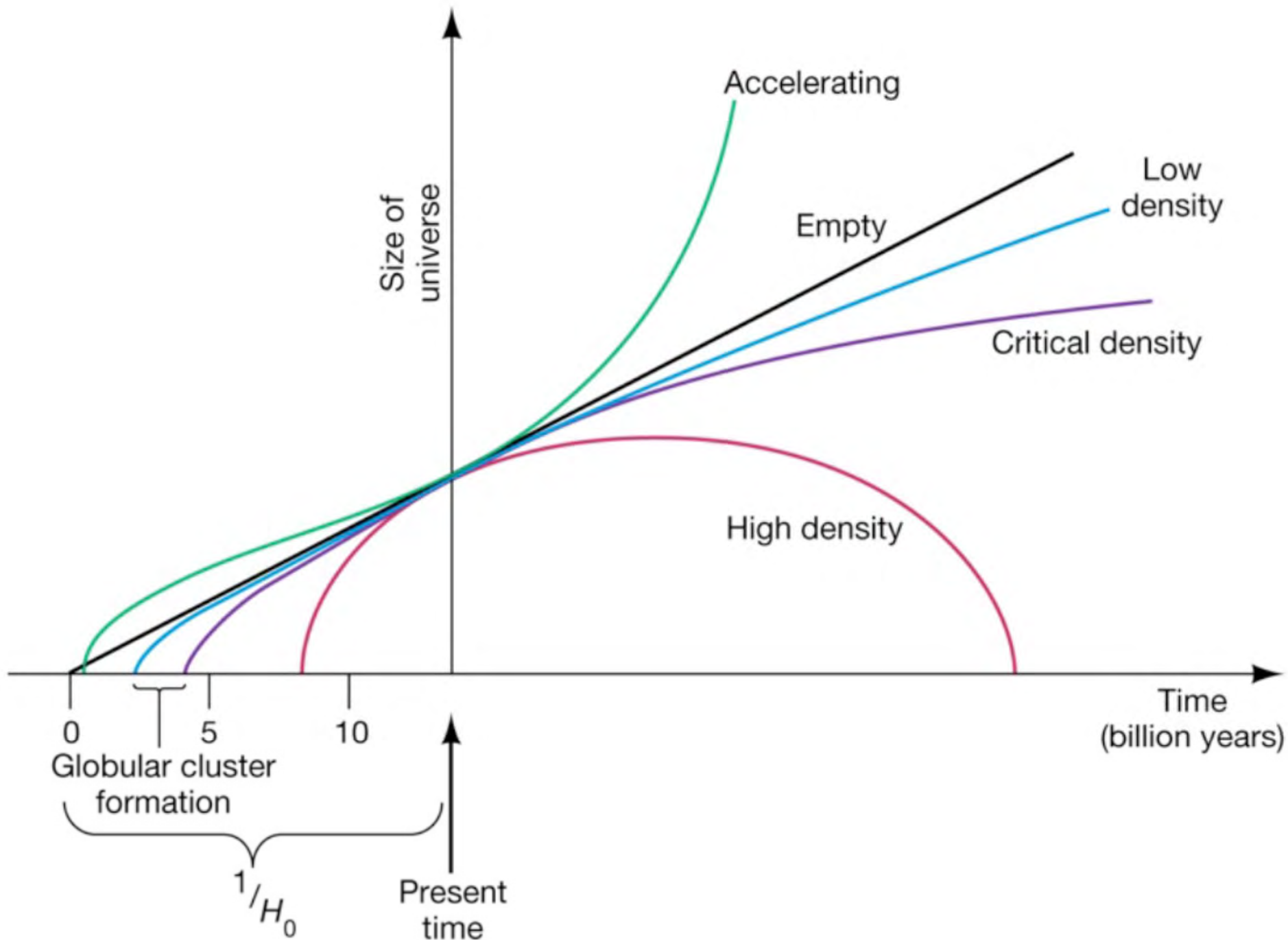
(c)

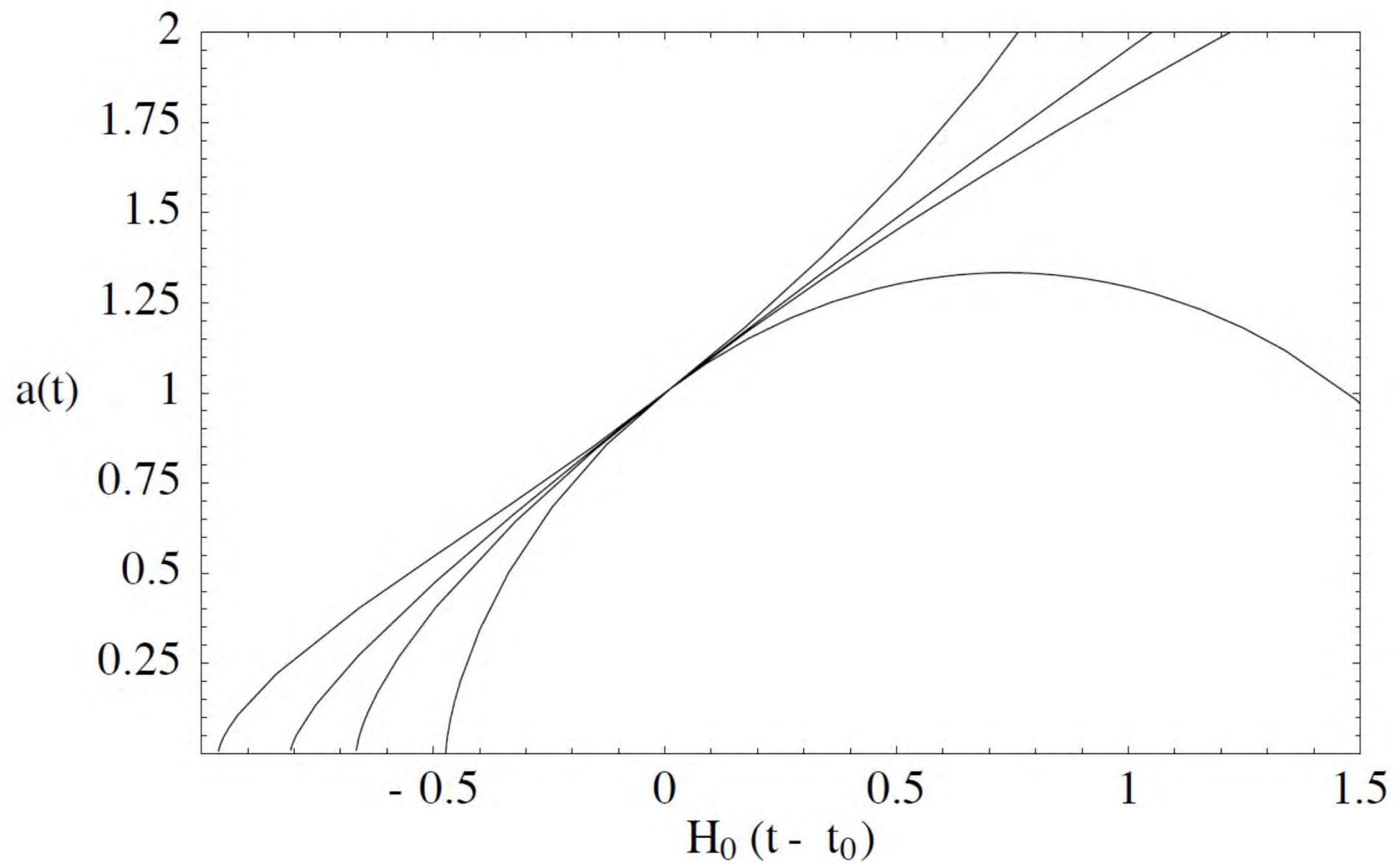


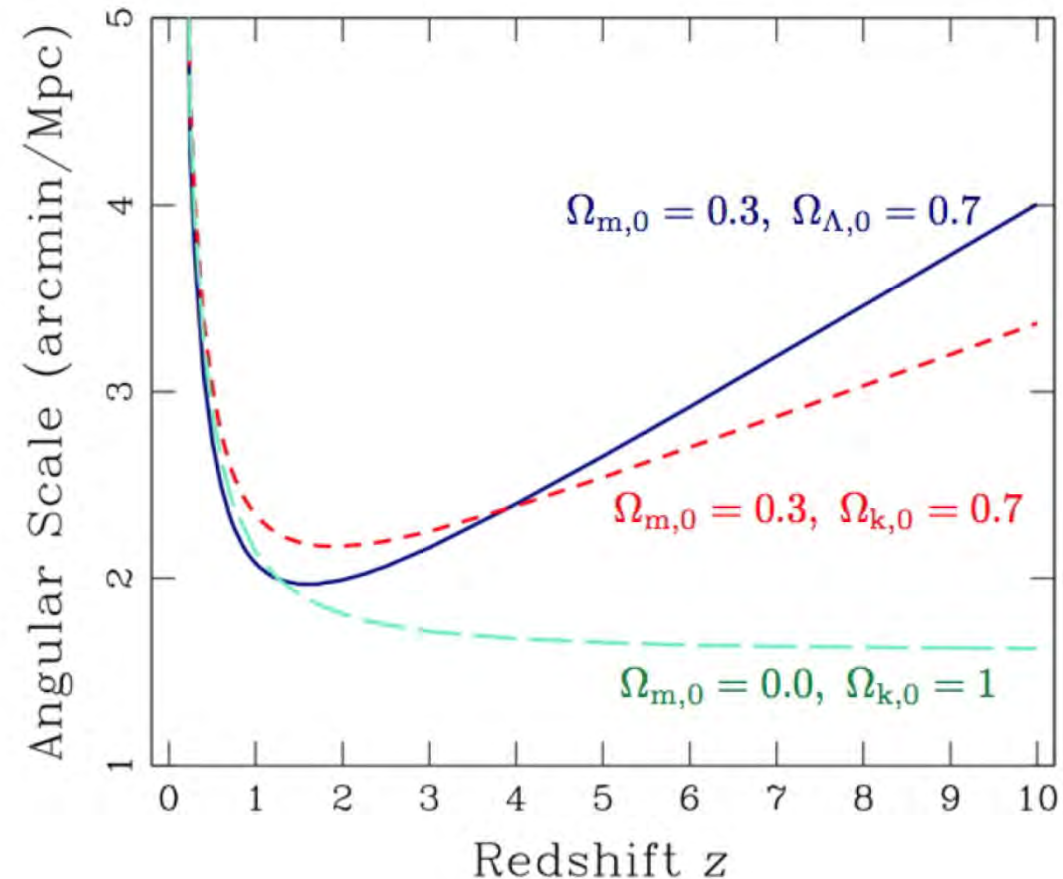
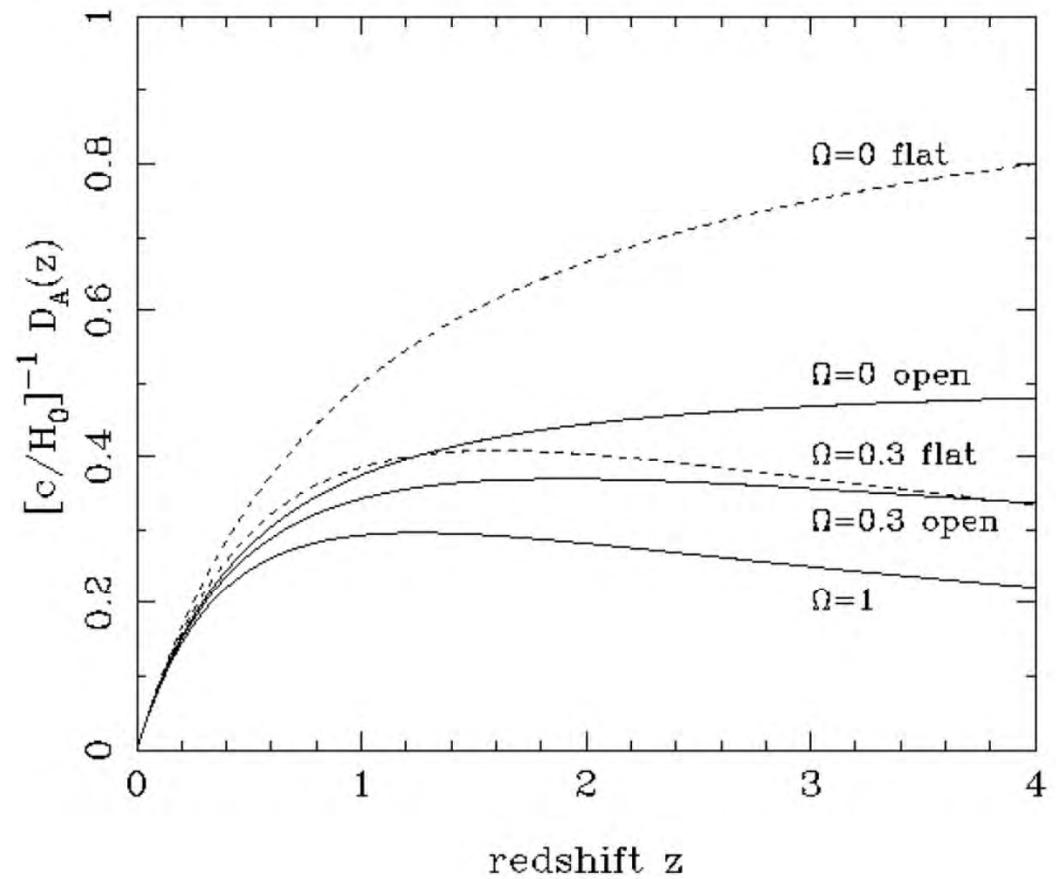
(a)

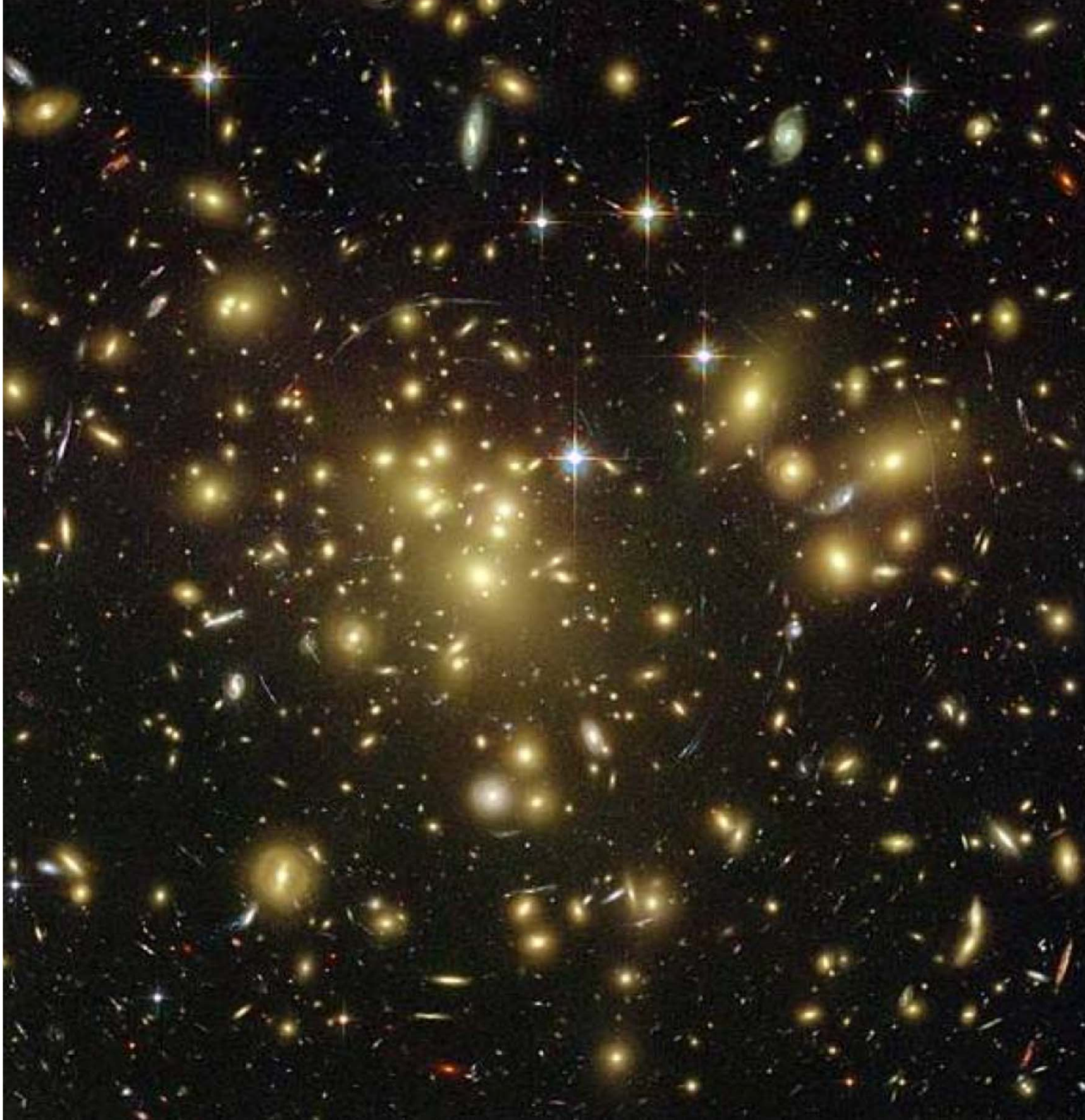


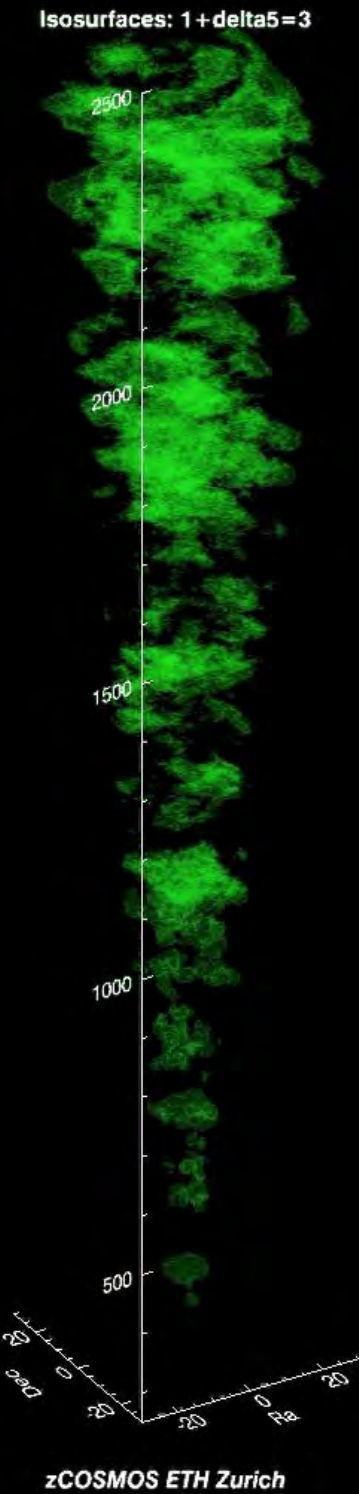
(b)



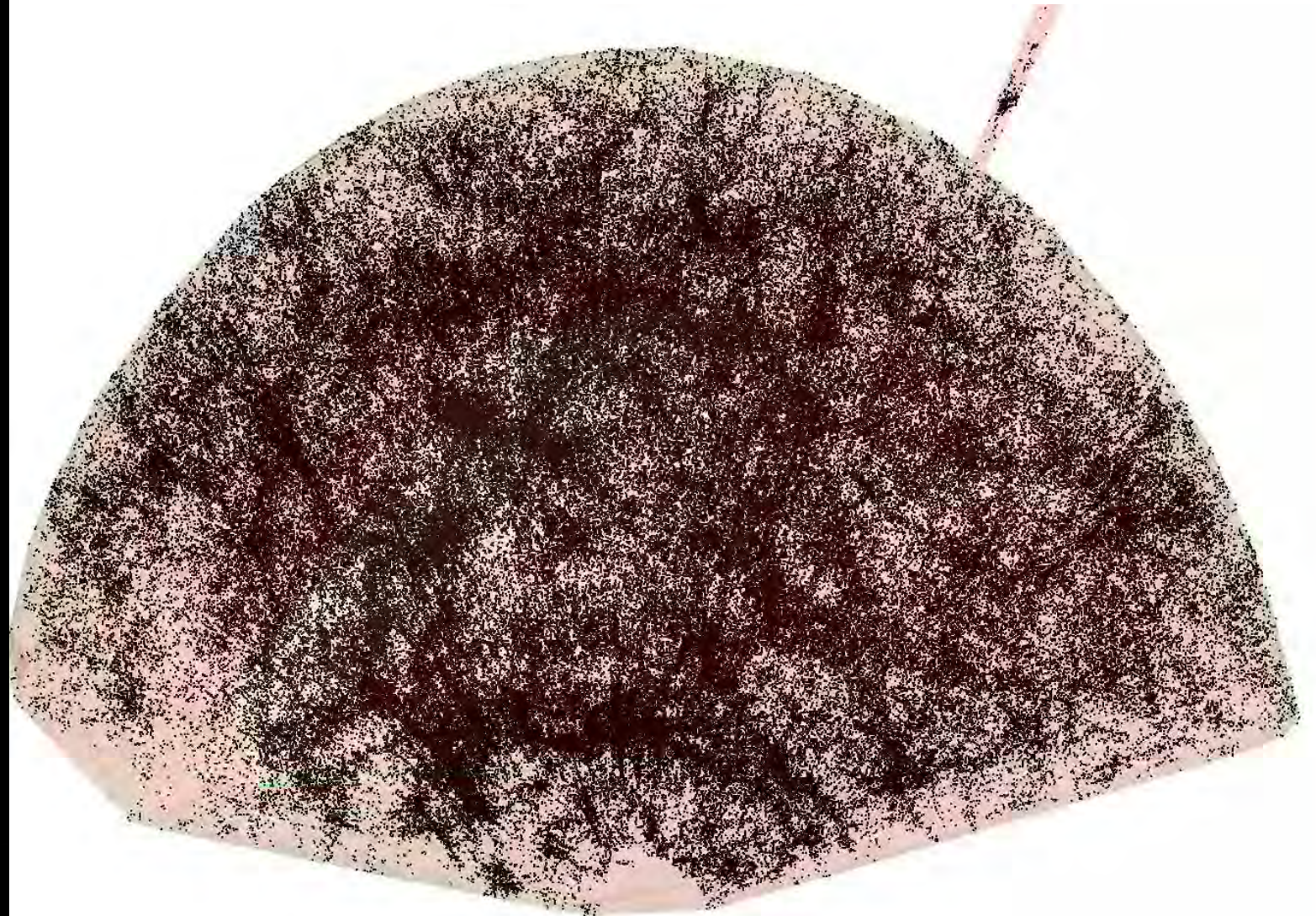








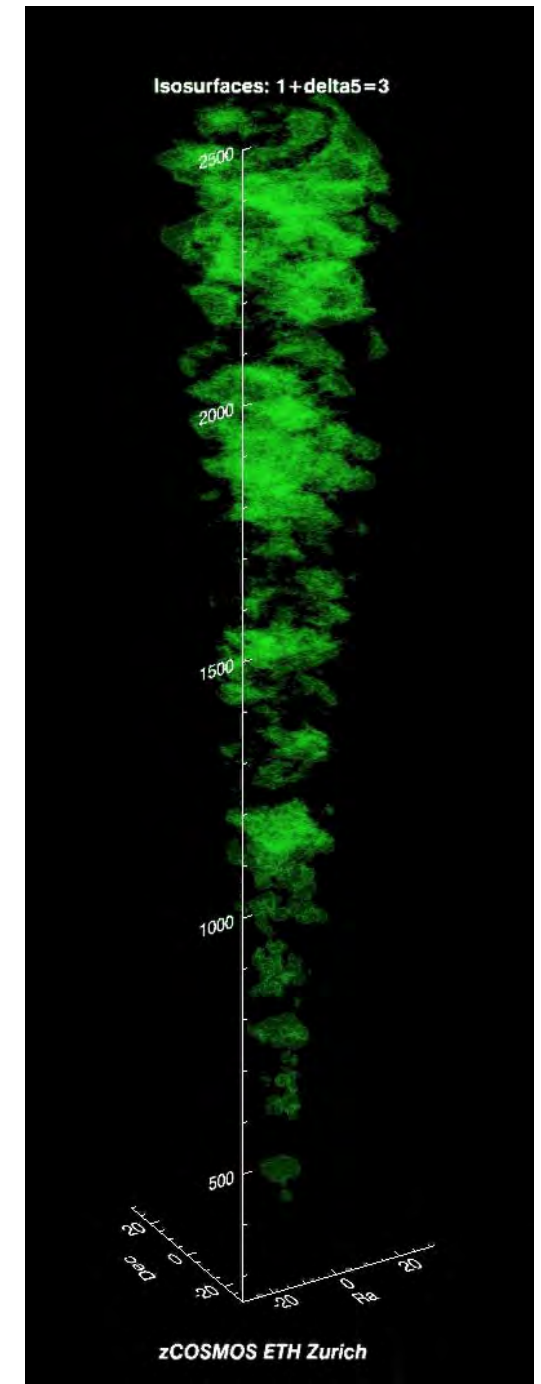
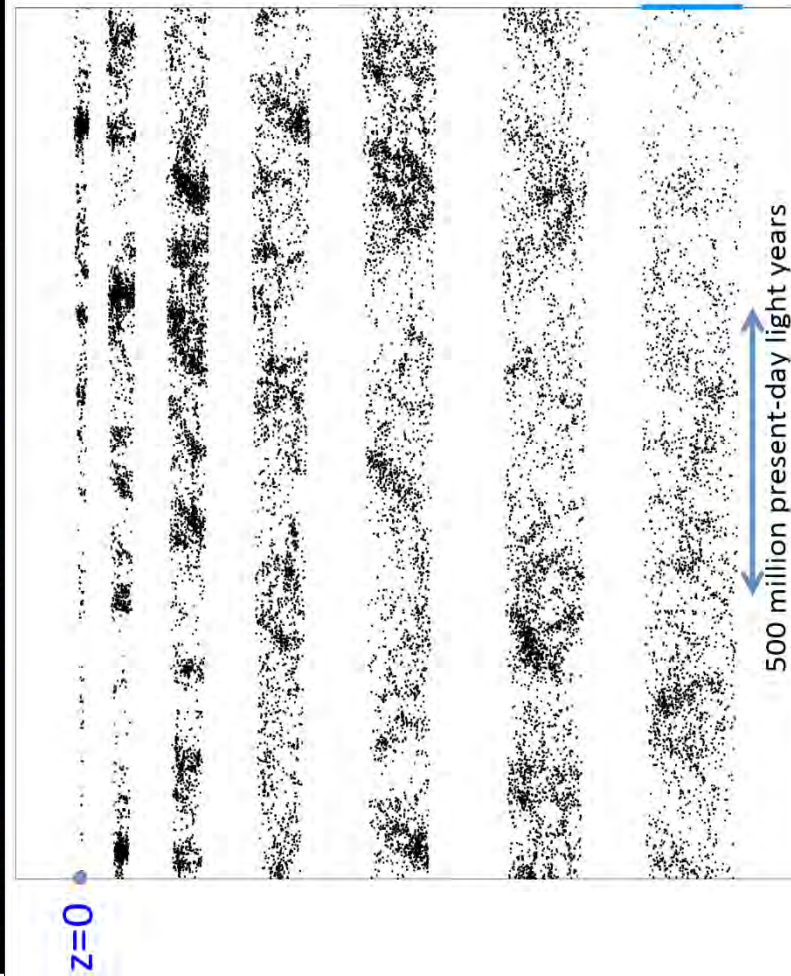
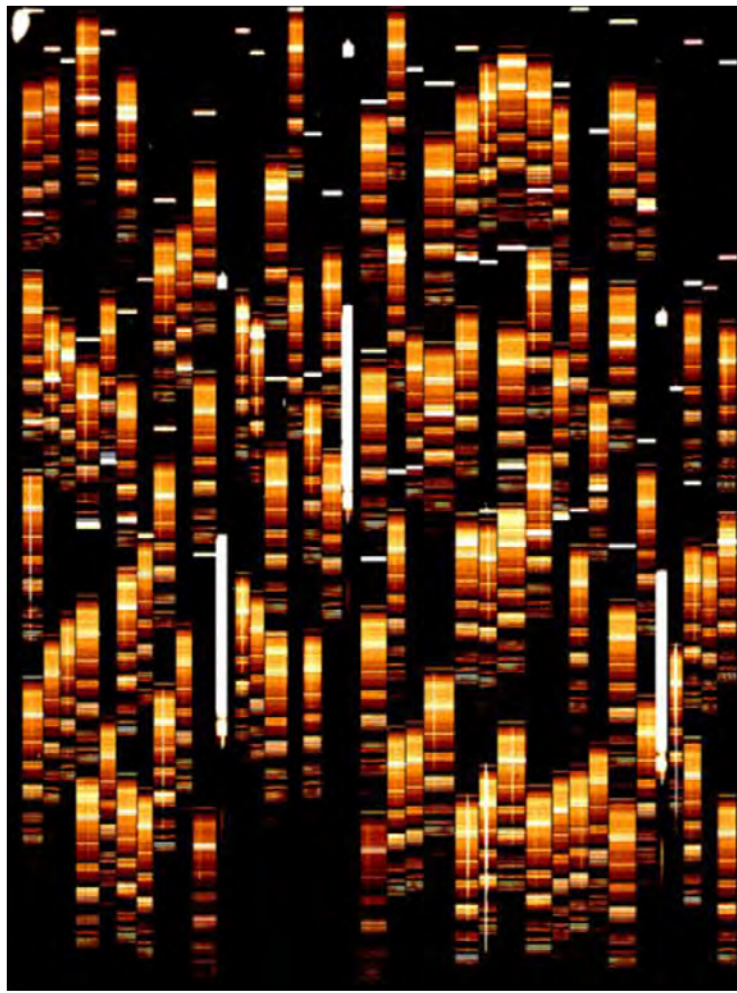
Large surveys since the past decade (SDSS, COSMOS, GOODS, VVDS, DEEP, GAMA, VIPERS etc.)



zCOSMOS + SDSS DR7 visualized by Yingjie Peng

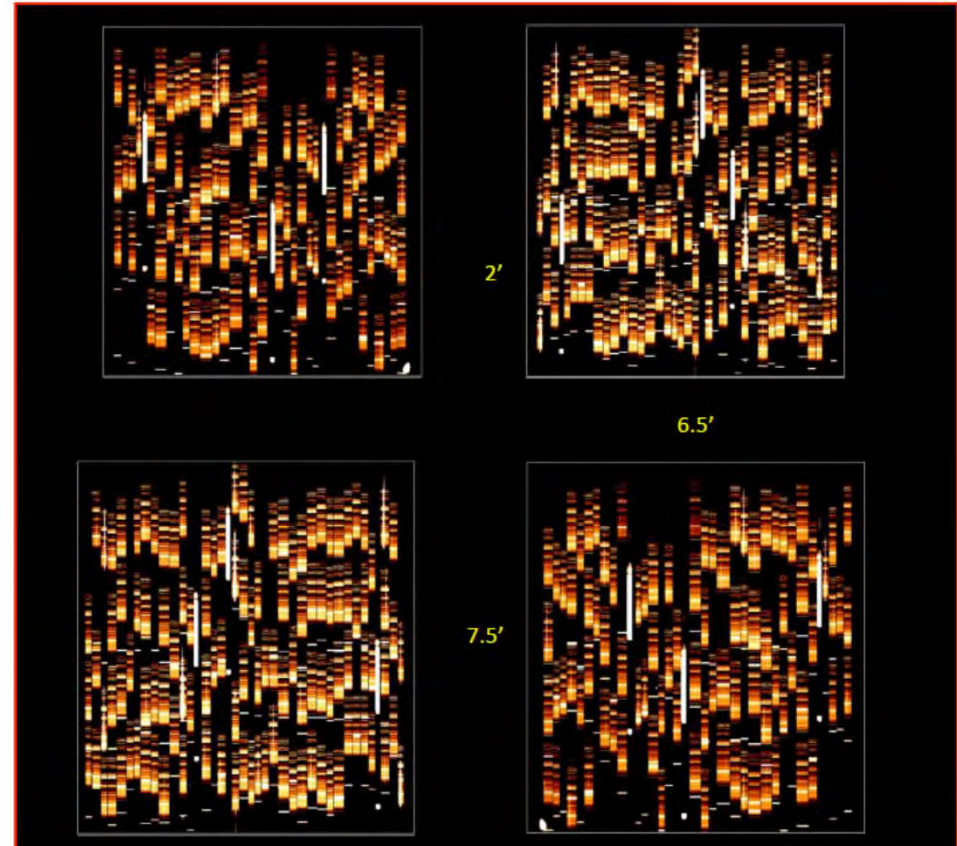
Large surveys enables new approach (SDSS, COSMOS, GOODS, DEEP etc.)

zCOSMOS is an approved Large Program on the ESO 8m VLT. 600 hours of observation are used to carry out a major redshift survey with the VIMOS spectrograph on the COSMOS field.



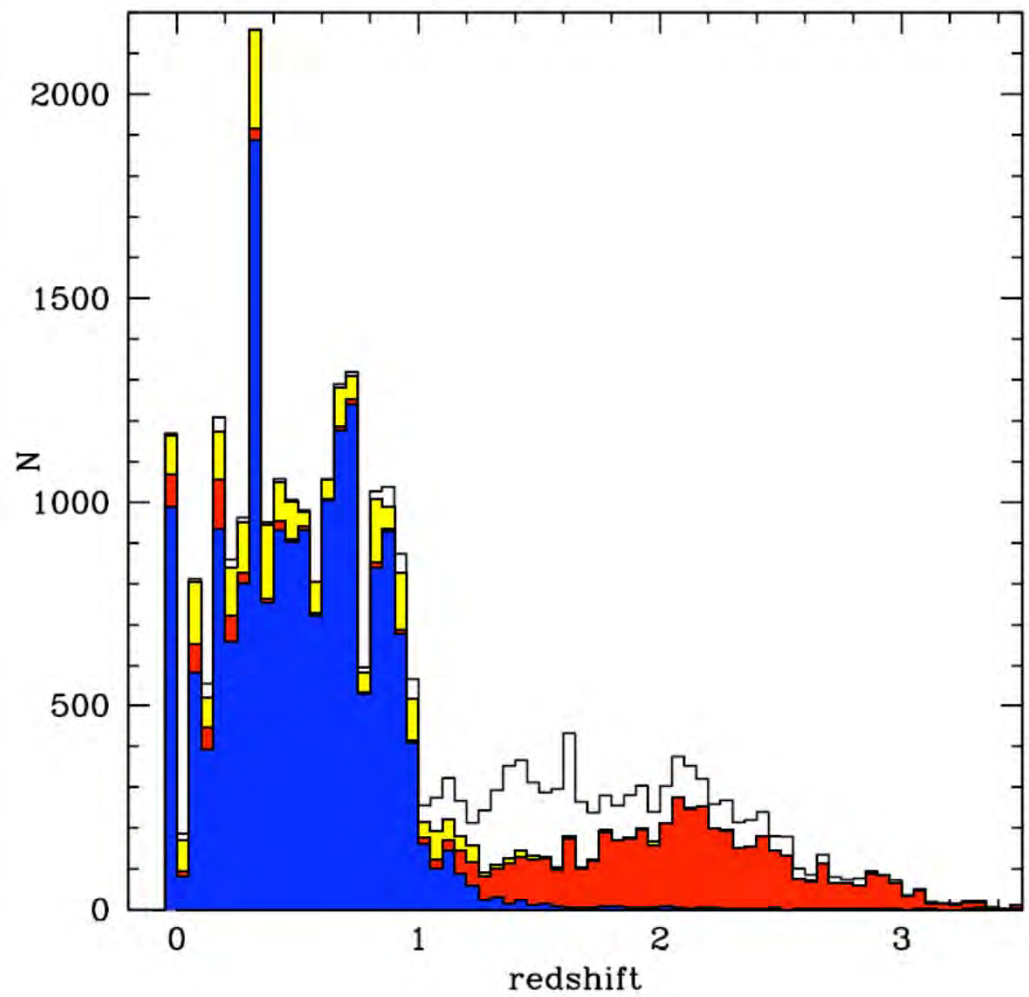
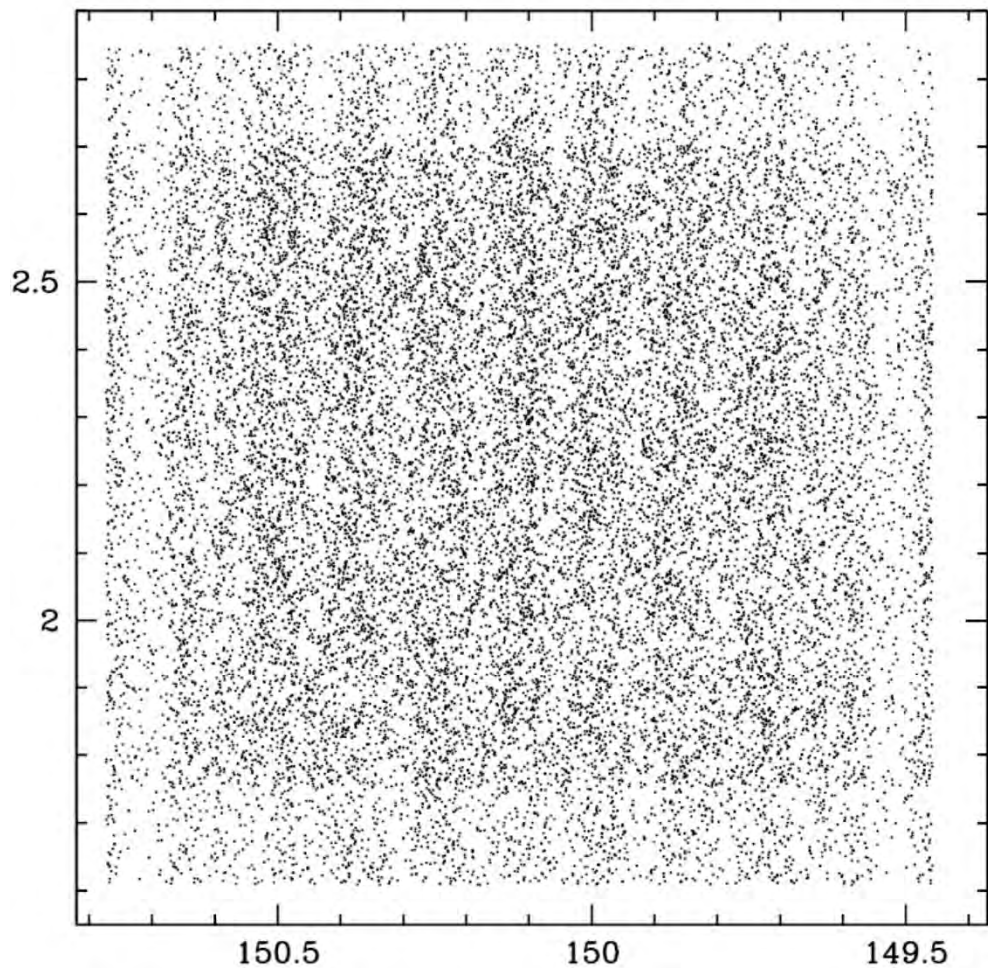
	fields	selection	N_{galaxies}	sampling	success
VVDS	$4 \times 4 \text{ deg}^2$	$I_{AB} < 22.5$	35,000	~15%	~ 80%
	$2 \times 2 \text{ deg}^2$	$I_{AB} < 24$	12,000	<10%	
	$1 \times 2 \text{ deg}^2$	$I_{AB} < 24.5$	1,000	<10%	
DEEP-2	$4 \times 1 \text{ deg}^2$	$BRI + R_{AB} < 24$	35,000 @ $0.8 < z < 1.4$	~60%	75%
zCOSMOS	$1 \times 2 \text{ deg}^2$	$I_{AB} < 22.5$	20,000 @ $0 < z < 1.2$	~70%	85%
		$gzK + B_{AB} < 25.5$	5,000 @ $1.5 < z < 3$	~70%	30-80%

- Generally with multi-slit spectrographs, e.g. VIMOS on VLT, DEIMOS on Keck.
- Can fibres work below sky?
- Badly need effective NIR multi-object spectrograph
 - FMOS (fibres)
 - MOSFIRE (slits)
 - KMOS (optical probes)



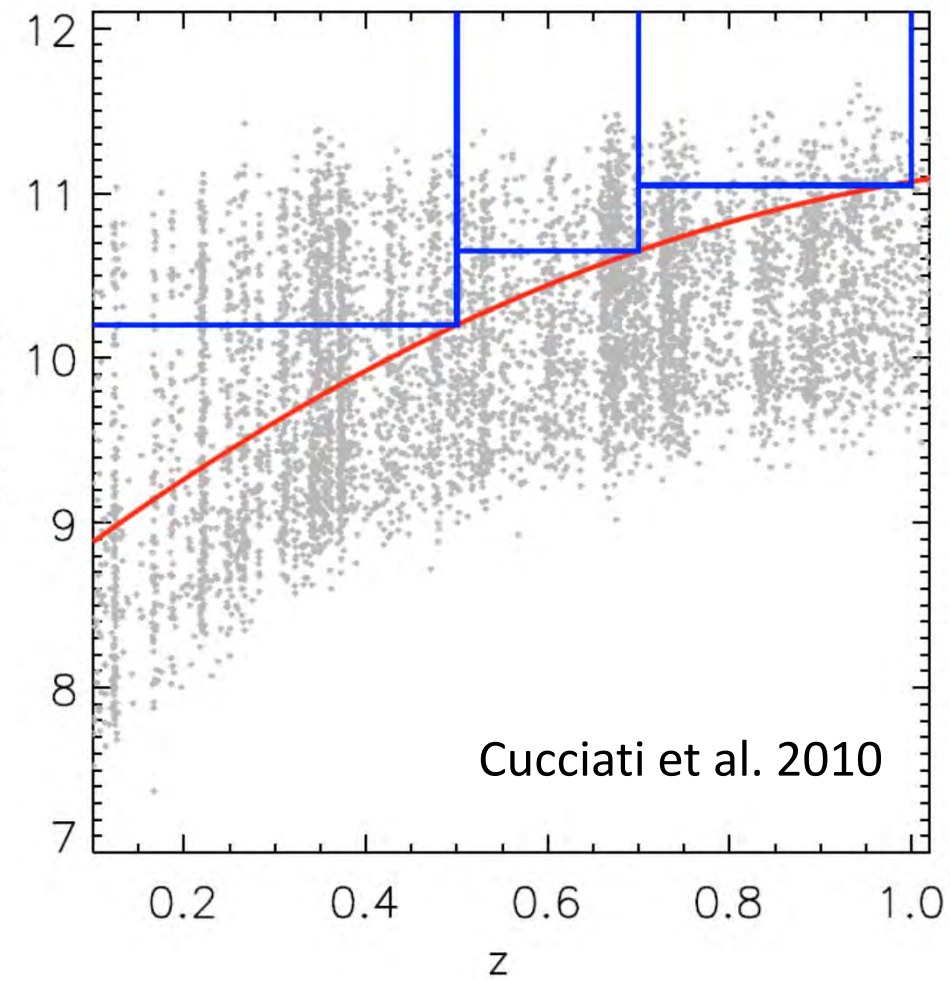
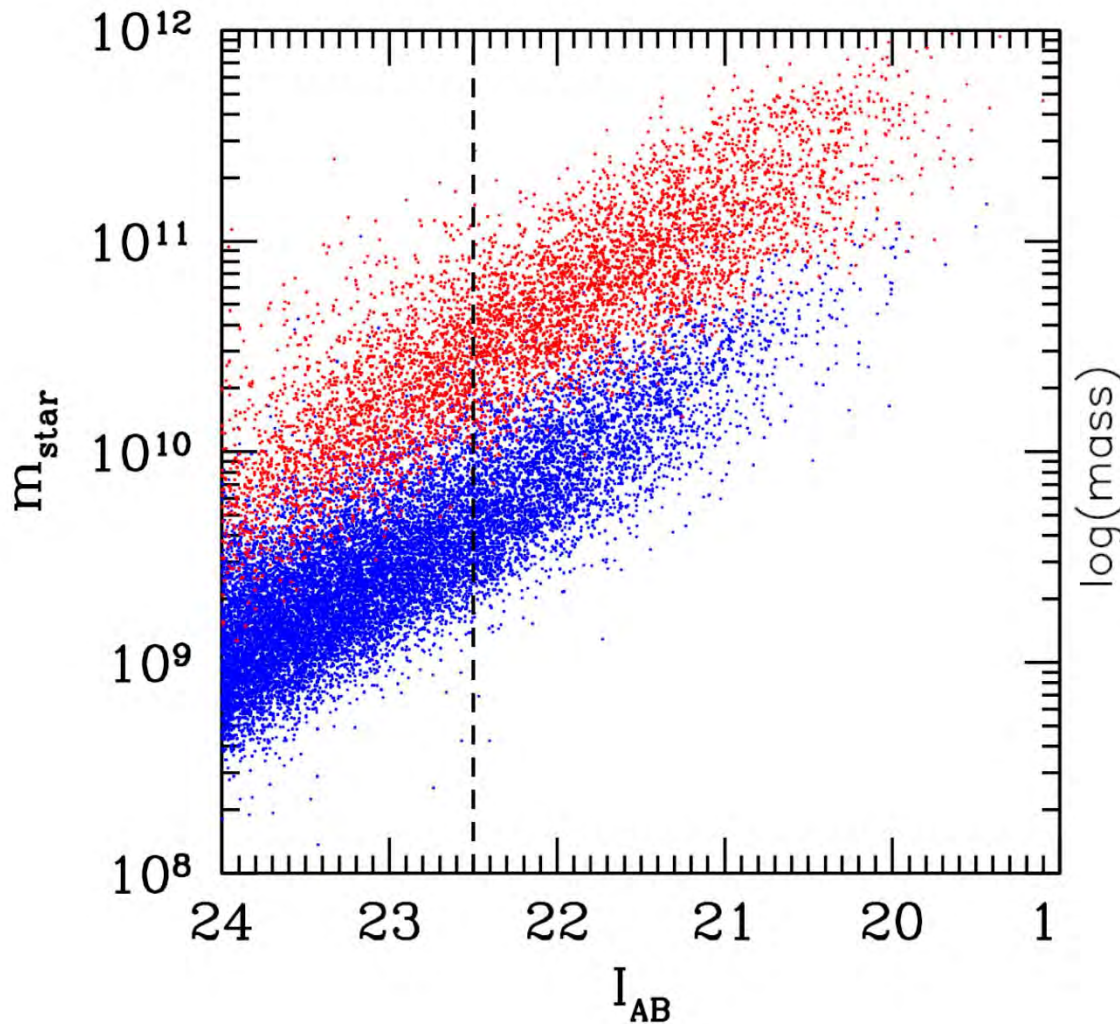
zCOSMOS

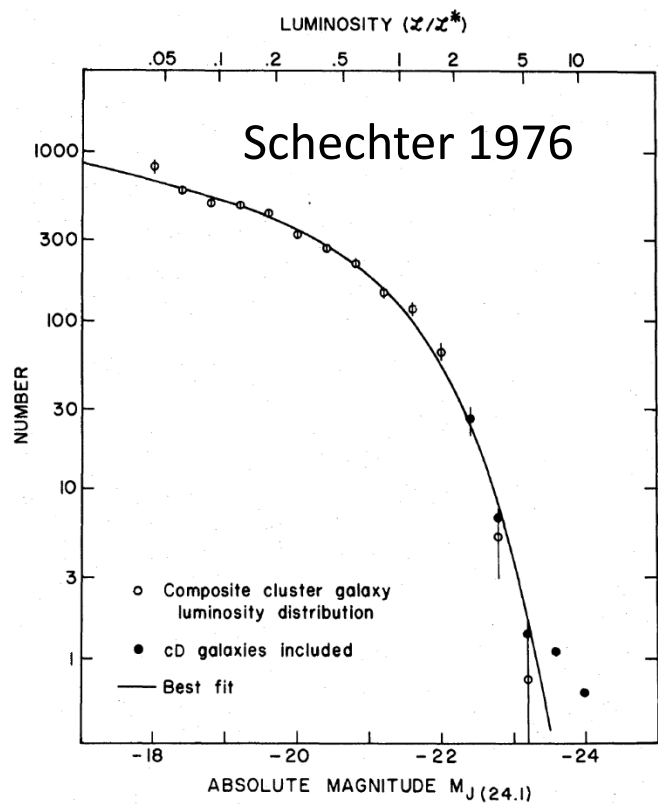
- 20,000 galaxies $I_{AB} < 22.5$ @ $0.1 < z < 1.4$ over 2 deg^2
- 5,000 galaxies BzK & ugr $B_{AB} < 25.25$ @ $1.4 < z < 3.0$ in central 1 deg^2



Mass and other (in)completeness in sky surveys

Almost all samples ultimately selected by apparent brightness.

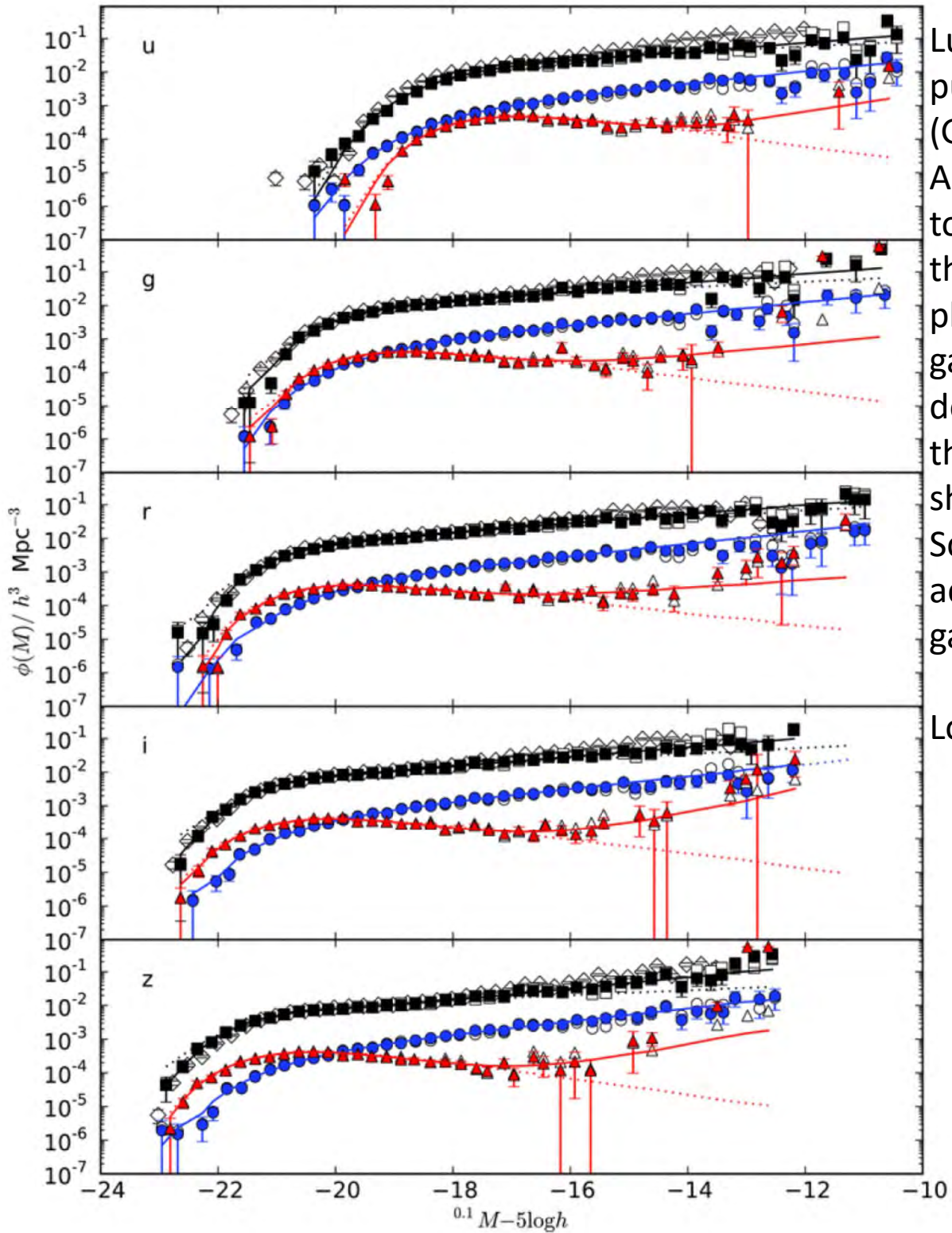




$$\phi(m)dm = e^{-\frac{m}{M^*}} \phi^* \left(\frac{m}{M^*}\right)^{\alpha_s} \frac{dm}{M^*}$$

Binggeli's (1987) cartoon of Paul Schechter and his function. Quite why it has this form buries **details** under foot.





Luminosity functions of nearby galaxies ($z < 0.1$) published by the Galaxy and Mass Assembly (GAMA) project from data obtained with the Anglo-Australian telescope. The five panels refer to LFs in five different wavelength bands, from the ultraviolet, u , to the infrared, z . The LF is plotted separately for blue (i.e. star-forming) galaxies and red galaxies whose light is dominated by old stars. The black squares are for the combined blue and red samples. Dotted lines show the best fit to the data assuming a Schechter function. The GAMA team accumulated spectra of many thousands of galaxies to construct these LFs.

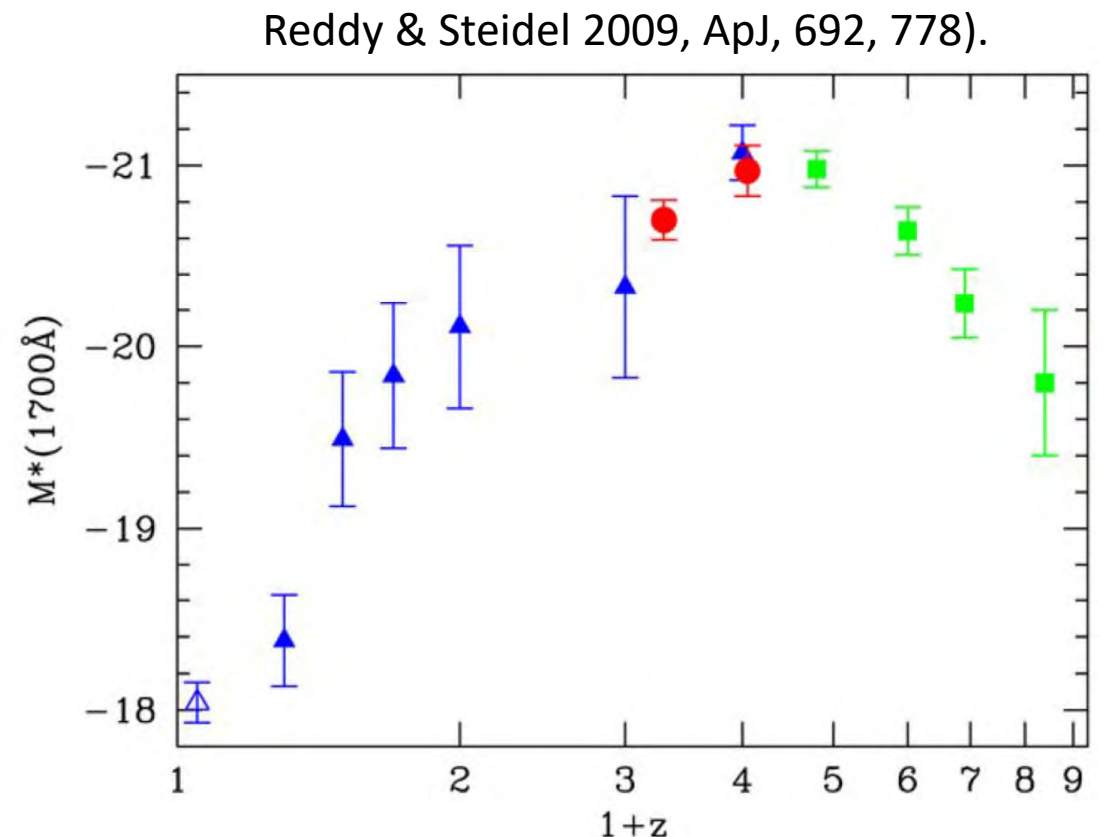
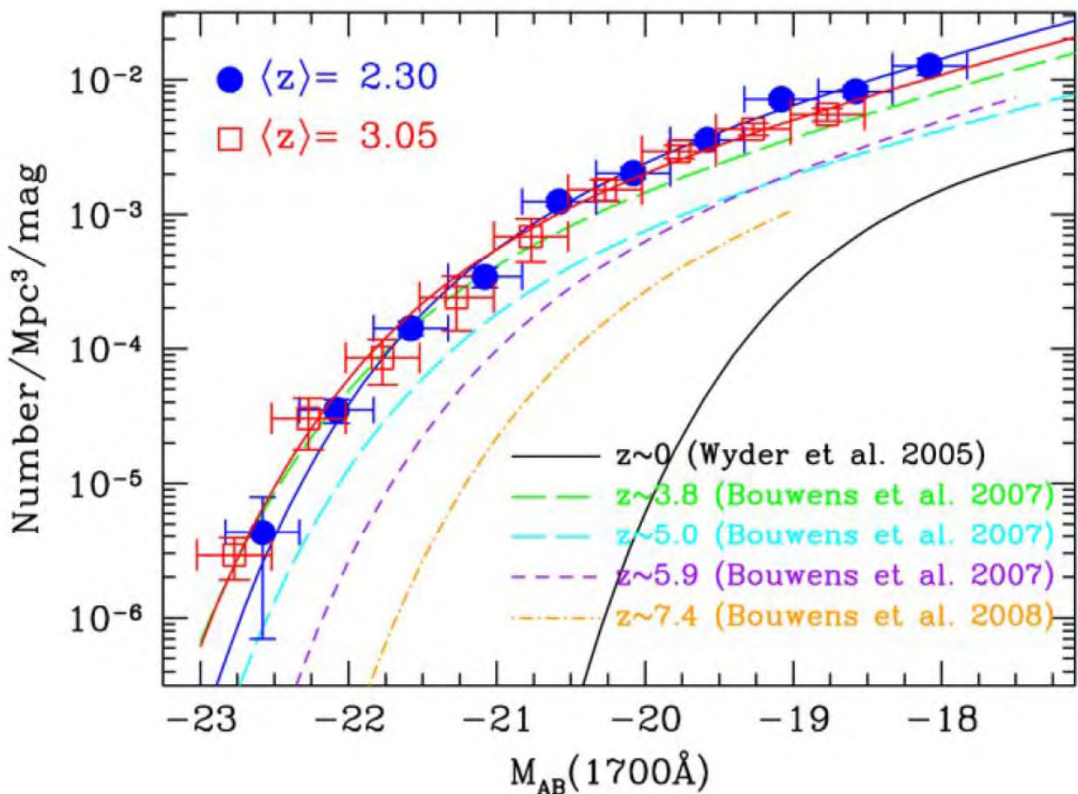
Loveday et al. 2012, MNRAS, 420, 1239

the LF of galaxies in visible light (in the V-band) is well-fitted by a Schechter function with typical parameters:

$$\alpha = -1.25$$

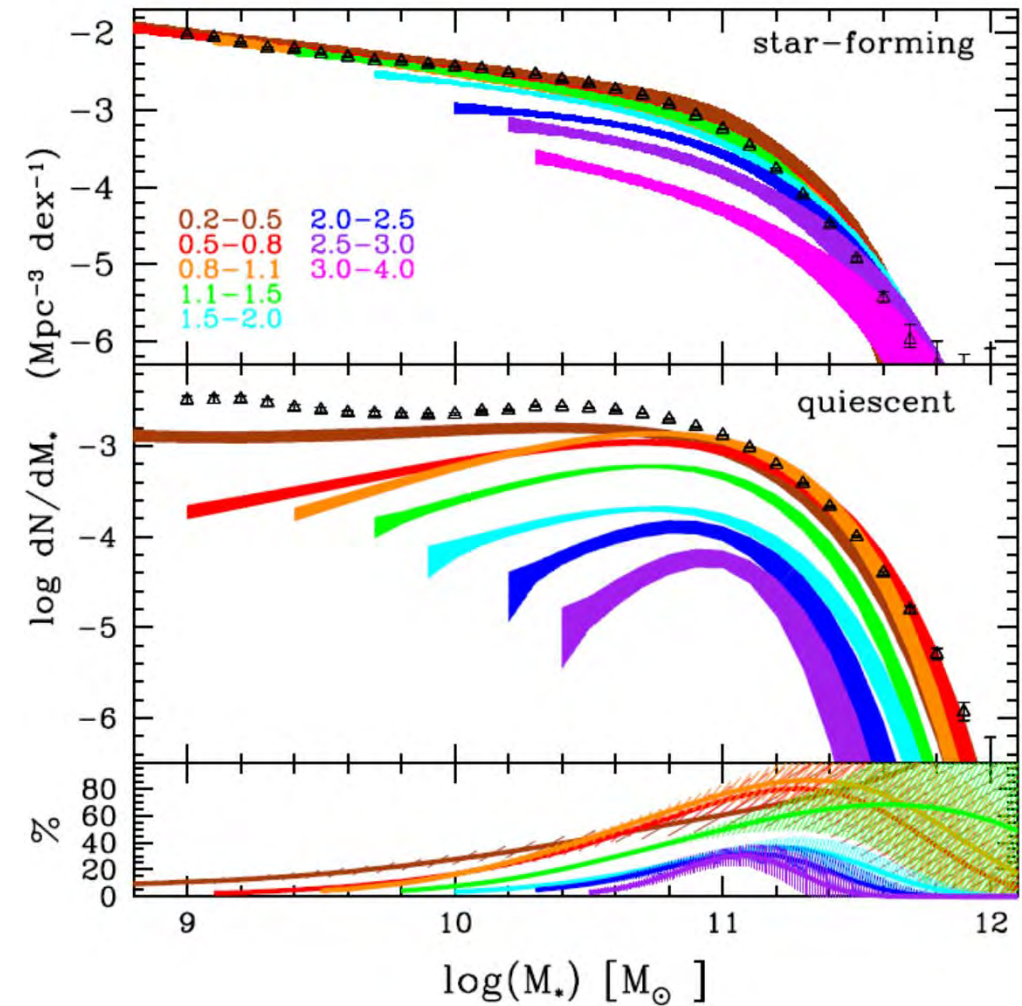
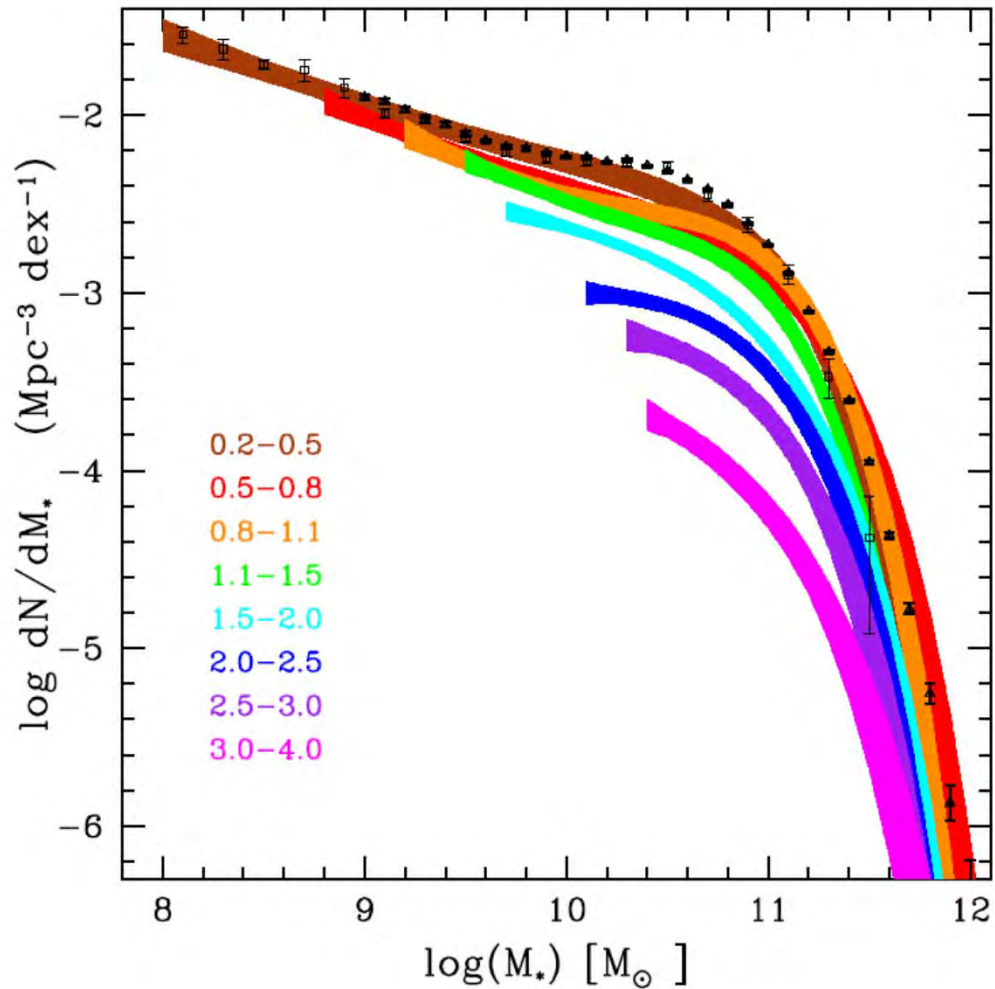
$$L^* = 1.0 \times 10^{10} h^{-2} L_{\odot V}$$

$$\phi^* = 1.2 \times 10^{-2} h^3 \text{ Mpc}^{-3}$$

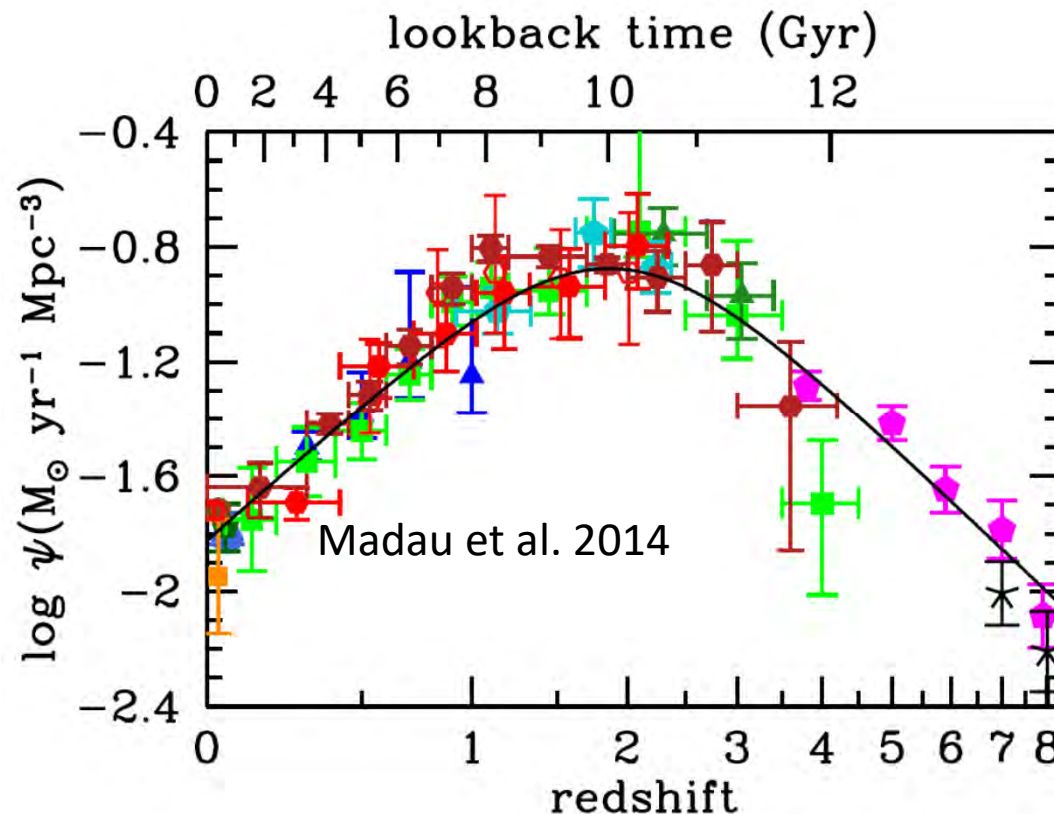


Left: Evolution of the ultraviolet (UV) luminosity function from $z = 7.4$ to $z = 0$.

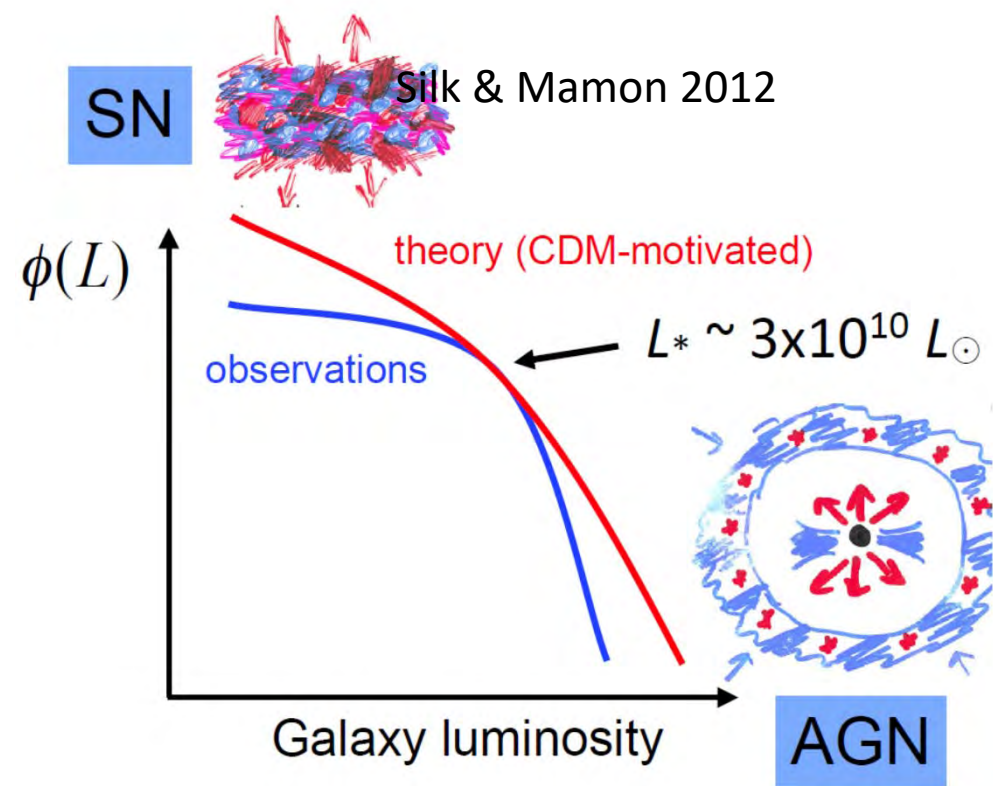
Right: Evolution of the characteristic UV luminosity (or absolute magnitude, M^* , at 1700 Å) with redshift.

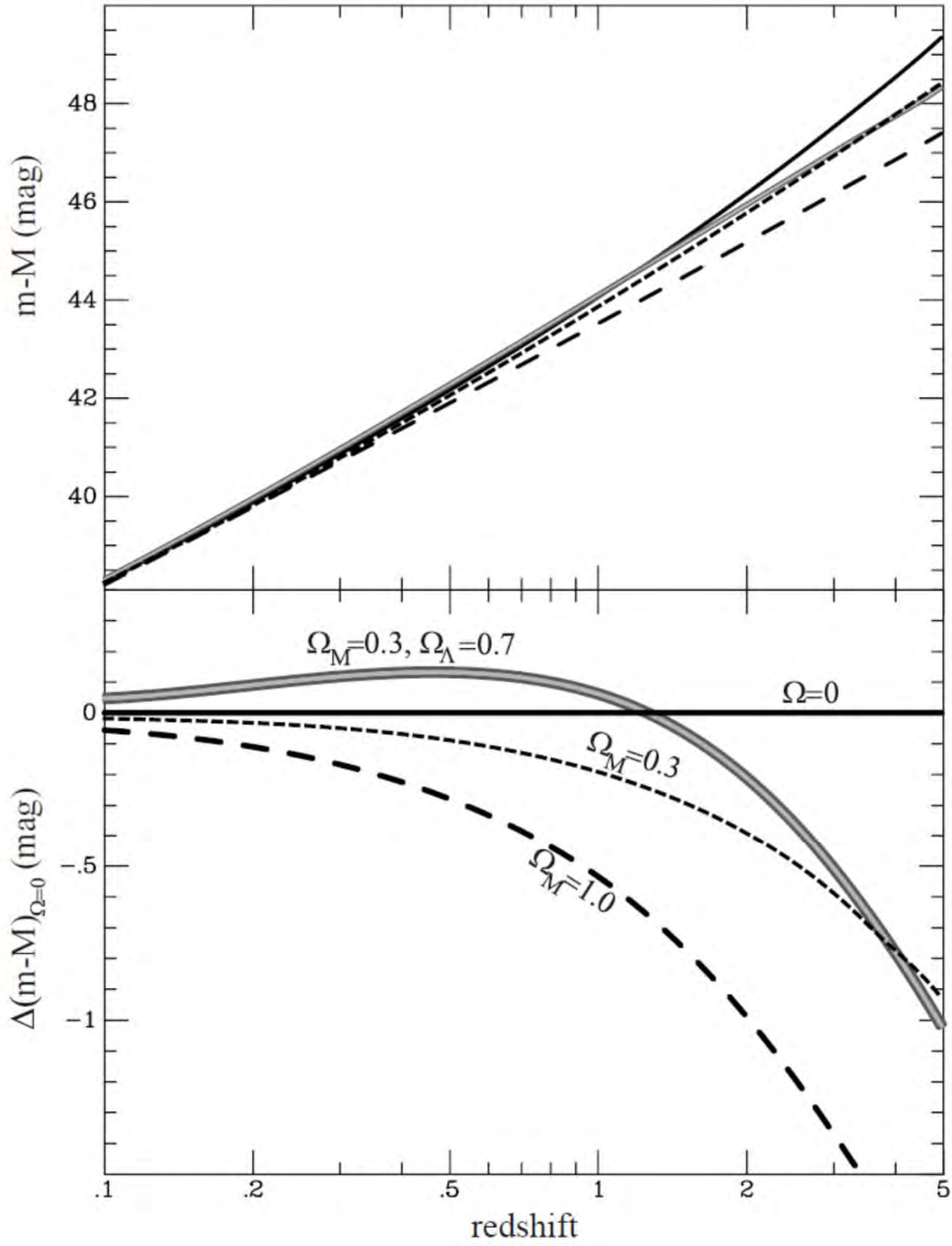


The Cosmic Star Formation History



Luminosity function and feedback

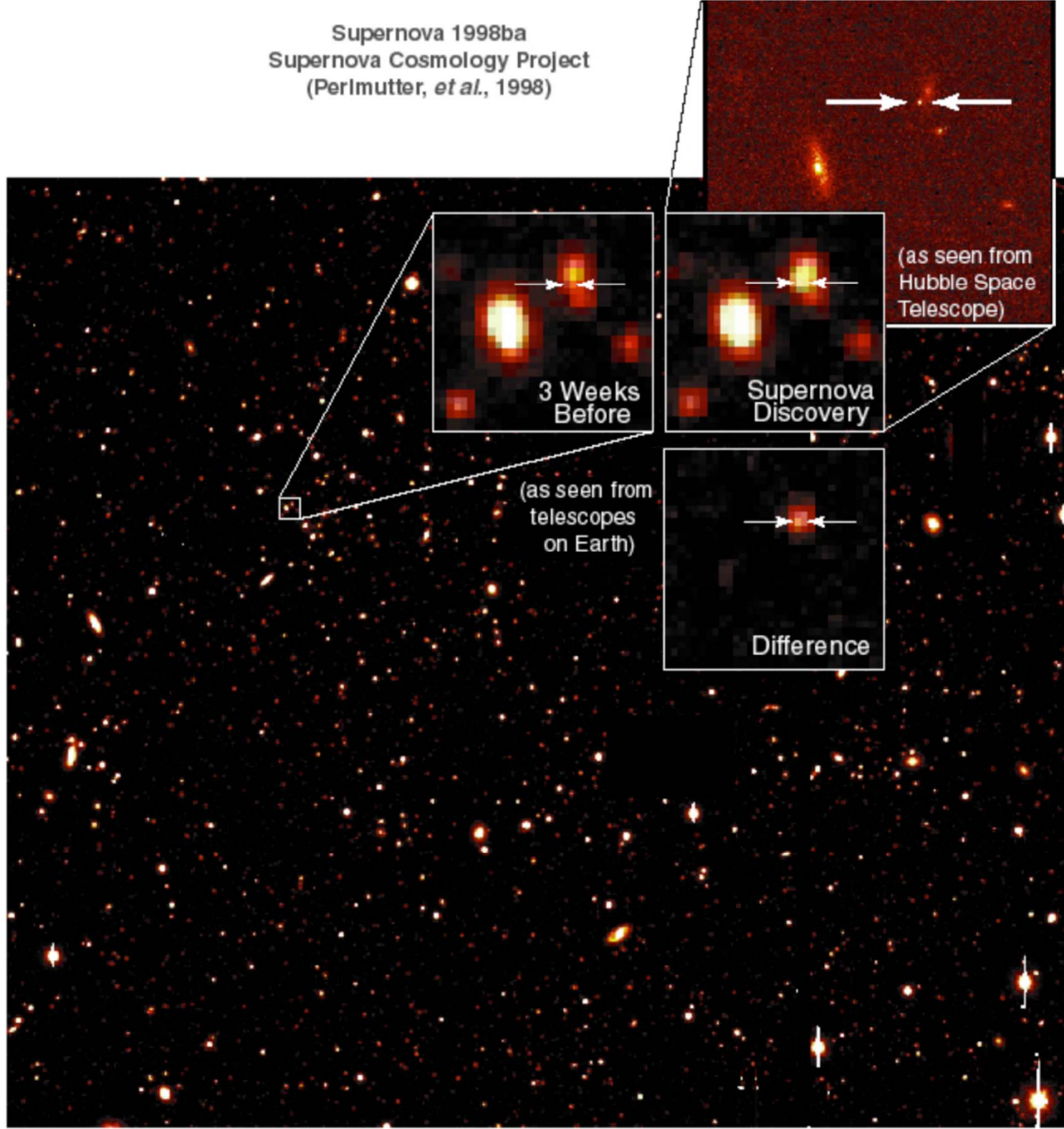




The distance modulus as a function of redshift for four relevant cosmological models, as indicated.

In the lower panel the empty universe ($\Omega_{m,0} = \Omega_{\Lambda,0} = 0$) has been subtracted from the other models to highlight the differences.

Supernova 1998ba
Supernova Cosmology Project
(Perlmutter, *et al.*, 1998)



The superb resolution of the Hubble Space Telescope allows a more accurate measurement of the light curves of high redshift supernovae than is possible from the ground.

Supernova Search in the Era of Wide-field Surveys

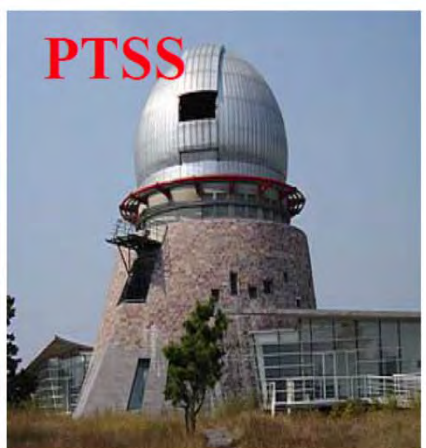


PTF *yesterday*
The Palomar Transient Factory
(2009-2012)
General synoptic transient survey

iPTF *today*
Intermediate Palomar Transient Factory
(2013-2016)
Focused mini-surveys



104+ papers, 3283+ citations



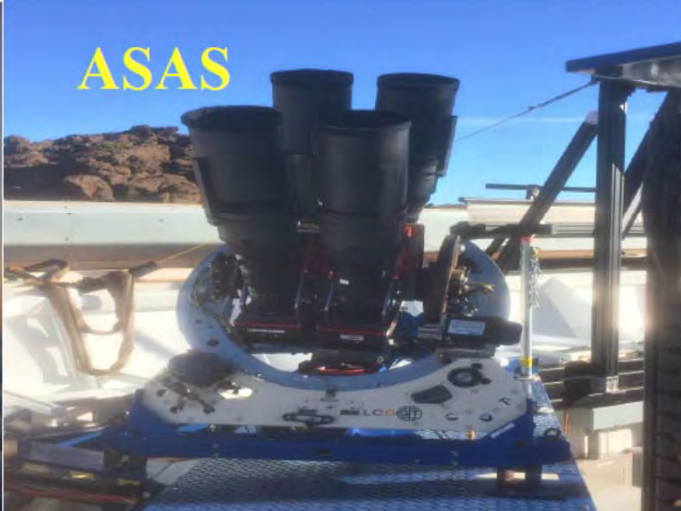
ZTF *tomorrow*
The Zwicky Transient Facility
(2017-2020)
High-cadence, wide-area survey



ATLAS

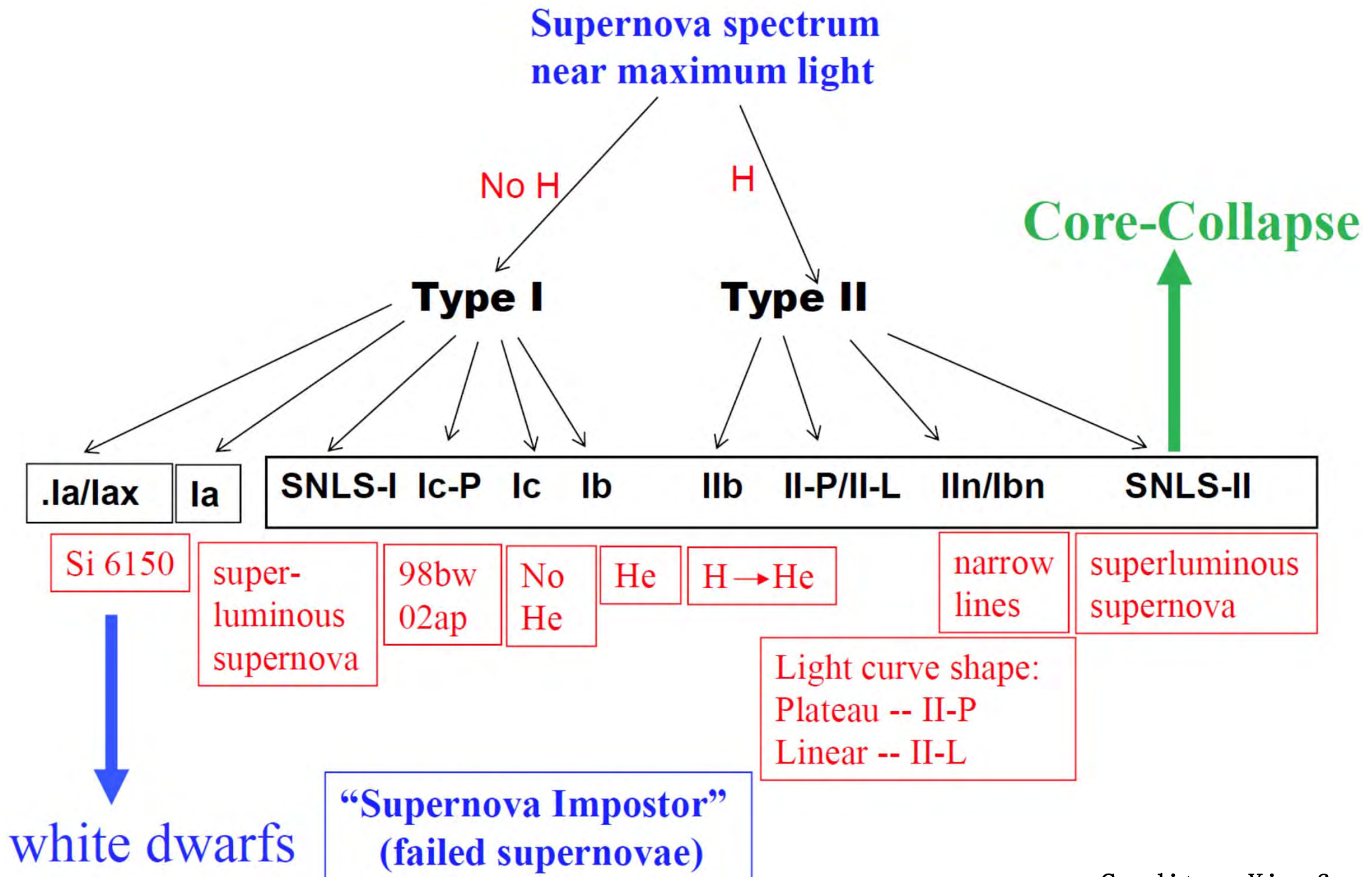


PanStarrs
Credits: Xiaofeng Wang
Tsinghua University

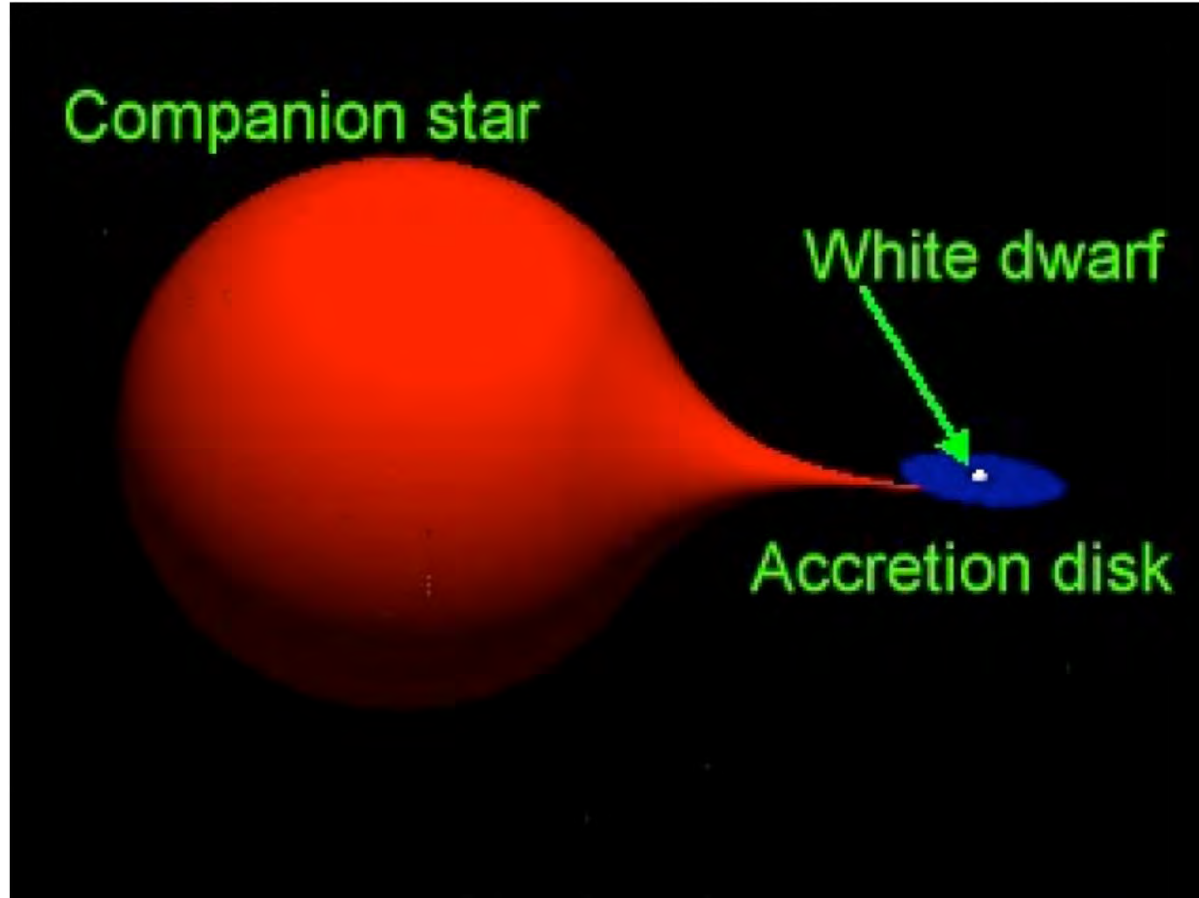


CRTS

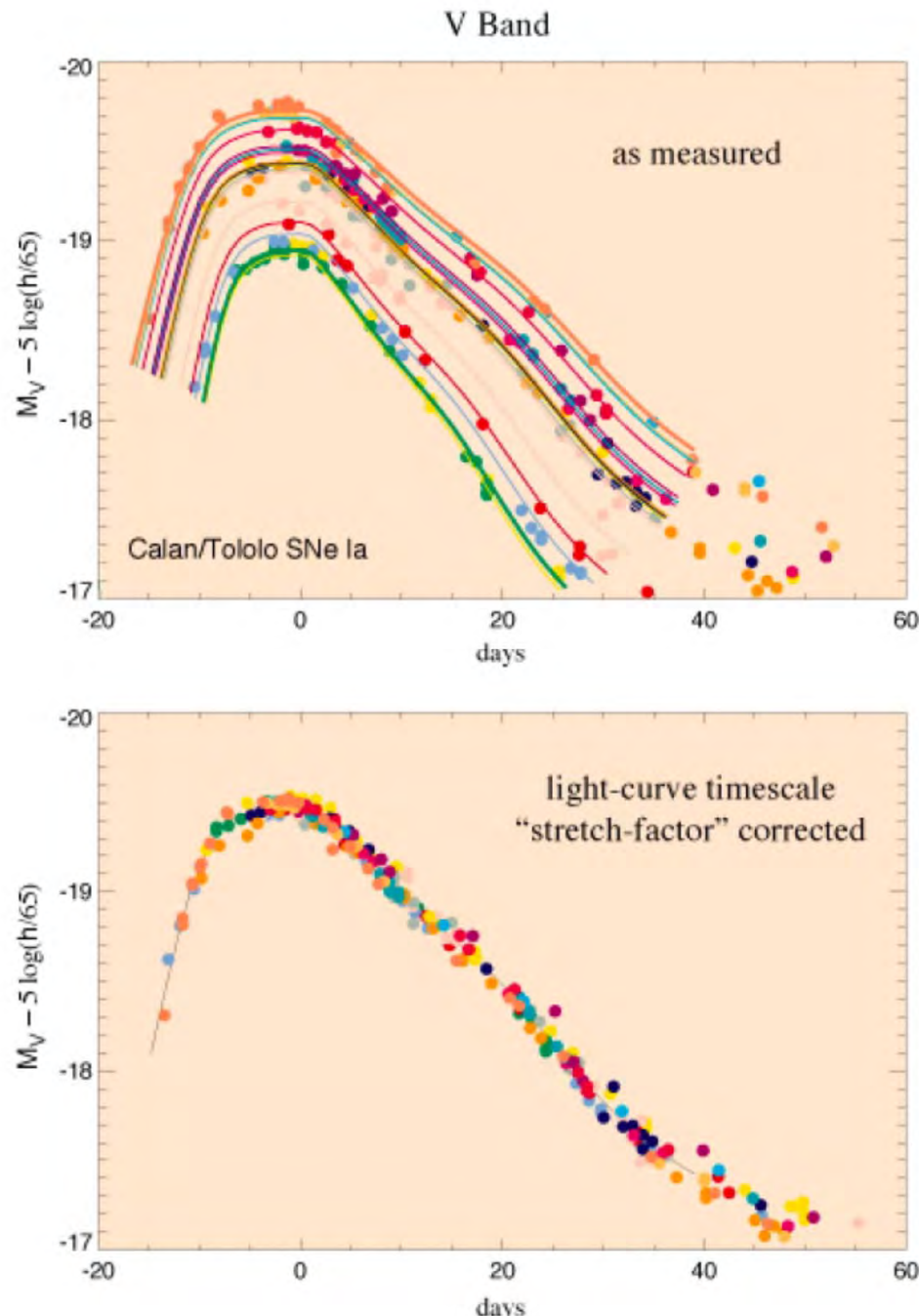
Supernova Taxonomy



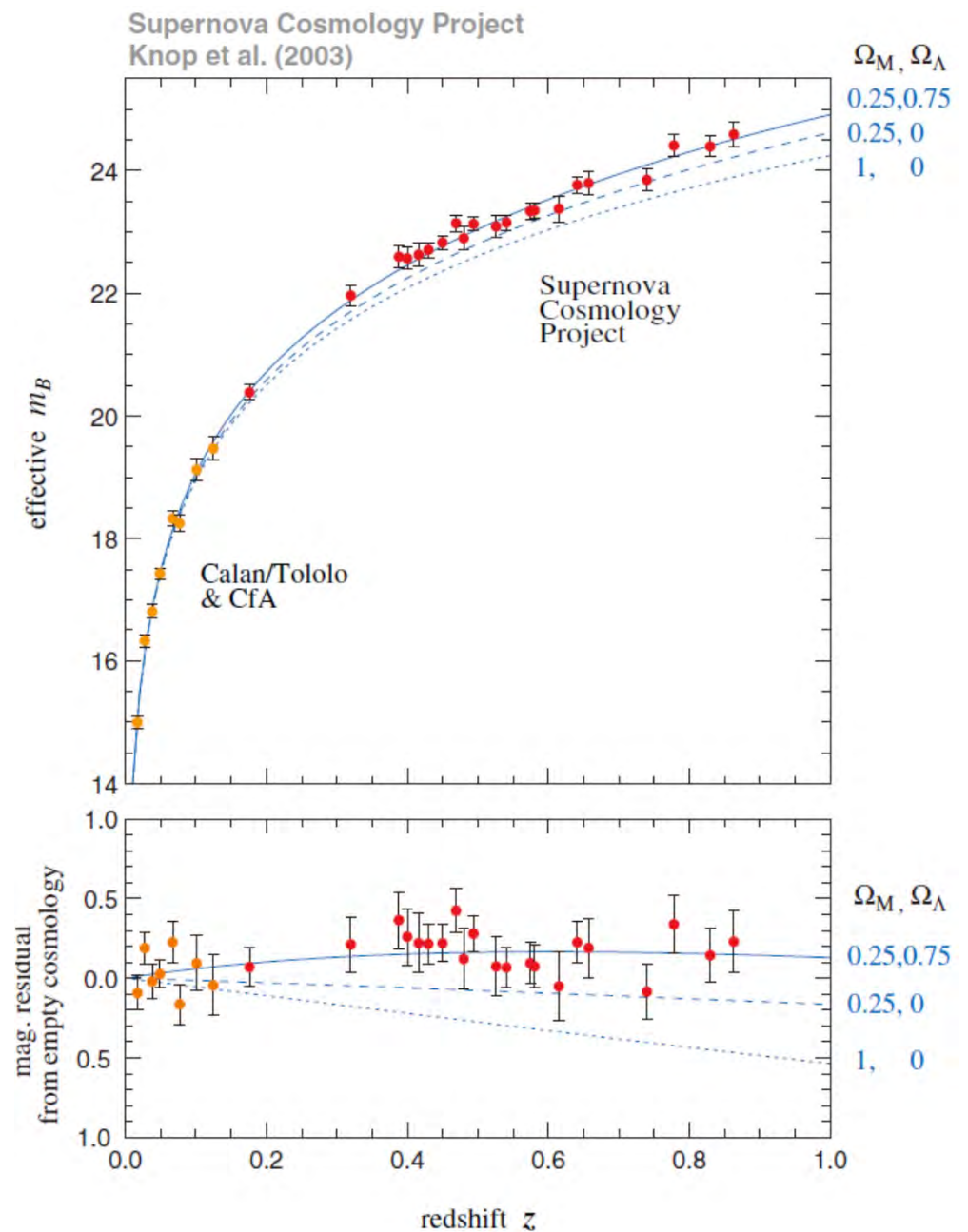
Credits: Xiaofeng Wang
Tsinghua University



Schematic representation of the stellar progenitor of a Type Ia supernova.



Light curves of type Ia SN before (top) and after (bottom) application of the correction
(Reproduced from <http://supernova.lbl.gov>).

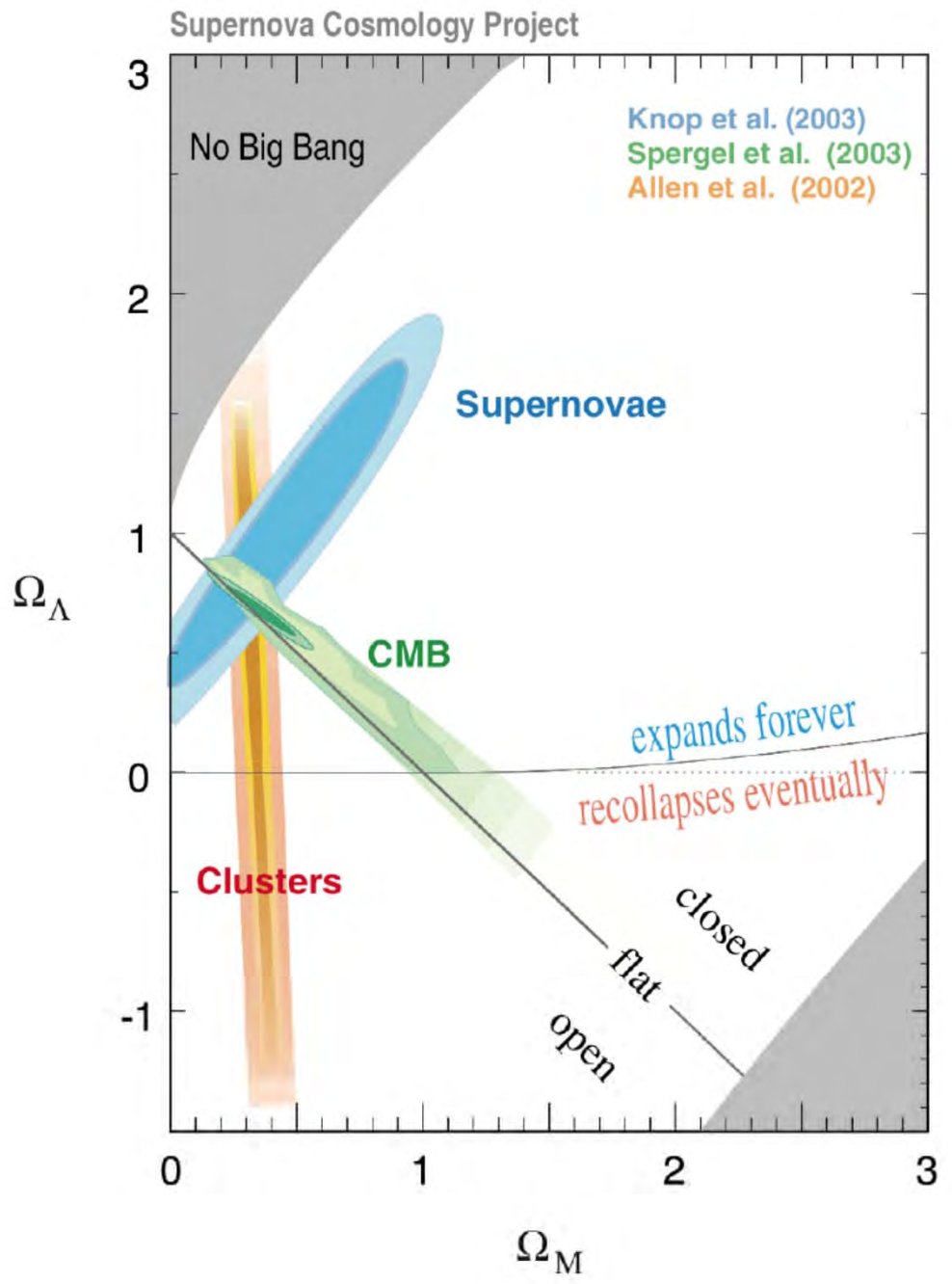
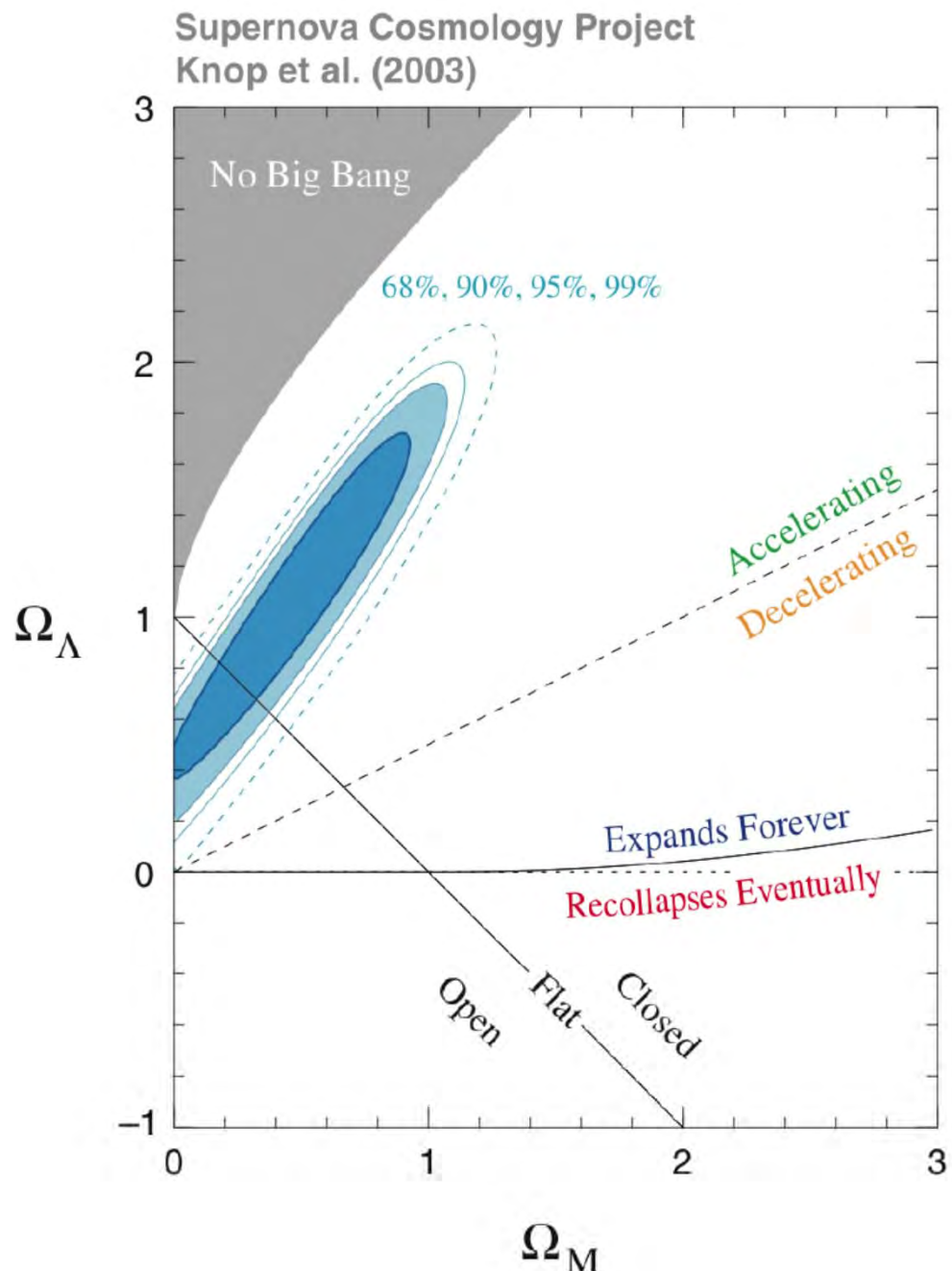


Hubble diagram for SNe of type Ia up to $z = 0.86$. The observed B-band magnitudes of the SNe at maximum light are compared with the predictions for three cosmological models, as indicated. The lower panel shows the difference relative to an empty universe.



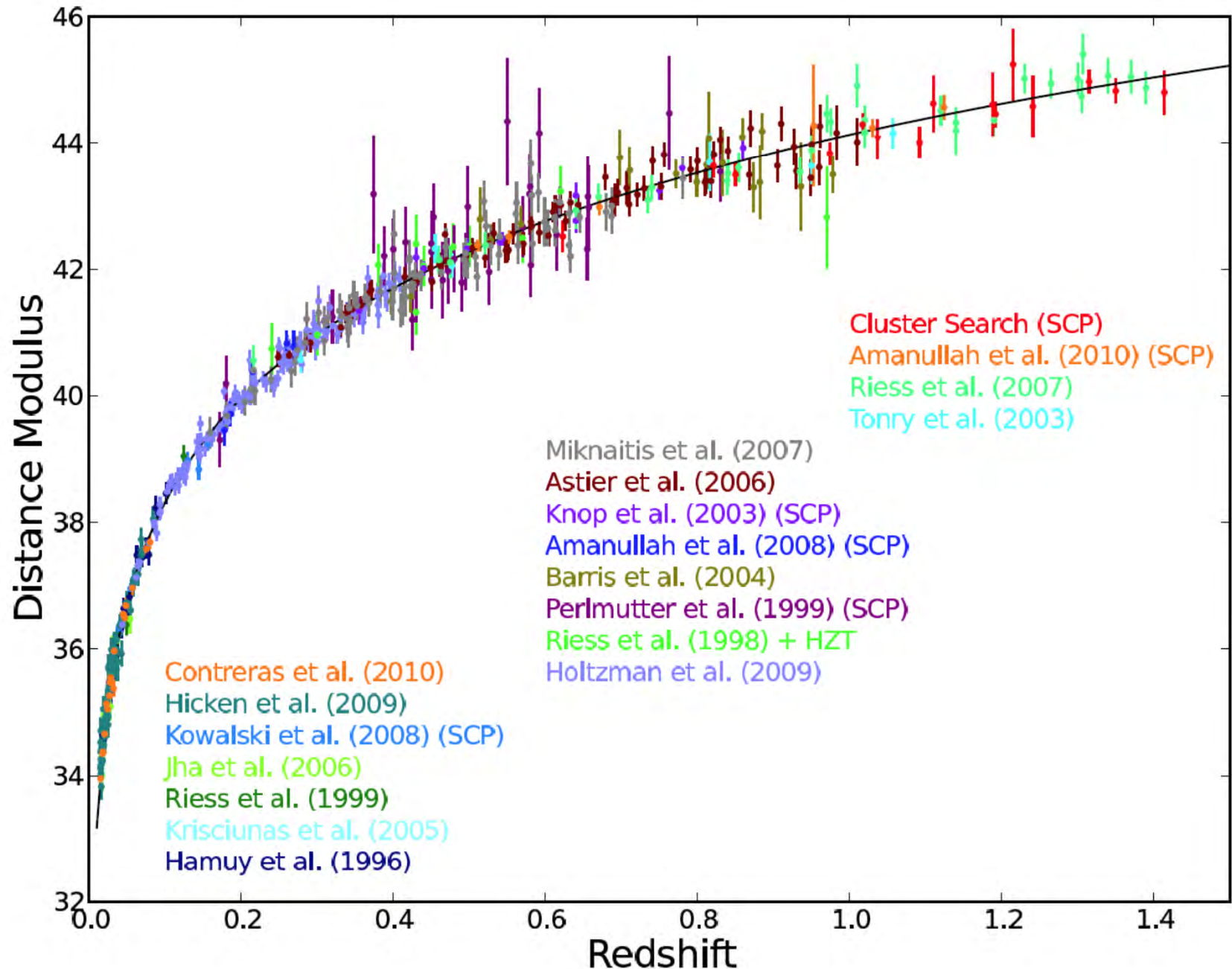
Johns Hopkins University; University Of California At Berkeley; Australian National University

From left, Adam Riess, Saul Perlmutter and Brian Schmidt shared the Nobel Prize in physics awarded Tuesday.

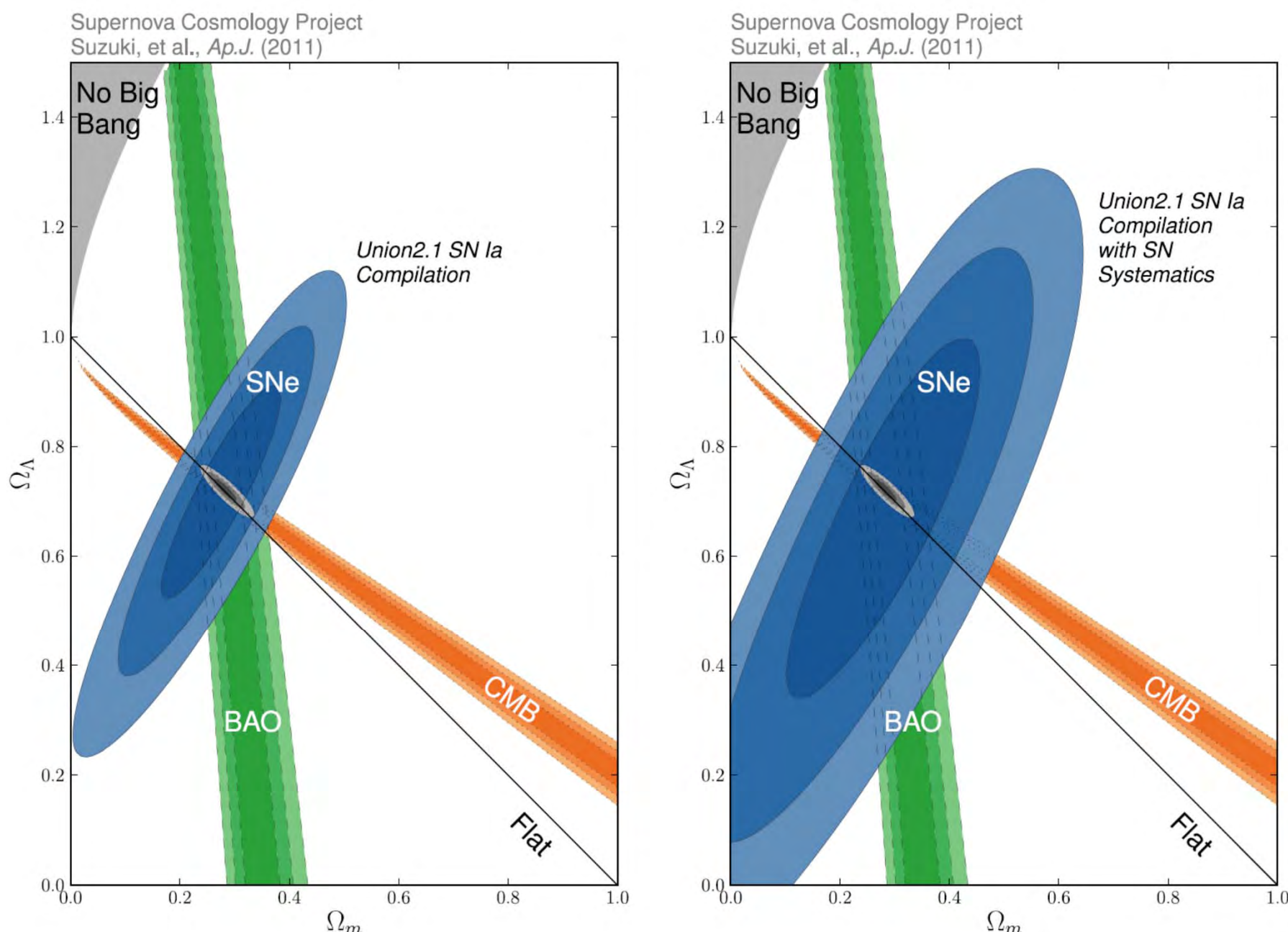


Left: Likelihood contours in the $\Omega_{m,0}$ - $\Omega_{\Lambda,0}$ plane.

Right: Joint likelihood contours in the $\Omega_{m,0}$ - $\Omega_{\Lambda,0}$ plane from type Ia supernovae, the angular power spectrum of the cosmic background radiation, and massive galaxy clusters.

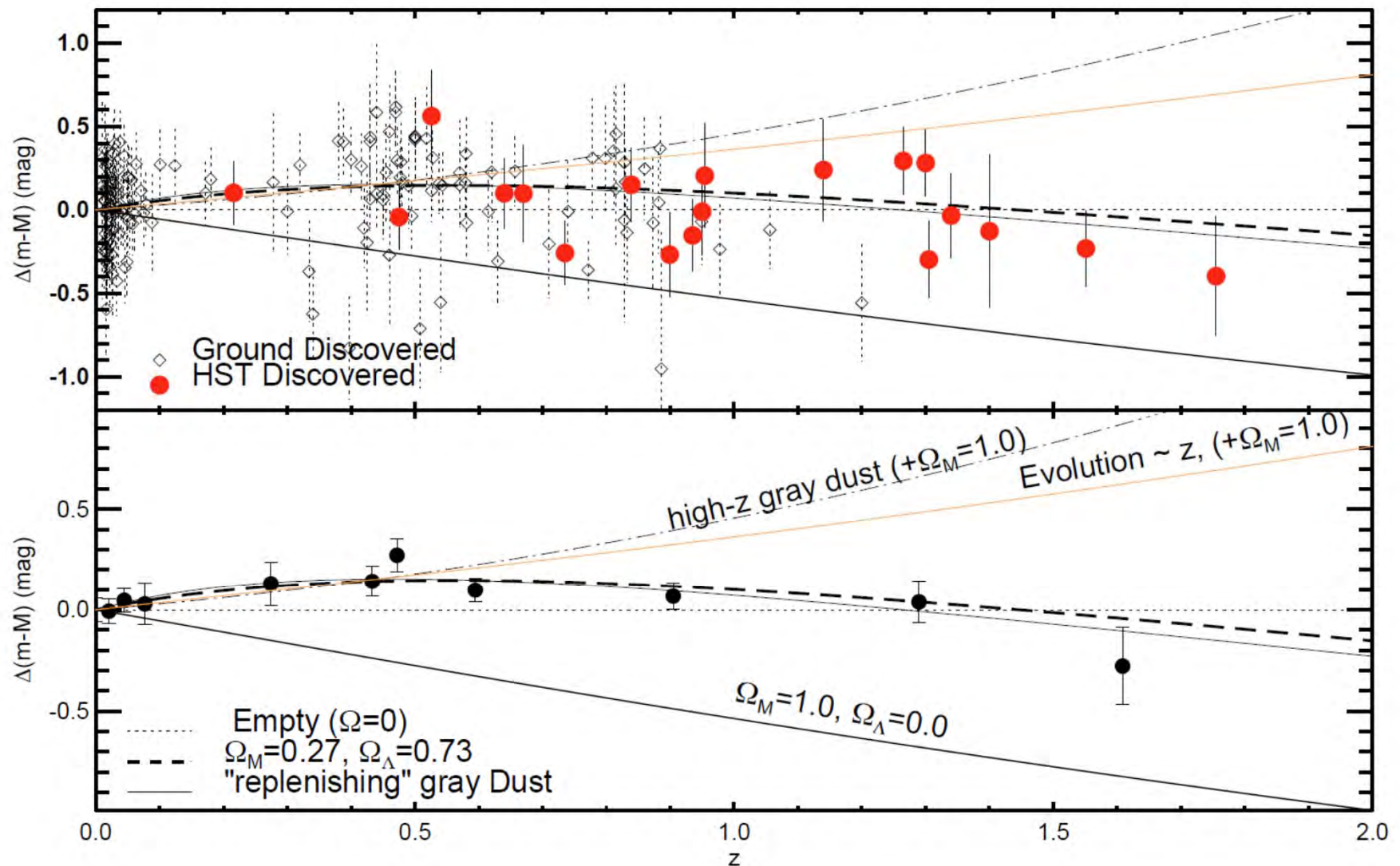


Suzuki+ 2012



Left: Joint likelihood contours (68%, 95%, and 99.7% confidence limits) in the $\Omega_{m,0}$ - $\Omega_{\Lambda,0}$ plane for a recent compilation of SN Ia data, together with the WMAP measure of the temperature anisotropies of the CMB, and the large-scale distribution of galaxies in the nearby Universe (BAO).

Right: Same as left, but including systematic uncertainties in the SN Ia luminosity.



SNIa residual Hubble diagram comparing cosmological models and models with astrophysical dimming (reproduced from Riess et al. 2004, ApJ, 607, 665). Data and models are shown relative to an empty universe model ($\Omega_{m,0} = \Omega_{\Lambda,0} = 0$).

[astro-ph #7] Current velocity data on dwarf galaxy NGC1052-DF2 do not constrain it to lack dark matter

0 votes @ETH-
Extragalactic

(12 votes from 11 institutions)

Please [log in](#) or [create an account](#) to vote!

[Nicolas F. Martin](#)^{1†}, [Michelle L. M. Collins](#), [Nicolas Longeard](#), [Erik Tollerud](#)

¹MPIA, Heidelberg

†Listed affiliation is based on previous publications and was not specified in this preprint.

ArXiv #: [1804.04136](#) ([PDF](#), [PS](#), [ADS](#), [Papers](#), [Other](#))

Comments: 5 pages, 5 figures. Submitted to ApJL

Originally posted [04/12/2018](#)



GA

It was recently proposed that the globular cluster system of the very low surface-brightness galaxy NGC1052-DF2 is dynamically very cold, leading to the conclusion that this dwarf galaxy has little or no dark matter. Here, we show that a robust statistical measure of the velocity dispersion of the tracer globular clusters implies a mundane velocity dispersion and a poorly constrained mass-to-light ratio. Models that include the possibility that some of the tracers are field contaminants do not yield a more constraining inference. We derive only a weak constraint on the mass-to-light ratio of the system within the half-light radius or within the radius of the furthest tracer ($M/L_V < 8.1$ at the 90-percent confidence level). Typical mass-to-light ratios measured for dwarf galaxies of the same stellar mass as NGC1052-DF2 are well within this limit. With this study, we emphasize the need to properly account for measurement uncertainties and to stay as close as possible to the data when determining dynamical masses from very small data sets of tracers.

[astro-ph #10] Measured and found wanting: reconciling mass-estimates of ultra-diffuse galaxies

0 votes @ETH-
Extragalactic

(12 votes from 10 institutions)

Please [log in](#) or [create an account](#) to vote!

[Chervin F. P. Laporte](#), [Adriano Agnello](#), [Julio F. Navarro](#)^{1†}

¹U.Victoria

†Listed affiliation is based on previous publications and was not specified in this preprint.

ArXiv #: [1804.04139](#) ([PDF](#), [PS](#), [ADS](#), [Papers](#), [Other](#))

Comments: Submitted to MNRAS, 5 pages, 4 figures, 1 table ready to be used for future observational considerations (e.g. use of 11 GCs vs 10)

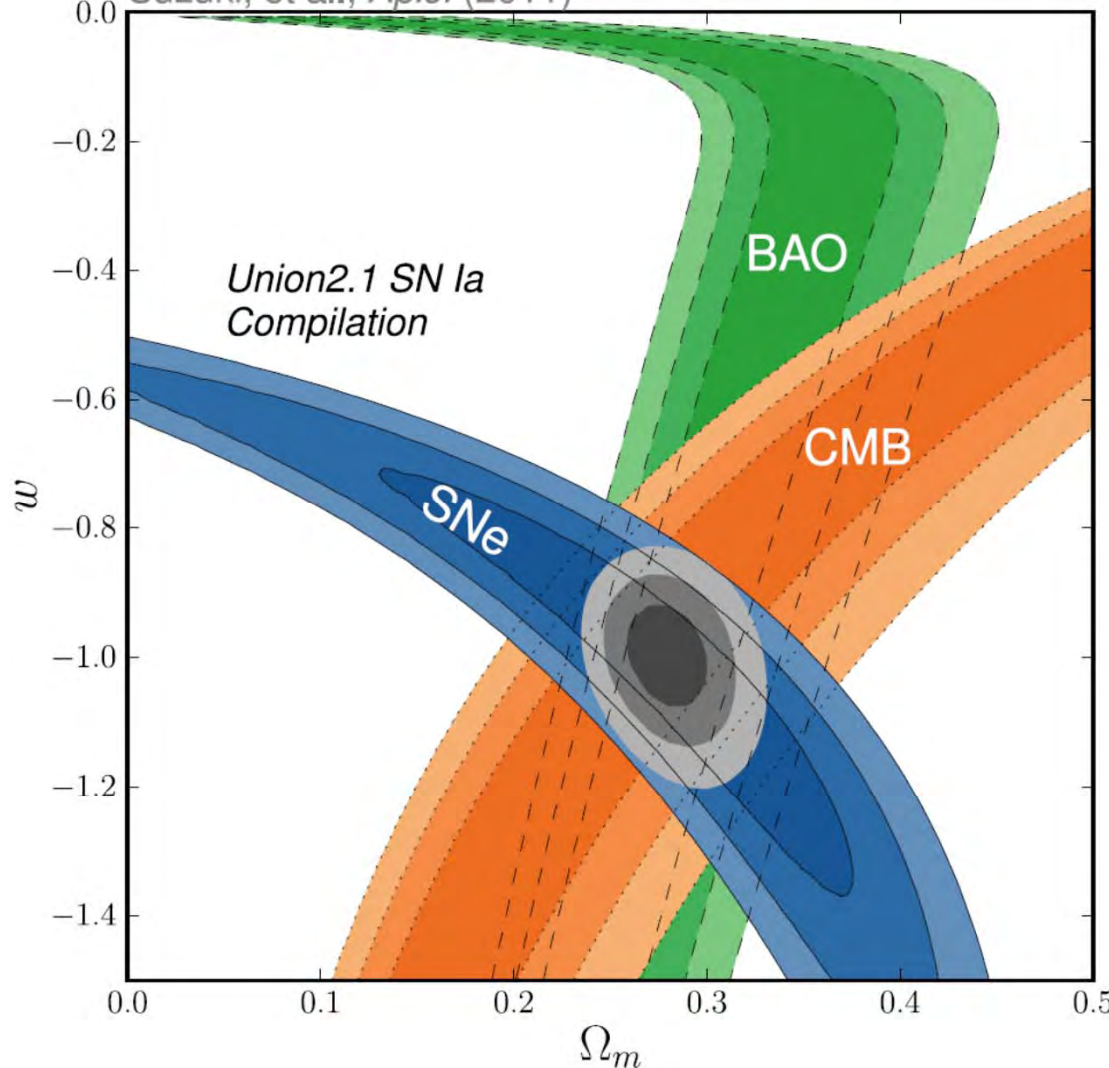
Originally posted [04/12/2018](#)



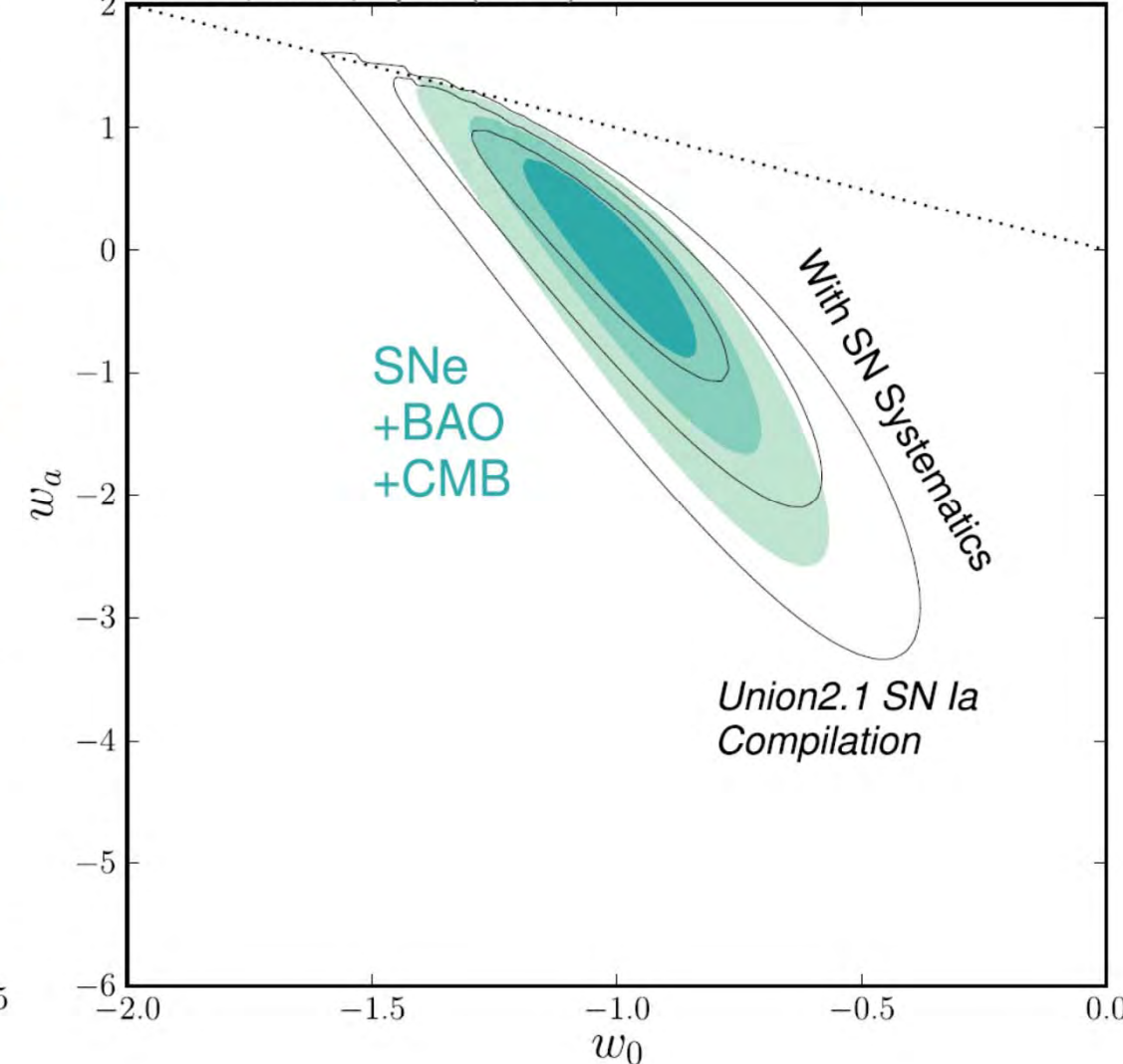
GA

The virial masses of ultra-diffuse galaxies (UDGs) have been estimated using the kinematics and abundance of their globular cluster populations, leading to disparate results. Some studies conclude that UDGs reside in massive dark matter halos while others, controversially, argue for the existence of UDGs with no dark matter at all. Here we show that these results arise because the uncertainties of these mass estimates have been substantially underestimated. Indeed, applying the same procedure to the well-studied Fornax dwarf spheroidal would conclude that it has an "overmassive" dark halo or, alternatively, that it lacks dark matter. We corroborate our argument with self-consistent mocks of tracers in cosmological halos, showing that masses from samples with $5 < N < 10$ tracers (assuming no measurement errors) are uncertain by at least an order of magnitude. Finally, we estimate masses of UDGs with HST imaging in Coma and show that their recent mass measurements (with adequate uncertainties) are in agreement with that of other dwarfs, such as Fornax.. We also provide bias and scatter factors for a range of sample sizes and measurement errors, of wider applicability.

Supernova Cosmology Project
Suzuki, et al., Ap.J. (2011)



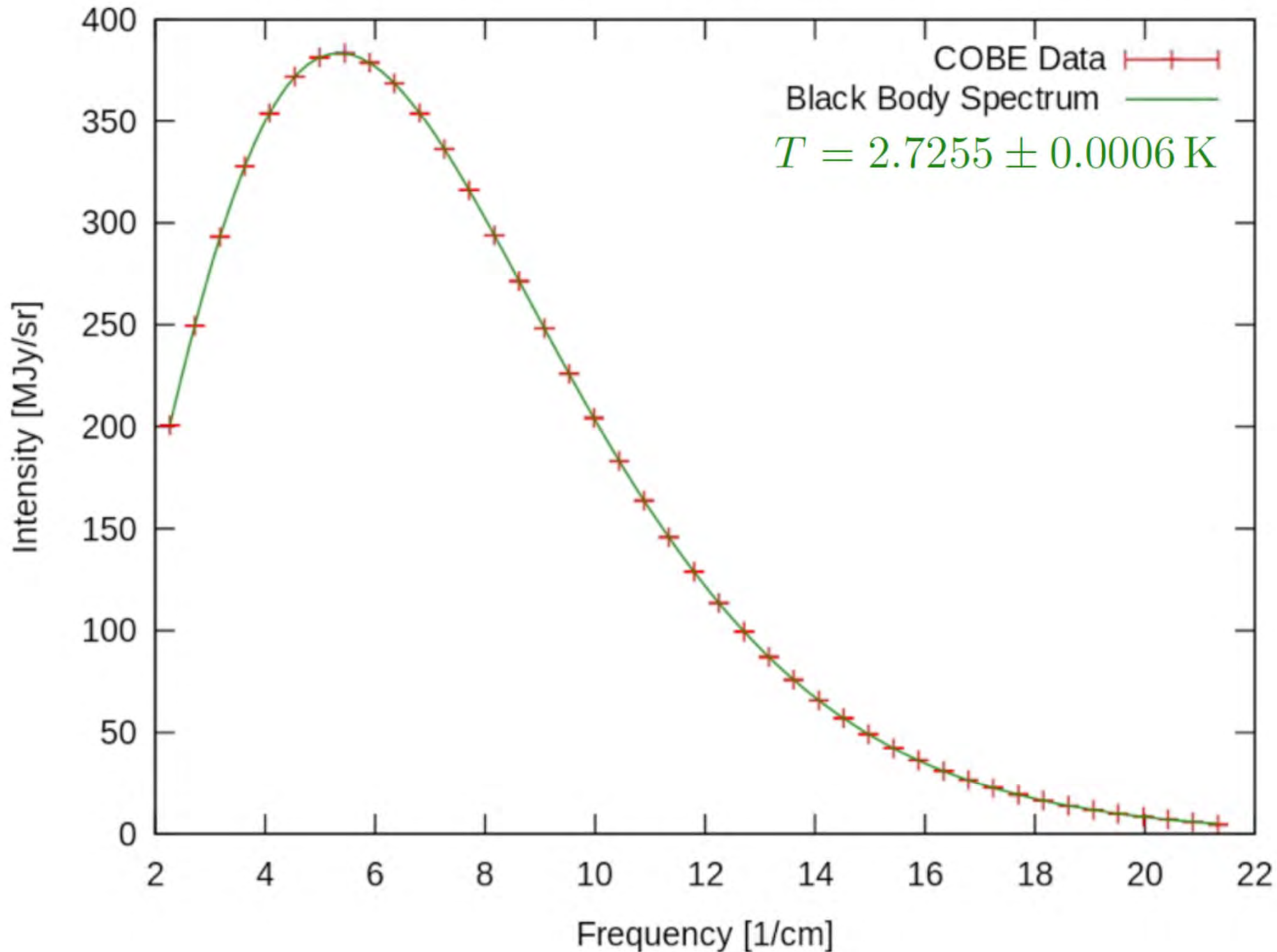
Supernova Cosmology Project
Suzuki, et al., Ap.J. (2011)

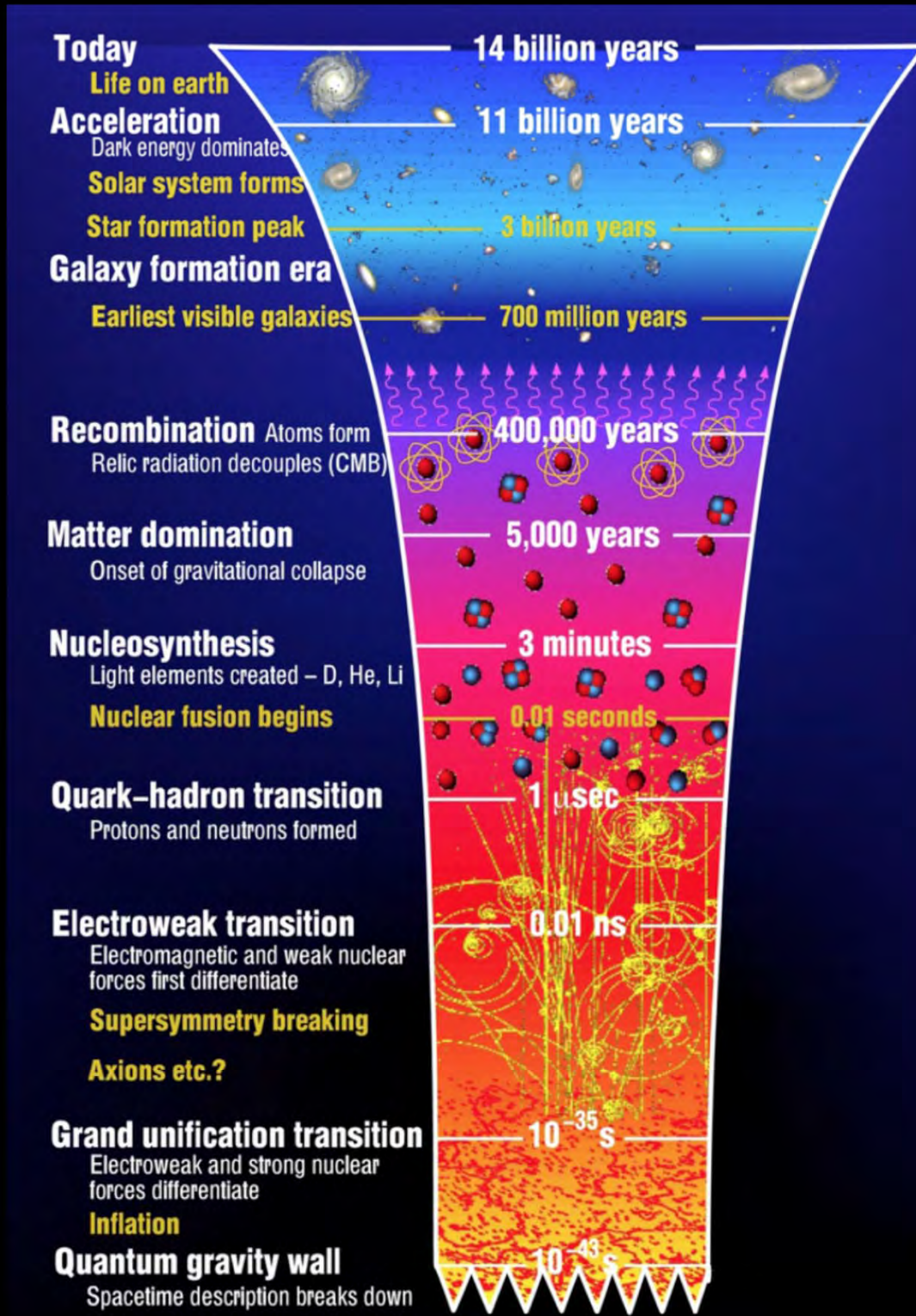


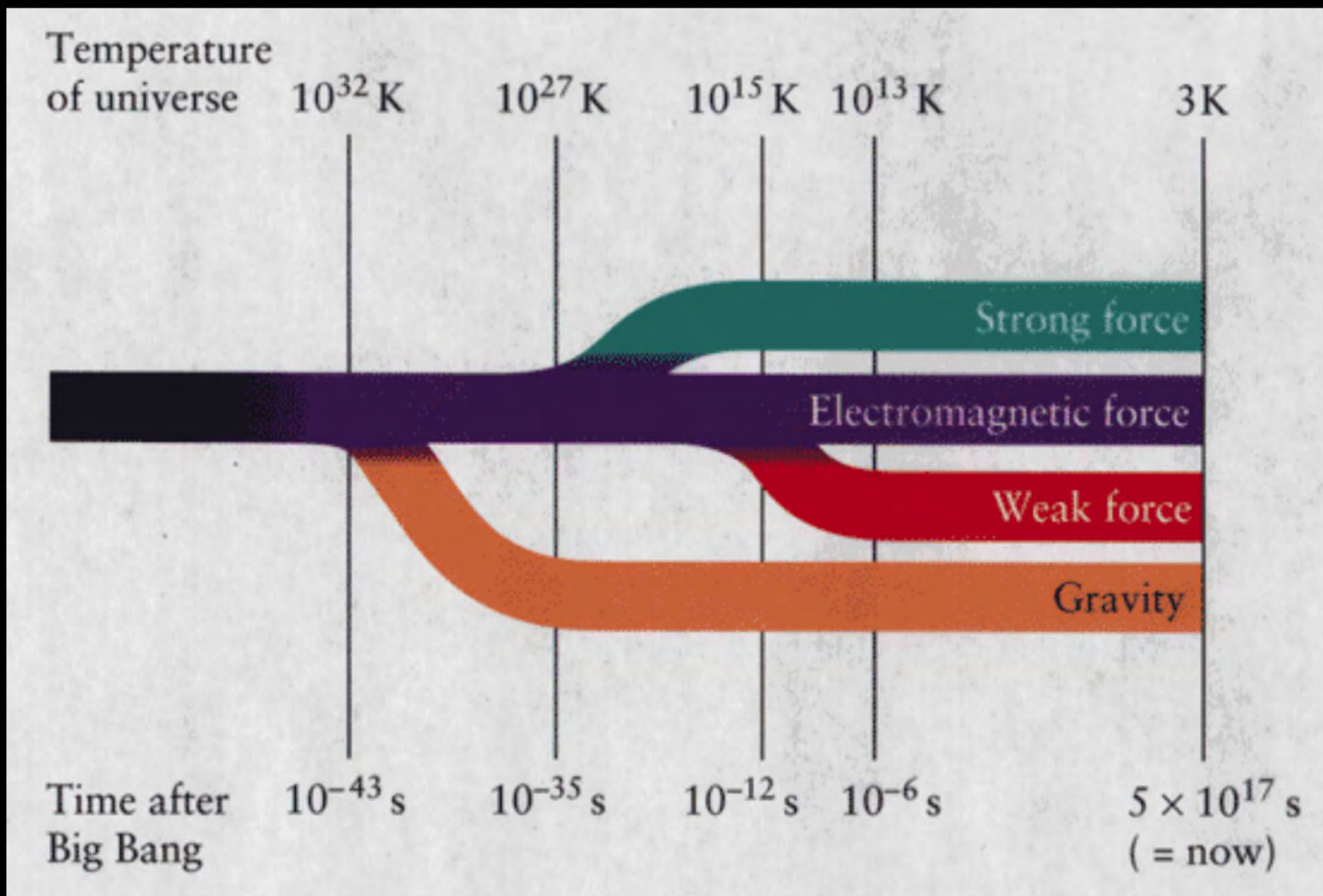
Left: Joint likelihood contours (68%, 95%, and 99.7% confidence limits) for $\Omega_{m,0}$ and the parameter w in the equation of state of dark energy.

Right: Joint confidence contours between the parameters w_0 and w_a .

Cosmic Microwave Background Spectrum from COBE





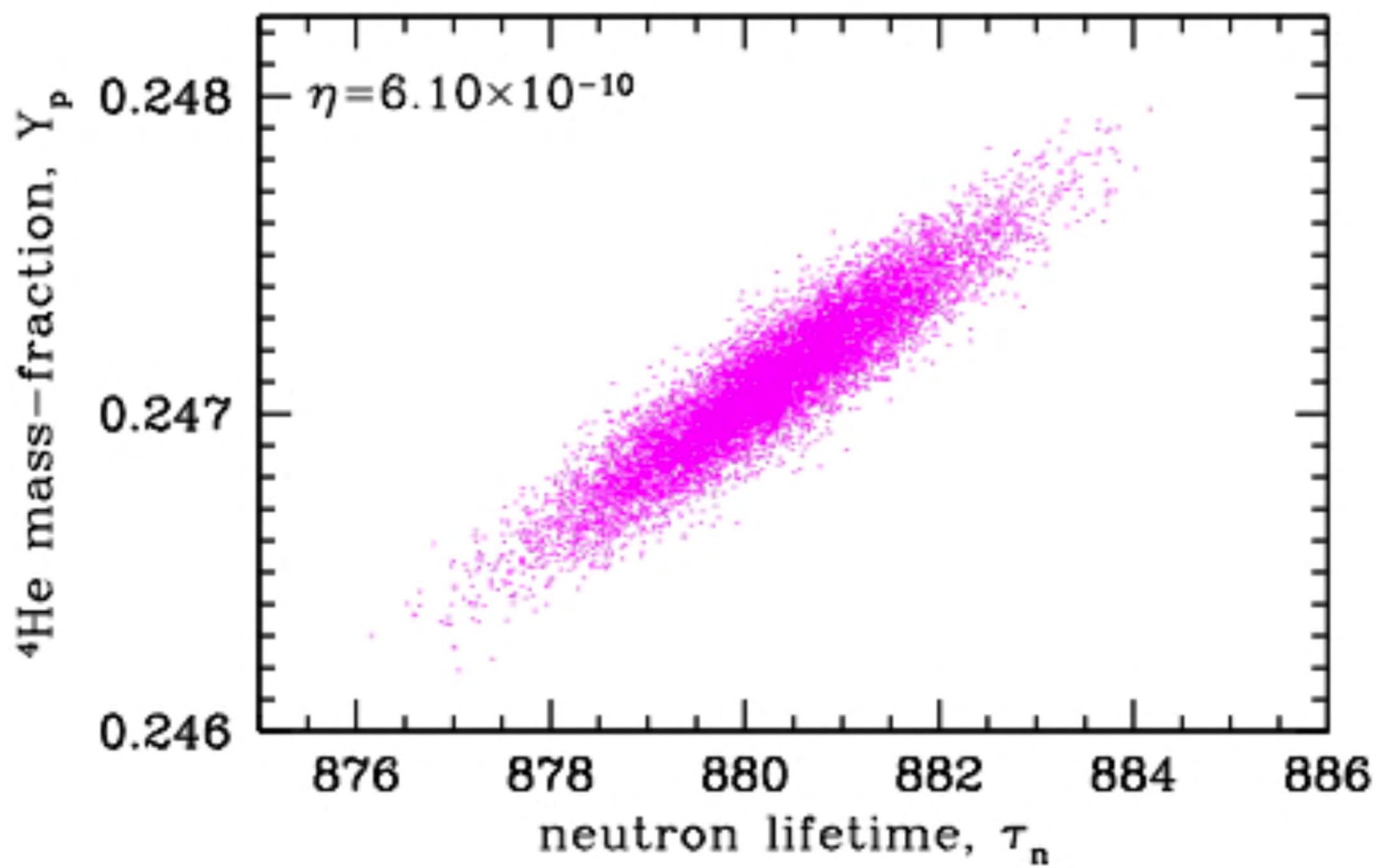


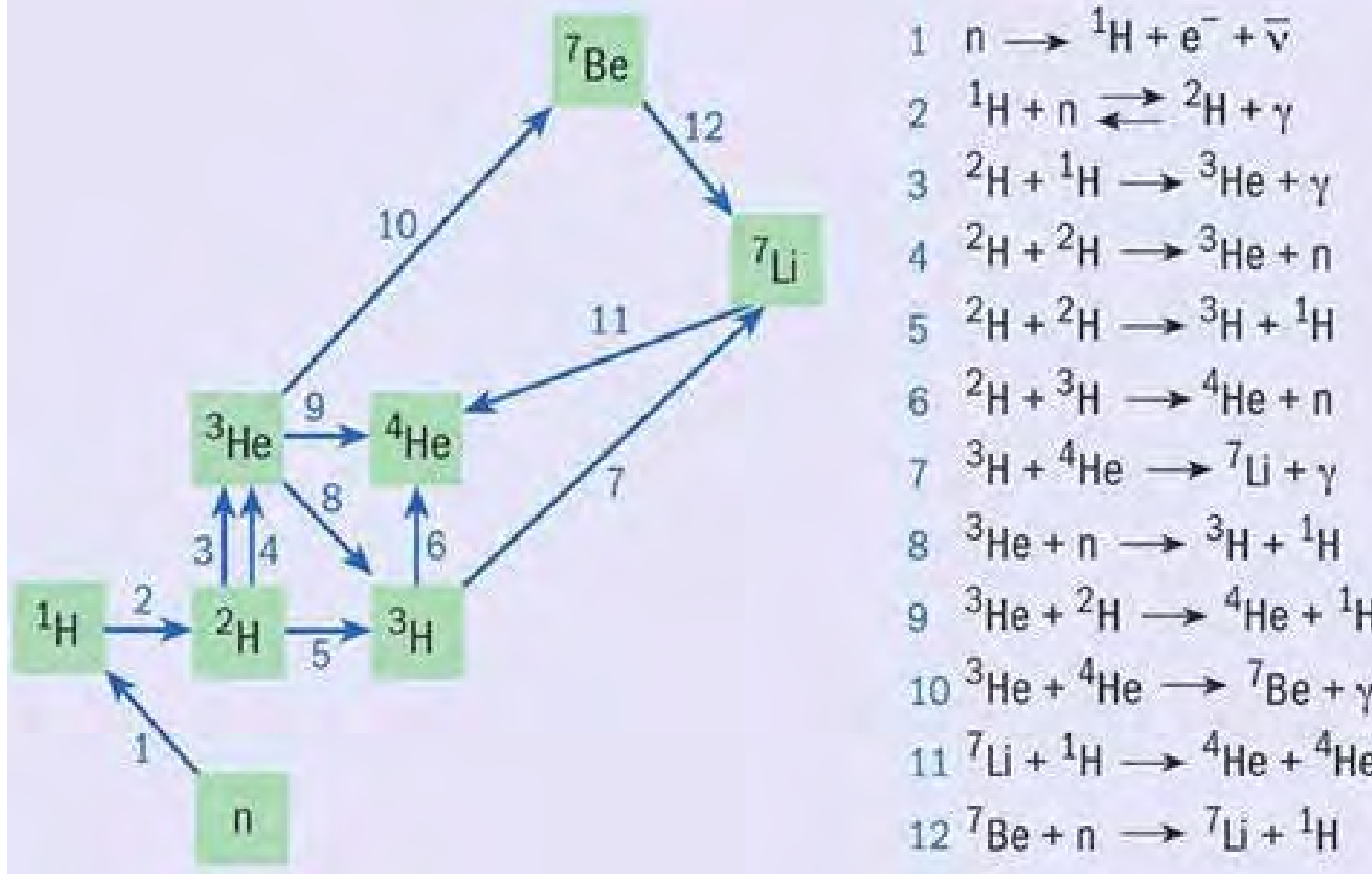
The four fundamental interactions became distinct with the falling temperature of the Universe.

Three Generations of Matter (Fermions)

	I	II	III	
mass →	2.4 MeV/c ²	1.27 GeV/c ²	171.2 GeV/c ²	0
charge →	2/3	2/3	2/3	0
spin →	1/2	1/2	1/2	1
name →	u up	c charm	t top	γ photon
Quarks				
	4.8 MeV/c ² -1/3 1/2 d down	104 MeV/c ² -1/3 1/2 s strange	4.2 GeV/c ² -1/3 1/2 b bottom	0 0 1 g gluon
Leptons				
	<2.2 eV/c ² 0 1/2 ν _e electron neutrino	<0.17 MeV/c ² 0 1/2 ν _μ muon neutrino	<15.5 MeV/c ² 0 1/2 ν _τ tau neutrino	91.2 GeV/c ² 0 1 Z ⁰ Z boson
	0.511 MeV/c ² -1 1/2 e electron	105.7 MeV/c ² -1 1/2 μ muon	1.777 GeV/c ² -1 1/2 τ tau	80.4 GeV/c ² ±1 1 W [±] W boson
Gauge Bosons				

The Standard Model of elementary particles with the three generations of matter and gauge bosons in the fourth column.

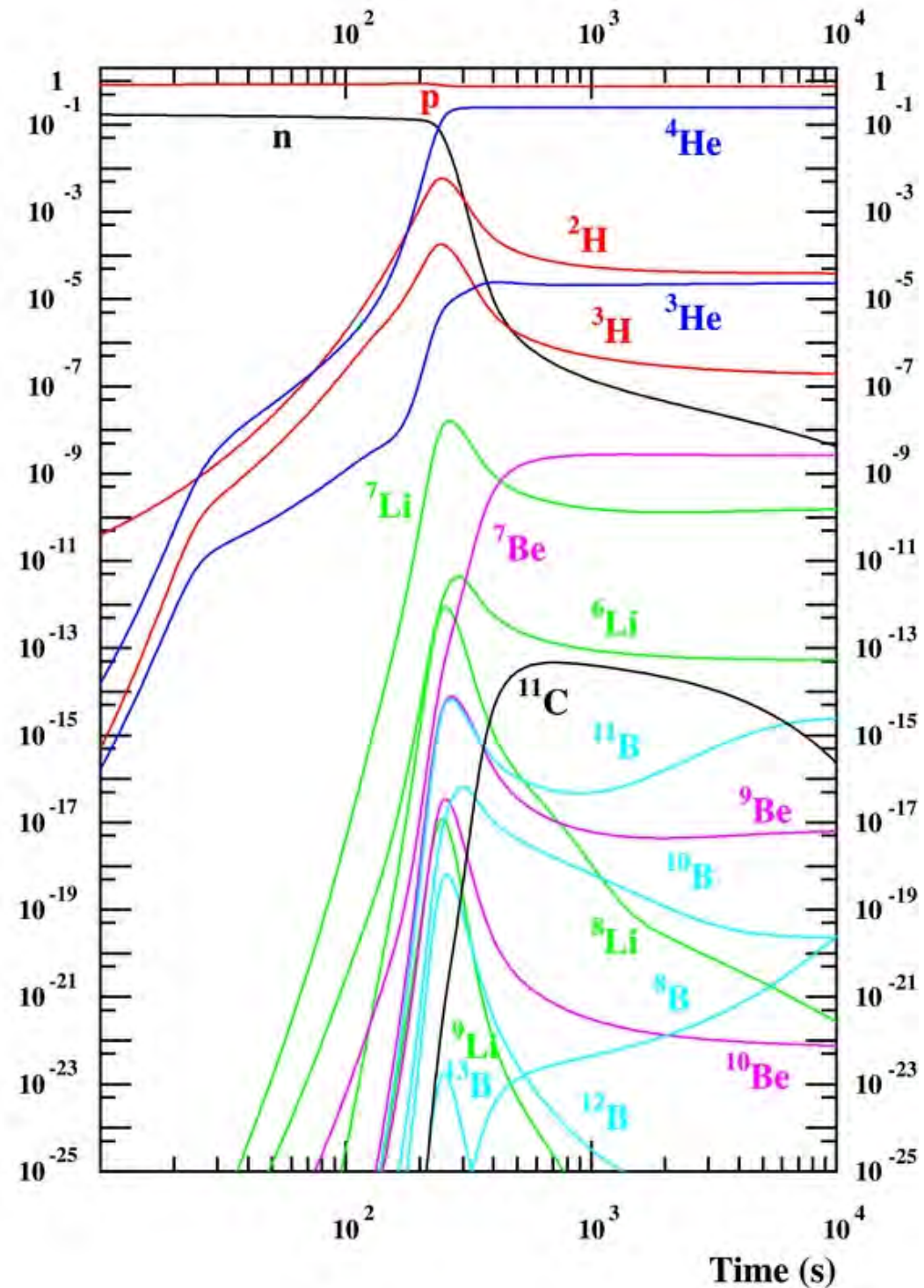




Nucleosynthesis - In the Big Bang theory of modern cosmology, there was a period in early universe that was favorable for the thermonuclear reactions. Light elements up to beryllium were generated about 3 minutes after Big Bang. The process lasted for about 15 minutes starting at temperature of 10^{10}K (at the high end of the thermonuclear reactions in the Figure. Initiation of the process depended on the baryon to photon ratio, too many photons would drive the $p + n \rightarrow D + \gamma$ reaction backward leaving no deuteron to proceed. Nucleosynthesis ended when temperature fell off with the cosmic expansion preventing elements heavier than beryllium to form. The calculation of mass abundances follows simple thermodynamic arguments and is insensitive to what happened before the process. Its agreement with observation presents a fairly reliable verification for the theory of Big Bang.

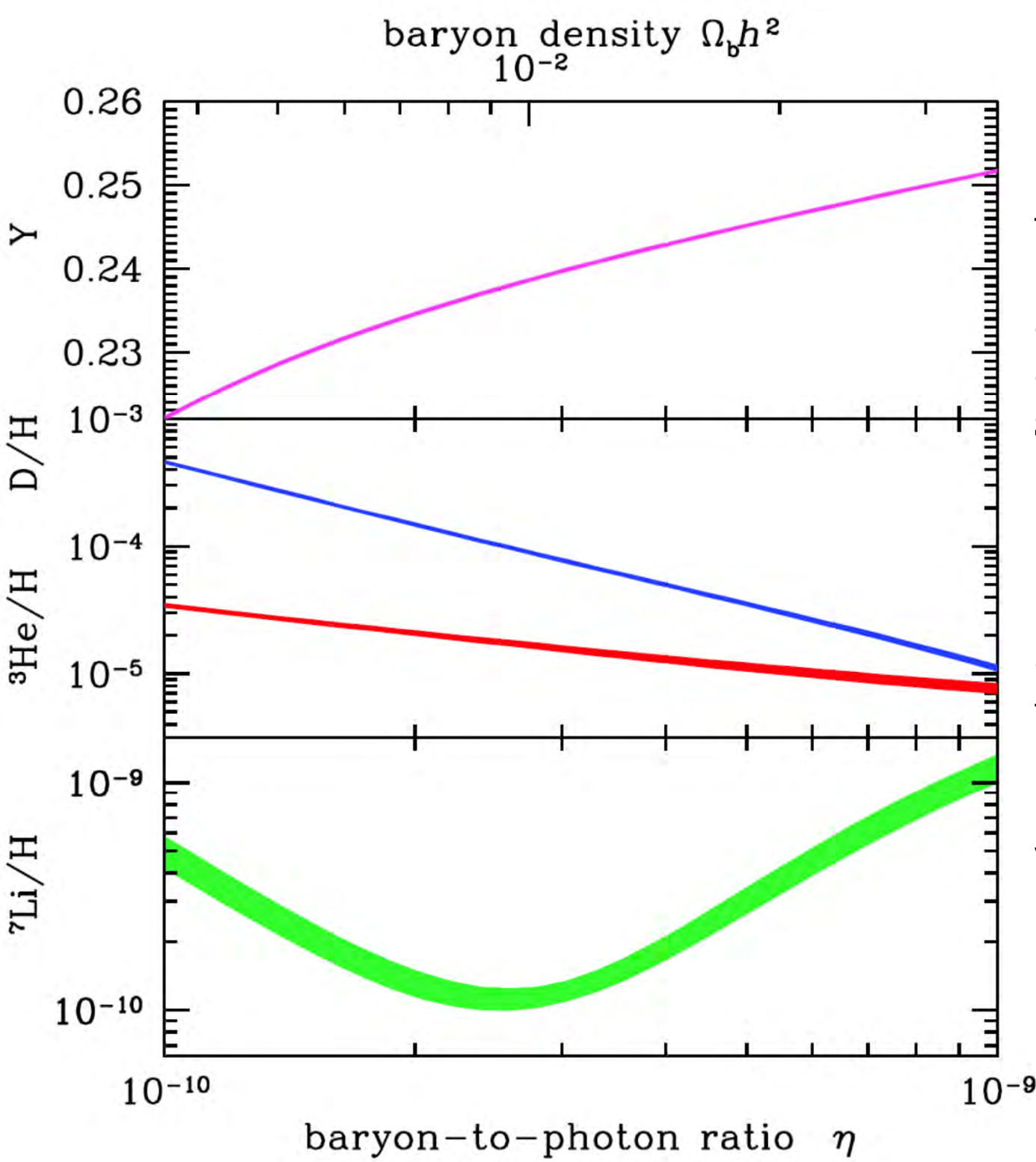
$$\Omega_B h^2 = \text{WMAP}$$

Mass fraction



Standard big bang nucleosynthesis production of H, He, Li, Be, and B isotopes as a function of time, for the baryon density taken from WMAP7.

Coc et al. 2011, The Astrophysical Journal, Volume 744, Number 2

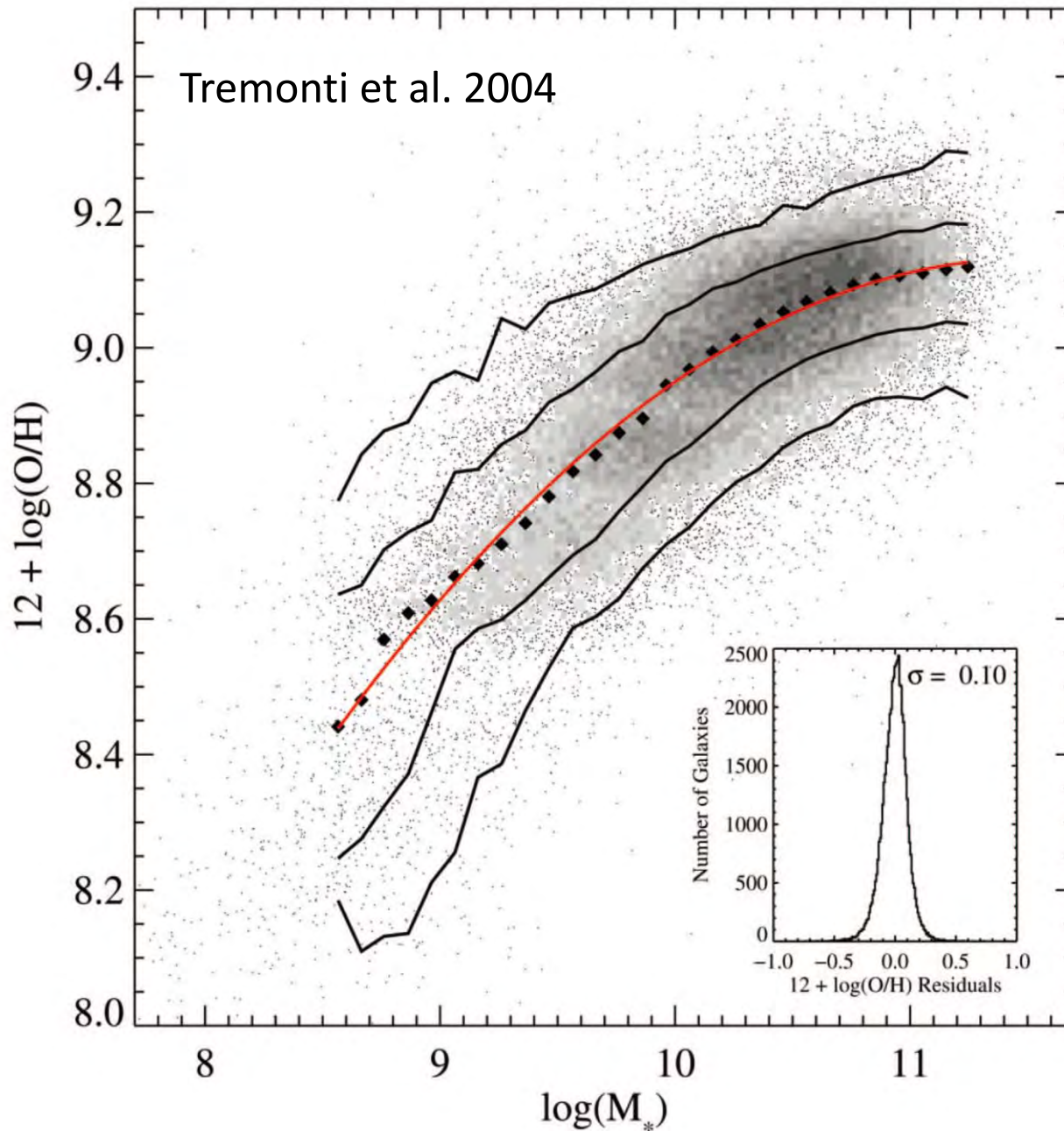


The abundances of light elements relative to H predicted by BBN calculations are shown as functions of $\eta = n_b/n_\gamma$ (bottom x-axis) and $\Omega_{b,0}h^2$ (top x-axis).

It is customary to express the primordial abundance of ^{4}He by mass (Y_p), and those of the other elements by number. The widths of the curves reflect the uncertainties in the predictions, propagated from uncertainties in the experimental values of the relevant nuclear reaction rates.

(Figure reproduced from Cyburt et al. 2015).

Mass- metallicity relation (MZR)



Mass- metallicity relation (MZR) in SDSS

Chemical Evolution

Faisst et al. 2016

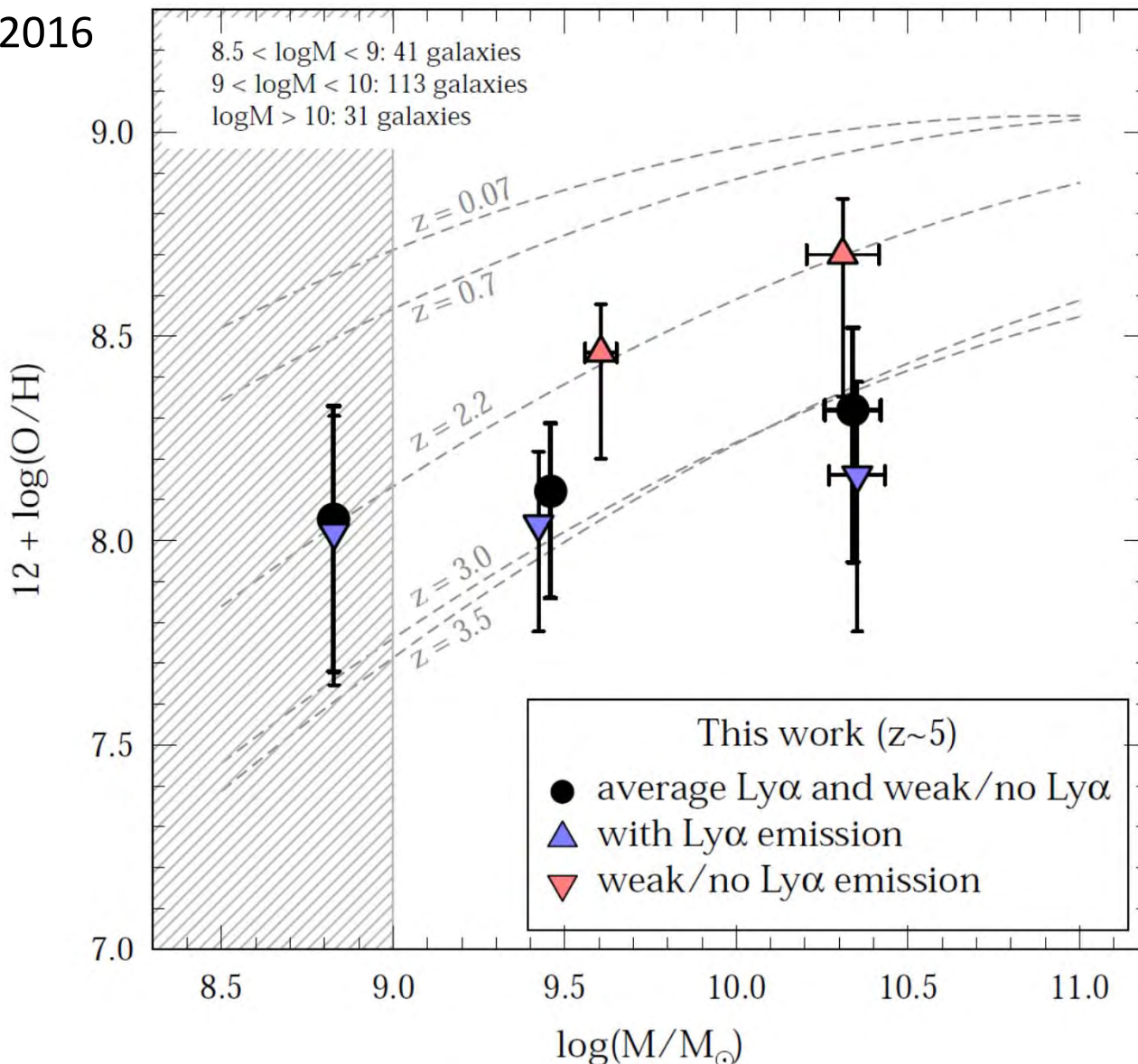


FIG. 9.— Gas phase metallicity as a function of stellar mass for galaxies at different redshifts. The large symbols show our results at $z \sim 5$ split in galaxies with Ly α emission (blue), weak/no Ly α emission (red), and the average of both (black). The metallicities are obtained by a simultaneous fit to all the absorption complexes (see text). The dashed lines show different measurements from the literature at $z = 0.07$ (Kewley & Ellison 2008), $z = 0.7, 2.2, 3.5$ (Maiolino et al. 2008), and $z = 3.0$ (Mannucci et al. 2009). Ly α emitting galaxies at $z \sim 5$ have a metal content similar to $z \sim 3 - 3.5$ galaxies and only a weak dependence on stellar mass. Galaxies devoid of Ly α emission show a higher metallicity at fixed mass comparable to $z \sim 2$ galaxies together with a stronger dependence on stellar mass. This is indicative of them being more evolved systems and highlights the diversity amongst $z \sim 5$ galaxies.

Fundamental Metallicity Relation (FMR)

Mannucci et al. 2010

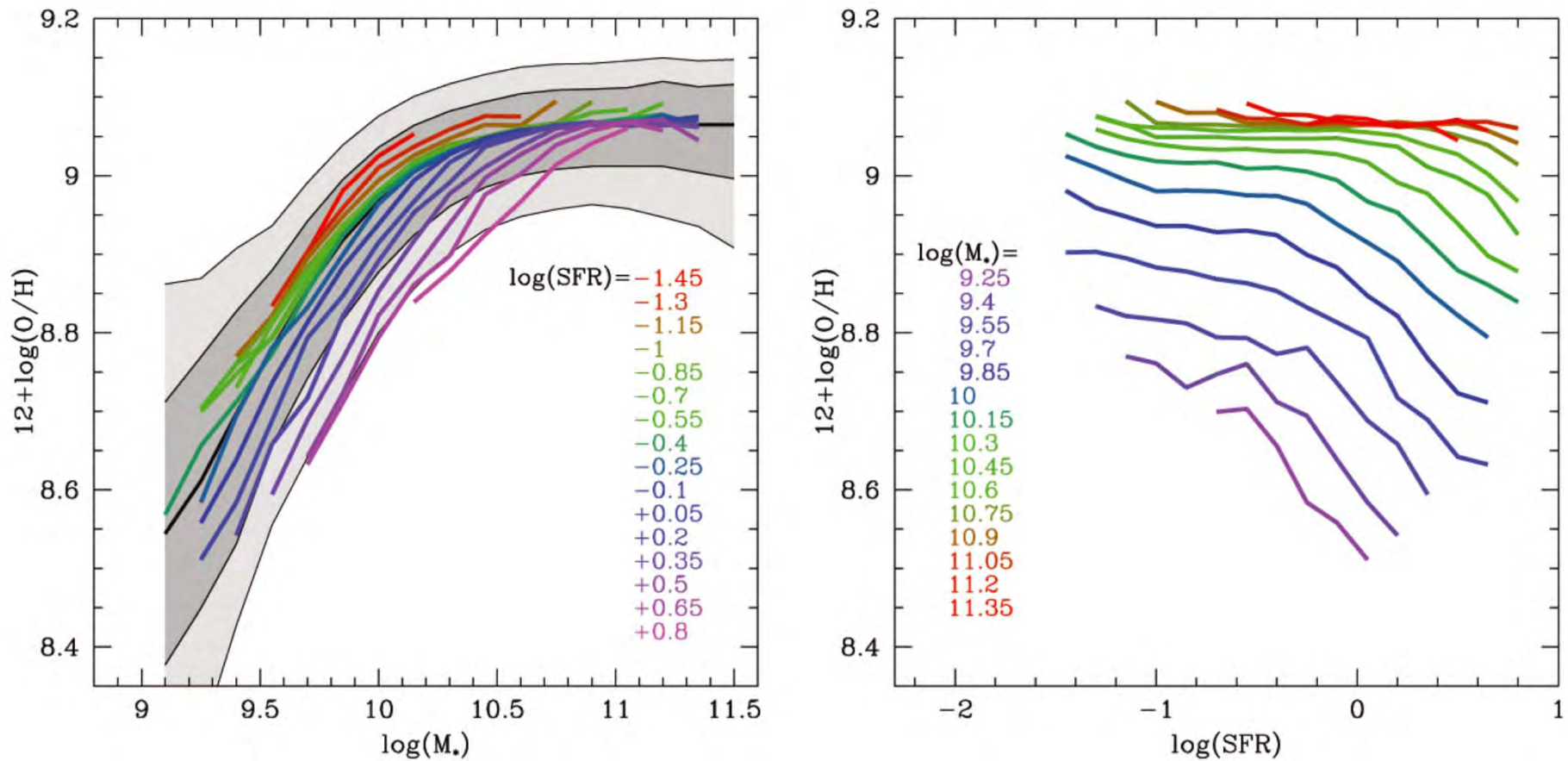
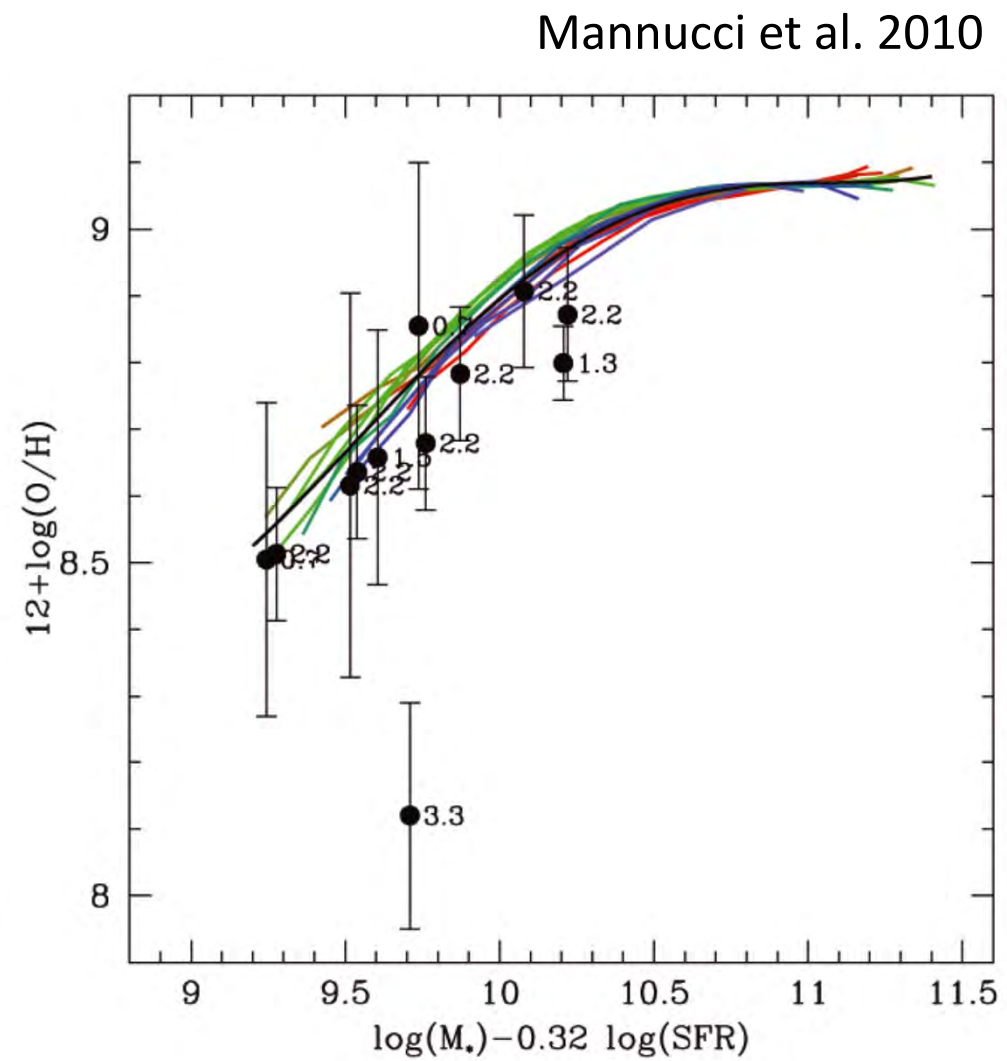
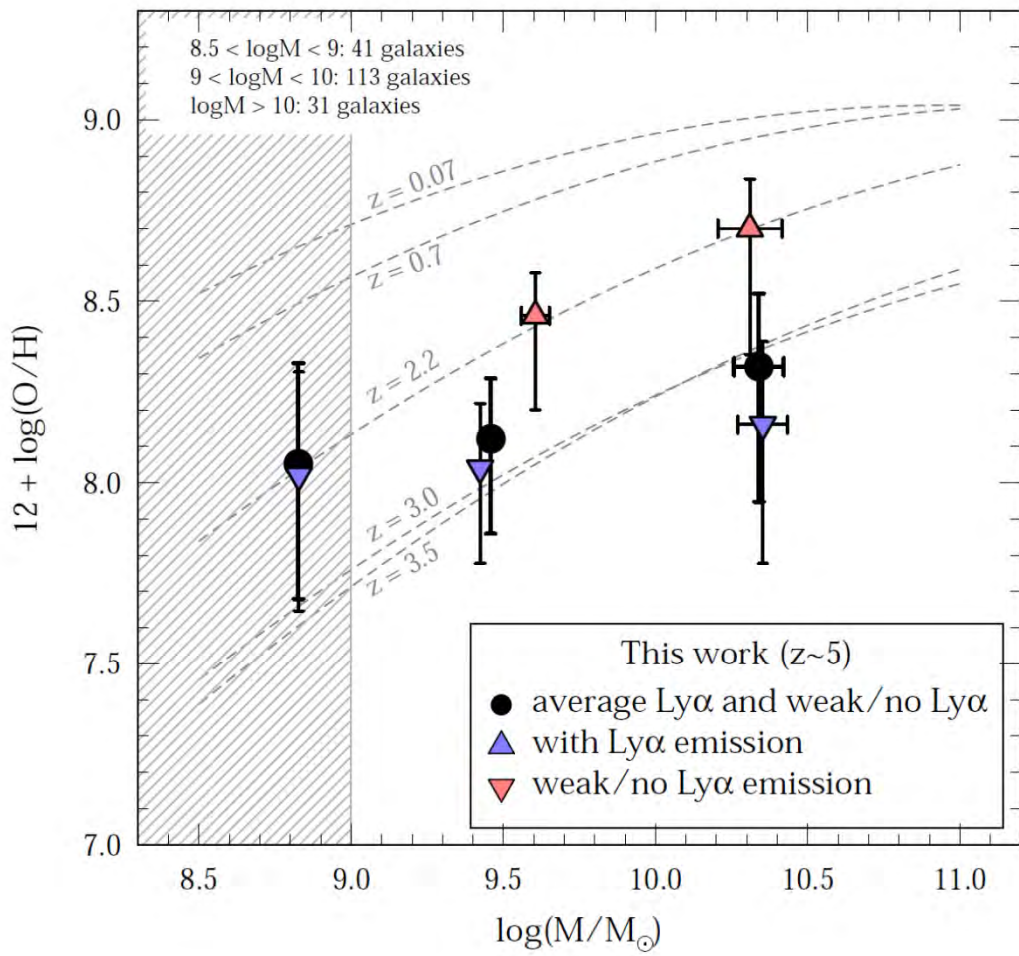
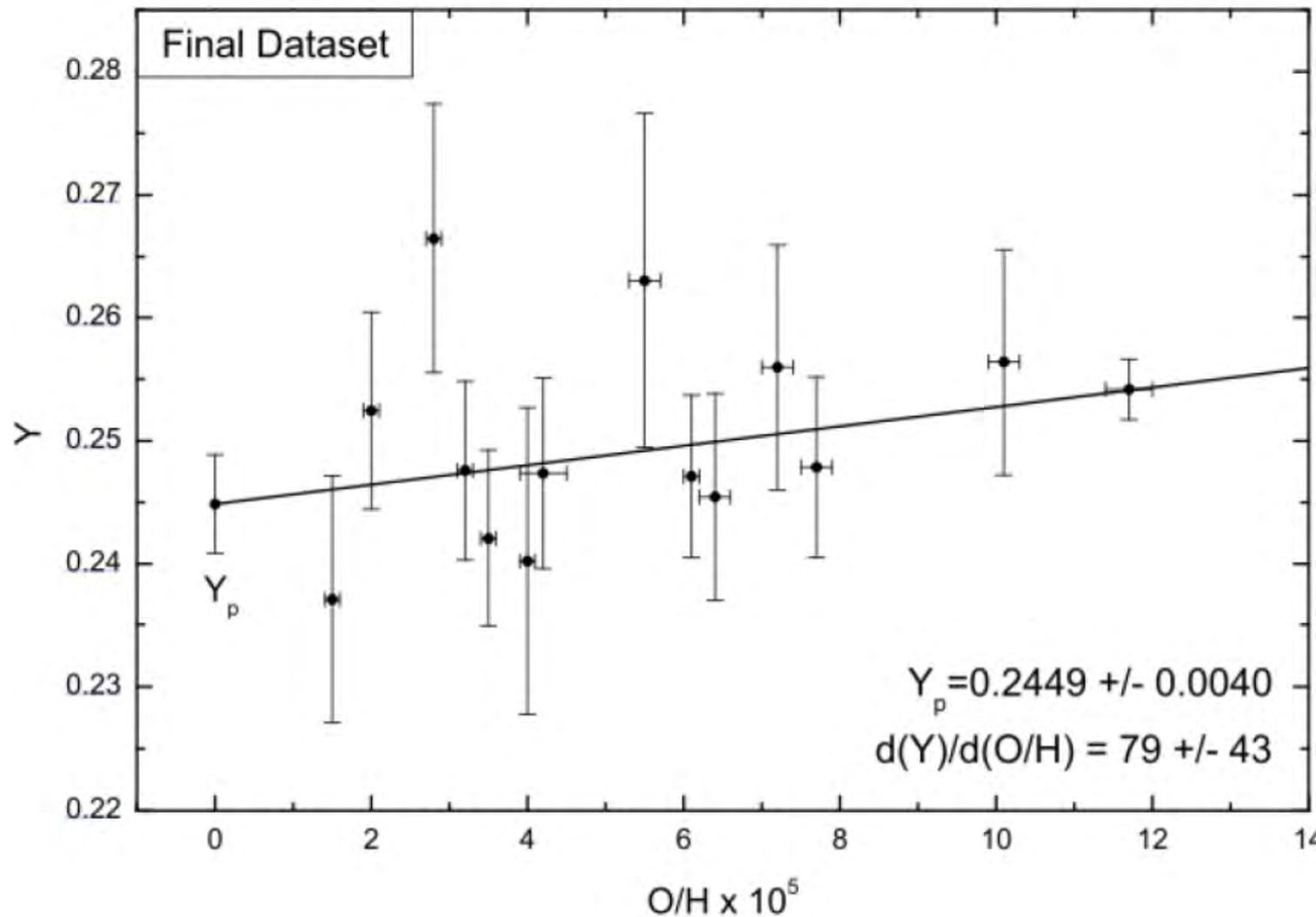


Figure 1. Left-hand panel: the mass–metallicity relation of local SDSS galaxies. The grey-shaded areas contain 64 and 90 per cent of all SDSS galaxies, with the thick central line showing the median relation. The coloured lines show the median metallicities, as a function of M_* , of SDSS galaxies with different values of SFR. Right-hand panel: median metallicity as a function of SFR for galaxies of different M_* . At all M_* with $\log(M_*) < 10.7$, metallicity decreases with increasing SFR at constant mass.

Fundamental Metallicity Relation (FMR)



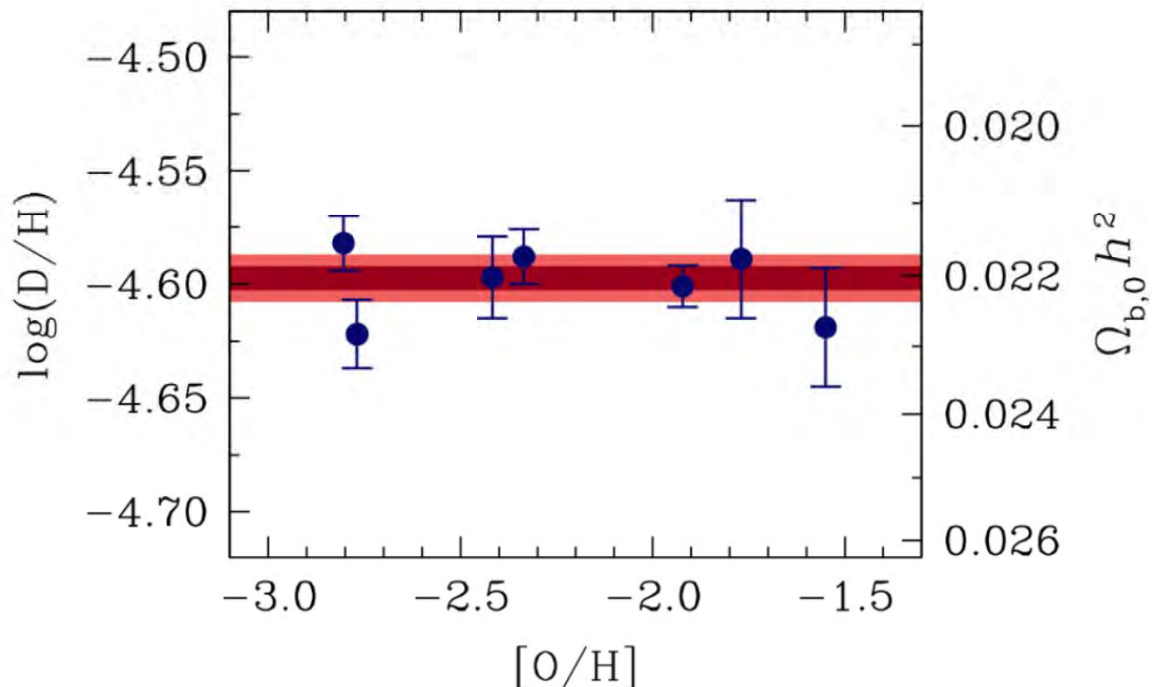
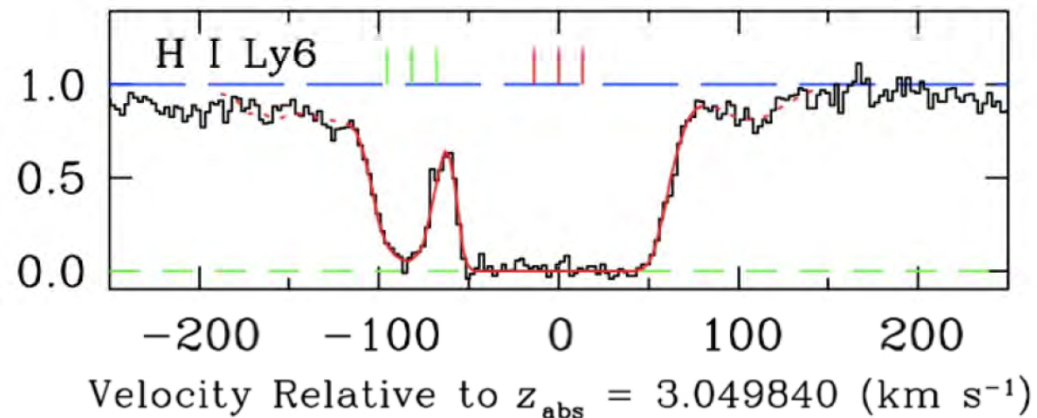


The abundance of ${}^4\text{He}$ by mass in the lowest metallicity dwarf galaxies known, plotted as a function of the O abundance. For comparison, in the Sun, in the Orion nebula, and generally in the Milky Way galaxy $(\text{O}/\text{H})_0 \sim 5 \times 10^{-4}$; thus, the galaxies with the lowest O abundance in this figure have $(\text{O}/\text{H}) \sim 0.04 (\text{O}/\text{H})_0$. The authors of this study (Aver et al. 2015) and a shallow gradient in the regression of Y with $d(\text{O}/\text{H})$: $d(Y) = d(\text{O}/\text{H}) = 79 \pm 43$ and deduce $Y_p = 0.245 \pm 0.004$. However, a zero gradient would be an almost equally good fit to the data. This illustrates one of the uncertainties in the determination of the primordial value of Y .

Precision Measures of (D/H) [Cooke et al. 2017]

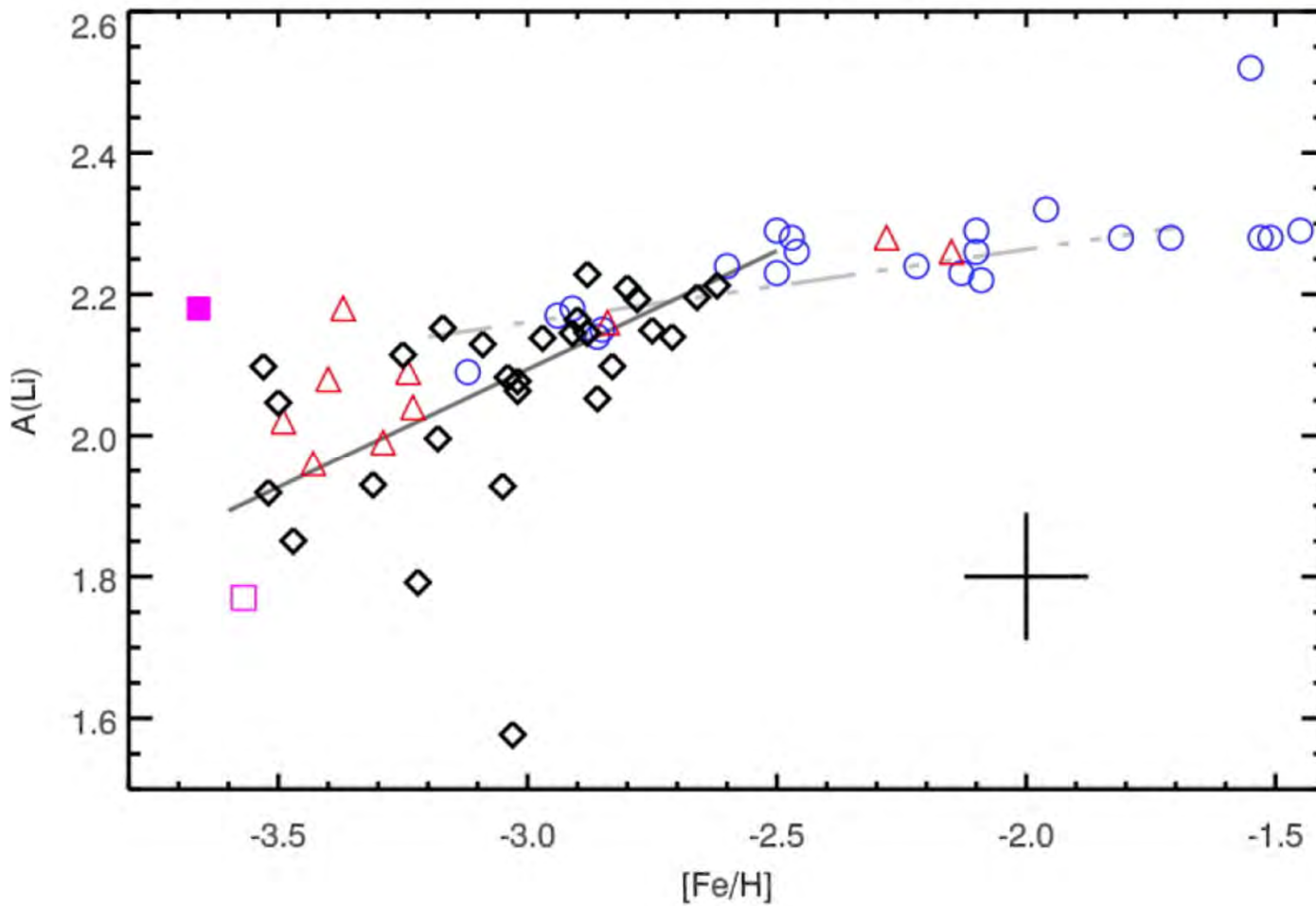
$$100\Omega_{b,0}h^2(\text{BBN}) = 2.235 \pm 0.05$$

(Random + Systematic Error)



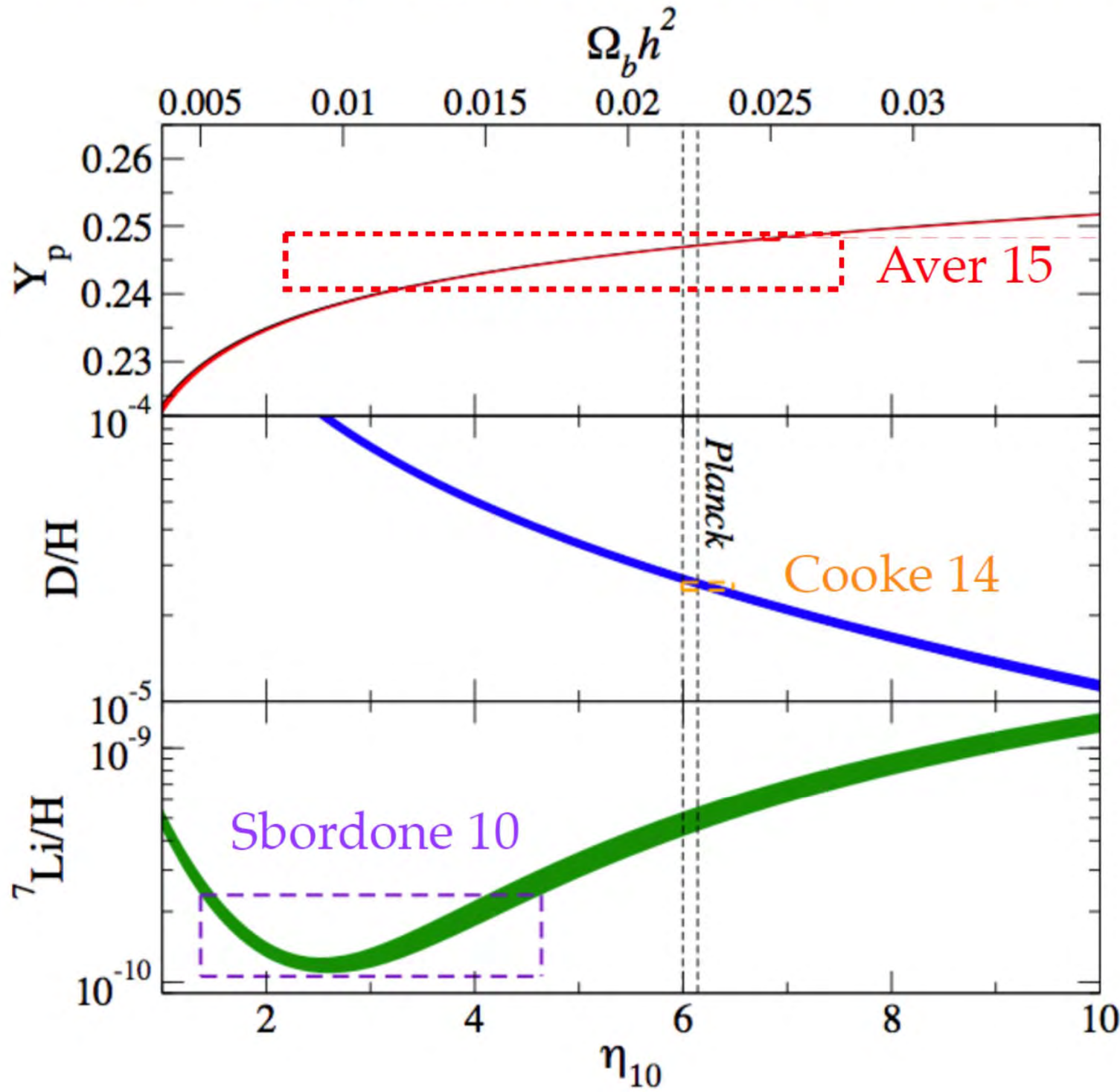
Left: The D I component is clearly resolved at $v = -82$ km/s in the transition from the $n = 1$ to the $n = 7$ energy level of H I seen in absorption against the quasar J1419+0829.

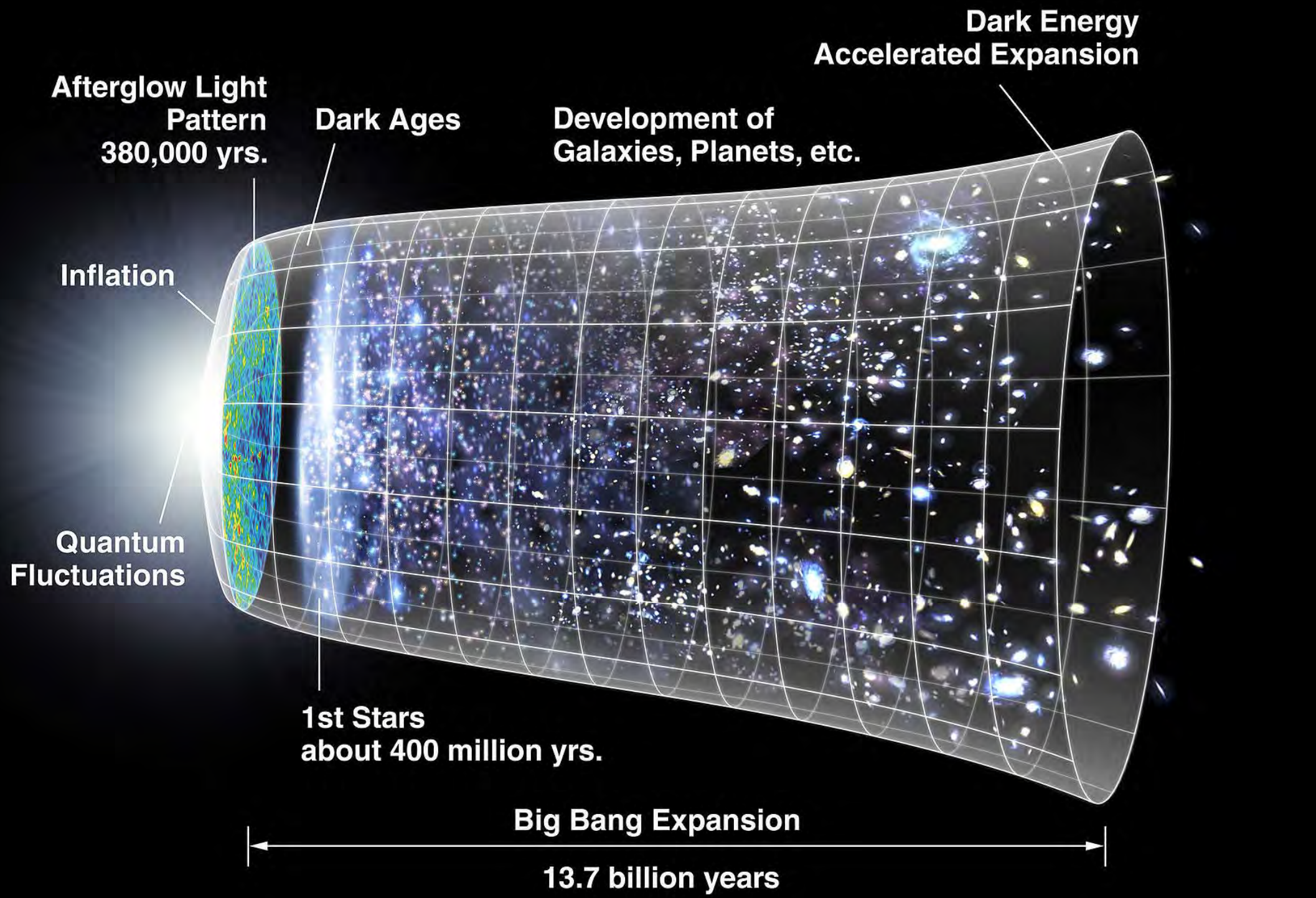
Right: The seven high-precision determinations of (D/H) from quasar absorption line spectroscopy. The dark and light red bands show the 1 and 2 σ confidence limits on $(\text{D}/\text{H})_p$. Figures adapted from Cooke et al. (2014, 2017).



A collection of ^7Li abundance measurements in metal-poor halo stars, from Sbordone et al. (2010). The different symbols refer to different data sets brought together here. Typical errors are indicated by the black cross. The Li abundance scale (y-axis) is defined as $A(\text{Li}) = \log(\text{Li}/\text{H}) + 12$.

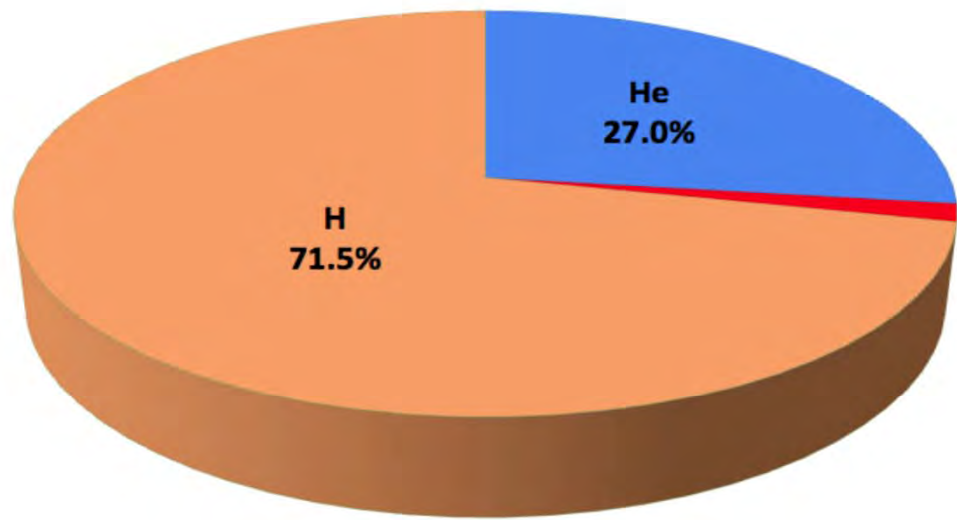
BBN theory confronts observations 2015





Cosmic Inventory

Component	Ω (ρ/ρ_c)
Dark Energy	0.691 ± 0.006
Matter (baryonic and non-baryonic)	0.312 ± 0.009
Baryons (Total)	0.0488 ± 0.0004
Baryons in stars and stellar remnants	~ 0.003
Neutrinos	~ 0.001
Photons (CMB)	5×10^{-5}



He
27.0%

Other
1.4%

Mg
5.3%

Si
5.0%

Ne
9.4%

Fe
9.7%

Other
4.9%

C
17.7%

N
5.2%

O
42.9%

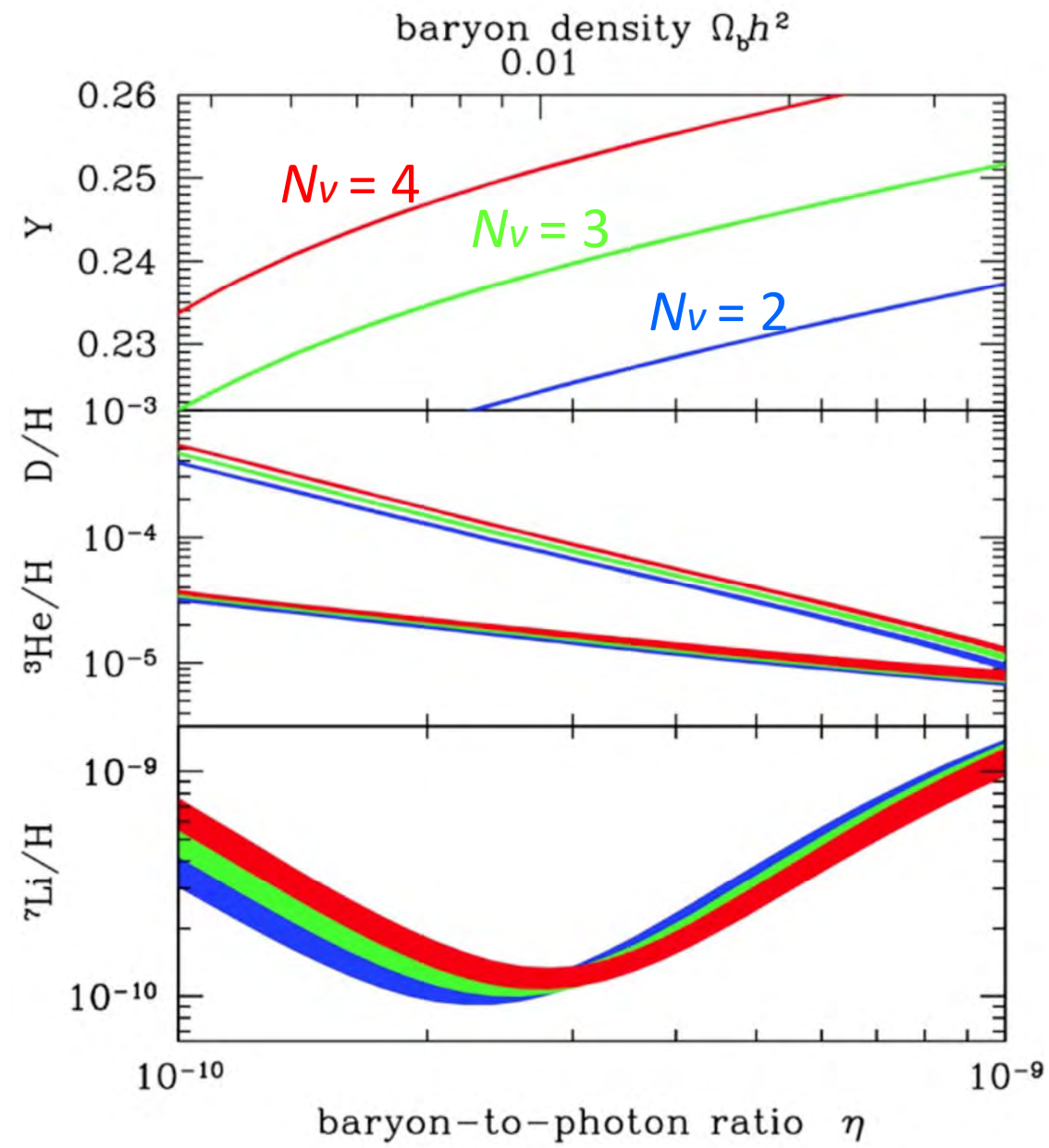
Solar chemical composition

Protosolar bulk abundances by mass

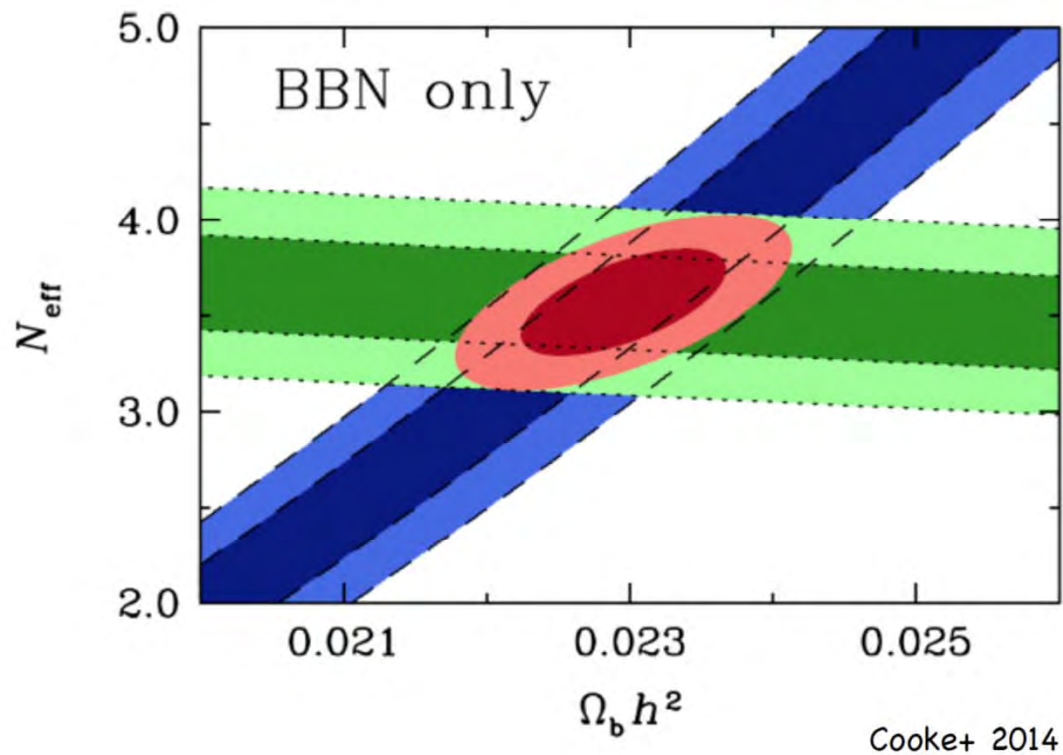
Asplund et al. 2009, ARAA, 47, 481

Three Generations of Matter (Fermions)

	I	II	III	
mass →	2.4 MeV/c ²	1.27 GeV/c ²	171.2 GeV/c ²	0
charge →	2/3 u	2/3 c	2/3 t	0
spin →	1/2 up	1/2 charm	1/2 top	1
name →				photon
Quarks	d	s	b	g
	4.8 MeV/c ² -1/3 d 1/2 down	104 MeV/c ² -1/3 s 1/2 strange	4.2 GeV/c ² -1/3 b 1/2 bottom	0 0 1 gluon
Leptons	e	ν_μ	ν_τ	Z ⁰
	<2.2 eV/c ² 0 e 1/2 electron neutrino	<0.17 MeV/c ² 0 ν_μ 1/2 muon neutrino	<15.5 MeV/c ² 0 ν_τ 1/2 tau neutrino	91.2 GeV/c ² 0 1 Z boson
Gauge Bosons	e	μ	τ	W [±]
	0.511 MeV/c ² -1 e 1/2 electron	105.7 MeV/c ² -1 μ 1/2 muon	1.777 GeV/c ² -1 τ 1/2 tau	80.4 GeV/c ² ±1 W [±] 1 W boson



Left: BBN predictions for light element from Cyburt et al. (2015).



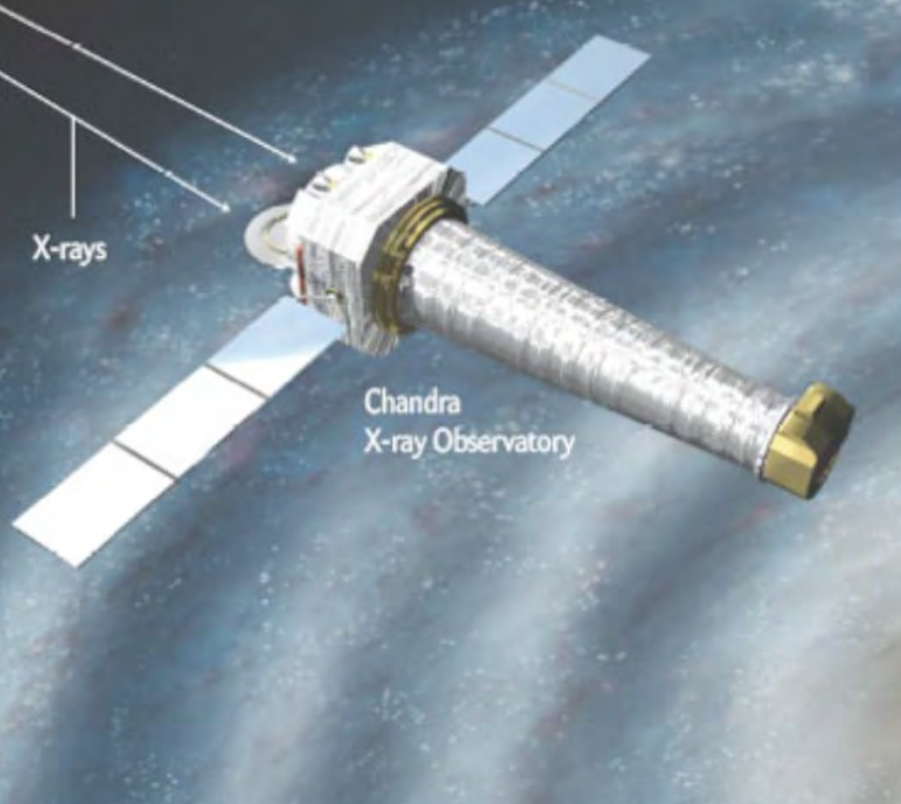
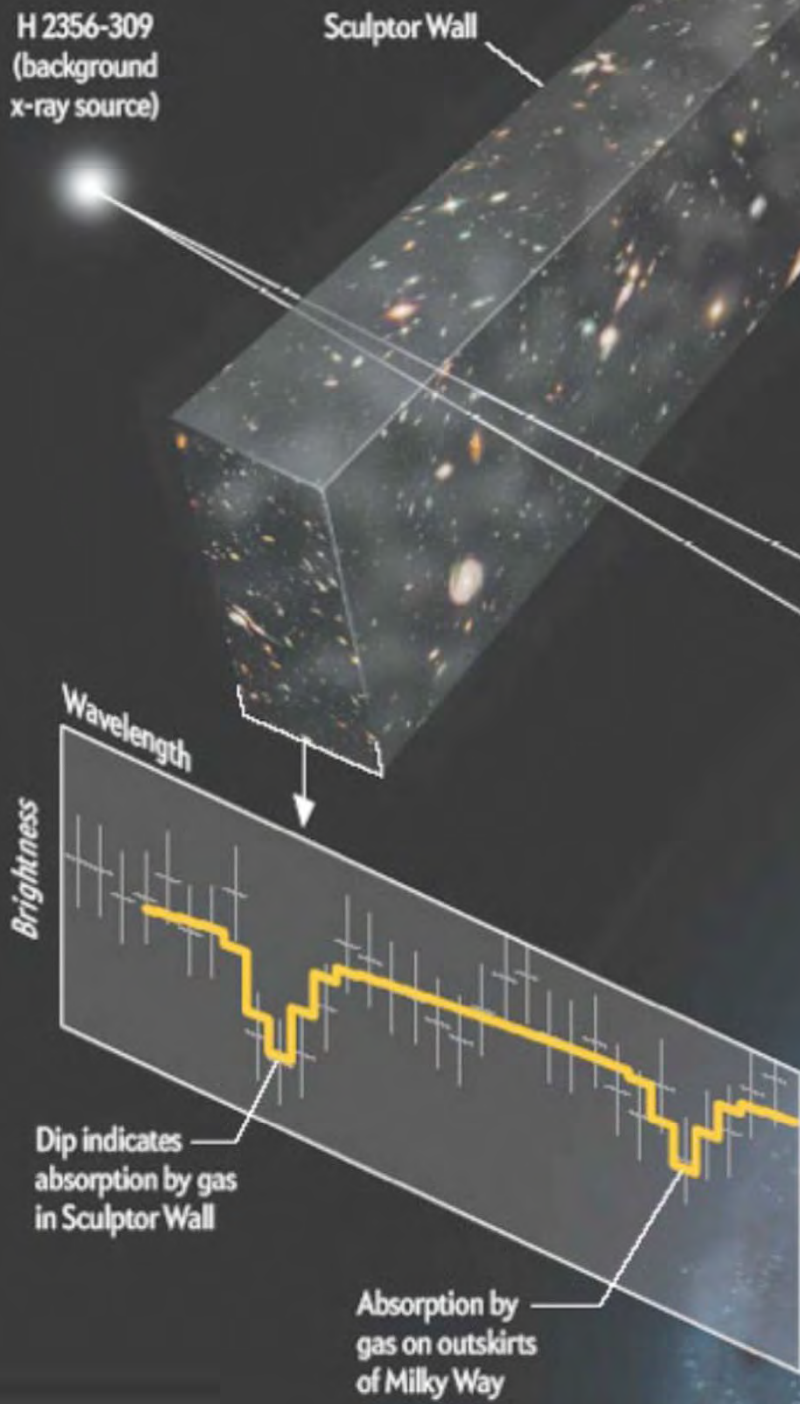
Right: Joint 1 σ (darker colours) and 2 σ (lighter colours) confidence contours for N_ν and $\Omega_{b,0}$ obtained from the measured values of Y_p and $(D/H)_p$ from Cooke et al. (2014).

Cosmic Inventory

Component	Ω (ρ/ρ_c)
Dark Energy	0.691 ± 0.006
Matter (baryonic and non-baryonic)	0.312 ± 0.009
Baryons (Total)	0.0488 ± 0.0004
Baryons in stars and stellar remnants	~ 0.003
Neutrinos	~ 0.001
Photons (CMB)	5×10^{-5}

Betrayed by Its Shadow

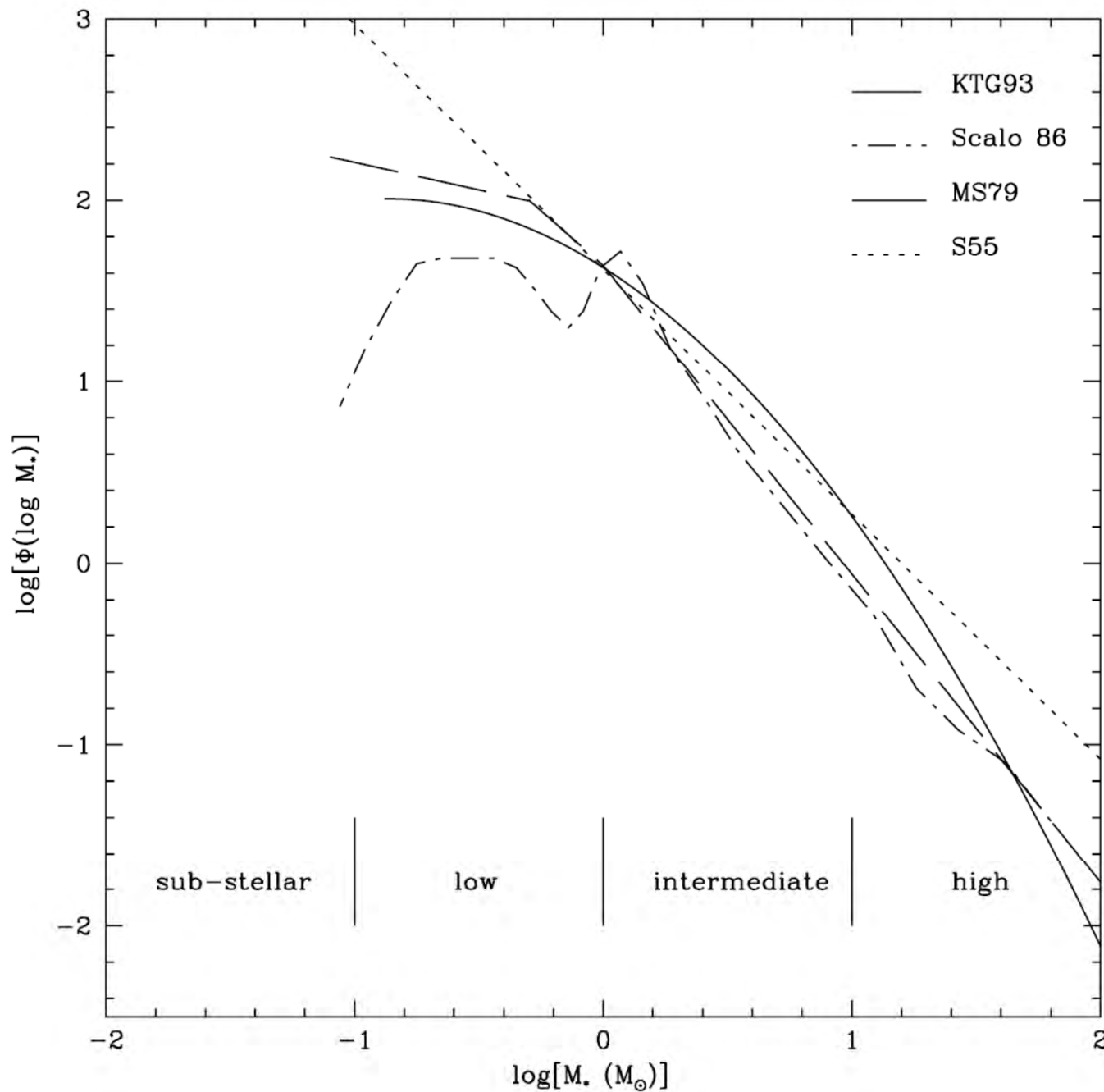
Astronomers think they may have found where the bulk of the normal matter in the universe lurks: not in galaxies but in a form of intergalactic gas (mostly hydrogen) called the warm-hot intergalactic medium, or WHIM. The name connotes that the gas is less than blazingly hot and, consequently, glows too feebly to see directly. Looking in the interstices of a giant filament of galaxies called the Sculptor Wall, astronomers saw, in essence, the WHIM's shadow: the gas absorbed x-rays from a background object at a distinctive wavelength.



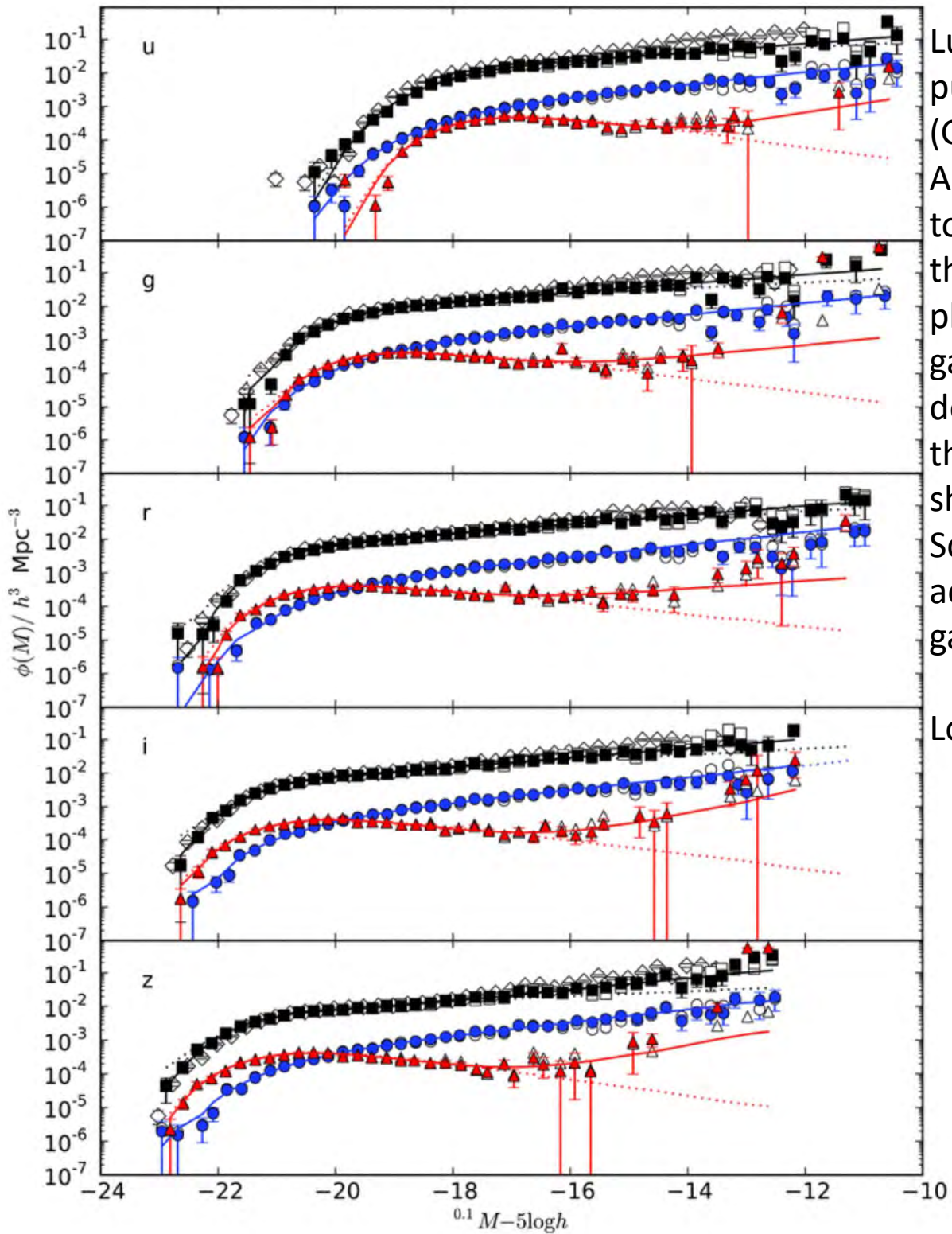
Phases of Interstellar Gas

Phase	T (K)	n_H (cm $^{-3}$)	Comments	Cool HI (CNM)	~ 100	30	
Coronal gas (HIM) $f_V \approx 0.5?$ $\langle n_H \rangle f_V \approx 0.002 \text{ cm}^{-3}$ (f_V ≡ volume filling factor)	$\gtrsim 10^{5.5}$	~ 0.004	Shock-heated Collisionally ionized Either expanding or in pressure equilibrium Cooling by: ◇ Adiabatic expansion ◇ X ray emission Observed by: • UV and x ray emission • Radio synchrotron emission	$f_V \approx 0.01$ $n_H f_V \approx 0.3 \text{ cm}^{-3}$			Heating by photoelectrons from dust Ionization by starlight, cosmic rays Cooling by: ◇ Fine structure line emission Observed by: • HI 21-cm emission, absorption • Optical, UV absorption lines
H II gas $f_V \approx 0.1$ $\langle n_H \rangle f_V \approx 0.02 \text{ cm}^{-3}$	10^4	$0.3 - 10^4$	Heating by photoelectrons from H, He Photoionized Either expanding or in pressure equilibrium Cooling by: ◇ Optical line emission ◇ Free-free emission ◇ Fine-structure line emission Observed by: • Optical line emission • Thermal radio continuum	Diffuse H ₂ $f_V \approx 0.001$ $n_H f_V \approx 0.1 \text{ cm}^{-3}$	$\sim 50 \text{ K}$	~ 100	Heating by photoelectrons from dust Ionization by starlight, cosmic rays Cooling by: ◇ Fine structure line emission Observed by: • HI 21-cm emission, absorption • CO 2.6-mm emission • optical, UV absorption lines
Warm HI (WNM) $f_V \approx 0.4$ $n_H f_V \approx 0.2 \text{ cm}^{-3}$	~ 5000	0.6	Heating by photoelectrons from dust Ionization by starlight, cosmic rays Pressure equilibrium Cooling by: ◇ Optical line emission ◇ Fine structure line emission Observed by: • HI 21 cm emission, absorption • Optical, UV absorption lines	Dense H ₂ $f_V \approx 10^{-4}$ $\langle n_H \rangle f_V \approx 0.2 \text{ cm}^{-3}$	$10 - 50$	$10^3 - 10^6$	Heating by photoelectrons from dust Ionization and heating by cosmic rays Self-gravitating: $p > p(\text{ambient ISM})$ Cooling by: ◇ CO line emission ◇ CI fine structure line emission Observed by: • CO 2.6-mm emission • dust FIR emission
				Cool stellar outflows	$50 - 10^3$	$1 - 10^6$	Observed by: • Optical, UV absorption lines • Dust IR emission • HI, CO, OH radio emission

Stellar Initial Mass Functions



Meyer+ 1999



Luminosity functions of nearby galaxies ($z < 0.1$) published by the Galaxy and Mass Assembly (GAMA) project from data obtained with the Anglo-Australian telescope. The five panels refer to LFs in five different wavelength bands, from the ultraviolet, u , to the infrared, z . The LF is plotted separately for blue (i.e. star-forming) galaxies and red galaxies whose light is dominated by old stars. The black squares are for the combined blue and red samples. Dotted lines show the best fit to the data assuming a Schechter function. The GAMA team accumulated spectra of many thousands of galaxies to construct these LFs.

Loveday et al. 2012, MNRAS, 420, 1239

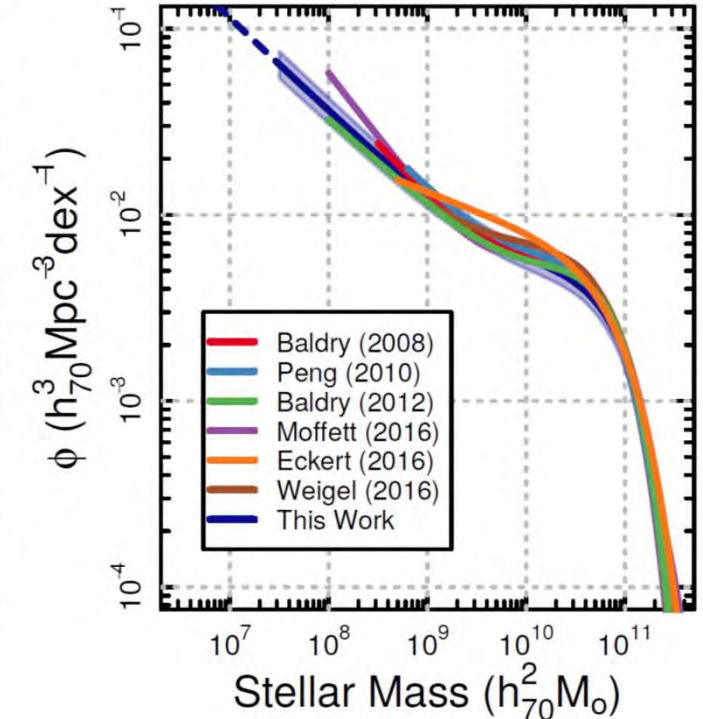
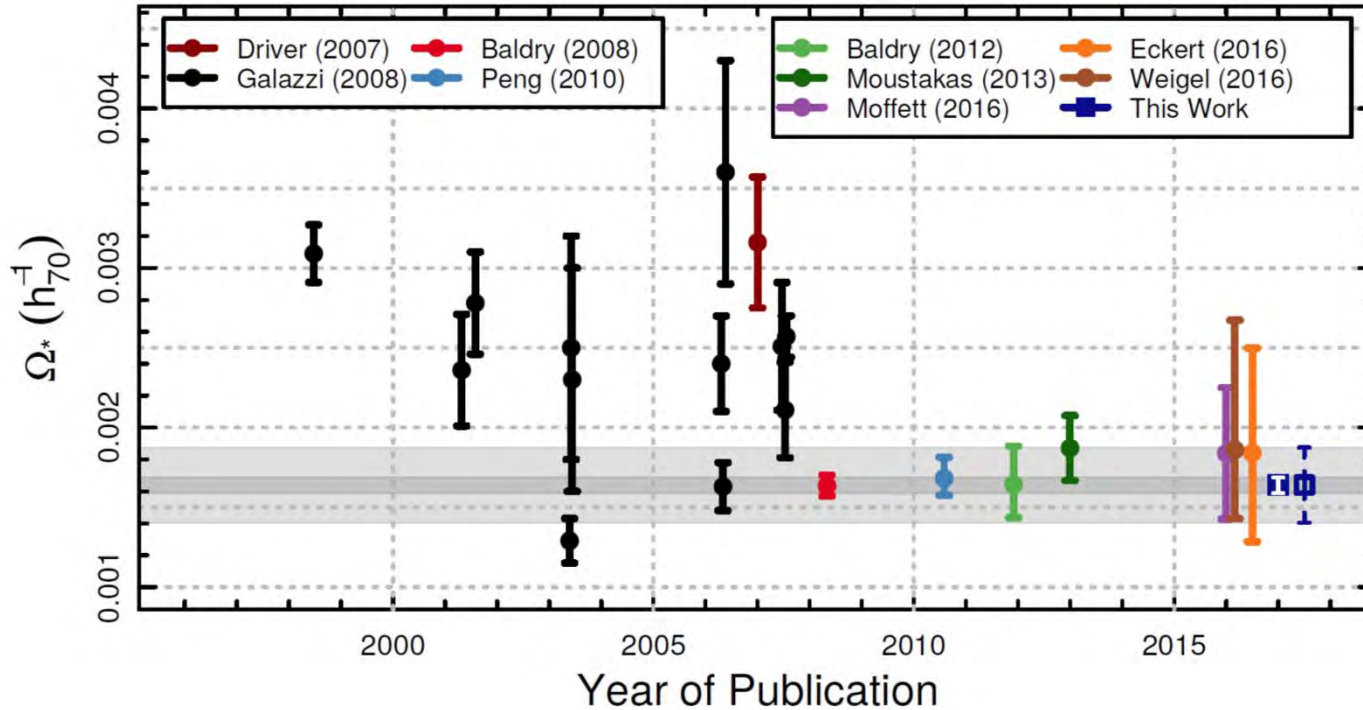
the LF of galaxies in visible light (in the V-band) is well-fitted by a Schechter function with typical parameters:

$$\alpha = -1.25$$

$$L^* = 1.0 \times 10^{10} h^{-2} L_{\odot V}$$

$$\phi^* = 1.2 \times 10^{-2} h^3 \text{ Mpc}^{-3}$$

Estimates of Ω_\star from Stellar Mass Function



$$\Omega_\star = 1.66 \pm 0.97 h_{70}^{-1} \times 10^{-3}$$

Wright et al. 2017

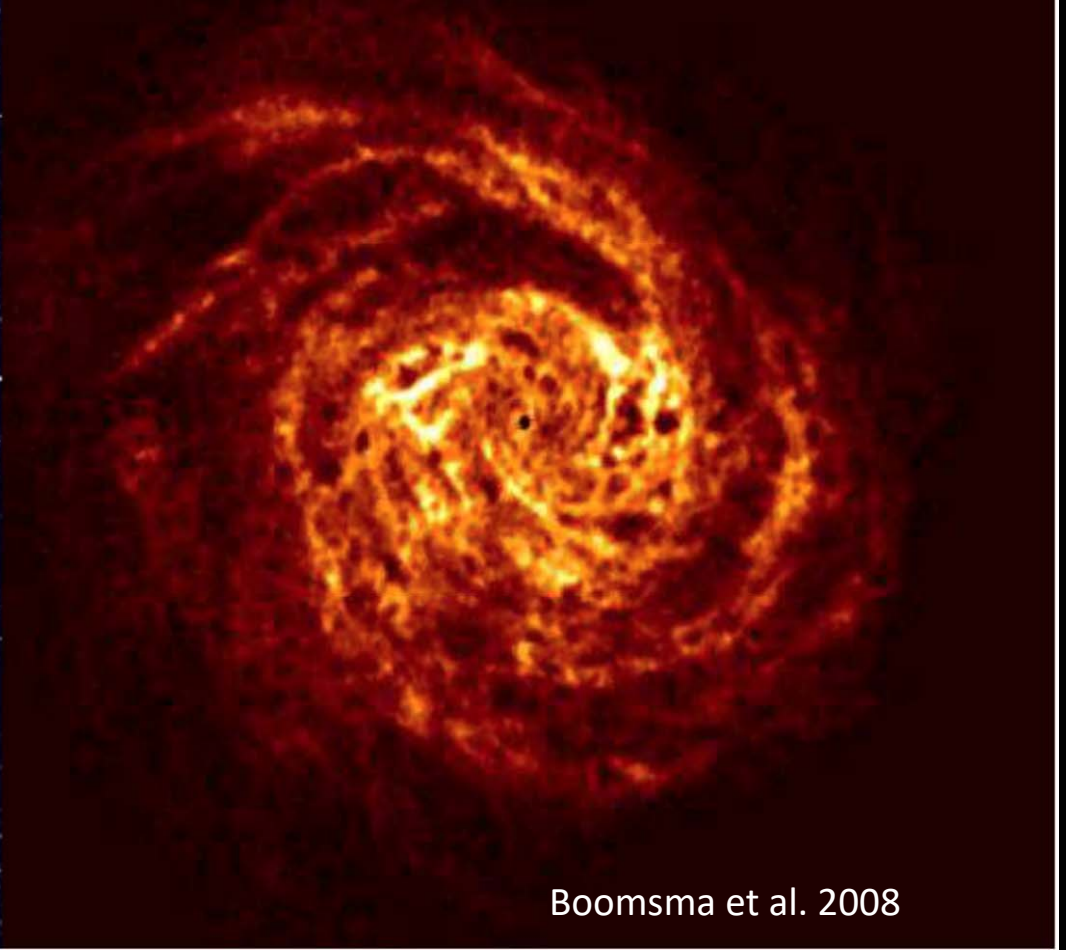
CSST/ LSST will be able to cover significantly larger area of sky than any current surveys (SDSS, GAMA...) in the local Universe, with better and deeper photometry, which will then provide better constraints on the stellar mass function and hence the estimate of Ω_\star .



optical

NGC6946 on the same scale

HI

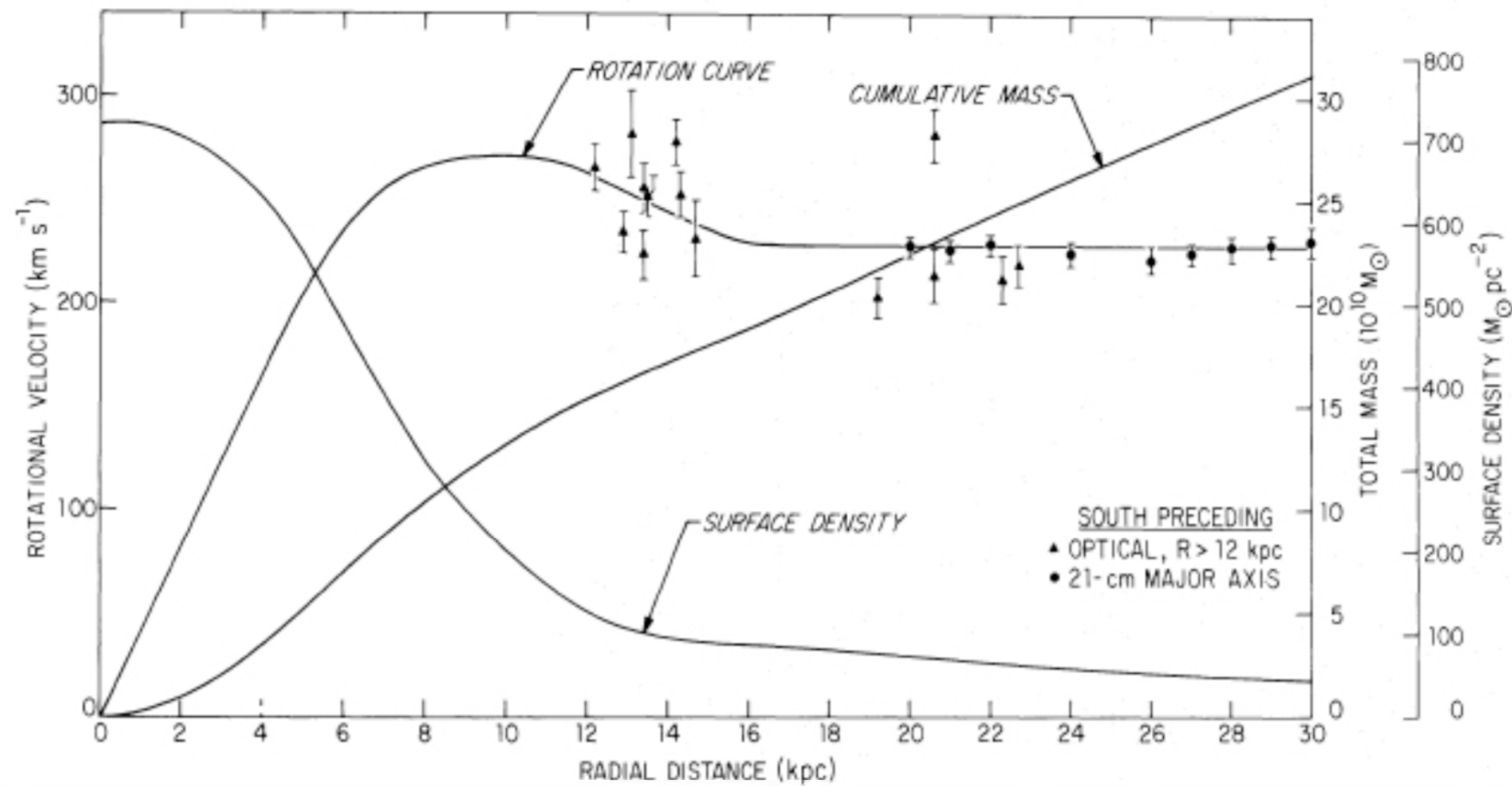


Boomsma et al. 2008

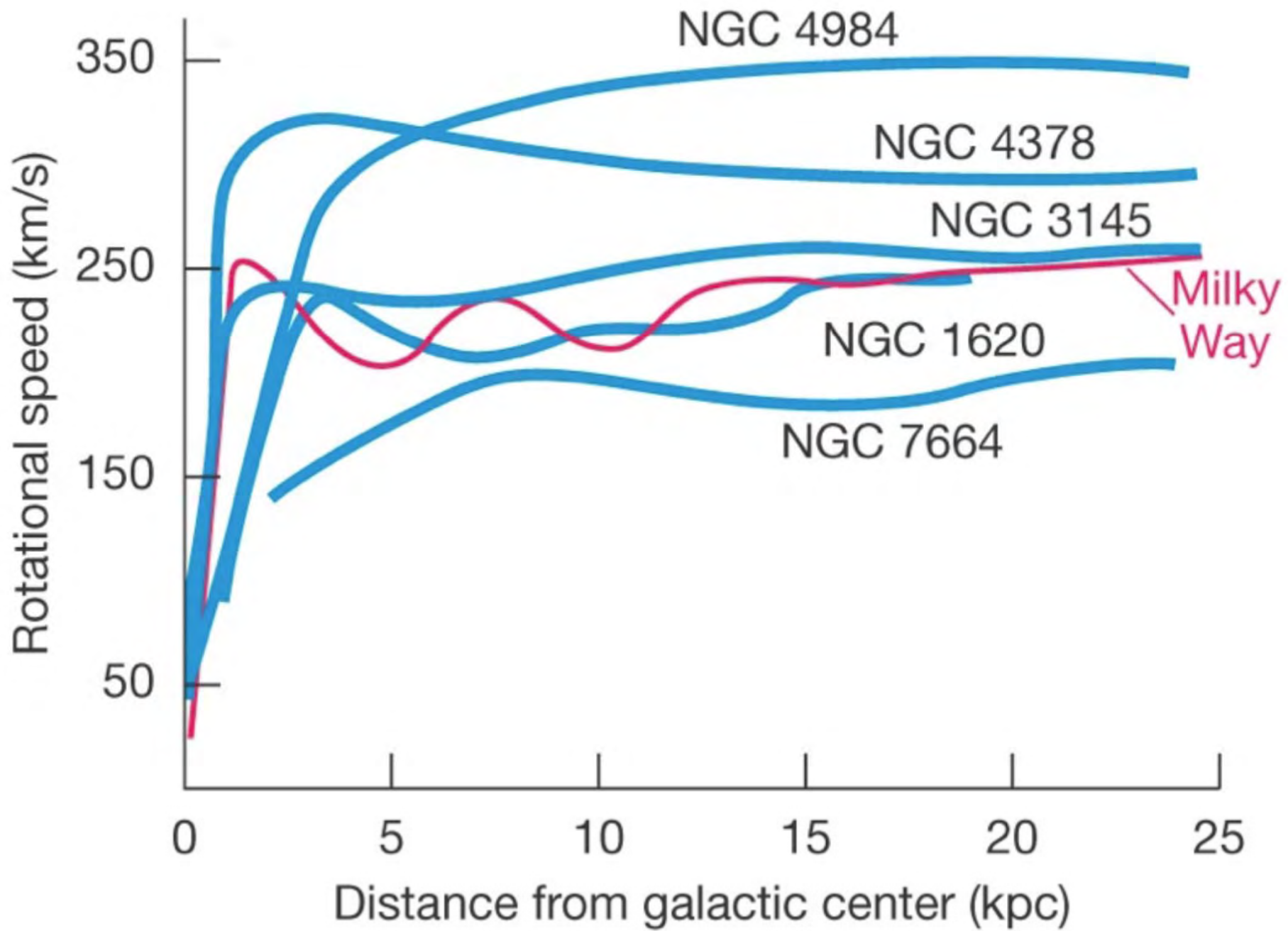
Why HI?

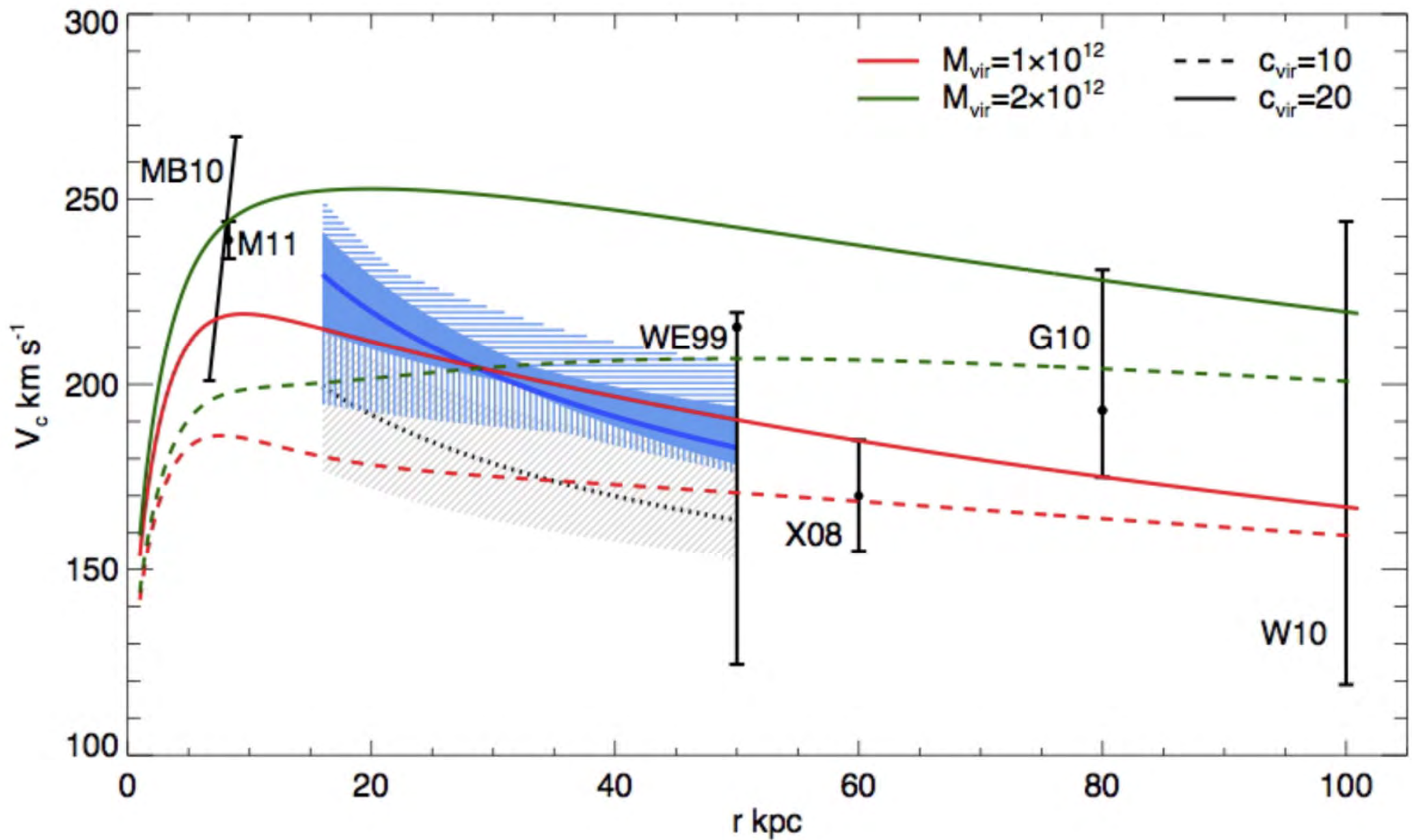
- the role of HI in the Galactic Recycling
- How do galaxies acquire gas?
- $SFR - M_{HI}$ – Stellar feedback
- The dependence of M_{HI} on environment
- Structure and the kinematics of the HI in nearby galaxies
- Interplay between the multiple phases of the gas (ionized, atomic, molecular) and how this connects to star formation.
- how is the activity of AGN connected to HI and how do AGN affect the gas content of galaxies?

Evolution with redshift

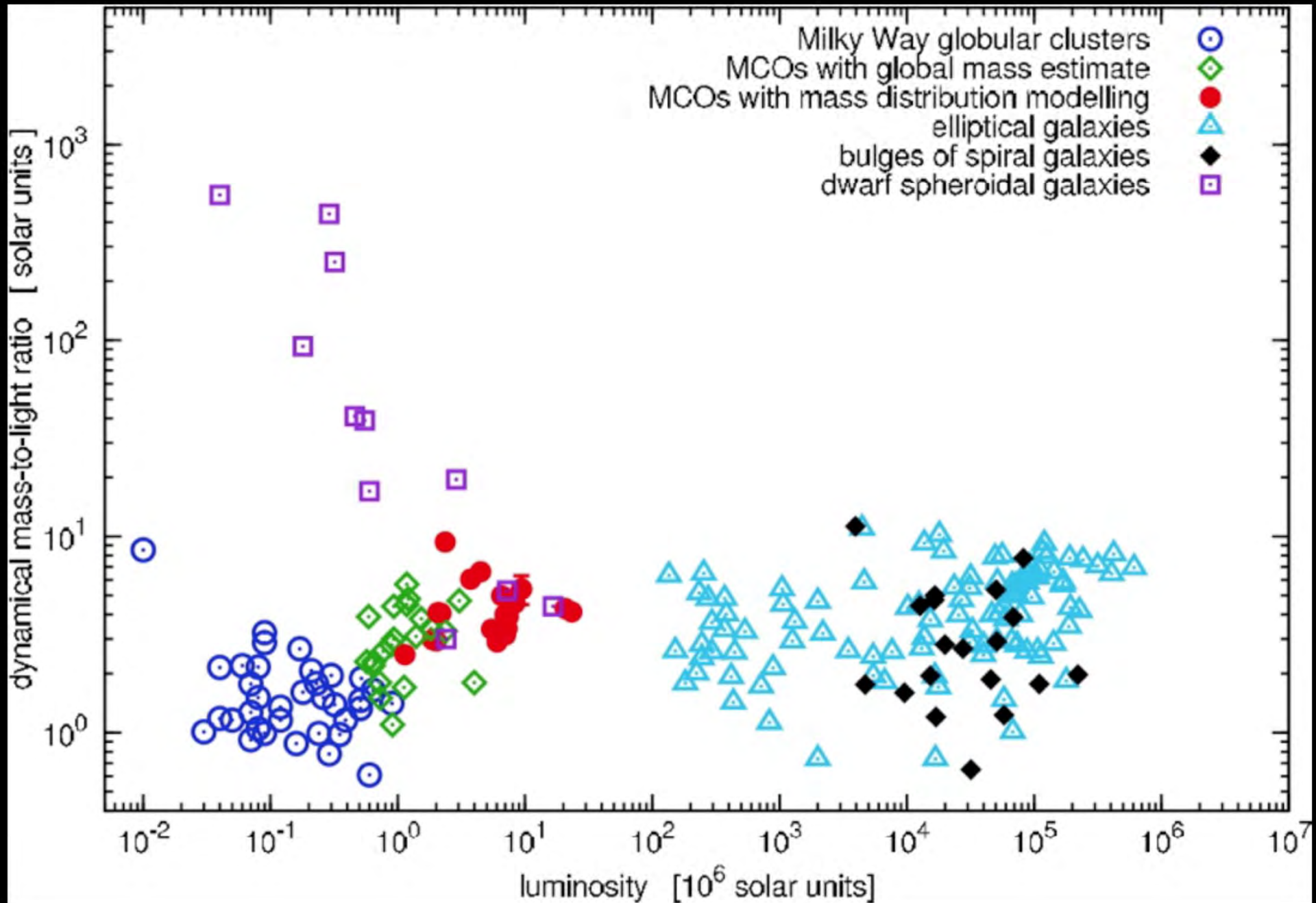


Roberts & Whitehurst 1975





Deason+ 2012



Dabringhausen+ 2008





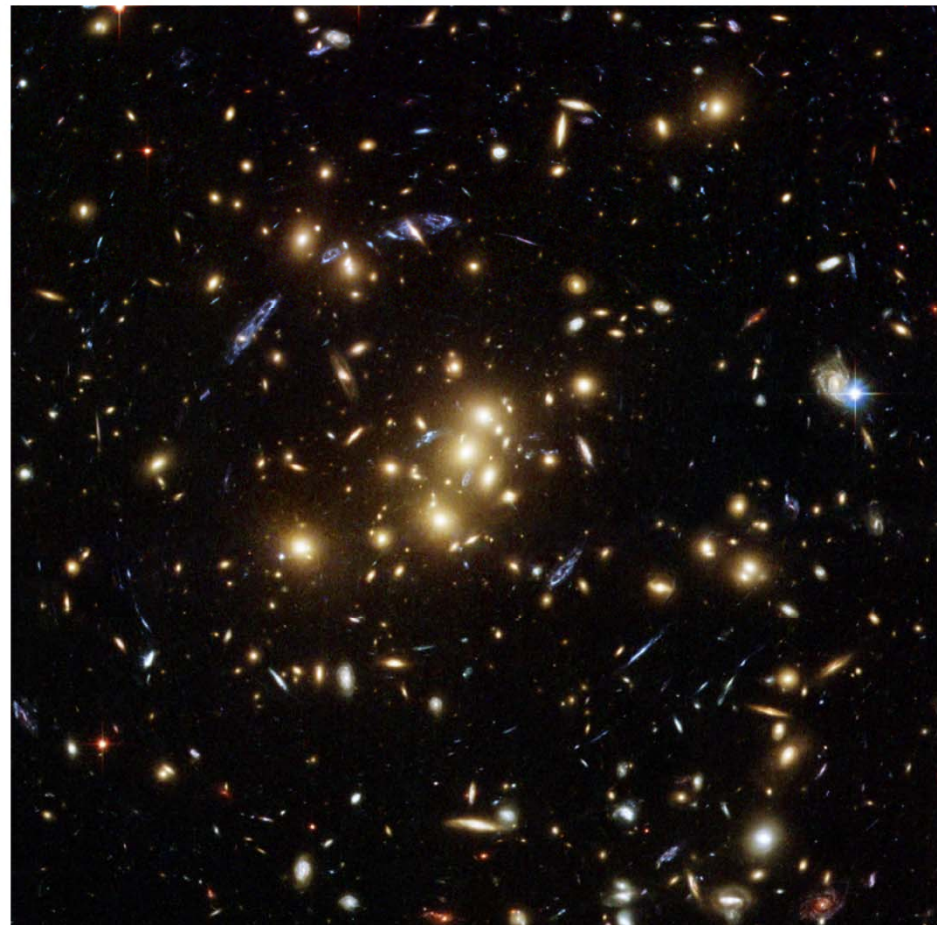
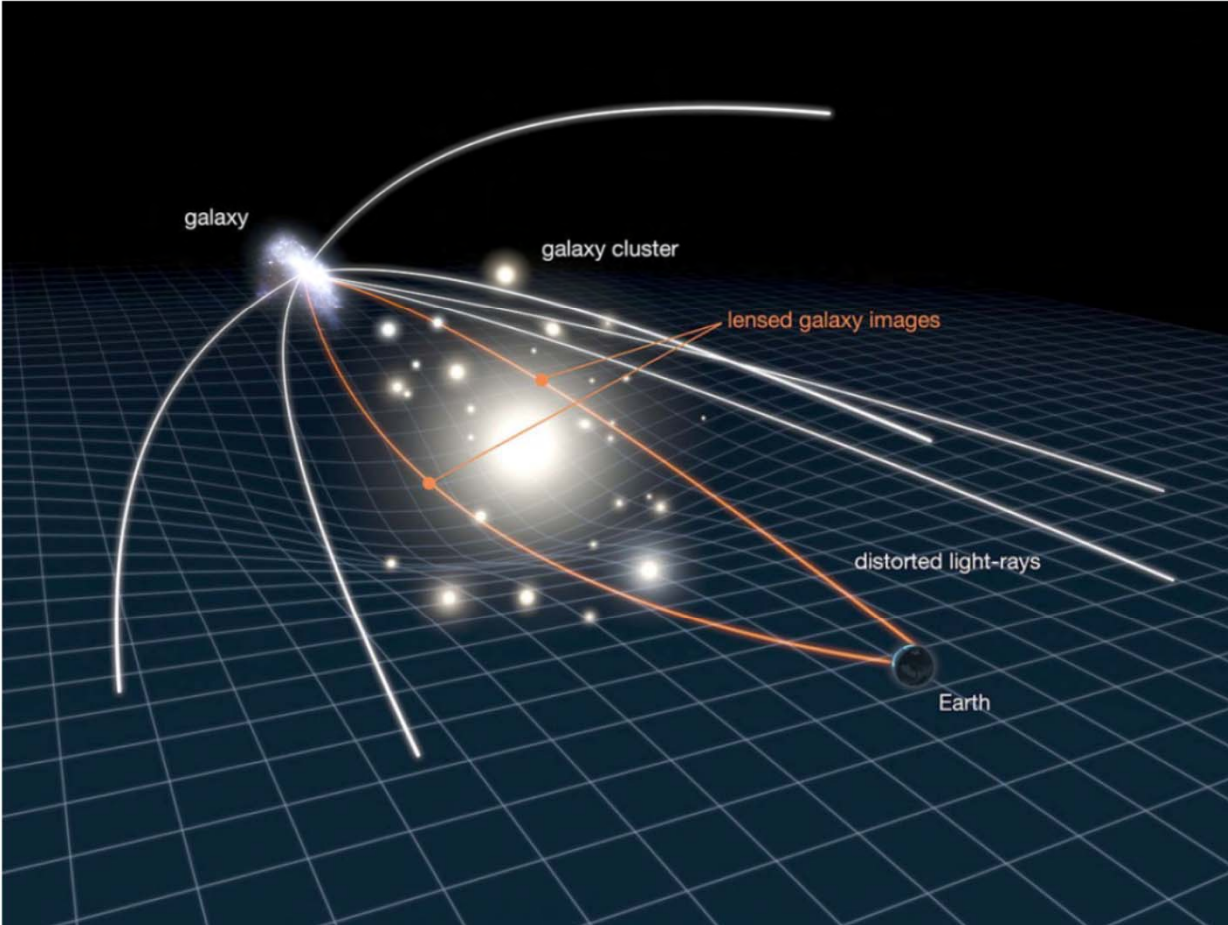
NASA, ESA, and the Hubble Heritage Team (STScI/AURA)





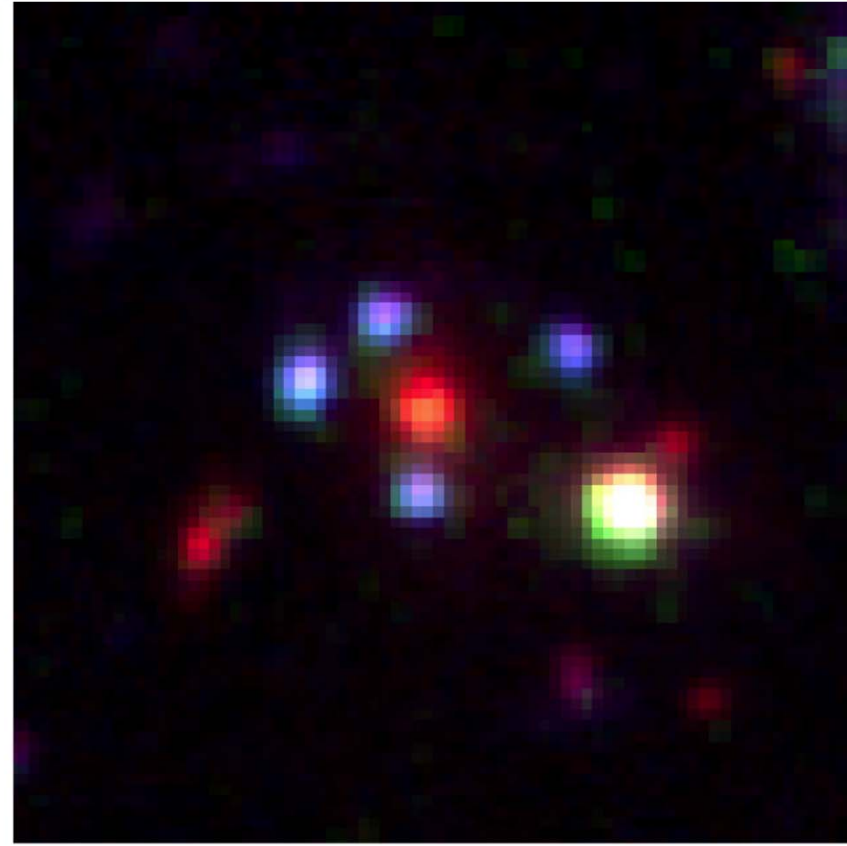
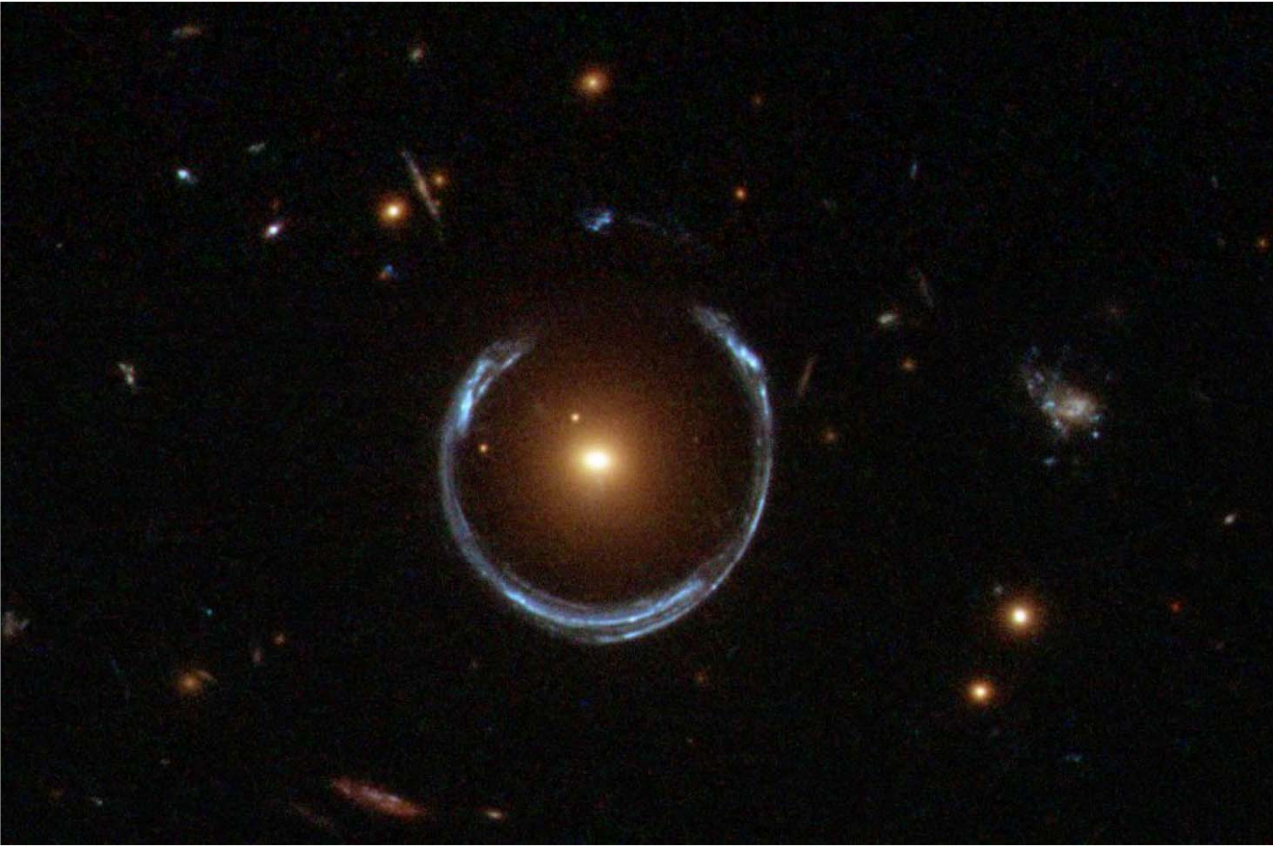
Left: The galaxy cluster Abell 383 imaged with the Hubble Space Telescope Advanced Camera for Surveys. This cluster is one of the largest concentrations of matter in the local Universe ($z = 0.1887$), with a mass $M \sim 7.5 \times 10^{14} M_\odot$.

Right: The Xray image of the cluster (shown here superimposed on the HST image taken in visible light) obtained by the Chandra observatory shows diffuse emission from intracluster gas at temperatures $\sim 5 \times 10^7$ K.



Left: Schematic representation of gravitational lensing by a galaxy cluster.

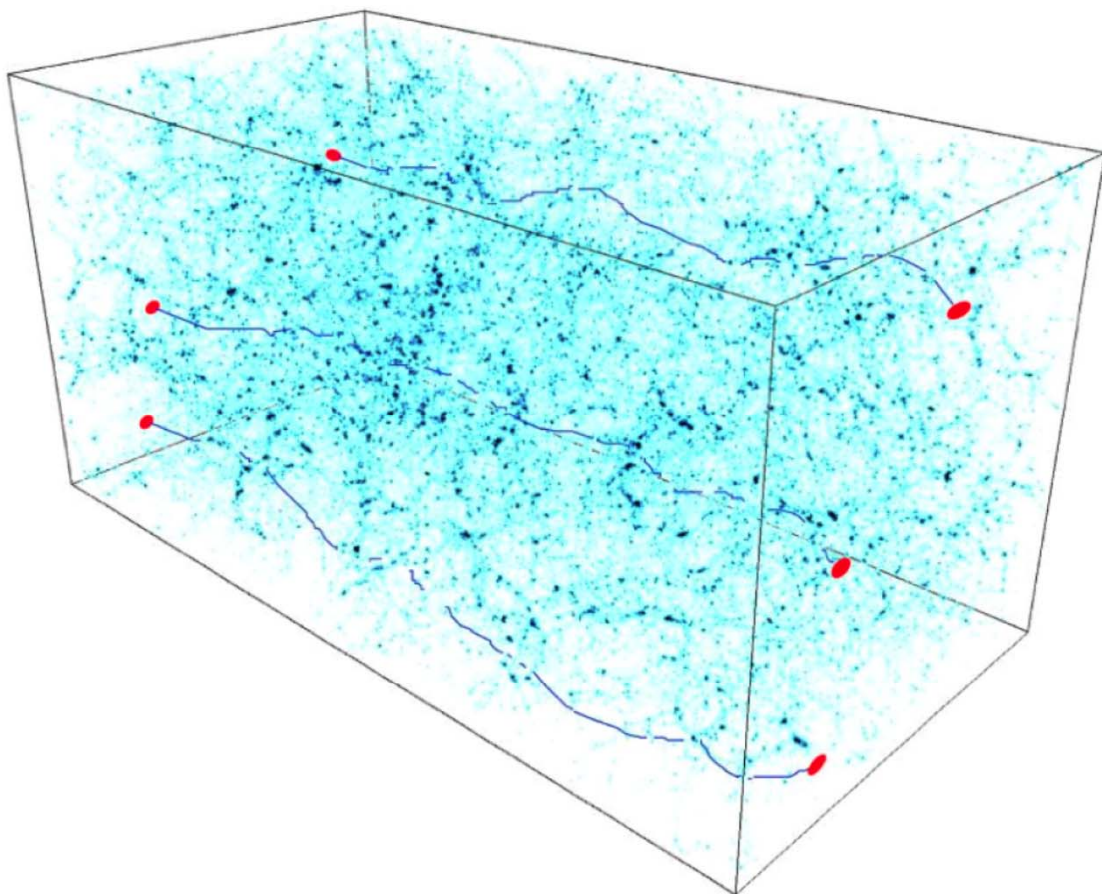
Right: The $z = 0.395$ galaxy cluster Cl0024+1652 imaged with the Hubble Space Telescope Advanced Camera for Surveys. With a mass $M = 5 \times 10^{14} M_{\odot}$, the cluster acts as a gravitational lens: the blue arcs in the HST field of view are images of background galaxies at $z >> 0.395$, stretched and magnified by the curvature of spacetime generated by the mass of the cluster.



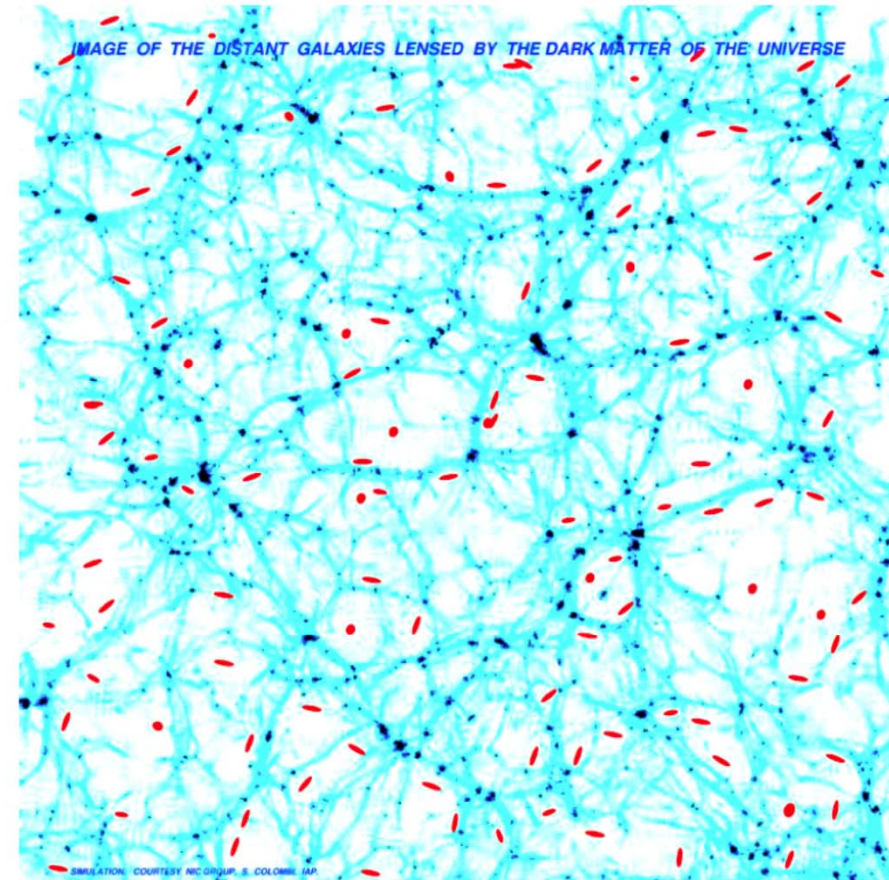
Left: HST image of the 'Cosmic Horseshoe', a star-forming galaxy at $z = 2.38115$ gravitationally lensed into a near-complete Einstein ring by a foreground massive ($M \sim 6 \times 10^{12} M_{\odot}$) red galaxy at $z = 0.444$.

Right: CSWA20, a blue star-forming galaxy at $z = 1.433$ gravitationally lensed into an Einstein cross (four images) by a foreground massive ($M \sim 4 \times 10^{12} M_{\odot}$) galaxy at $z = 0.741$. These galaxy-scale gravitational lenses not only give us the means to probe the distribution of dark matter in galactic halos, but also allow astronomers to study the physical properties of high redshift galaxies in much more detail than is normally the case (i.e. in the absence of gravitational magnification).

DEFLECTION OF LIGHT RAYS CROSSING THE UNIVERSE, EMITTED BY DISTANT GALAXIES



SIMULATION: COURTESY NIC GROUP, S. COLOMBI, IAP.



SIMULATION: COURTESY NIC GROUP, S. COLOMBI, IAP.

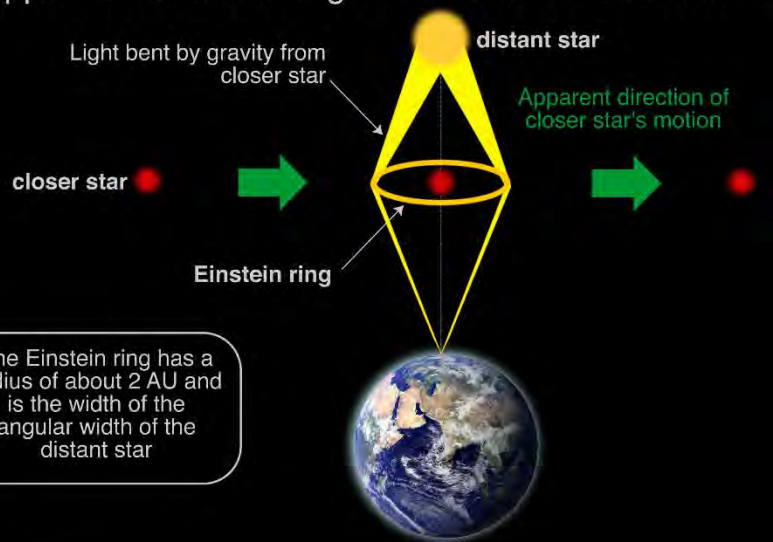
Cosmic shear is the weak lensing by the large-scale structure of the Universe.

Left: Light (shown in dark blue) from distant galaxies (red) is constantly being deflected.

Right: The observer sees distorted, correlated, images of the distant galaxies. The correlation of their shapes depends on the large-scale structure, and therefore cosmological parameters that determine the evolution of cosmic structure can be extracted from statistical analysis of the distortion pattern.

Gravitational Microlensing

The Earth, a close star, and a brighter, more distant star, happen to come into alignment for a few weeks or months



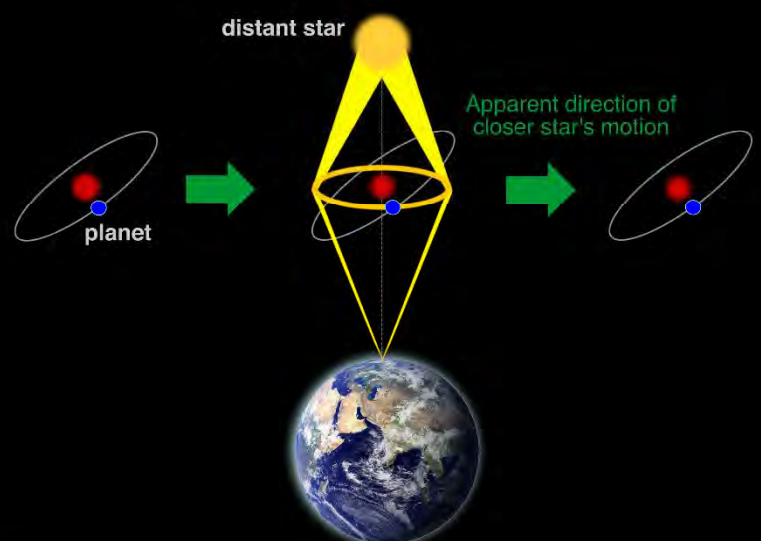
Gravity from the closer star acts as a lens and magnifies the distant star over the course of the transit.



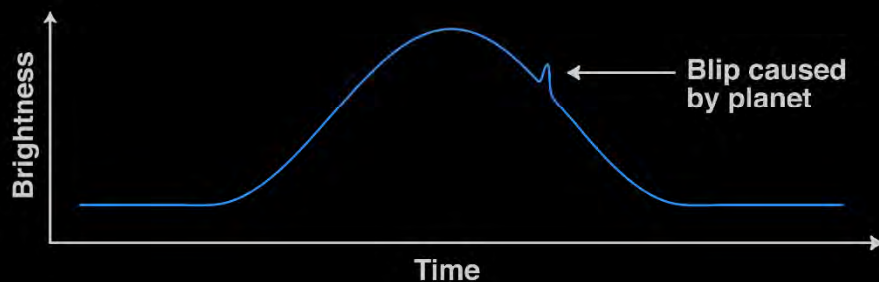
The change in brightness can be plotted on a graph



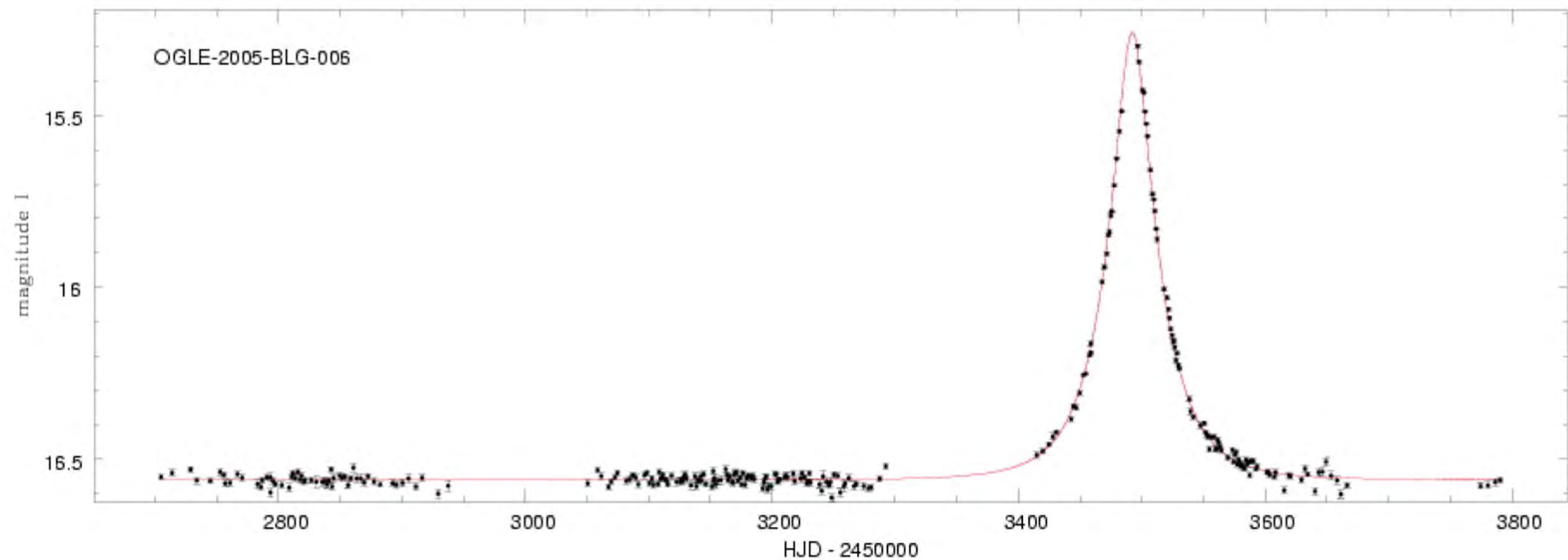
If there is a planet orbiting the closer star, and it happens to align with the Einstein ring, its mass will enhance the lens effect and increase the magnification for a short time

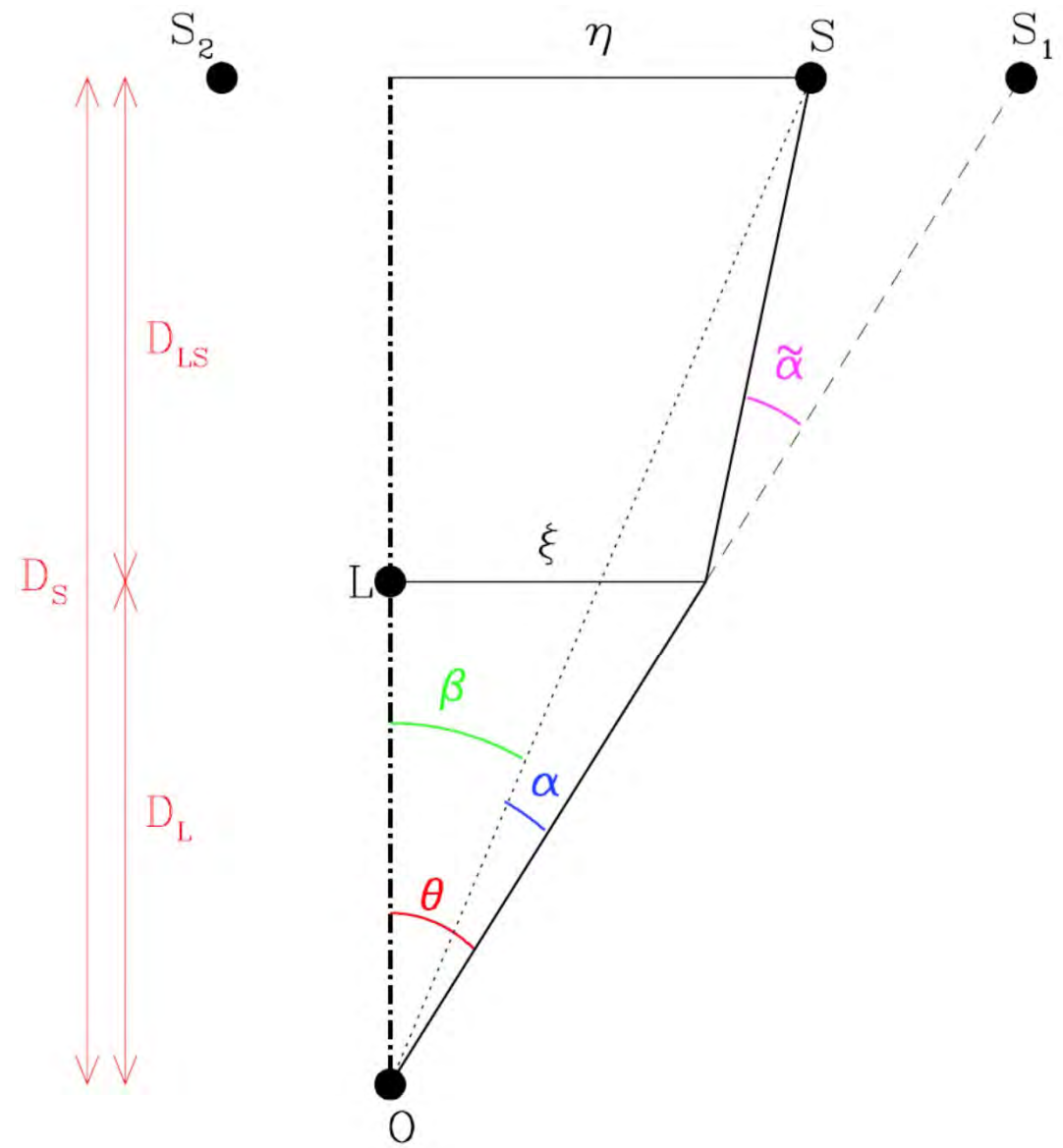
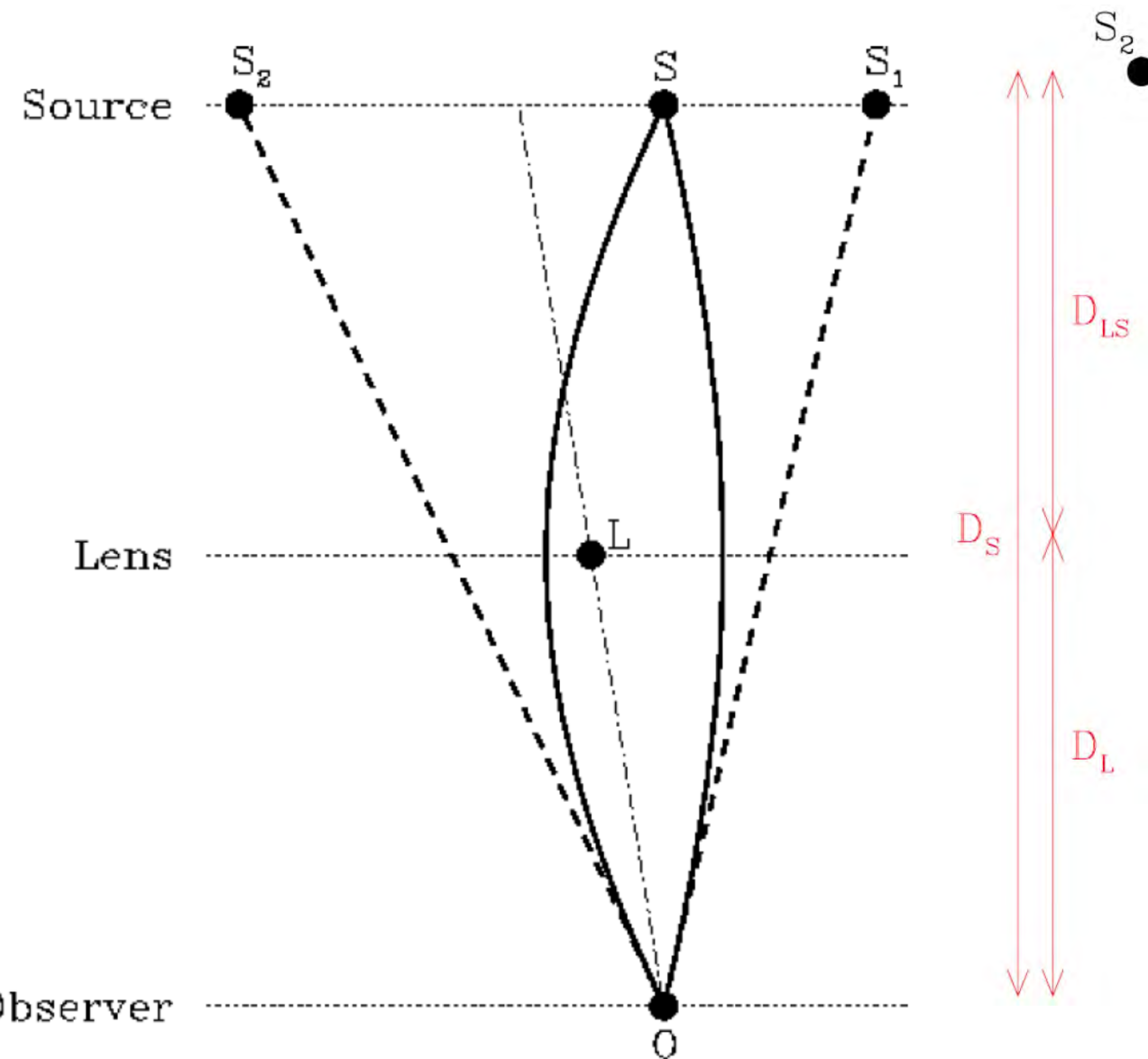


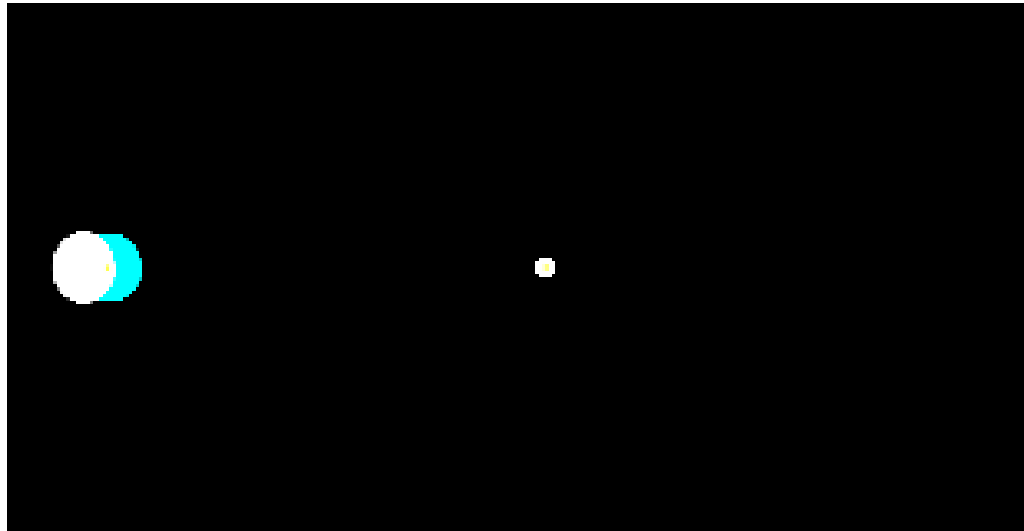
The planet causes a small blip on the graph



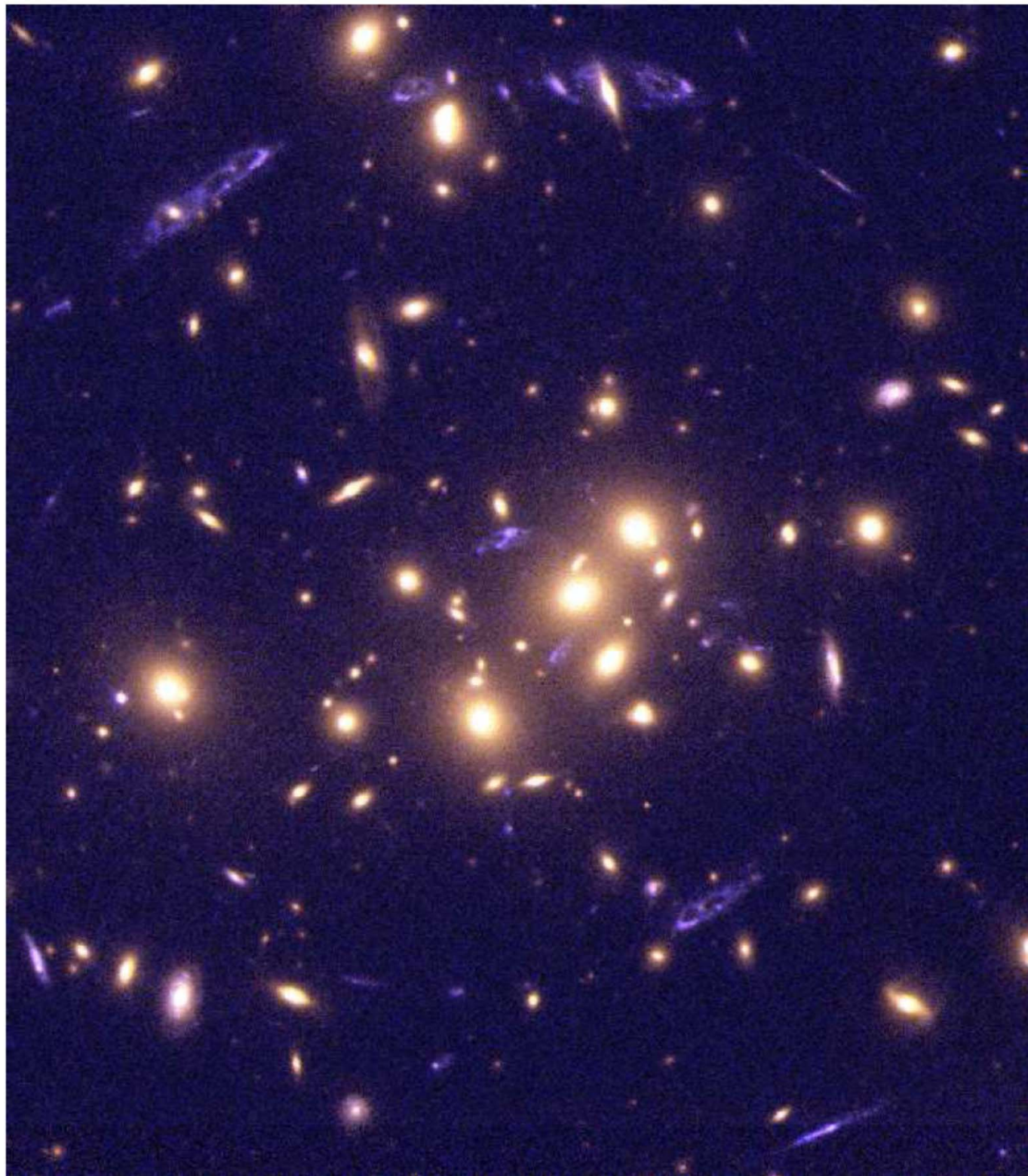
Light curve of a microlensing event.



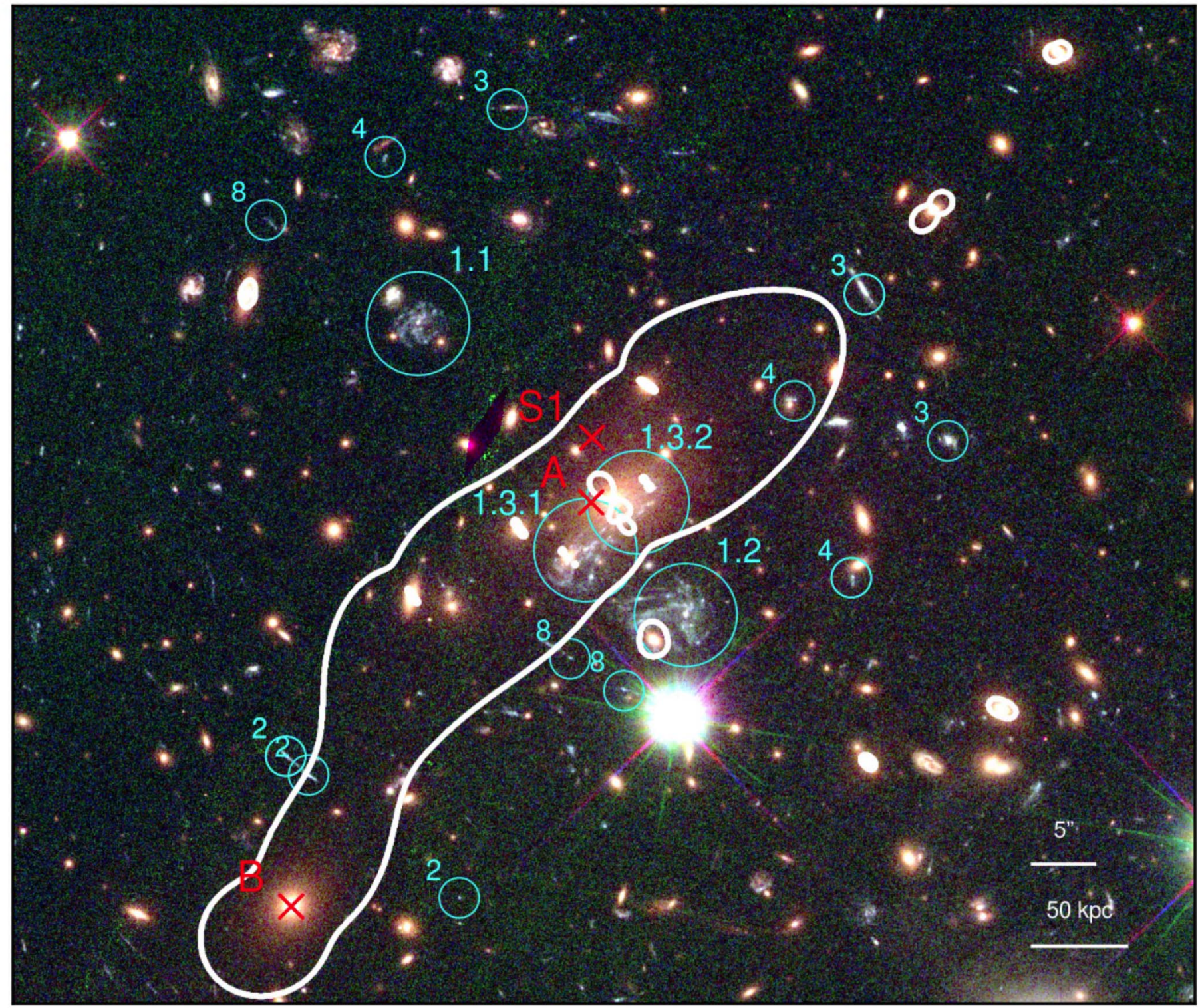




A light source passes behind a gravitational lens (point mass placed in the center of the image). The aqua circle is a source as it would be seen if there was no lens; white spots are the multiple images of the source.

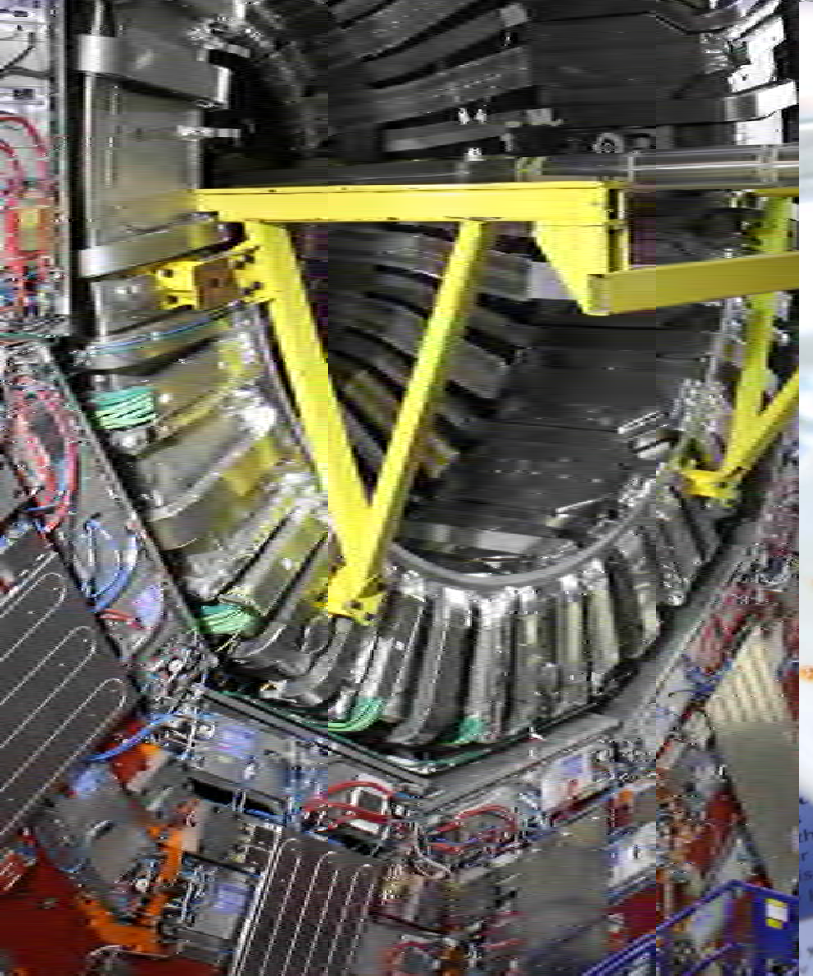


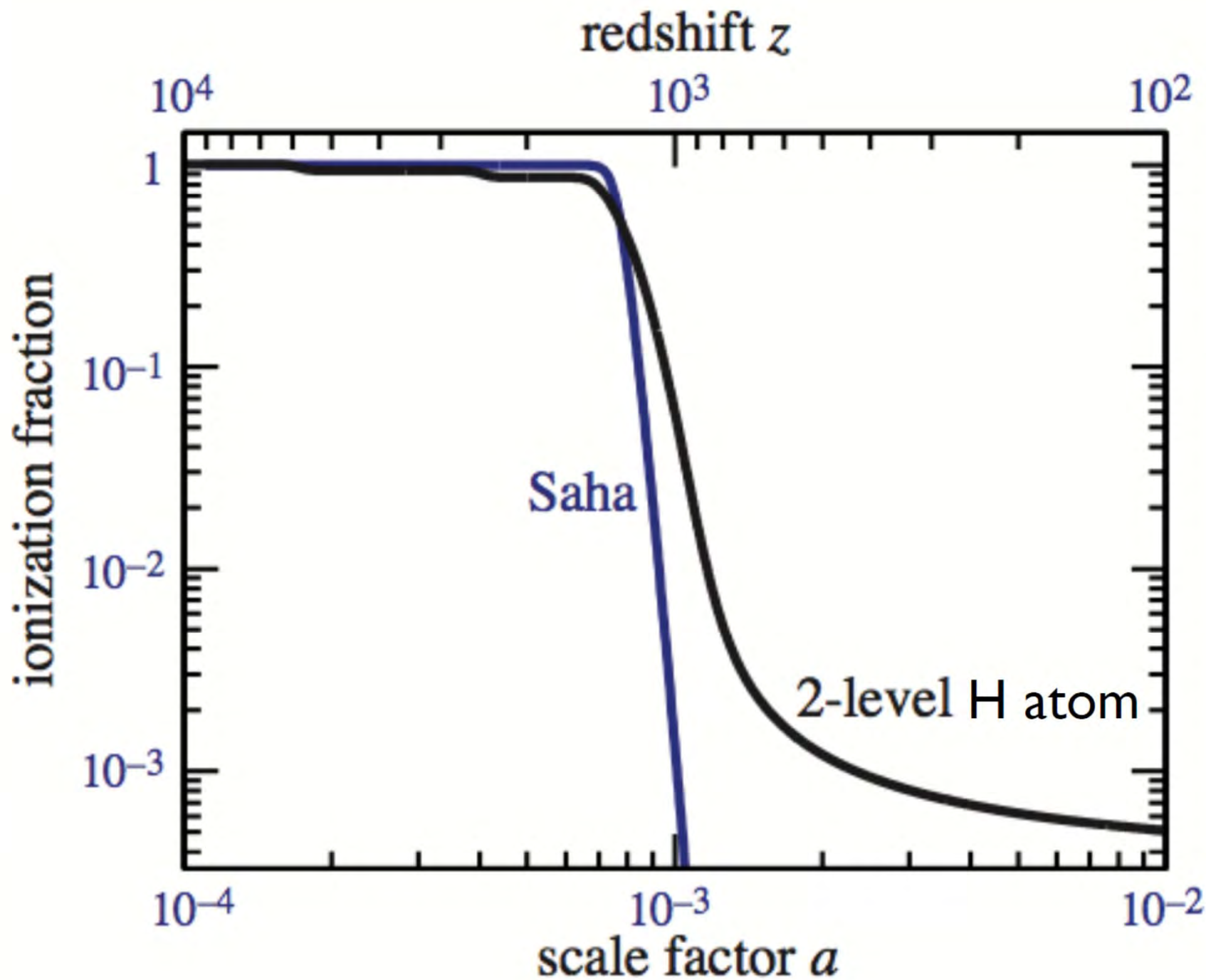
Galaxy Cluster CL0024 + 1654 ($z = 0.39$) with multiple images of a blue background galaxy. It shows very nicely the reddish images of cluster galaxies, the brightest of them concentrated around the center, and the bluish arcs.

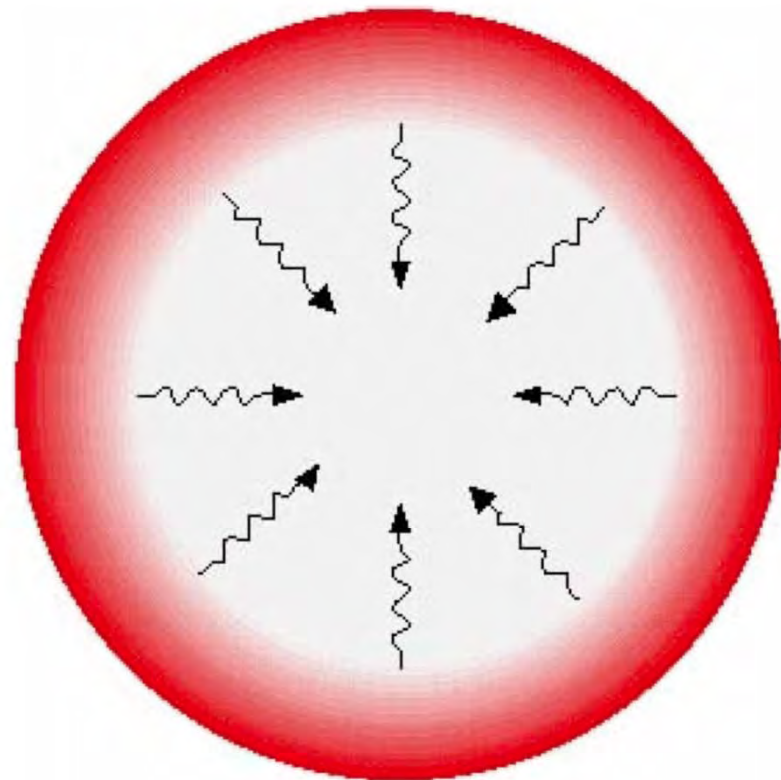








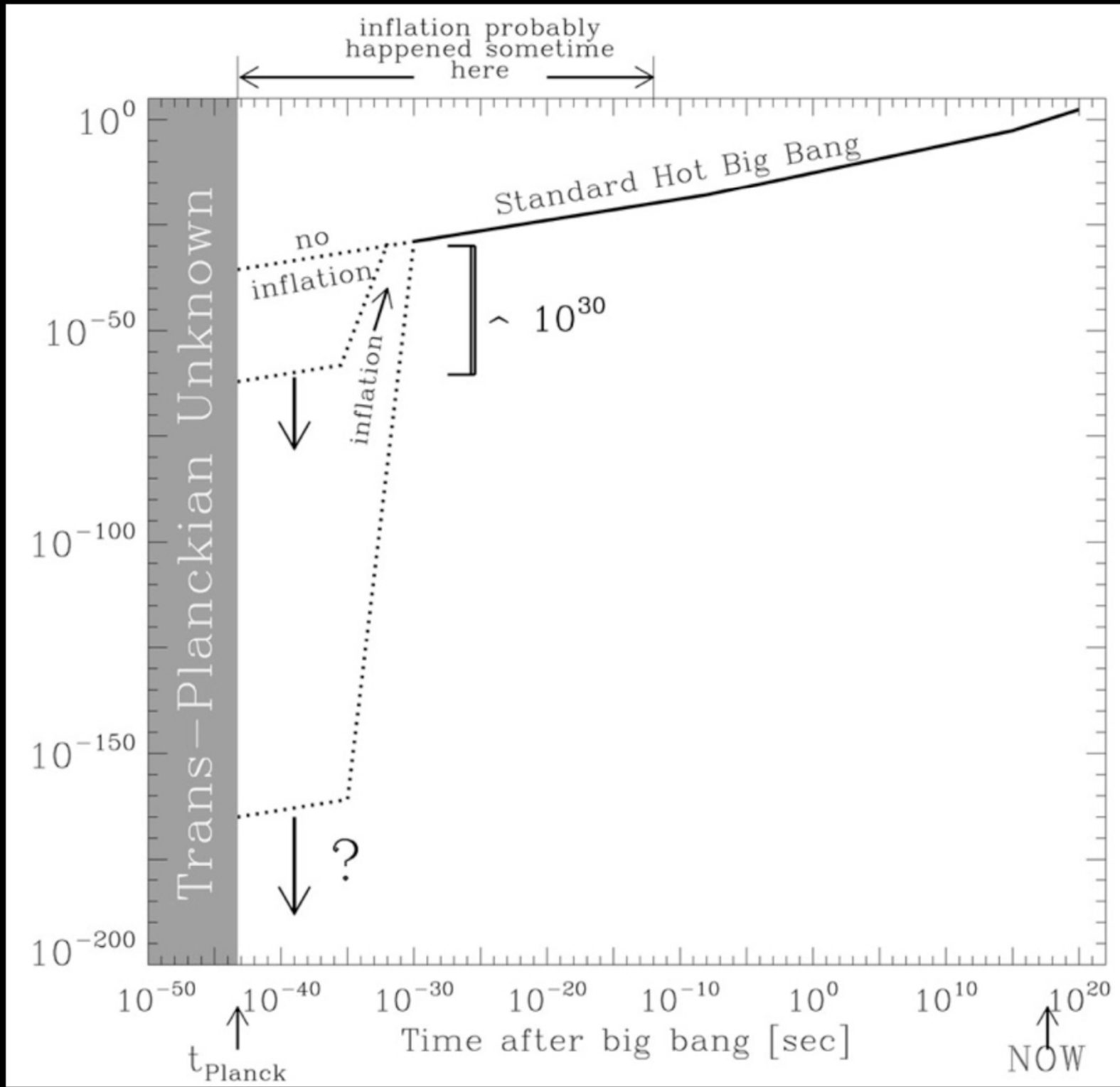


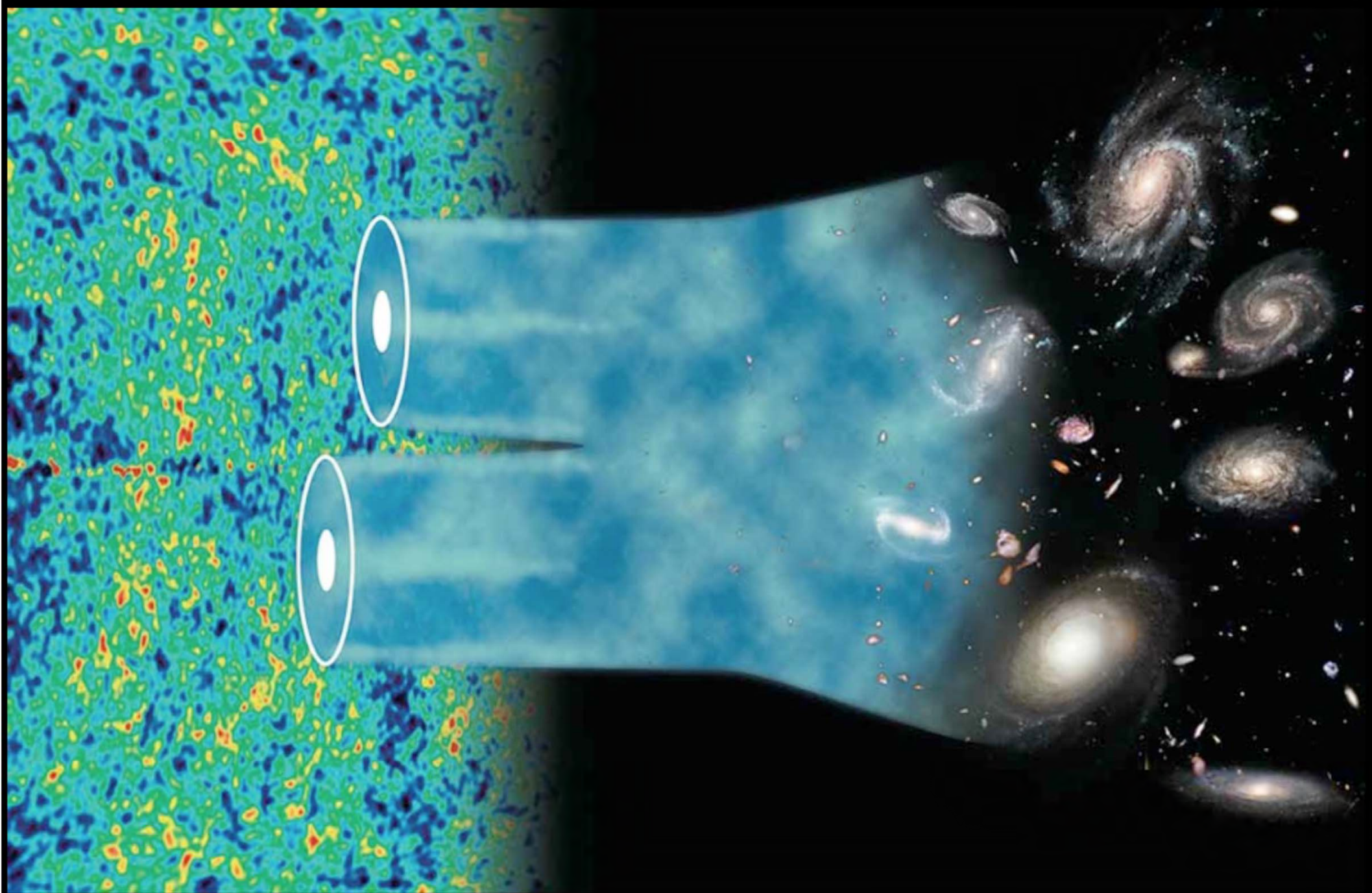


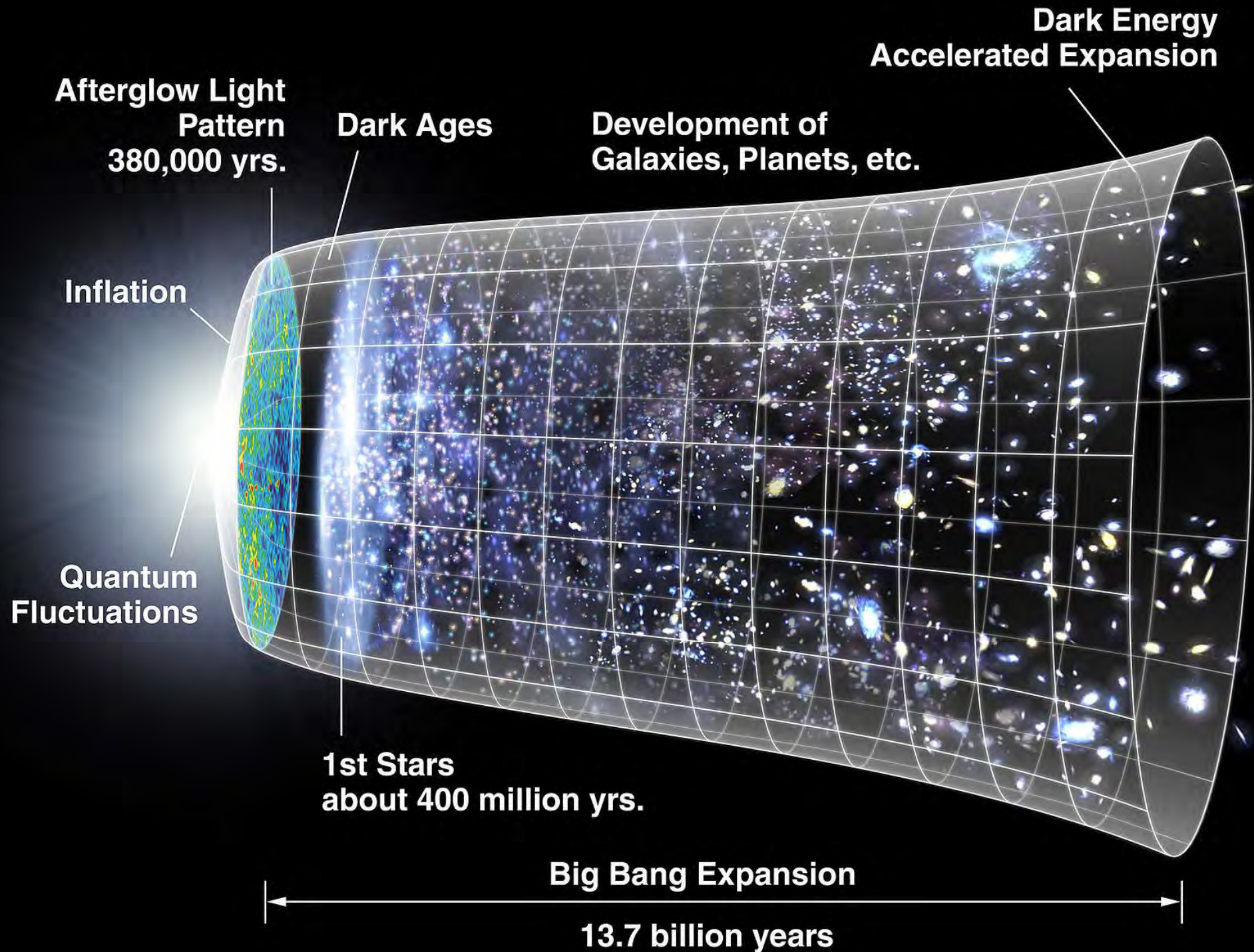
Event	Redshift	T (K)	t (Myr)
Radiation-Matter Equality	3380	9215	0.047
Recombination	1375	3750	0.251
Photon Decoupling	1090	2971	0.372
Last Scattering	1090	2971	0.372

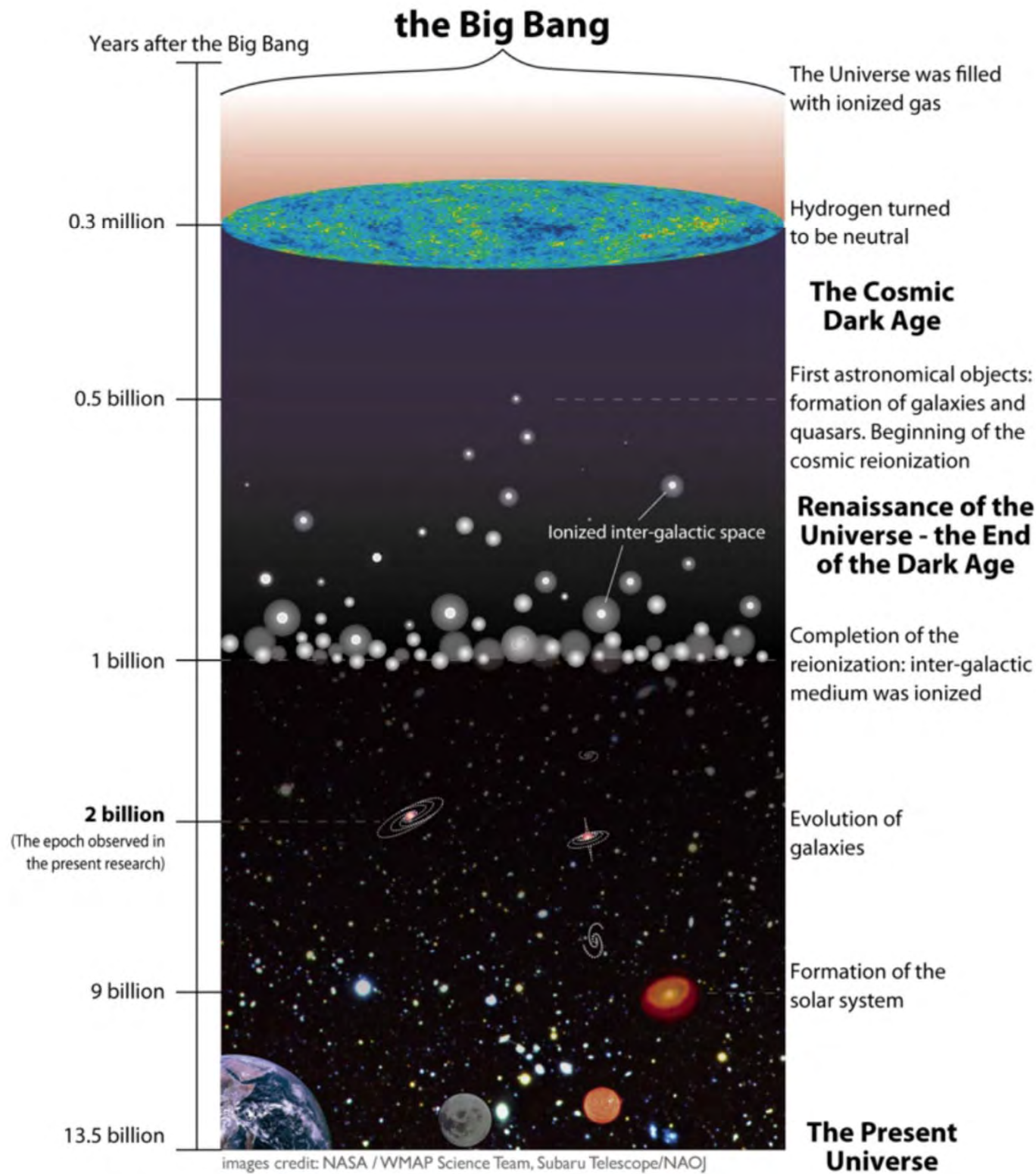
CMB parameters

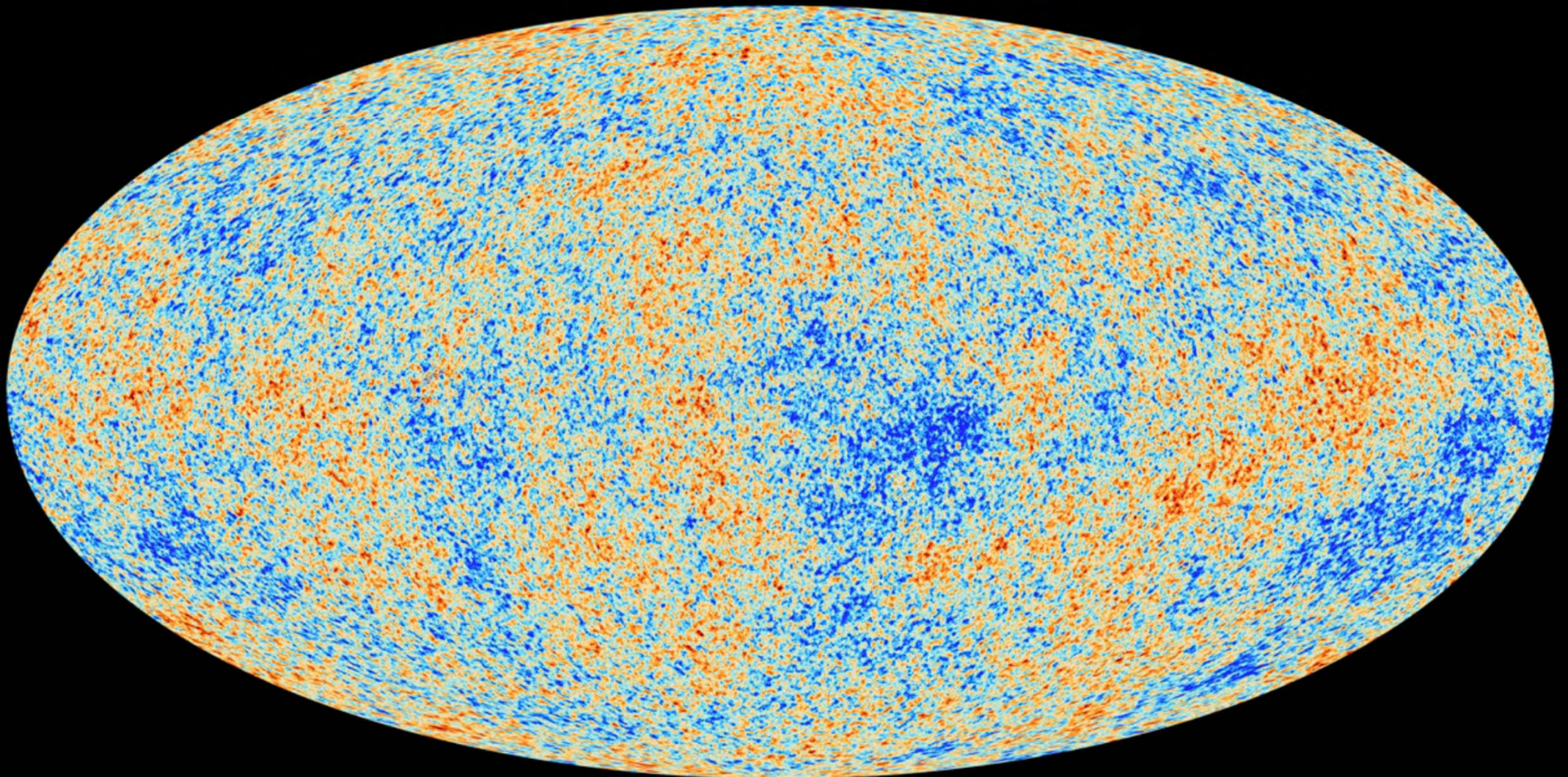
Property	Value
Temperature, T_{CMB}	2.7255 K
Peak Wavelength, λ_{peak}	0.106 cm
Number density of CMB photons, $n_{\gamma,0}$	411 cm^{-3}
Energy density of CMB photons, $u_{\gamma,0}$	0.26 eV cm^{-3}
Average photon energy, $\langle h\nu_{\text{CMB}} \rangle$	$6.34 \times 10^{-4} \text{ eV}$
Photon/Baryon ratio, $1/\eta$	1.64×10^9



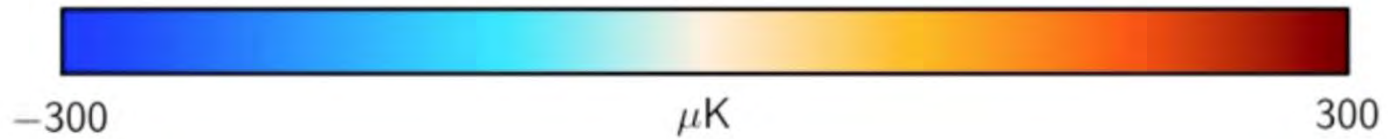
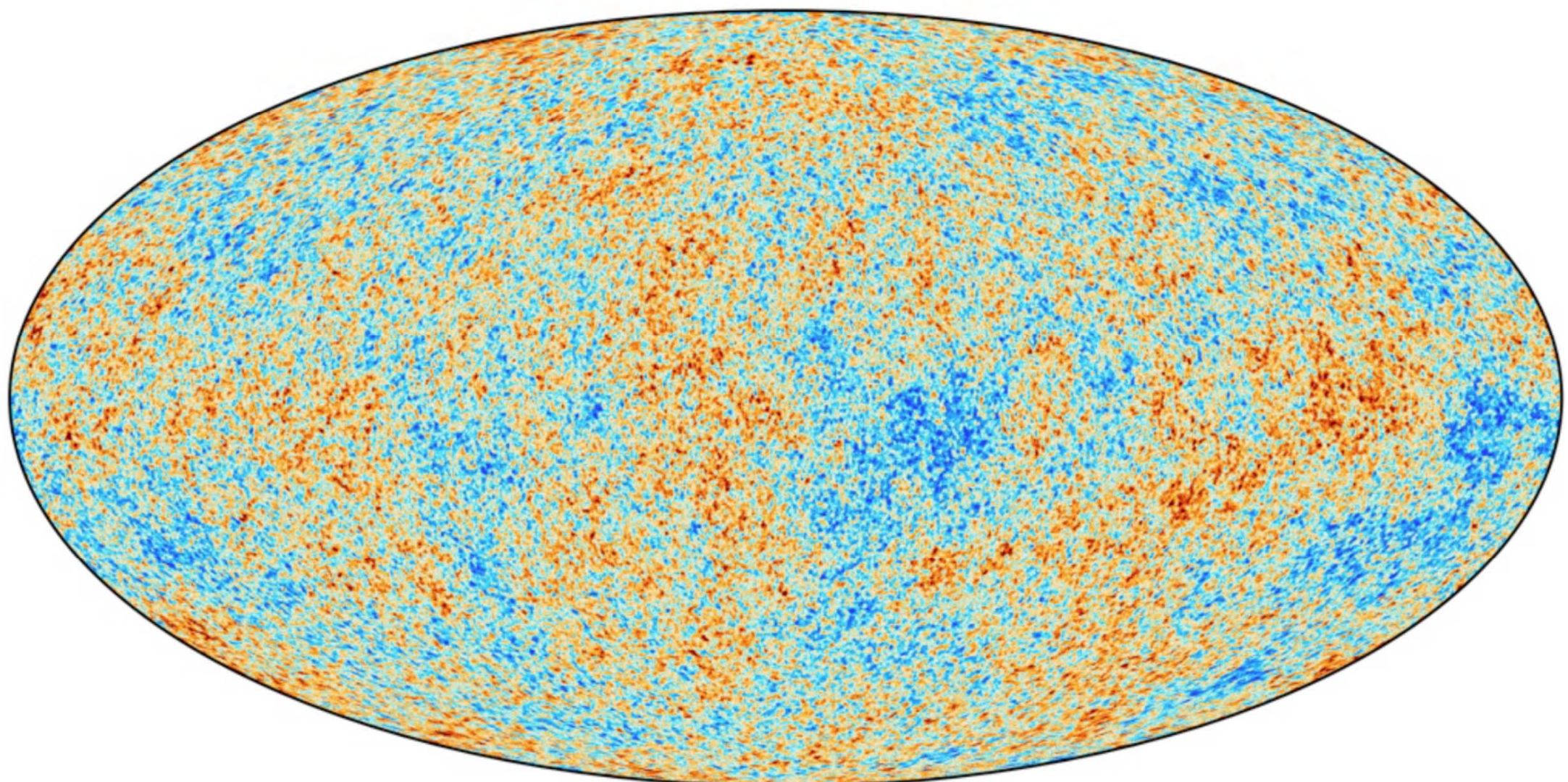








$$\frac{\delta T}{T}(\theta, \phi) = \frac{T(\theta, \phi) - \langle T \rangle}{\langle T \rangle}$$



List of spherical harmonics

$$Y_0^0(\theta, \varphi) = \frac{1}{2} \sqrt{\frac{1}{\pi}}$$

$$Y_1^{-1}(\theta, \varphi) = \frac{1}{2} \sqrt{\frac{3}{2\pi}} \sin \theta e^{-i\varphi}$$

$$Y_1^0(\theta, \varphi) = \frac{1}{2} \sqrt{\frac{3}{\pi}} \cos \theta$$

$$Y_1^1(\theta, \varphi) = \frac{-1}{2} \sqrt{\frac{3}{2\pi}} \sin \theta e^{i\varphi}$$

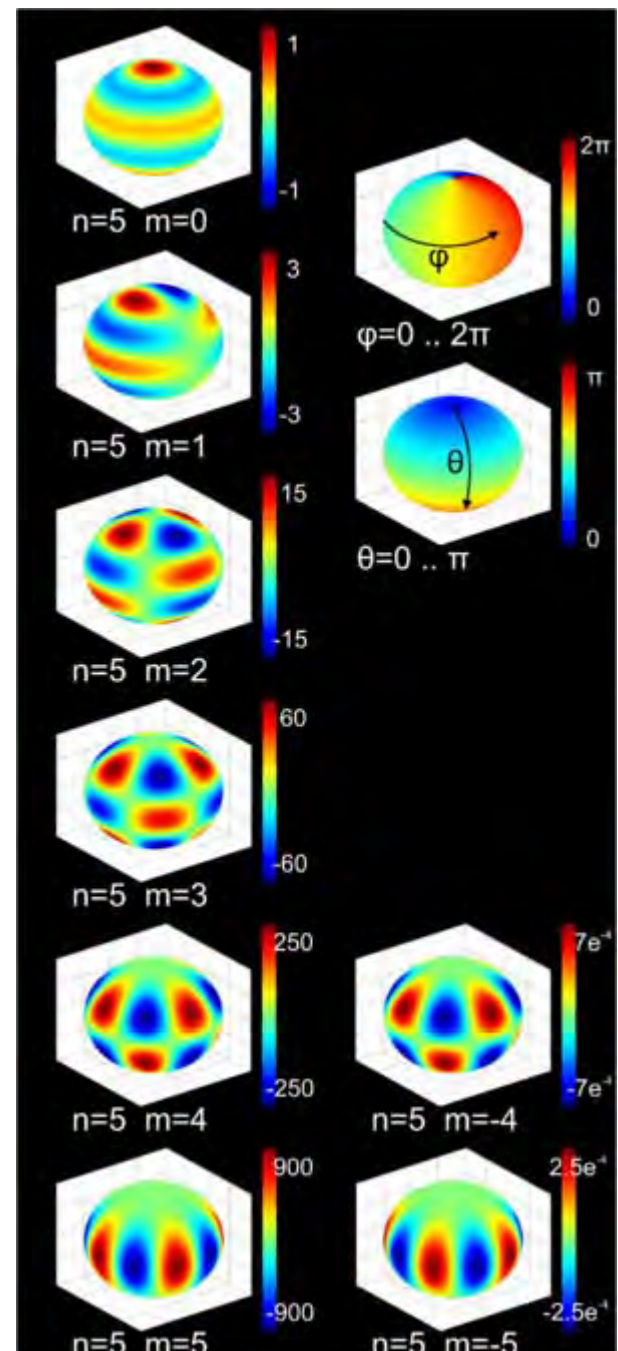
$$Y_2^{-2}(\theta, \varphi) = \frac{1}{4} \sqrt{\frac{15}{2\pi}} \sin^2 \theta e^{-2i\varphi}$$

$$Y_2^{-1}(\theta, \varphi) = \frac{1}{2} \sqrt{\frac{15}{2\pi}} \sin \theta \cos \theta e^{-i\varphi}$$

$$Y_2^0(\theta, \varphi) = \frac{1}{4} \sqrt{\frac{5}{\pi}} (3 \cos^2 \theta - 1)$$

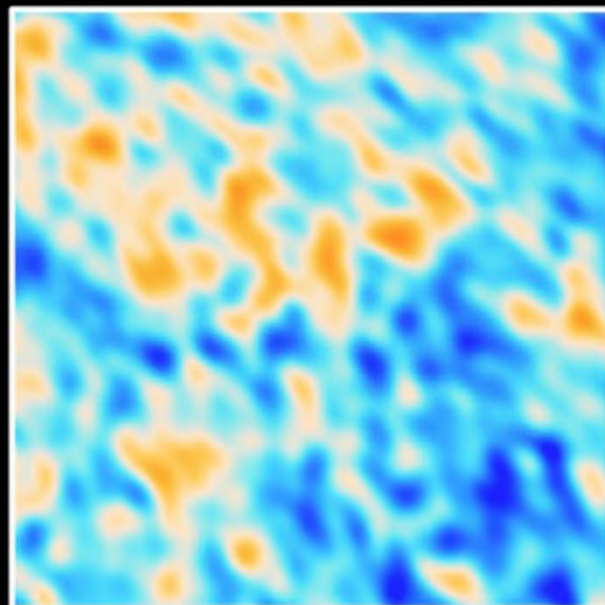
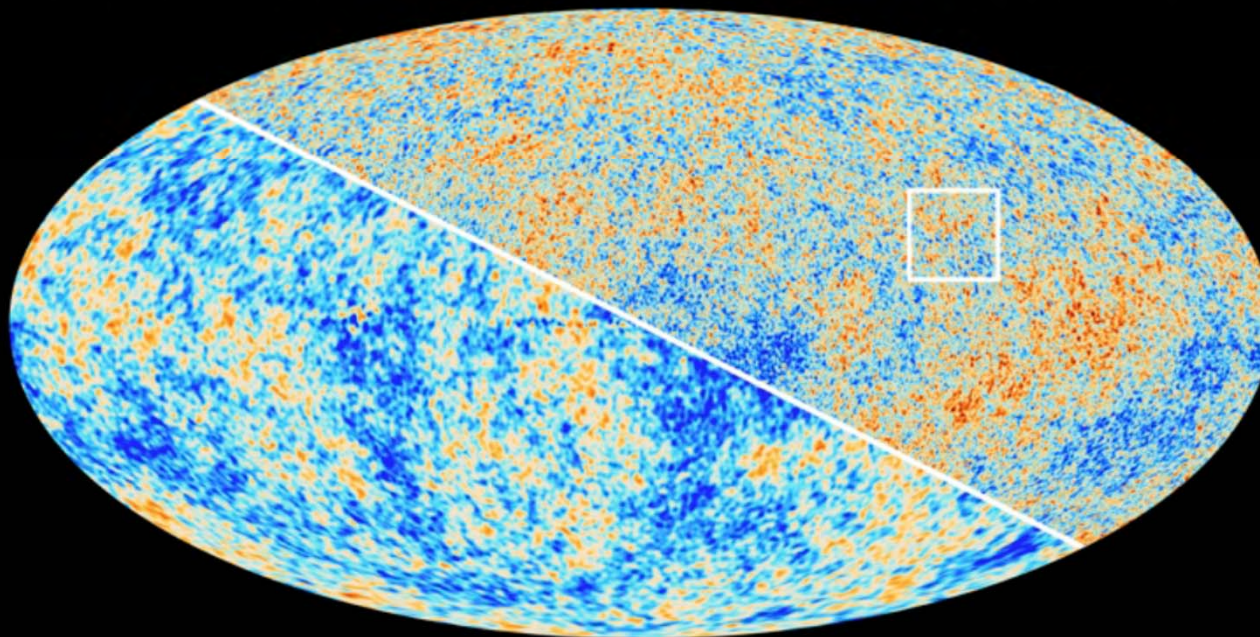
$$Y_2^1(\theta, \varphi) = \frac{-1}{2} \sqrt{\frac{15}{2\pi}} \sin \theta \cos \theta e^{i\varphi}$$

$$Y_2^2(\theta, \varphi) = \frac{1}{4} \sqrt{\frac{15}{2\pi}} \sin^2 \theta e^{2i\varphi}$$

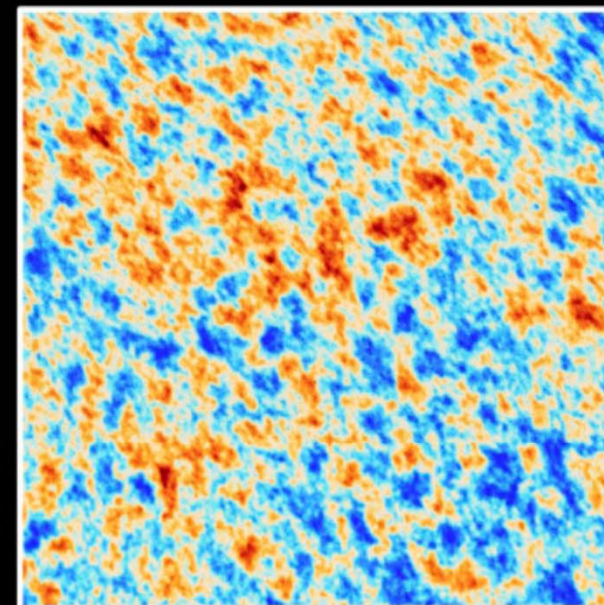


3D color plot of the spherical harmonics of degree $n = 5$. Note that $n = \ell$.

The Cosmic Microwave Background as seen by Planck and WMAP



WMAP



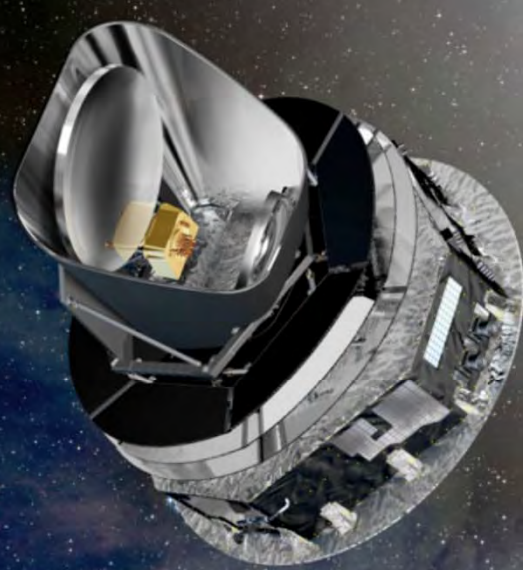
Planck



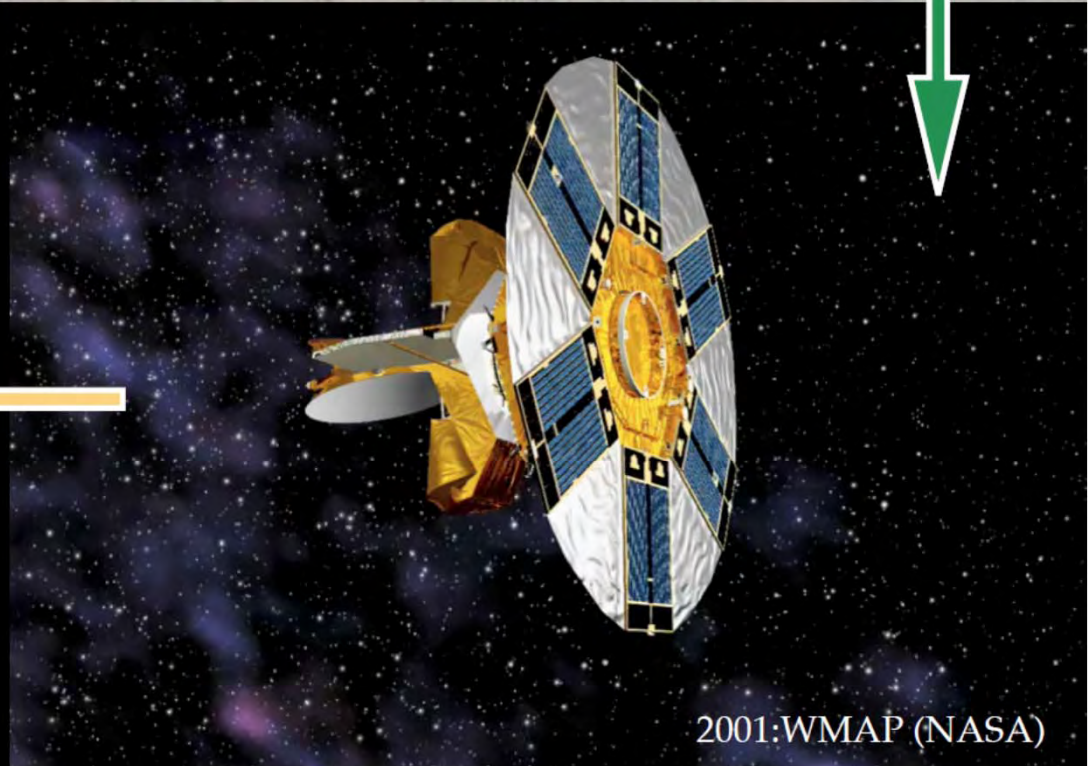
1989: COBE (NASA)



1998: BOOMERanG (Caltech / Rome)

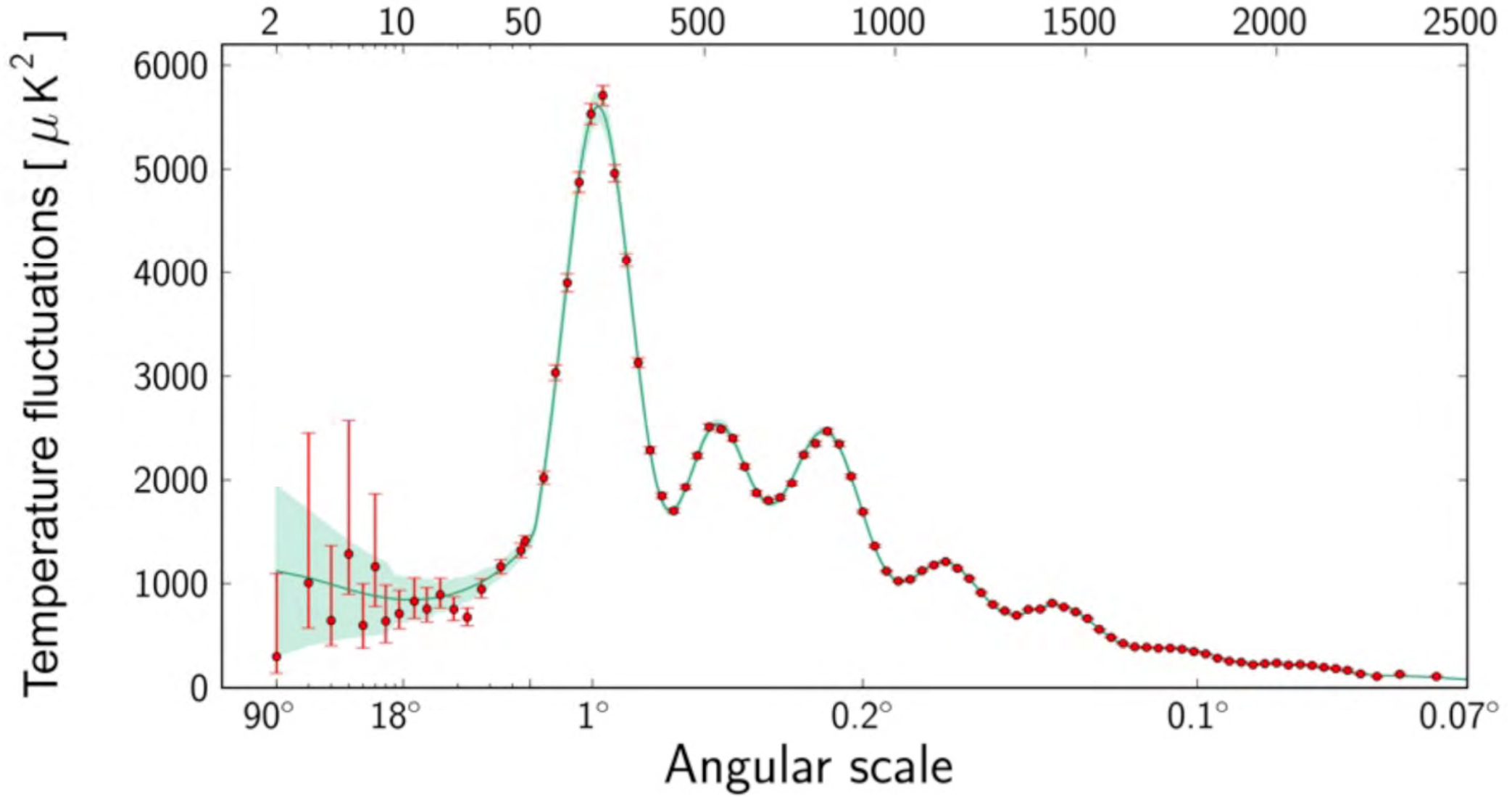


2009: Planck (ESA)

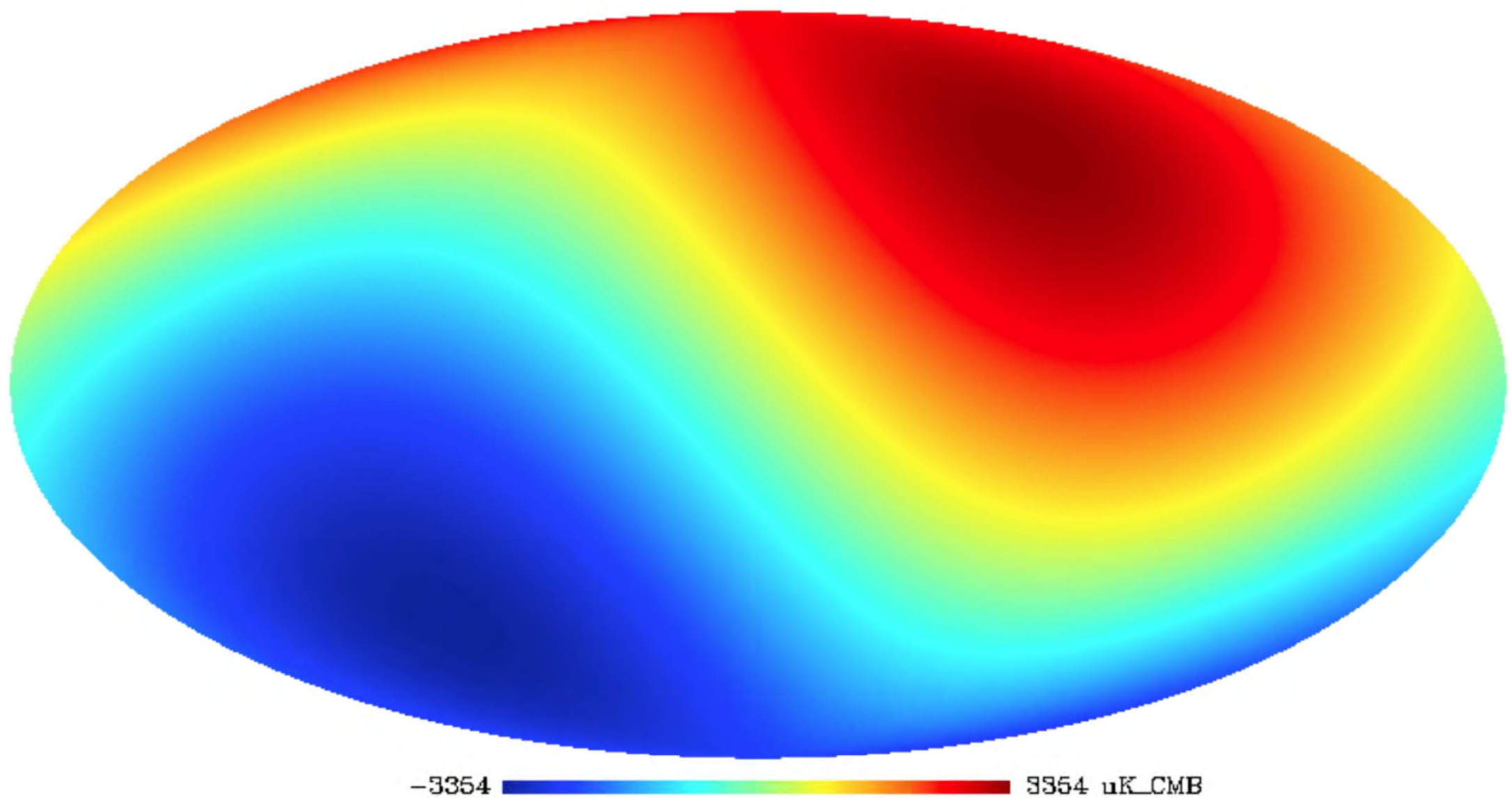


2001: WMAP (NASA)

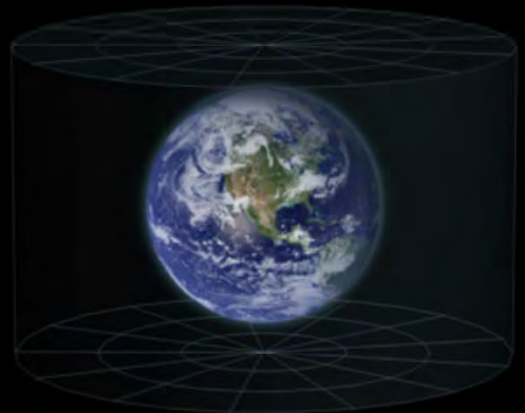
Multipole moment, ℓ



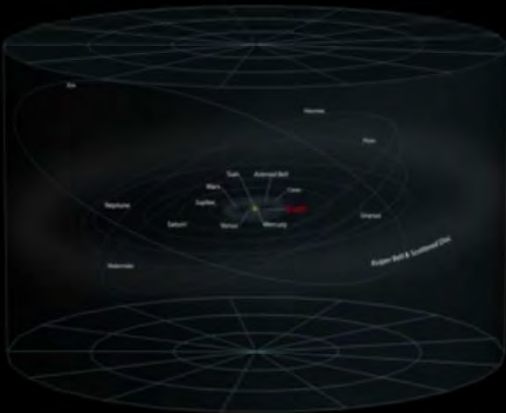
CMB dipole



Earth



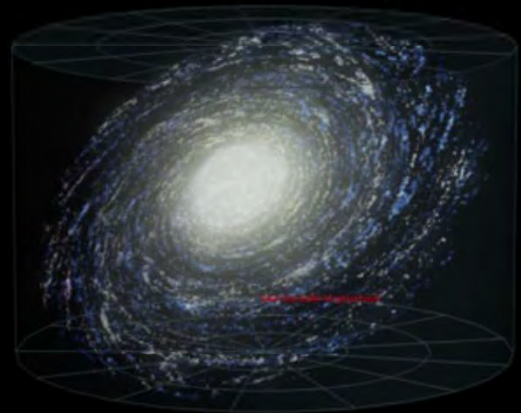
Solar System



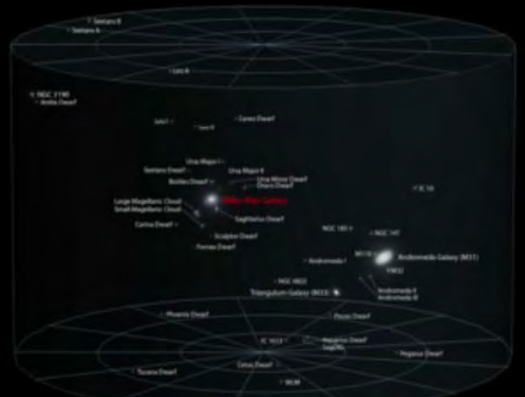
Solar Interstellar Neighborhood



Milky Way Galaxy

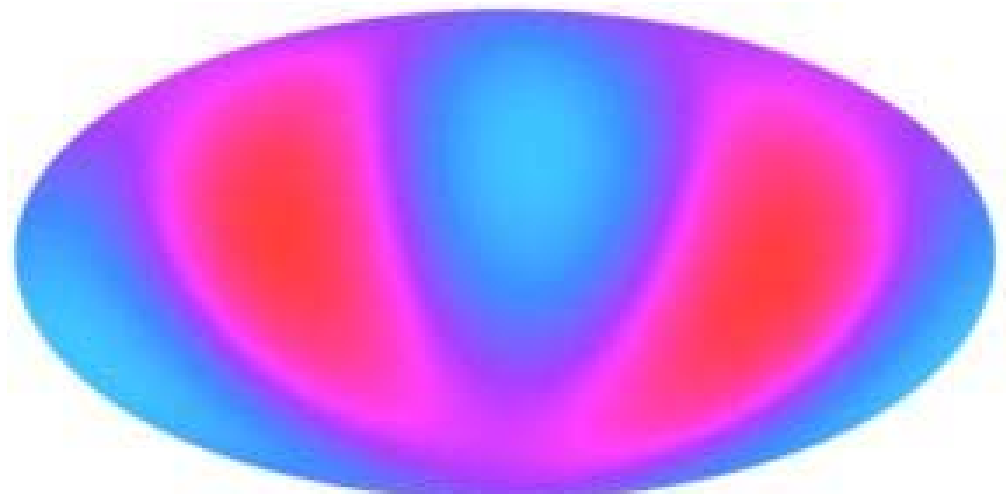


Local Galactic Group

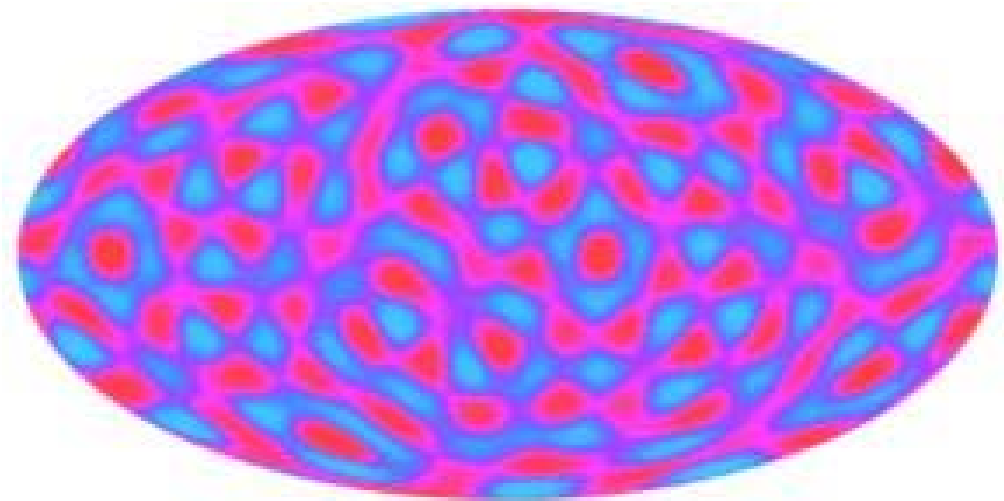


Virgo Supercluster





$\ell = 2$



$\ell = 16$

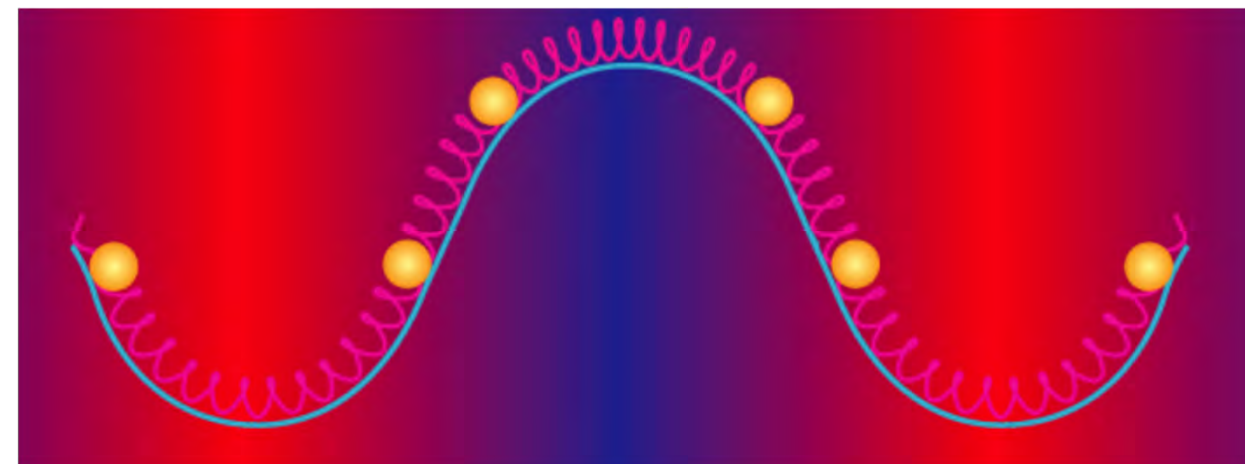
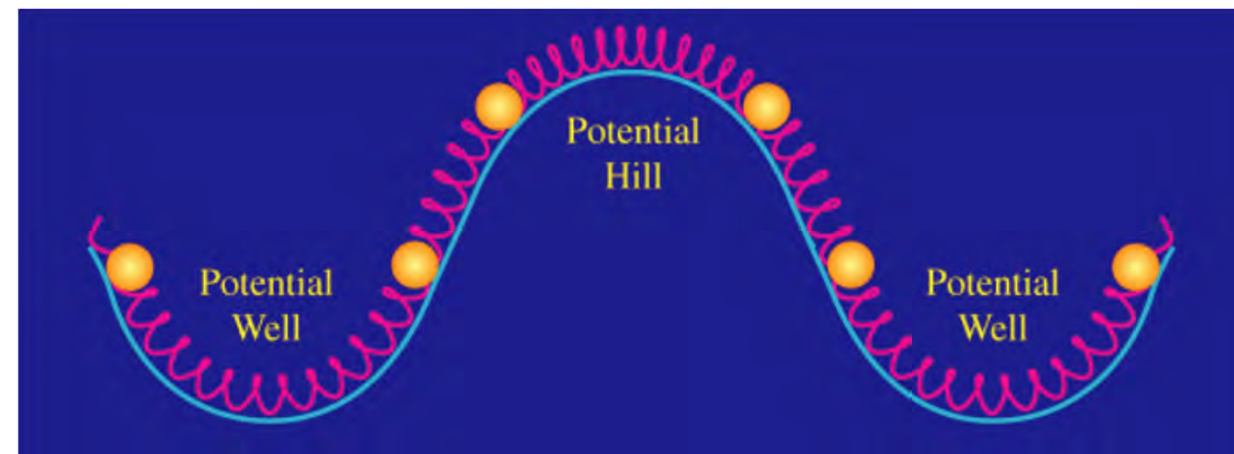
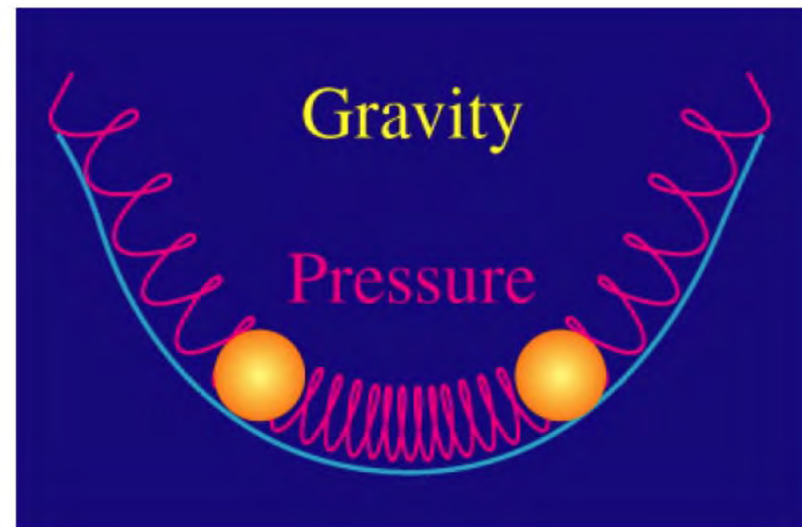
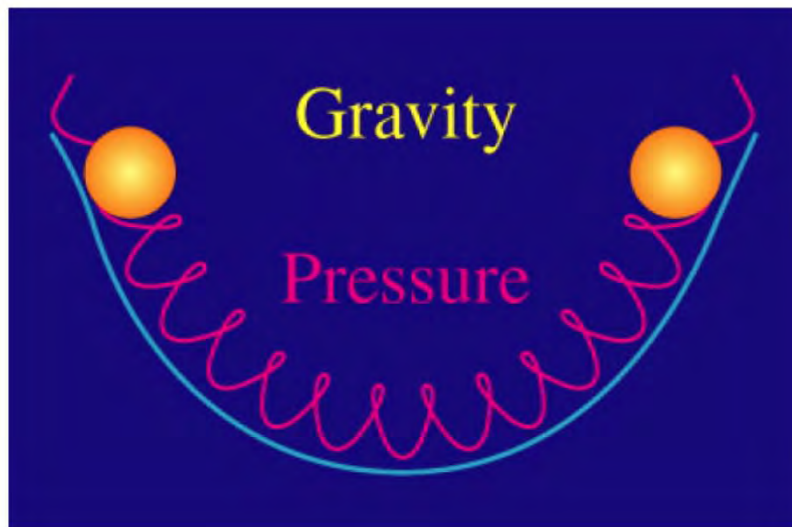
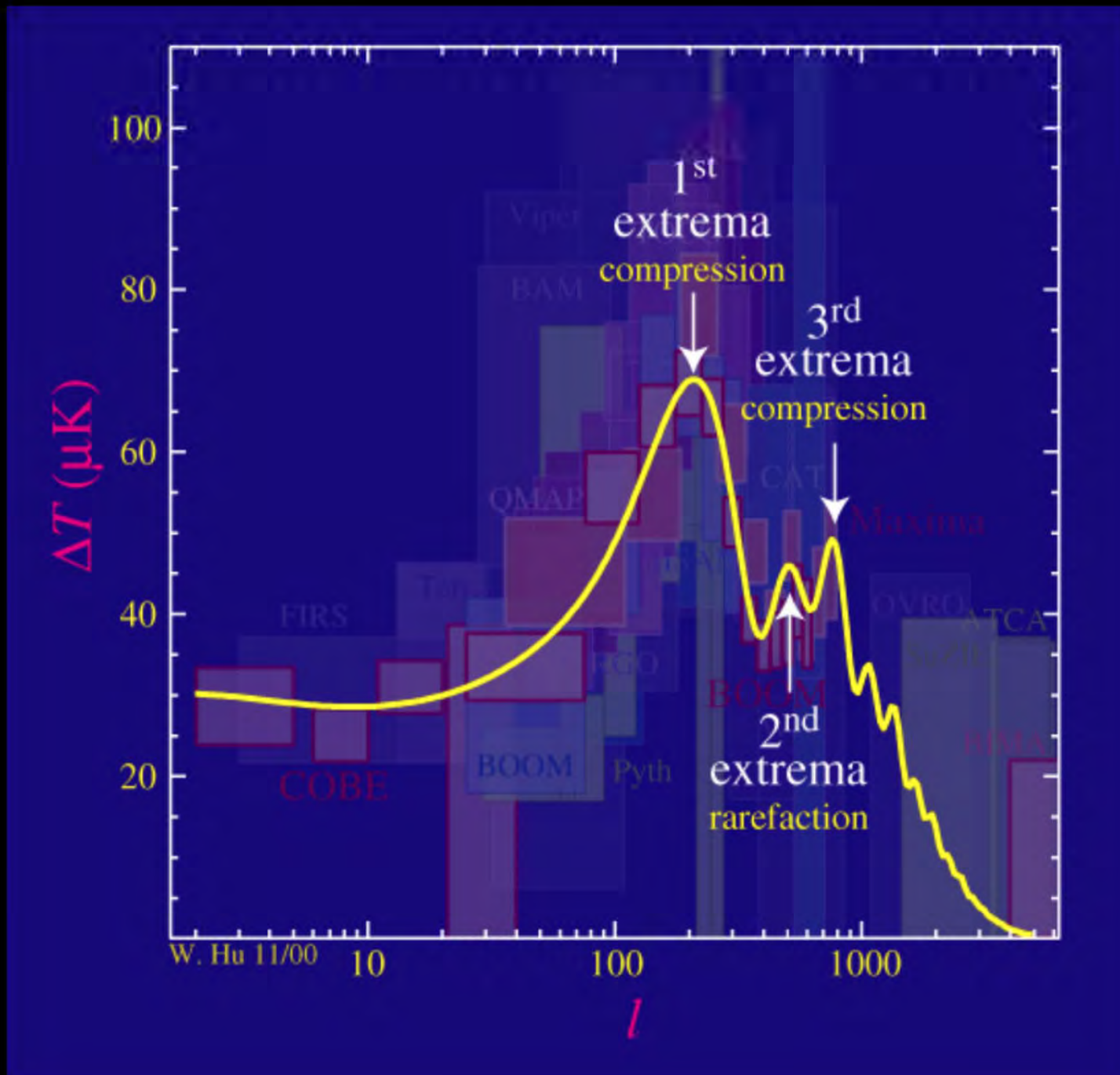
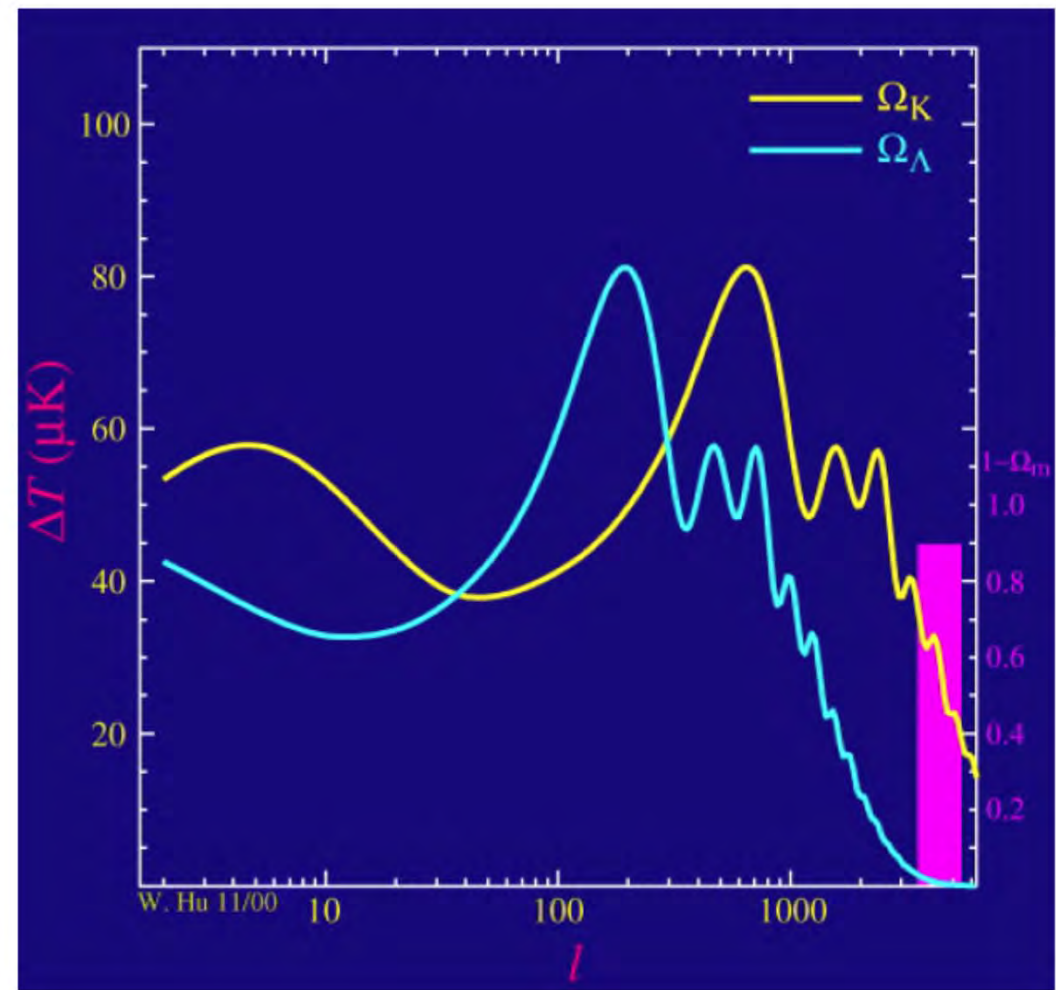
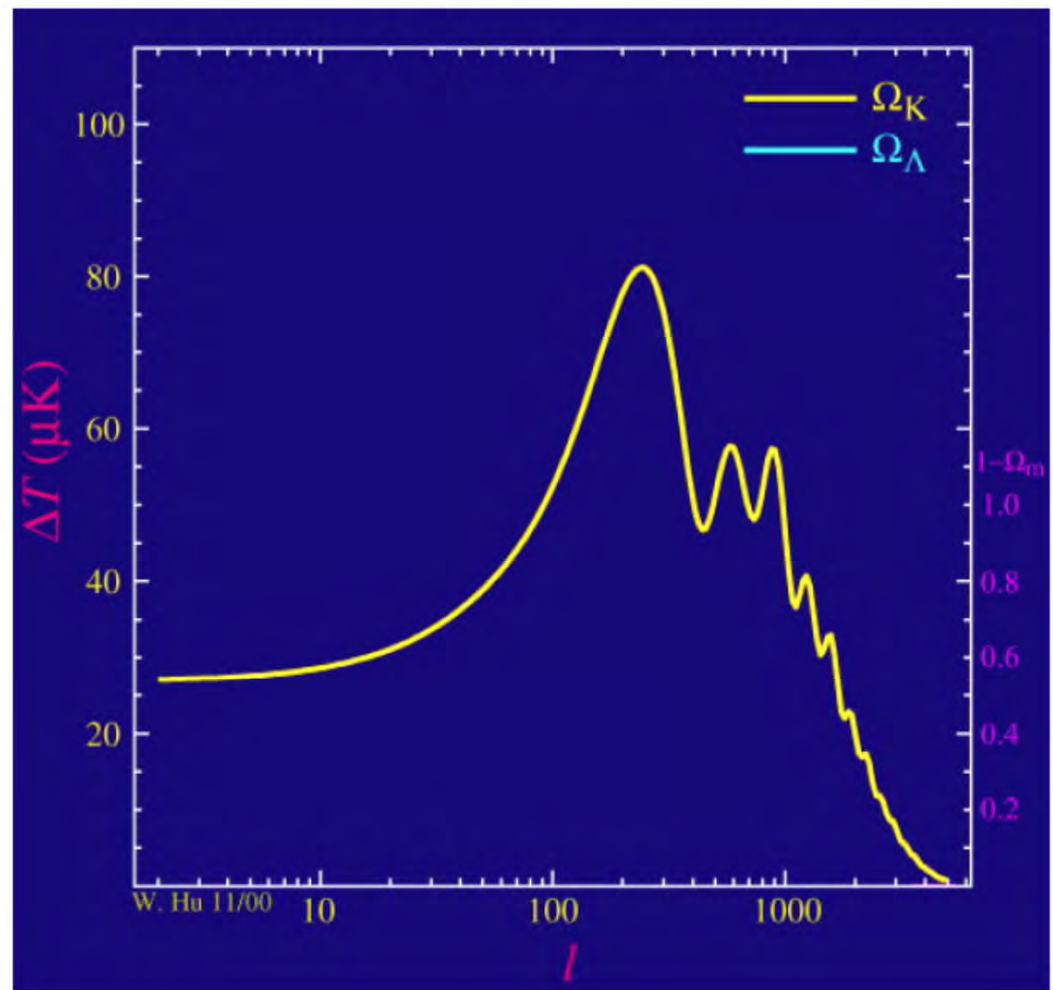


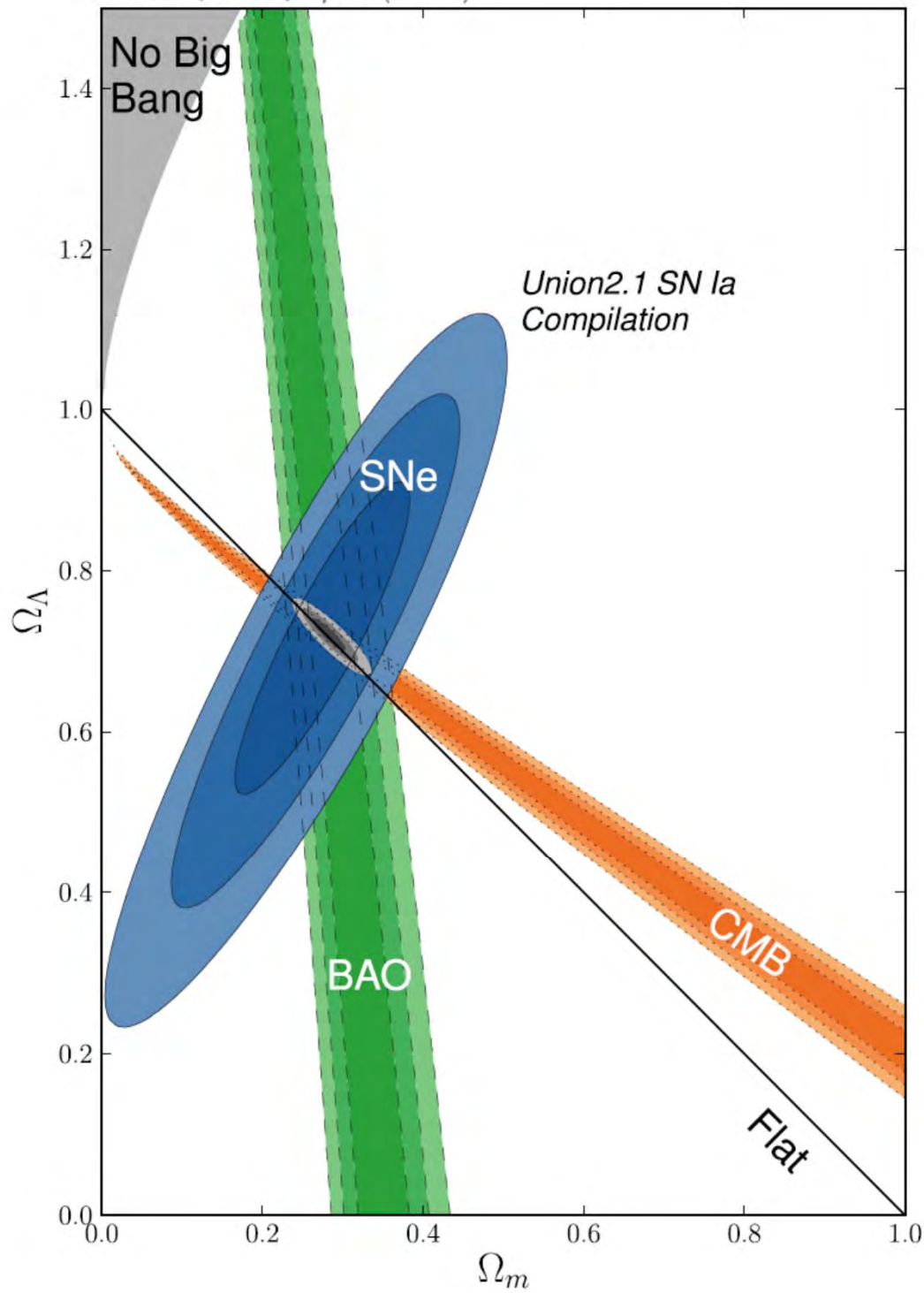
Figure credit: Wayne Hu

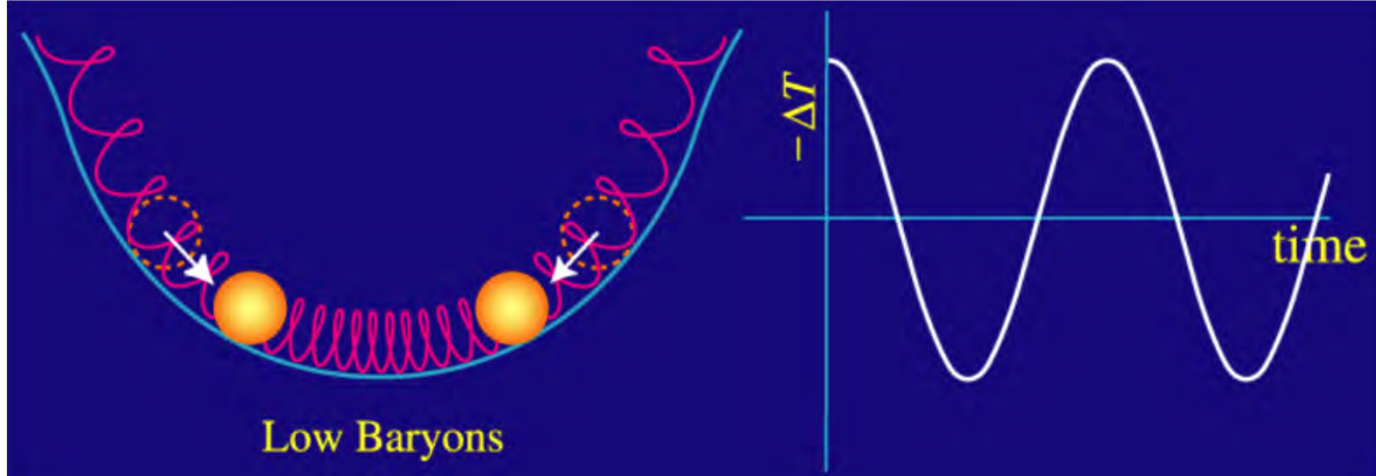


(Figure credit: Wayne Hu).

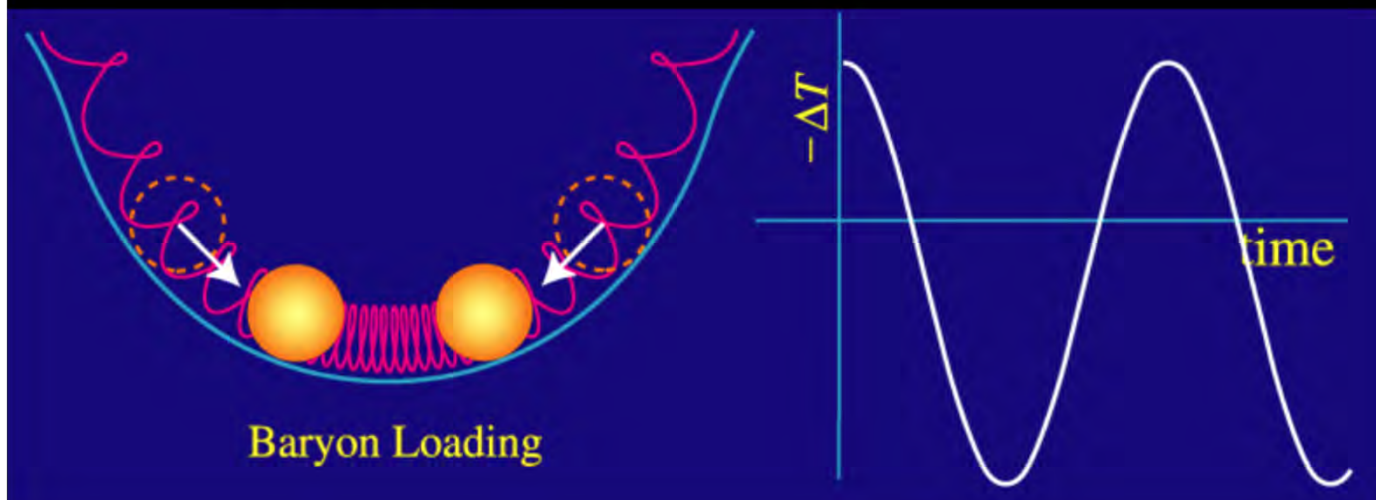


(Figure credit: Wayne Hu).

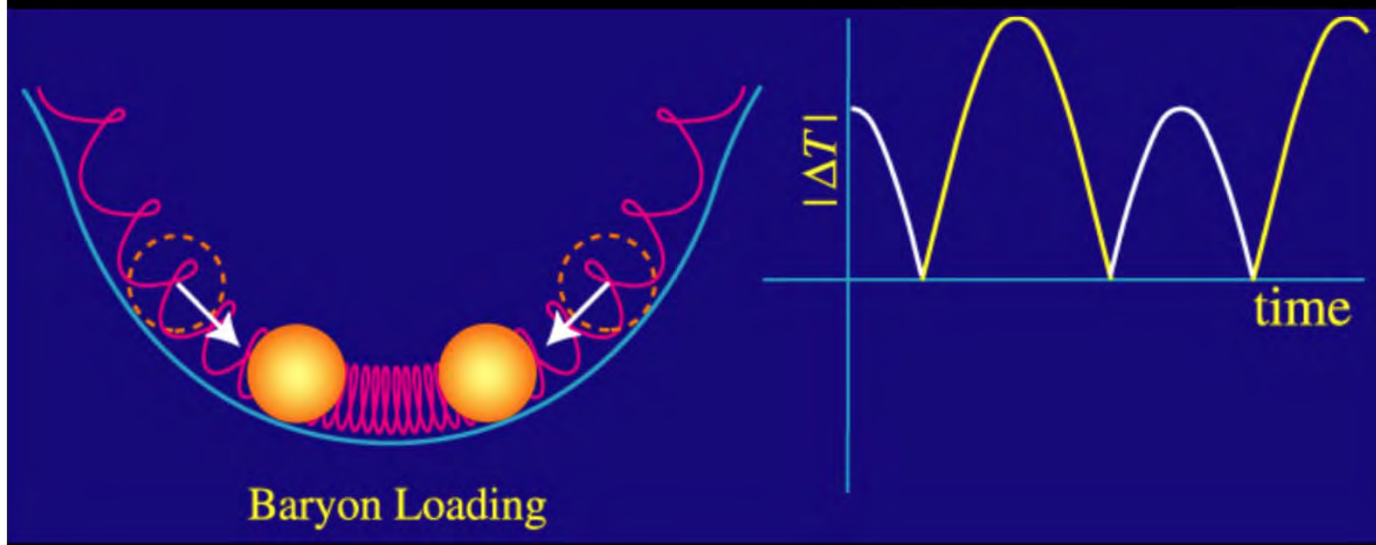




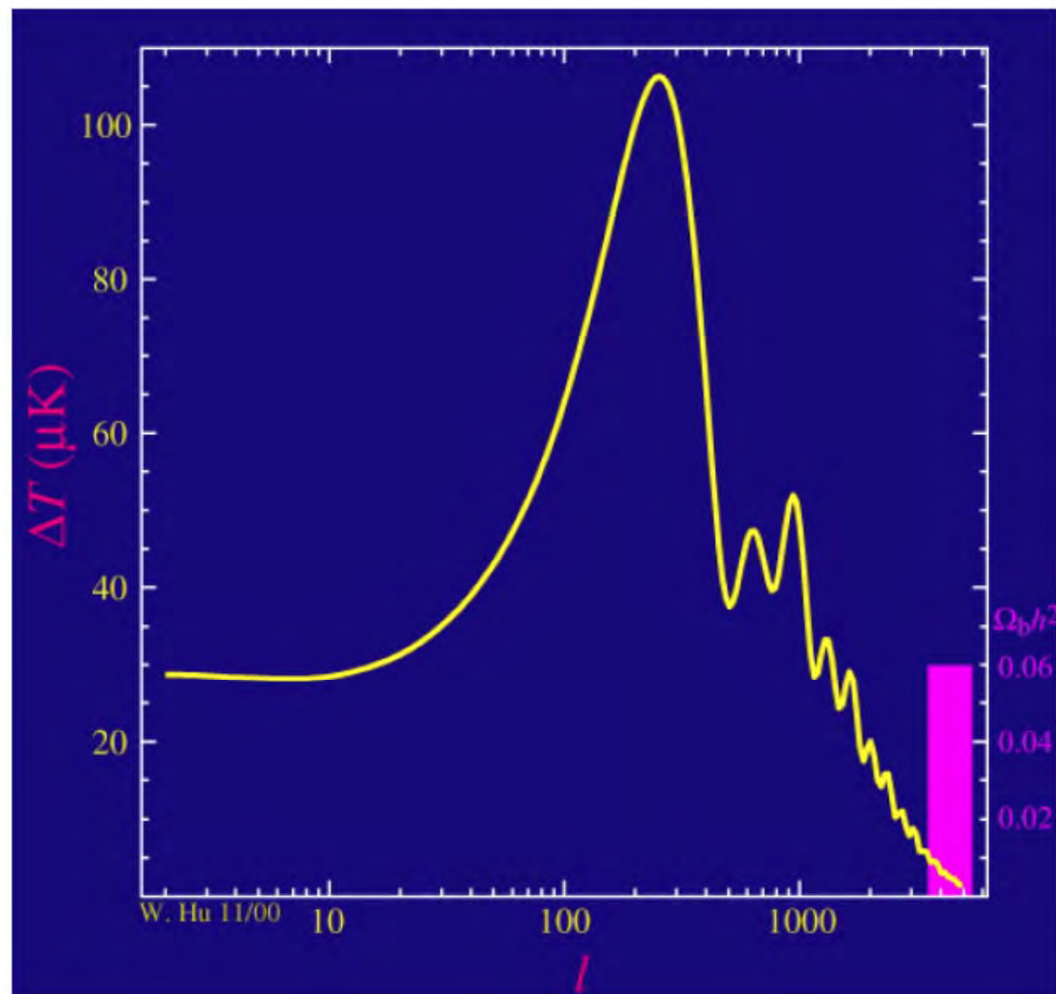
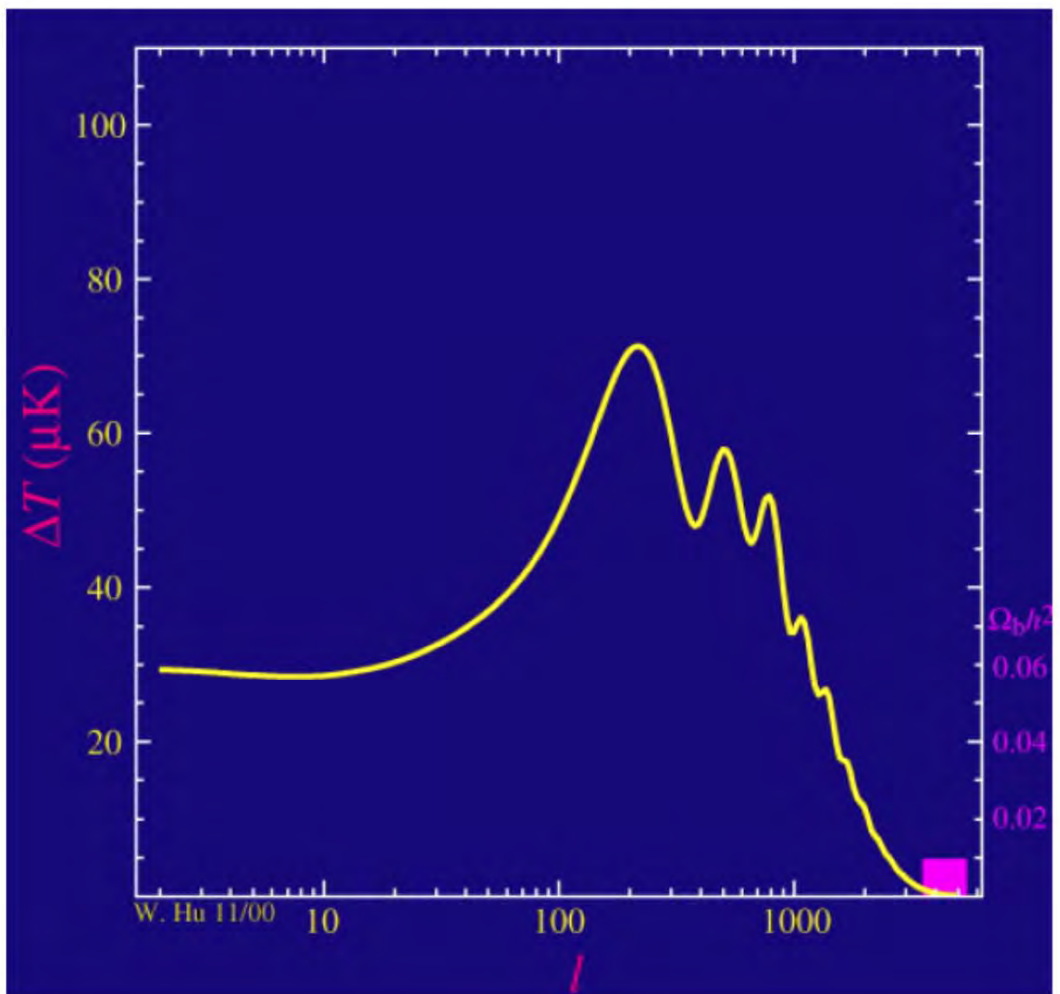
Low Baryons

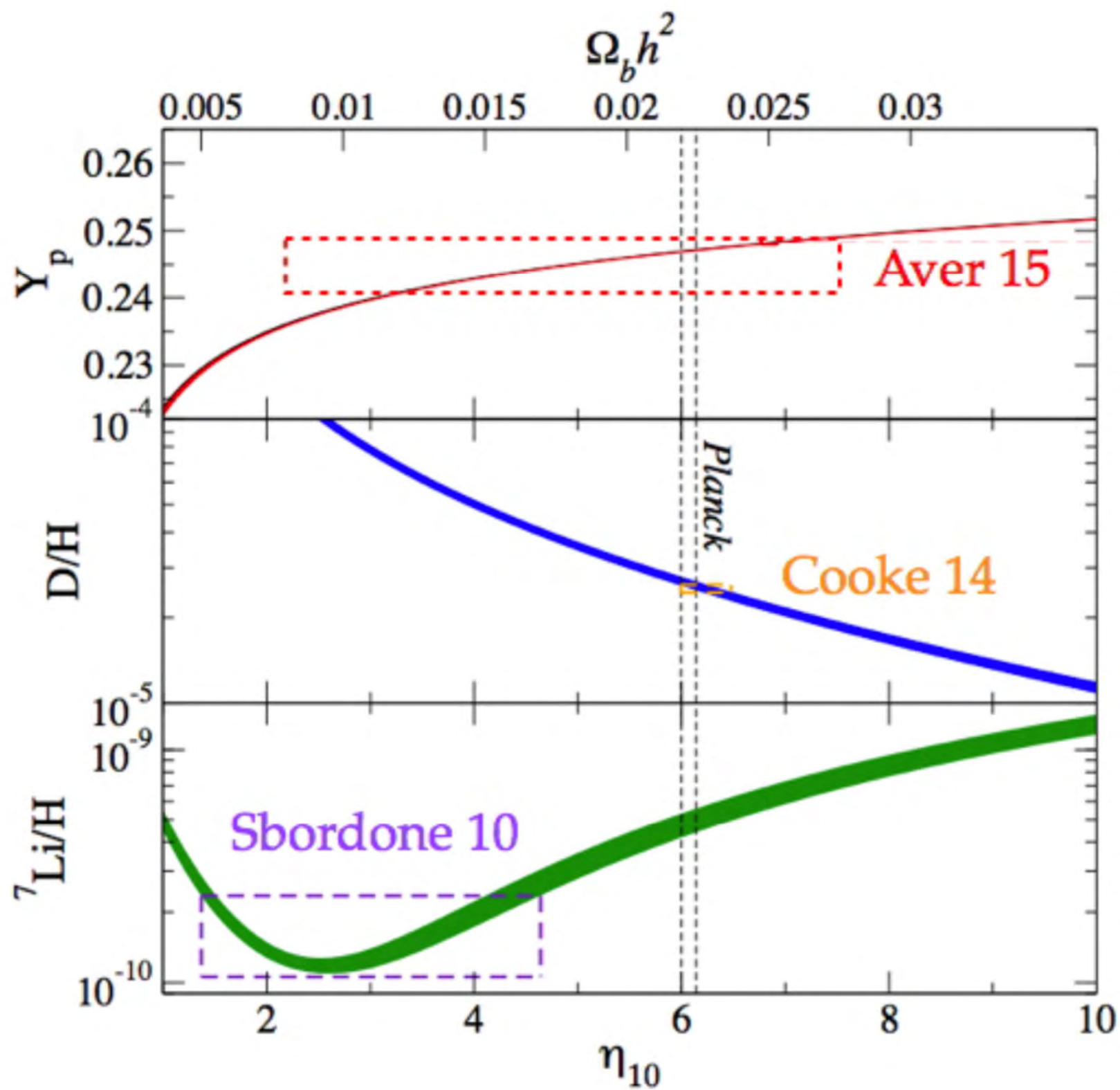


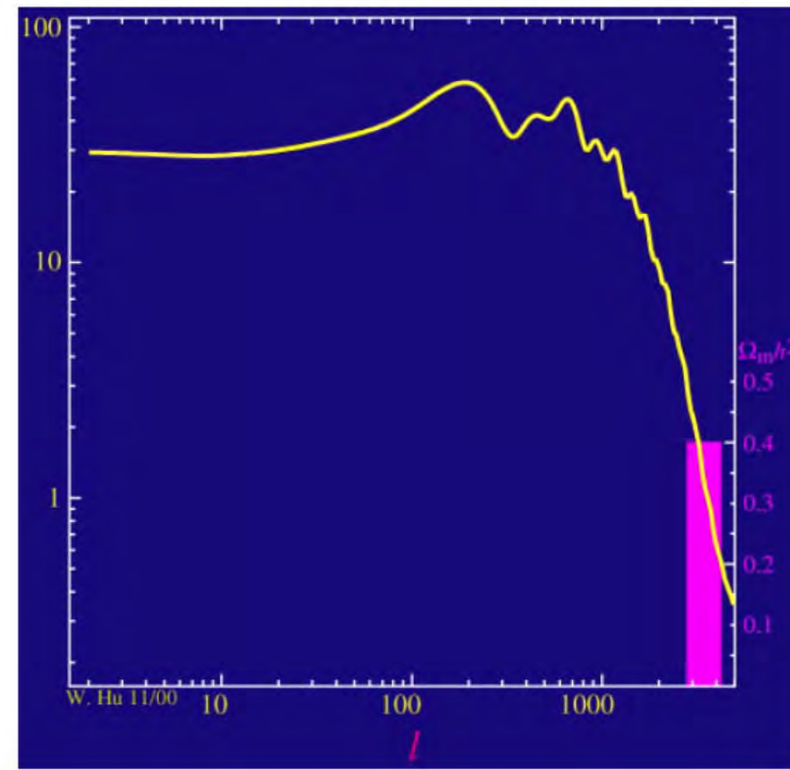
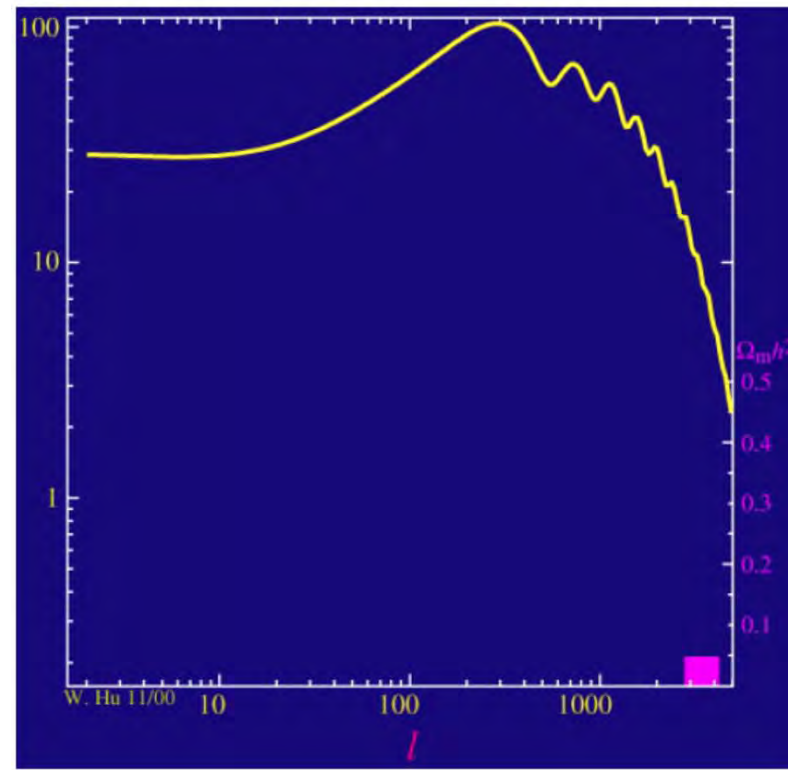
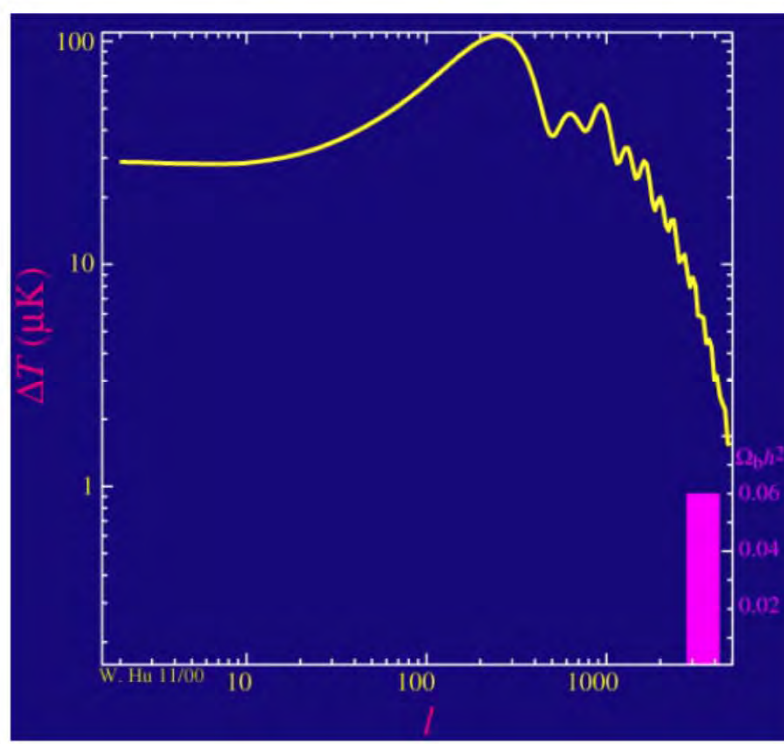
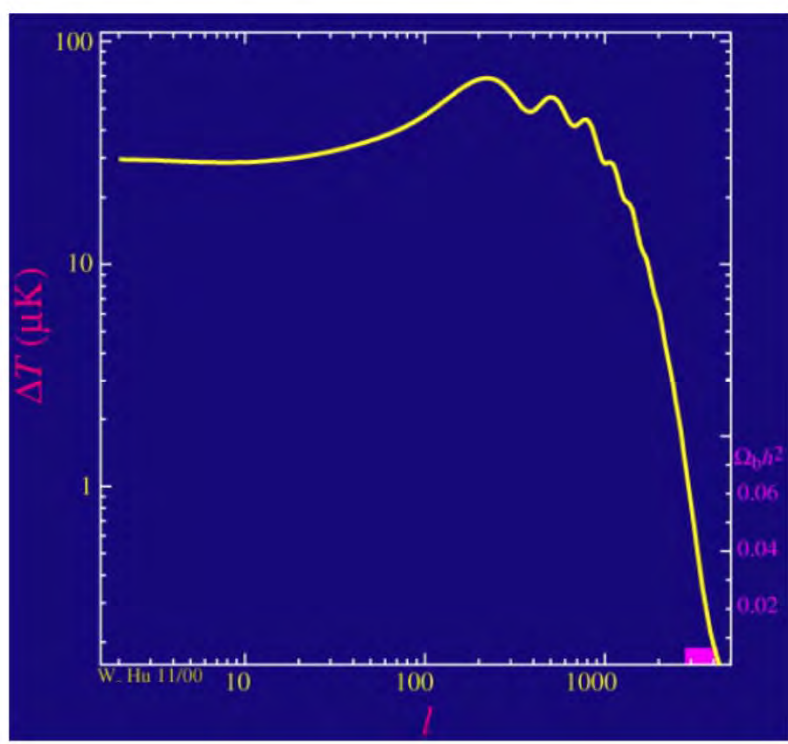
Baryon Loading



Baryon Loading







- [Find Similar Abstracts](#) (with [default settings below](#))
- [Full Refereed Journal Article \(PDF/Postscript\)](#)
- [Full Refereed Scanned Article \(GIF\)](#)
- [References in the article](#)
- [Citations to the Article \(1528\) \(Citation History\)](#)
- [Refereed Citations to the Article](#)
- [Associated Articles](#)
- [Also-Read Articles \(Reads History\)](#)
- [HEP/Spires Information](#)
- [Translate This Page](#)

Title: Perturbations of a Cosmological Model and Angular Variations of the Microwave Background

Authors: [Sachs, R. K.](#); [Wolfe, A. M.](#)

Publication: Astrophysical Journal, vol. 147, p.73 ([ApJ Homepage](#))

Publication Date: 01/1967

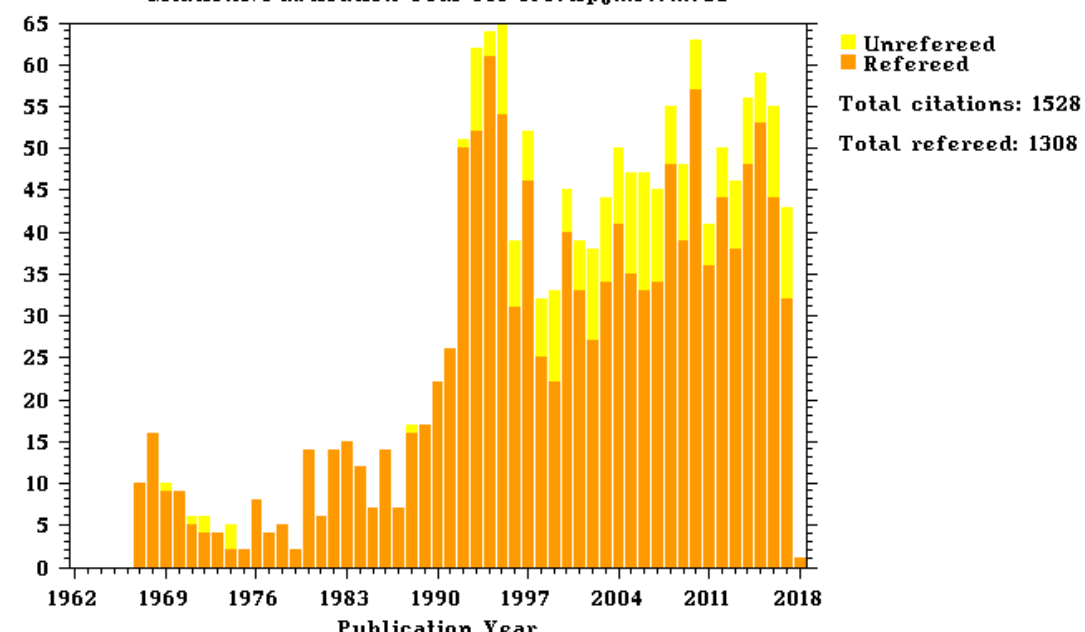
Origin: [ADS](#)

DOI: [10.1086/148982](https://doi.org/10.1086/148982)

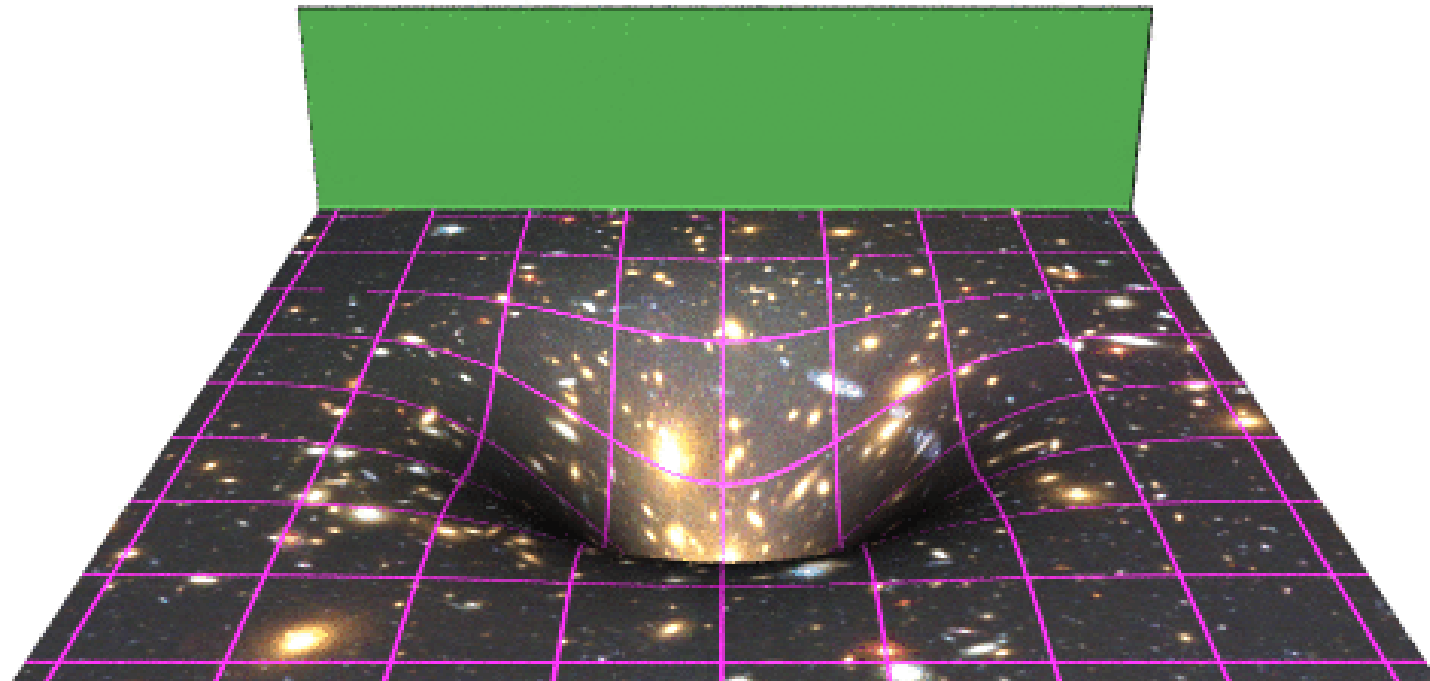
Bibliographic Code: [1967ApJ...147...73S](#)

We consider general-relativistic, spatially homogeneous, and isotropic $k = 0$ cosmological models with either pressure zero or pressure one-third the energy density. The equations for general linearized perturbations away from these models are explicitly integrated to obtain density fluctuations, rotational perturbations, and gravitational waves. The equations for light rays in the perturbed models are integrated. The models are used to estimate the anisotropy of the microwave radiation, assuming this radiation is cosmological. It is estimated that density fluctuations now of order 10 per cent with characteristic lengths now of order 1000 Mpc would cause anisotropies of order 1 per cent in the observed microwave temperature due to the gravitational redshift and other general-relativistic effects. The $p = 0$ models are compared in detail with corresponding Newtonian models. The perturbed Newtonian models do not contain gravitational waves, but the density perturbations and rotational perturbations are surprisingly similar.

Citations/Publication Year for 1967ApJ...147...73S



The Integrated Sachs-Wolfe Effect



Planck 2015 results. XIII. Cosmological parameters

Planck Collaboration: P. A. R. Ade¹⁰⁰, N. Aghanim⁷⁰, M. Arnaud⁸⁴, M. Ashdown^{80,7}, J. Aumont⁷⁰, C. Baccigalupi⁹⁹, A. J. Banday^{111,11}, R. B. Barreiro⁶, J. G. Bartlett^{1,78}, N. Bartolo^{36,77}, E. Battaner^{114,115}, R. Battye⁷⁹, K. Benabed^{11,10}, A. Benoît⁶⁸, A. Benoît-Lévy^{27,11,10}, J.-P. Bernard^{111,11}, M. Bersanelli^{39,58}, P. Bielewicz^{111,11,99}, A. Bonaldi⁷⁹, L. Bonavera⁷⁶, J. R. Bond¹⁰, J. Borrill^{16,104}, F. R. Bouchet^{71,102}, F. Boulanger⁷⁰, M. Bucher¹, C. Burigana^{37,37,59}, R. C. Butler⁵⁷, E. Calabrese¹⁰⁷, J.-F. Cardoso^{85,171}, A. Catalano^{86,83}, A. Challinor^{73,80,14}, A. Chamballu^{84,18,70}, R.-R. Chary⁶⁷, H. C. Chiang^{31,8}, J. Chluba^{26,80}, P. R. Christensen^{94,43}, S. Church¹⁰⁶, D. L. Clements⁶⁶, S. Colombi^{71,110}, L. P. L. Colombo^{25,78}, C. Combet⁶⁸, A. Coulais⁸³, B. P. Crill^{78,95}, A. Curto¹⁷⁶, F. Cuttaia⁵⁷, L. Danese⁹⁹, R. D. Davies⁷⁹, R. J. Davis⁹, P. de Bernardis³⁸, A. de Rosa⁵⁷, G. de Zotti^{54,99}, J. Delabrouille¹, F.-X. Désert⁶³, E. Di Valentino³, C. Dickinson⁷⁹, J. M. Diego⁷⁶, K. Dolag^{113,91}, H. Dole^{70,69}, S. Donzelli⁵⁸, O. Dore^{78,13}, M. Douspis⁷⁰, A. Duout^{71,66}, J. Dunkley¹⁰⁷, X. Dupac⁴⁶, G. Efstathiou^{80,73}, F. Elsner^{27,71,110}, T. A. Enßlin⁹¹, H. K. Eriksen⁷⁴, M. Farhang^{10,97}, J. Fergusson¹⁴, F. Finelli^{57,59}, O. Forni^{111,11}, M. Fraisse³⁶, A. Fraisse³¹, E. Franceschi⁵⁷, A. Frejsel⁹⁴, S. Galeotta⁵⁶, S. Galli⁷¹, K. Ganga¹, C. Gauthier^{1,90}, M. Gerbino³⁸, T. Ghosh⁷⁰, M. Giard^{111,11}, Y. Giraud-Héraud¹, E. Giusarma³⁸, E. Gjerløw⁷⁴, J. González-Nuevo^{6,99}, K. M. Gorski^{78,117}, S. Gratton^{80,73}, A. Gregorio^{40,56,62}, A. Gruppuso⁵⁷, J. E. Gudmundsson³¹, J. Hamann^{109,108}, F. K. Hansen⁷⁴, D. Hanson^{92,78,10}, D. L. Harrison^{73,80}, G. Helou¹³, S. Henrot-Versille³¹, C. Hernández-Monteagudo^{15,91}, D. Herranz¹⁶, S. R. Hildebrandt^{78,13}, E. Hivon^{71,110}, M. Hobson⁷, W. A. Holmes⁷⁸, A. Hornstrup¹⁹, W. Hovest⁹¹, Z. Huang¹⁰, K. M. Huffenberger²⁹, G. Hurier⁷⁰, A. H. Jaffe⁶⁶, T. R. Jaffe^{111,11}, W. C. Jones³¹, M. Juvela³⁰, E. Keihänen³⁰, R. Keskitalo¹⁶, T. S. Kisner⁸⁸, R. Kneissl^{45,9}, J. Knoche⁹¹, L. Knox³³, M. Kunz^{20,70,2}, H. Kurki-Suonio^{30,52}, G. Lagache^{57,0}, M. Lahteenmaki^{1,52}, J.-M. Lamarré⁸³, A. Lasenby^{7,80}, M. Lattanzi³⁷, C. R. Lawrence⁷⁸, J. P. Leahy⁷⁹, R. Leonardi⁴⁶, J. Lesgourgues^{109,98,82}, F. Levrier⁸³, A. Lewis²⁶, M. Liguori^{36,77}, P. B. Lilje⁷⁴, M. Linden-Vørnle¹⁹, M. López-Caniego^{46,76}, P. M. Lubin³⁴, J. F. Macías-Pérez⁵⁶, G. Maggio⁵⁶, N. Mandlesi^{17,3}, A. Mangilli^{70,81}, A. Marchini⁶⁰, P. G. Martin¹⁰, M. Martinelli¹¹⁶, E. Martínez-González⁷⁶, S. Mas³⁸, S. Matarrese^{36,77,49}, P. Mazzatorta⁴¹, P. McGehee⁶⁷, P. R. Meinhold³⁴, A. Melchiorri^{38,60}, J.-B. Melin¹⁸, L. Mendes⁴⁶, A. Menella^{59,58}, M. Migliaccio^{73,80}, M. Milloca³³, S. Mitra^{65,78}, M.-A. Miville-Deschénes^{70,10}, A. Moneti⁷¹, L. Montier^{111,11}, G. Morgante⁵⁷, D. Mortlock⁶⁶, A. Moss¹⁰¹, D. Munshi¹⁰⁰, J. A. Murphy⁹³, P. Naselsky^{94,43}, F. Natoli^{37,4,57}, C. B. Netterfield²², H. U. Nørgaard-Nielsen¹⁹, F. Novello⁷⁹, D. Novikov⁸⁹, I. Novikov^{94,39}, C. A. Oxborrow¹⁹, F. Paci⁹⁹, L. Pagano^{38,60}, F. Pajot⁷⁰, R. Paladini⁶⁷, D. Paoletti^{57,59}, B. Partridge⁵¹, F. Pasian⁵⁶, G. Patanchon¹, T. J. Pearson^{13,67}, O. Perdereau⁸¹, L. Perotto⁸⁹, F. Perrotta⁹⁹, V. Pettorino⁵⁰, D. Piacentini²⁵, M. Piat¹, E. Pierpaoli²⁵, D. Pietrobon⁷⁸, S. Plaszczynski⁸¹, E. Pointecouteau^{111,11}, G. Polenta^{45,5}, L. Popa⁷², G. W. Prat⁸⁴, G. Prézeau^{13,78}, S. Prunet^{71,110}, J.-L. Puget⁷⁰, J. P. Rachén^{23,91}, W. T. Reach¹¹², R. Rebolo^{15,17,44}, M. Reinecke⁹¹, M. Remazeilles^{79,70,1}, C. Renault⁸⁶, A. Renzi^{42,61}, I. Ristorcelli^{111,11}, G. Rocha^{78,13}, C. Rosset¹, M. Rossetti^{39,58}, G. Roudier^{1,83,78}, B. Rouillé d'Orfeuil⁸¹, M. Rowan-Robinson⁶, J. A. Rubino-Martí^{5,4}, B. Rusholme⁶⁷, N. Said³⁸, V. Salvatelli^{38,6}, L. Salvati³⁸, M. Sandri³⁷, D. Santos⁸⁶, M. Savelainen^{30,52}, G. Savini⁹⁶, D. Scott²⁴, M. D. Seifert^{78,13}, P. Serra⁷⁰, E. P. Shellard¹⁴, L. D. Spencer¹⁰⁰, M. Spinelli⁸¹, V. Stolyarov^{7,80,105}, R. Stompor¹, R. Sudiwala¹⁰⁰, R. Sunyaev^{91,103}, D. Sutton^{73,80}, A.-S. Suur-Uuski^{30,52}, J.-F. Sygnet⁷¹, J. A. Tauber⁶⁷, L. Terenzi^{38,57}, L. Toffolatti^{21,76,57}, M. Tomasi^{39,58}, M. Tristram⁸¹, T. Trombetti⁵⁷, M. Tucci²⁰, J. Tuovinen¹², M. Türler⁶⁴, G. Umana⁵³, L. Valenziano⁵⁷, J. Valiviita^{30,52}, B. Van Tent⁸⁷, P. Vielva⁷⁶, F. Villa⁵⁷, L. A. Wade⁷⁸, B. D. Wandelt^{71,10,35}, I. K. Wehus⁷⁸, M. White³², S. D. M. White⁹¹, A. Wilkinson⁷⁹, D. Yvon¹⁸, A. Zacchei⁵⁶, and A. Zonca³⁴

(Affiliations can be found after the references)

February 5 2015

ABSTRACT

This paper presents cosmological results based on full-mission *Planck* observations of temperature and polarization anisotropies of the cosmic microwave background (CMB) radiation. Our results are in very good agreement with the 2013 analysis of the *Planck* nominal-mission temperature data, but with increased precision. The temperature and polarization power spectra are consistent with the standard spatially-flat six-parameter Λ CDM cosmology with a power-law spectrum of adiabatic scalar perturbations (denoted “base Λ CDM” in this paper). From the *Planck* temperature data combined with *Planck* lensing, for this cosmology we find a Hubble constant, $H_0 = (67.8 \pm 0.9) \text{ km s}^{-1}\text{Mpc}^{-1}$, a matter density parameter $\Omega_m = 0.308 \pm 0.012$, and a tilted scalar spectral index with $n_s = 0.968 \pm 0.006$, consistent with the 2013 analysis. (In this abstract we quote 68 % confidence limits on measured parameters and 95 % upper limits on other parameters.) We present the first results of polarization measurements with the Low Frequency Instrument at large angular scales. Combined with the *Planck* temperature and lensing data, these measurements give a reionization optical depth of $\tau = 0.066 \pm 0.016$, corresponding to a reionization redshift of $z_{\text{re}} = 8.8^{+1.7}_{-1.4}$. These results are consistent with those from WMAP polarization measurements cleaned for dust emission using 353 GHz polarization maps from the High Frequency Instrument. We find no evidence for any departure from base Λ CDM in the neutrino sector of the theory. For example, combining *Planck* observations with other astrophysical data we find $N_{\text{eff}} = 3.15 \pm 0.23$ for the effective number of relativistic degrees of freedom, consistent with the value $N_{\text{eff}} = 3.046$ of the Standard Model of particle physics. The sum of neutrino masses is constrained to $\sum m_\nu < 0.23 \text{ eV}$. The spatial curvature of our Universe is found to be very close to zero with $|\Omega_k| < 0.005$. Adding a tensor component as a single-parameter extension to base Λ CDM we find an upper limit on the tensor-to-scalar ratio of $r_{0.02} < 0.11$, consistent with the *Planck* 2013 results and consistent with the B -mode polarization constraints from a joint analysis of BICEP2, *Keck Array*, and *Planck* (BKP) data. Adding the BKP B -mode data to our analysis leads to a tighter constraint of $r_{0.002} < 0.09$ and disfavours inflationary models with a $V(\phi) \propto \phi^2$ potential. The addition of *Planck* polarization data leads to strong constraints on deviations from a purely adiabatic spectrum of fluctuations. We find no evidence for any contribution from isocurvature perturbations or from cosmic defects. Combining *Planck* data with other astrophysical data, including Type Ia supernovae, the equation of state of dark energy is constrained to $w = -1.006 \pm 0.045$, consistent with the expected value for a cosmological constant. The standard big bang nucleosynthesis predictions for the helium and deuterium abundances for the best-fit *Planck* base Λ CDM cosmology are in excellent agreement with observations. We also analyse constraints on annihilating dark matter and on possible deviations from the standard recombination history. In both cases, we find no evidence for new physics. The *Planck* results for base Λ CDM are in good agreement with baryon acoustic oscillation data and with the JLA sample of Type Ia supernovae. However, as in the 2013 analysis, the amplitude of the fluctuation spectrum is found to be higher than inferred from some analyses of rich cluster counts and weak gravitational lensing. We show that these tensions cannot easily be resolved with simple modifications of the base Λ CDM cosmology. Apart from these tensions, the base Λ CDM cosmology provides an excellent description of the *Planck* CMB observations and many other astrophysical data sets.

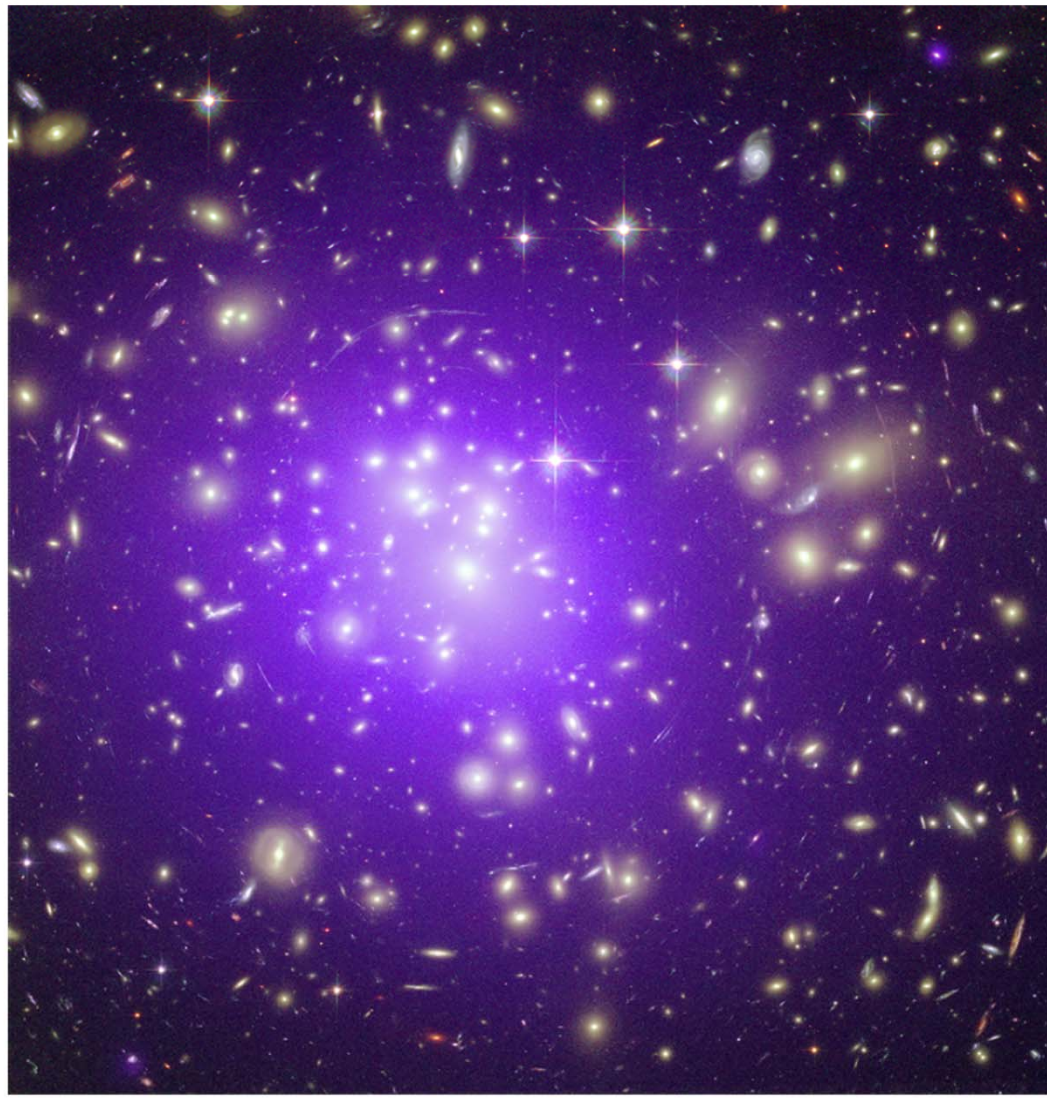
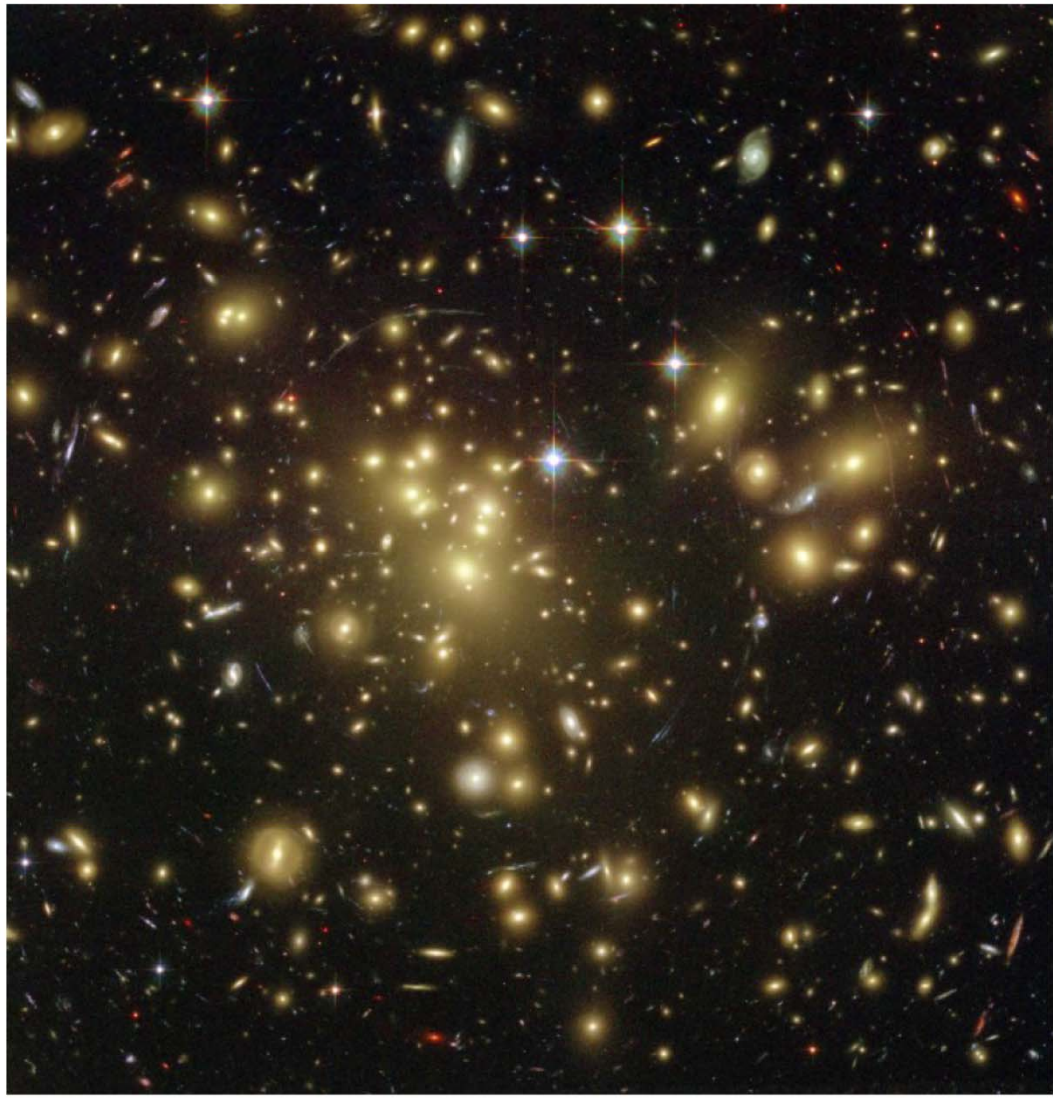
Key words. Cosmology: observations – Cosmology: theory – cosmic microwave background – cosmological parameters

Table 4. Parameter 68 % confidence limits for the base ΛCDM model from *Planck* CMB power spectra, in combination with lensing reconstruction (“lensing”) and external data (“ext,” BAO+JLA+ H_0). Nuisance parameters are not listed for brevity (they can be found in the *Planck Legacy Archive* tables), but the last three parameters give a summary measure of the total foreground amplitude (in μK^2) at $\ell = 2000$ for the three high- ℓ temperature spectra used by the likelihood. In all cases the helium mass fraction used is predicted by BBN (posterior mean $Y_p \approx 0.2453$, with theoretical uncertainties in the BBN predictions dominating over the *Planck* error on $\Omega_b h^2$).

Parameter	TT+lowP 68 % limits	TT+lowP+lensing 68 % limits	TT+lowP+lensing+ext 68 % limits	TT,TE,EE+lowP 68 % limits	TT,TE,EE+lowP+lensing 68 % limits	TT,TE,EE+lowP+lensing+ext 68 % limits
$\Omega_b h^2$	0.02222 ± 0.00023	0.02226 ± 0.00023	0.02227 ± 0.00020	0.02225 ± 0.00016	0.02226 ± 0.00016	0.02230 ± 0.00014
$\Omega_c h^2$	0.1197 ± 0.0022	0.1186 ± 0.0020	0.1184 ± 0.0012	0.1198 ± 0.0015	0.1193 ± 0.0014	0.1188 ± 0.0010
$100\theta_{\text{MC}}$	1.04085 ± 0.00047	1.04103 ± 0.00046	1.04106 ± 0.00041	1.04077 ± 0.00032	1.04087 ± 0.00032	1.04093 ± 0.00030
τ	0.078 ± 0.019	0.066 ± 0.016	0.067 ± 0.013	0.079 ± 0.017	0.063 ± 0.014	0.066 ± 0.012
$\ln(10^{10} A_s)$	3.089 ± 0.036	3.062 ± 0.029	3.064 ± 0.024	3.094 ± 0.034	3.059 ± 0.025	3.064 ± 0.023
n_s	0.9655 ± 0.0062	0.9677 ± 0.0060	0.9681 ± 0.0044	0.9645 ± 0.0049	0.9653 ± 0.0048	0.9667 ± 0.0040
H_0	67.31 ± 0.96	67.81 ± 0.92	67.90 ± 0.55	67.27 ± 0.66	67.51 ± 0.64	67.74 ± 0.46
Ω_Λ	0.685 ± 0.013	0.692 ± 0.012	0.6935 ± 0.0072	0.6844 ± 0.0091	0.6879 ± 0.0087	0.6911 ± 0.0062
Ω_m	0.315 ± 0.013	0.308 ± 0.012	0.3065 ± 0.0072	0.3156 ± 0.0091	0.3121 ± 0.0087	0.3089 ± 0.0062
$\Omega_m h^2$	0.1426 ± 0.0020	0.1415 ± 0.0019	0.1413 ± 0.0011	0.1427 ± 0.0014	0.1422 ± 0.0013	0.14170 ± 0.00097
$\Omega_m h^3$	0.09597 ± 0.00045	0.09591 ± 0.00045	0.09593 ± 0.00045	0.09601 ± 0.00029	0.09596 ± 0.00030	0.09598 ± 0.00029
σ_8	0.829 ± 0.014	0.8149 ± 0.0093	0.8154 ± 0.0090	0.831 ± 0.013	0.8150 ± 0.0087	0.8159 ± 0.0086
$\sigma_8 \Omega_m^{0.5}$	0.466 ± 0.013	0.4521 ± 0.0088	0.4514 ± 0.0066	0.4668 ± 0.0098	0.4553 ± 0.0068	0.4535 ± 0.0059
$\sigma_8 \Omega_m^{0.25}$	0.621 ± 0.013	0.6069 ± 0.0076	0.6066 ± 0.0070	0.623 ± 0.011	0.6091 ± 0.0067	0.6083 ± 0.0066
z_{re}	$9.9^{+1.8}_{-1.6}$	$8.8^{+1.7}_{-1.4}$	$8.9^{+1.3}_{-1.2}$	$10.0^{+1.7}_{-1.5}$	$8.5^{+1.4}_{-1.2}$	$8.8^{+1.2}_{-1.1}$
$10^9 A_s$	$2.198^{+0.076}_{-0.085}$	2.139 ± 0.063	2.143 ± 0.051	2.207 ± 0.074	2.130 ± 0.053	2.142 ± 0.049
$10^9 A_s e^{-2r}$	1.880 ± 0.014	1.874 ± 0.013	1.873 ± 0.011	1.882 ± 0.012	1.878 ± 0.011	1.876 ± 0.011
Age/Gyr	13.813 ± 0.038	13.799 ± 0.038	13.796 ± 0.029	13.813 ± 0.026	13.807 ± 0.026	13.799 ± 0.021
z_*	1090.09 ± 0.42	1089.94 ± 0.42	1089.90 ± 0.30	1090.06 ± 0.30	1090.00 ± 0.29	1089.90 ± 0.23
r_*	144.61 ± 0.49	144.89 ± 0.44	144.93 ± 0.30	144.57 ± 0.32	144.71 ± 0.31	144.81 ± 0.24
$100\theta_*$	1.04105 ± 0.00046	1.04122 ± 0.00045	1.04126 ± 0.00041	1.04096 ± 0.00032	1.04106 ± 0.00031	1.04112 ± 0.00029
z_{drag}	1059.57 ± 0.46	1059.57 ± 0.47	1059.60 ± 0.44	1059.65 ± 0.31	1059.62 ± 0.31	1059.68 ± 0.29
r_{drag}	147.33 ± 0.49	147.60 ± 0.43	147.63 ± 0.32	147.27 ± 0.31	147.41 ± 0.30	147.50 ± 0.24
k_D	0.14050 ± 0.00052	0.14024 ± 0.00047	0.14022 ± 0.00042	0.14059 ± 0.00032	0.14044 ± 0.00032	0.14038 ± 0.00029
z_{eq}	3393 ± 49	3365 ± 44	3361 ± 27	3395 ± 33	3382 ± 32	3371 ± 23
k_{eq}	0.01035 ± 0.00015	0.01027 ± 0.00014	0.010258 ± 0.000083	0.01036 ± 0.00010	0.010322 ± 0.000096	0.010288 ± 0.000071
$100\theta_{\text{eq}}$	0.4502 ± 0.0047	0.4529 ± 0.0044	0.4533 ± 0.0026	0.4499 ± 0.0032	0.4512 ± 0.0031	0.4523 ± 0.0023
f_{2000}^{143}	29.9 ± 2.9	30.4 ± 2.9	30.3 ± 2.8	29.5 ± 2.7	30.2 ± 2.7	30.0 ± 2.7
$f_{2000}^{143+217}$	32.4 ± 2.1	32.8 ± 2.1	32.7 ± 2.0	32.2 ± 1.9	32.8 ± 1.9	32.6 ± 1.9
f_{2000}^{217}	106.0 ± 2.0	106.3 ± 2.0	106.2 ± 2.0	105.8 ± 1.9	106.2 ± 1.9	106.1 ± 1.8

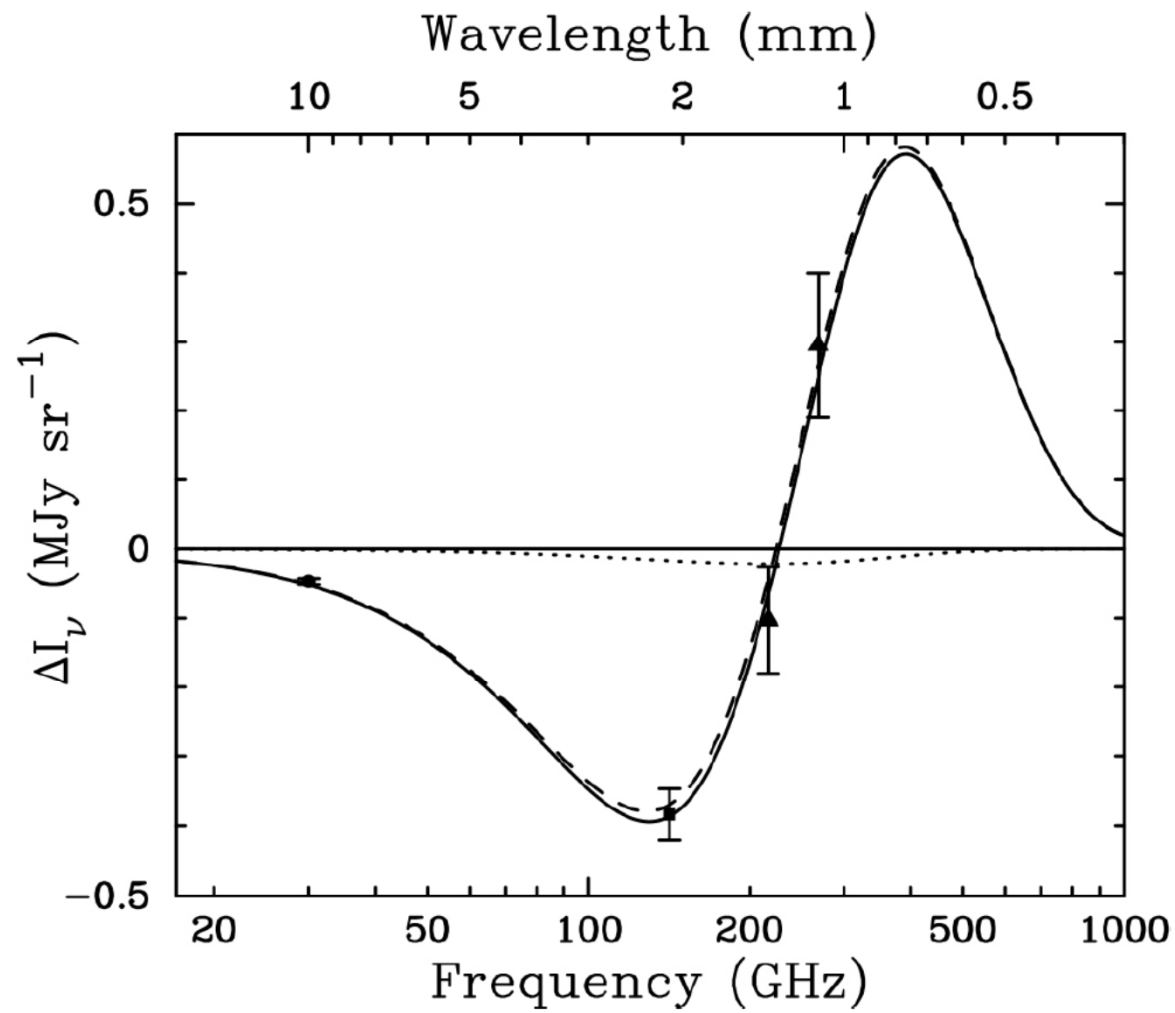
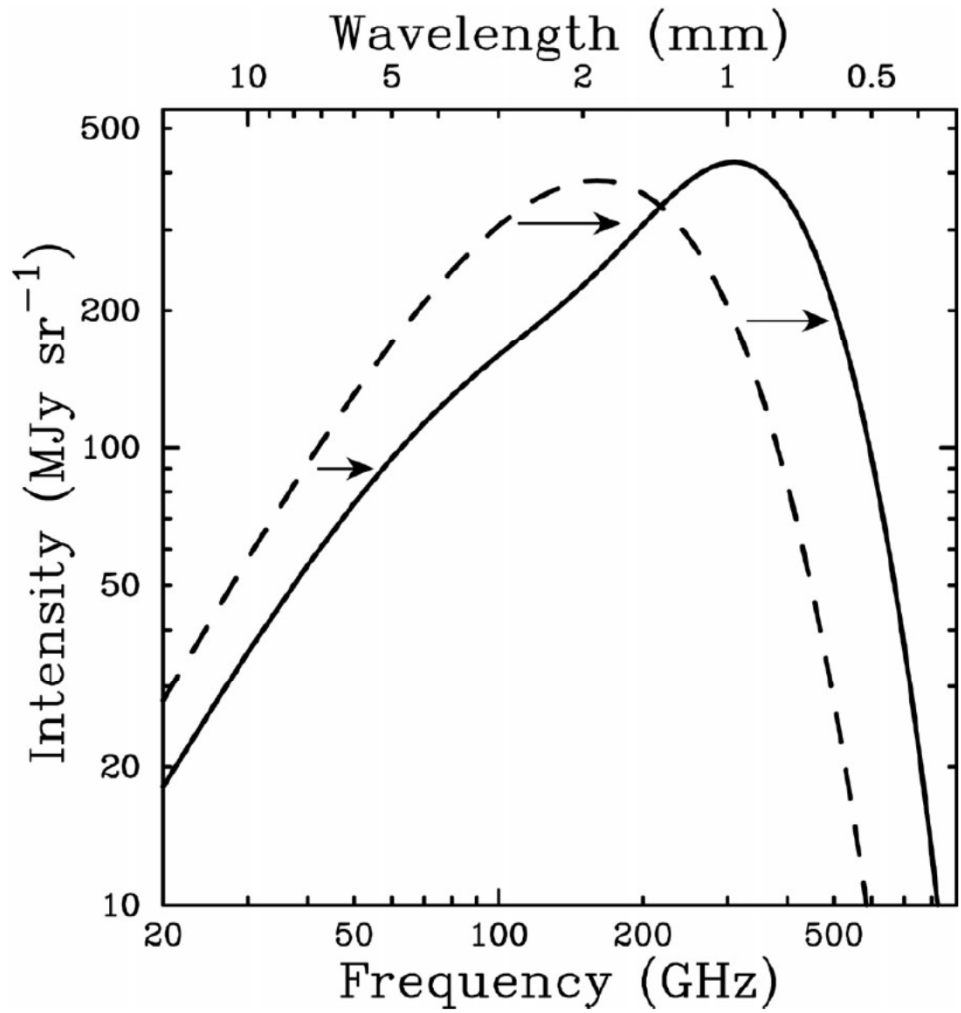
Table 5. Constraints on 1-parameter extensions to the base ΛCDM model for combinations of *Planck* power spectra, *Planck* lensing, and external data (BAO+JLA+ H_0 , denoted “ext”). Note that we quote 95 % limits here.

Parameter	TT	TT+lensing	TT+lensing+ext	TT,TE,EE	TT,TE,EE+lensing	TT,TE,EE+lensing+ext
Ω_K	$-0.052^{+0.049}_{-0.055}$	$-0.005^{+0.016}_{-0.017}$	$-0.0001^{+0.0054}_{-0.0052}$	$-0.040^{+0.038}_{-0.041}$	$-0.004^{+0.015}_{-0.015}$	$0.0008^{+0.0040}_{-0.0039}$
Σm_ν [eV]	< 0.715	< 0.675	< 0.234	< 0.492	< 0.589	< 0.194
N_{eff}	$3.13^{+0.64}_{-0.63}$	$3.13^{+0.62}_{-0.61}$	$3.15^{+0.41}_{-0.40}$	$2.99^{+0.41}_{-0.39}$	$2.94^{+0.38}_{-0.38}$	$3.04^{+0.33}_{-0.33}$
Y_p	$0.252^{+0.041}_{-0.042}$	$0.251^{+0.040}_{-0.039}$	$0.251^{+0.035}_{-0.036}$	$0.250^{+0.026}_{-0.027}$	$0.247^{+0.026}_{-0.027}$	$0.249^{+0.025}_{-0.026}$
$dn_s/d \ln k$	$-0.008^{+0.016}_{-0.016}$	$-0.003^{+0.015}_{-0.015}$	$-0.003^{+0.015}_{-0.014}$	$-0.006^{+0.014}_{-0.014}$	$-0.002^{+0.013}_{-0.013}$	$-0.002^{+0.013}_{-0.013}$
$r_{0.002}$	< 0.103	< 0.114	< 0.114	< 0.0987	< 0.112	< 0.113
w	$-1.54^{+0.62}_{-0.50}$	$-1.41^{+0.64}_{-0.56}$	$-1.006^{+0.085}_{-0.091}$	$-1.55^{+0.58}_{-0.48}$	$-1.42^{+0.62}_{-0.56}$	$-1.019^{+0.075}_{-0.080}$



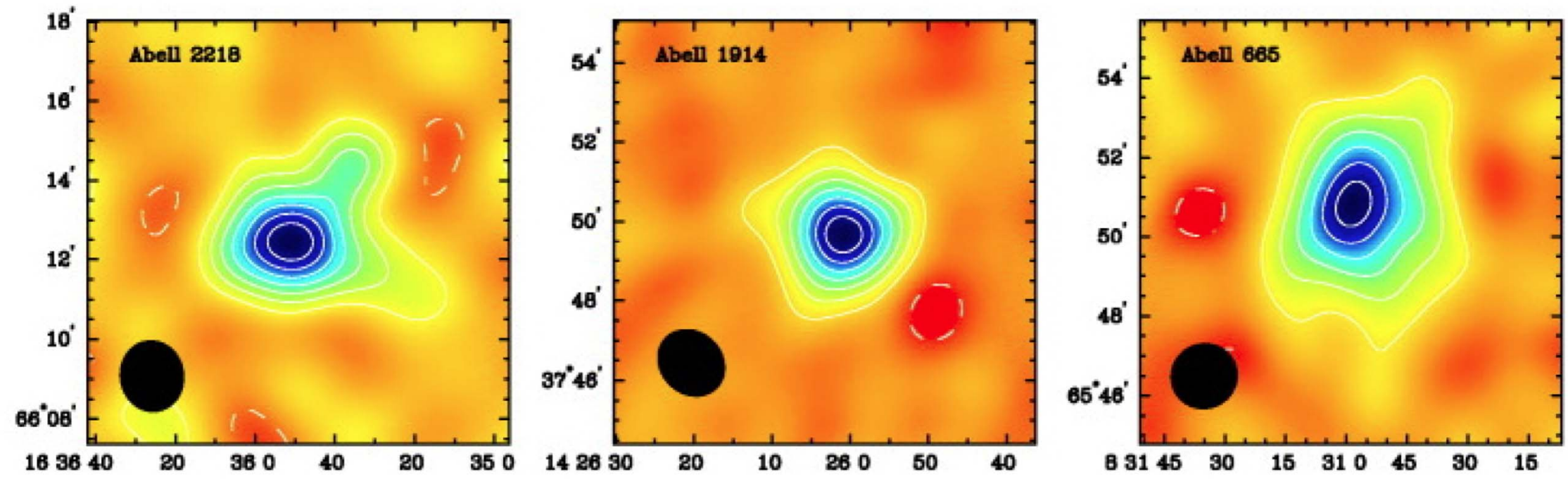
Left: The galaxy cluster Abell 1689 observed with the Hubble Space Telescope Advanced Camera for Surveys. This cluster is one of the largest concentrations of matter in the local Universe ($z = 0.1828$), with a mass $M \sim 10^{15} M_\odot$

Right: The X-ray image of the cluster (shown here superimposed on the HST image taken in visible light) obtained by the Chandra observatory shows diffuse emission from intracluster gas at temperatures $T \times 10^8$ K.

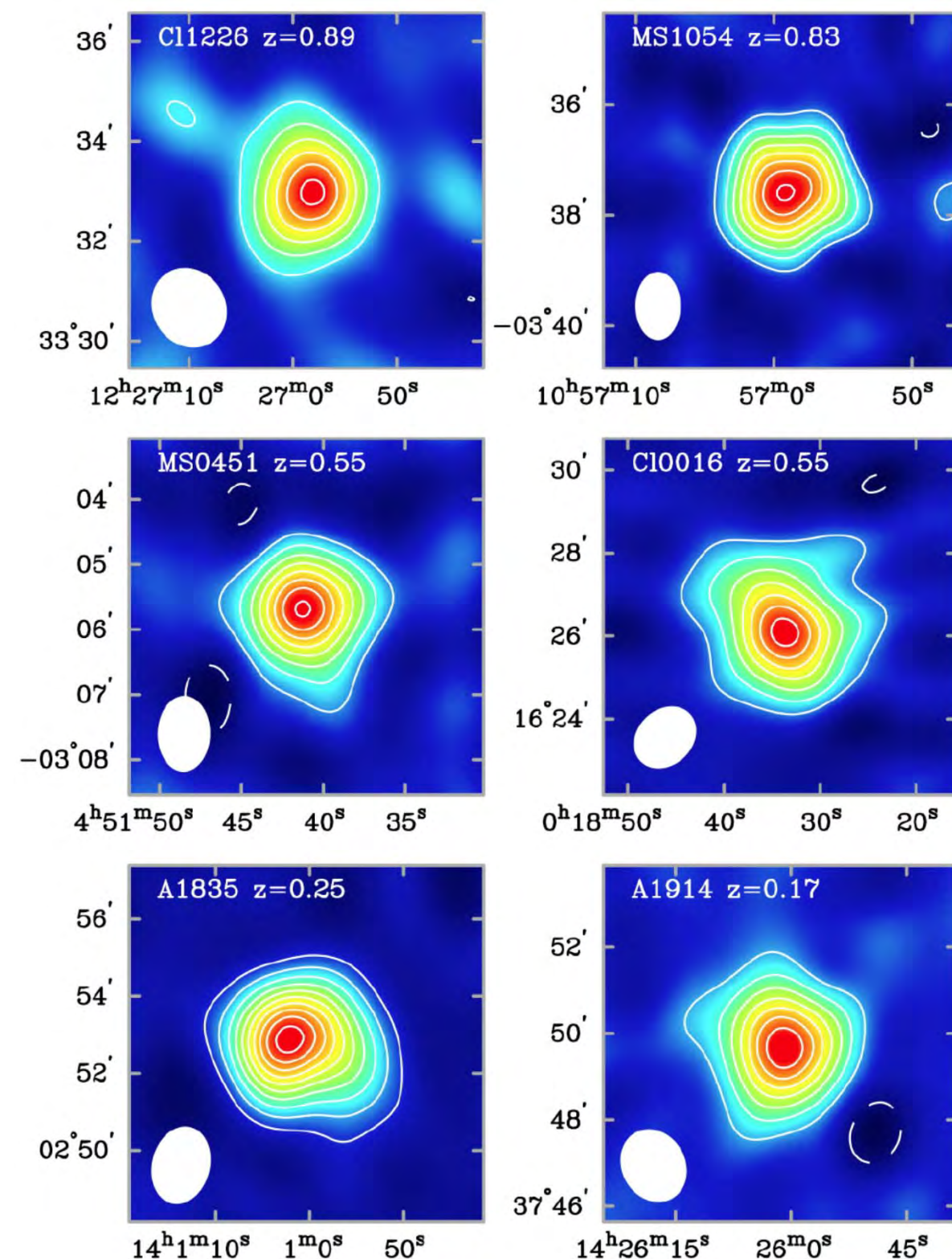


Left: Inverse Compton scattering by energetic electrons in the intracluster medium of massive galaxy clusters alters the blackbody spectrum of CMB photons travelling through the cluster (dashed line: intrinsic spectrum; continuous line: emerging spectrum). This is the Sunyaev-Zel'dovich effect, named from the two Russian cosmologists who predicted it in 1970.

Right: Difference between the intensity of the CMB and the signal through the cluster of galaxies Abell 2163. ΔI_ν is negative at frequencies lower than 218 GHz (wavelengths longer than 1.4 mm), and positive at higher frequencies. (Figures reproduced from Carlstrom et al. 2002).



Sunyaev-Zel'dovich maps of three clusters of galaxies, showing the temperature difference of the measured CMB relative to the average CMB temperature (or, at a fixed frequency, the difference in radiation intensities). The black ellipse in each image shows the instrumental resolution. For each of the clusters shown here, the spatial dependence of the SZ effect is clearly visible. (Figure reproduced from Grego et al. 2001).



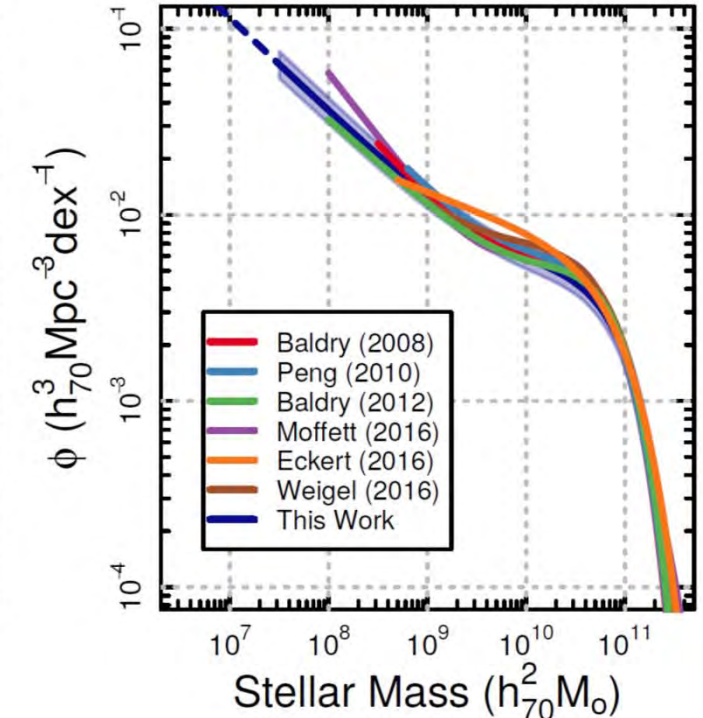
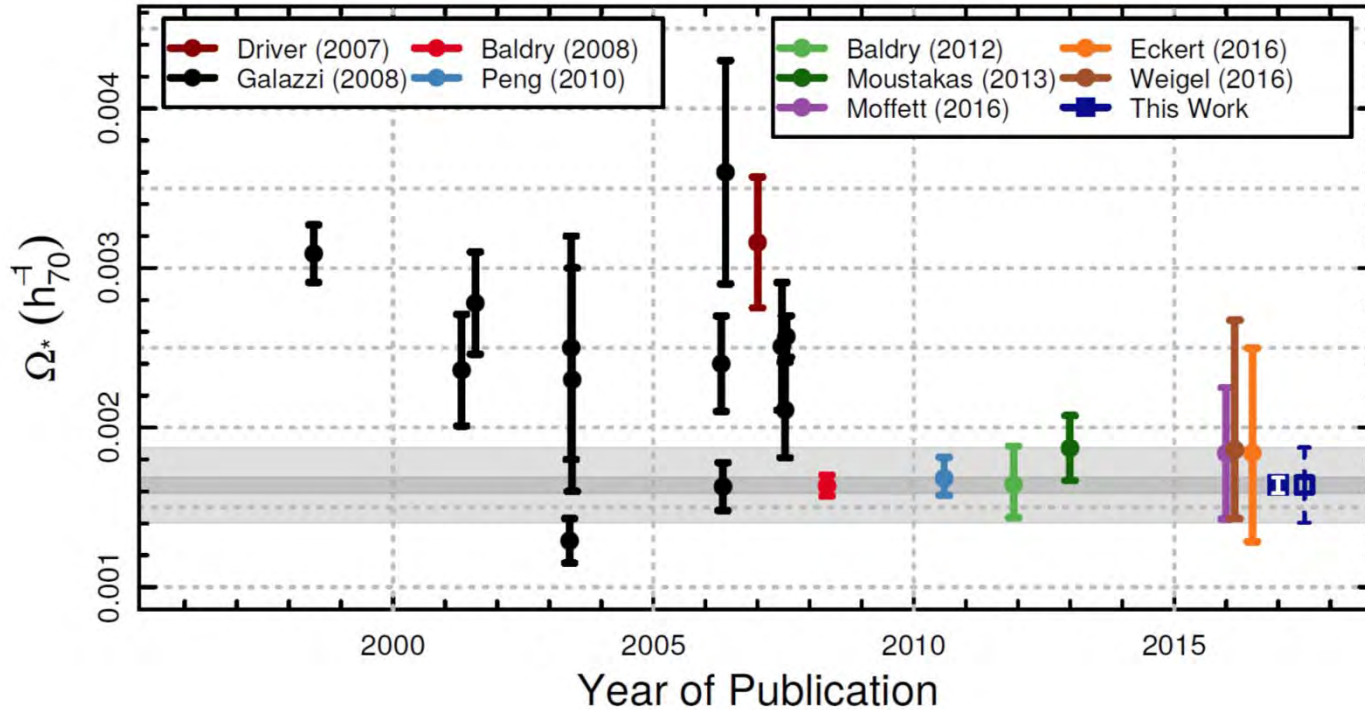
S-Z effect in six clusters at different redshifts, from $z = 0.17$ to $z = 0.89$.

The colour coding is such that red corresponds to the largest values of $|\Delta I_\nu / I_\nu|$ and blue to the lowest. The strength of the S-Z signal falls off from the core to the outskirts of each cluster, reflecting the decrease of the integral $\int n_e T \, dl$ with projected distance from the centre.

All of the clusters shown have similar high X-ray luminosities and, as can be seen, the strengths of their S-Z signals are similar, illustrating the independence of the S-Z effect on redshift.

These images were obtained with the Owens Valley Radio Observatory at a frequency of 30 GHz ($\lambda = 1$ cm). (Figure reproduced from Carlstrom et al. 2002).

Estimates of Ω_\star from Stellar Mass Function



$$\Omega_\star = 1.66 \pm 0.97 h_{70}^{-1} \times 10^{-3}$$

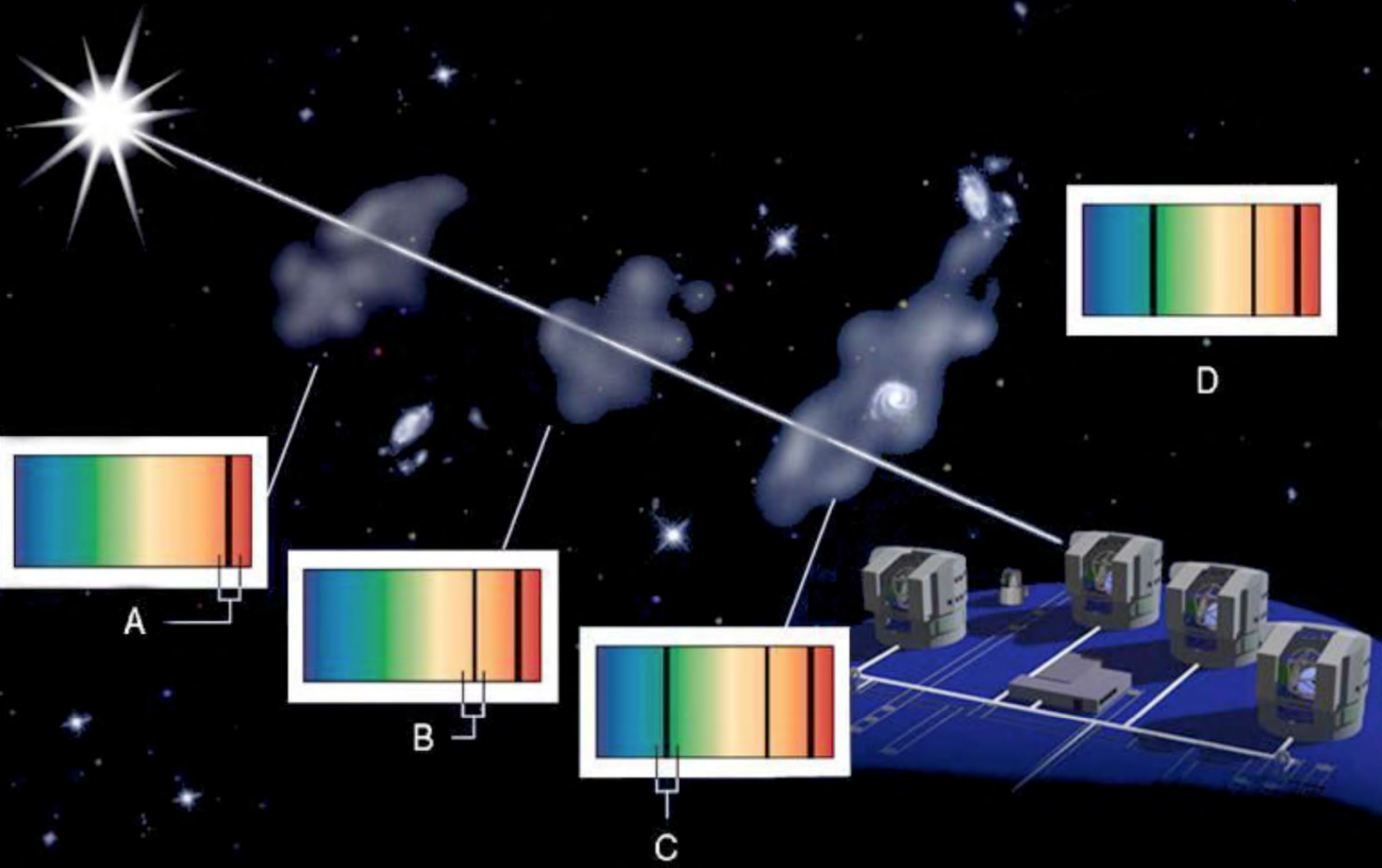
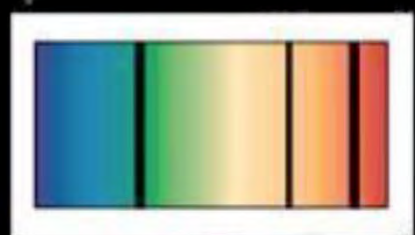
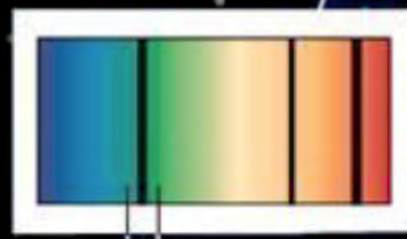
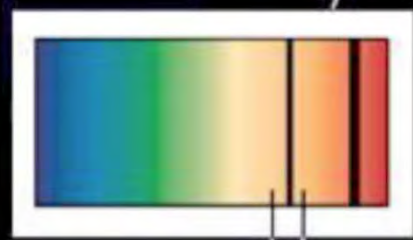
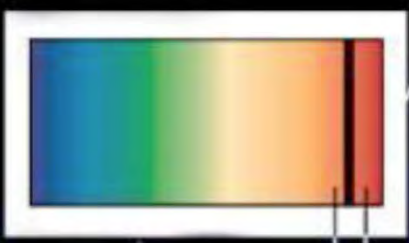
Wright et al. 2017

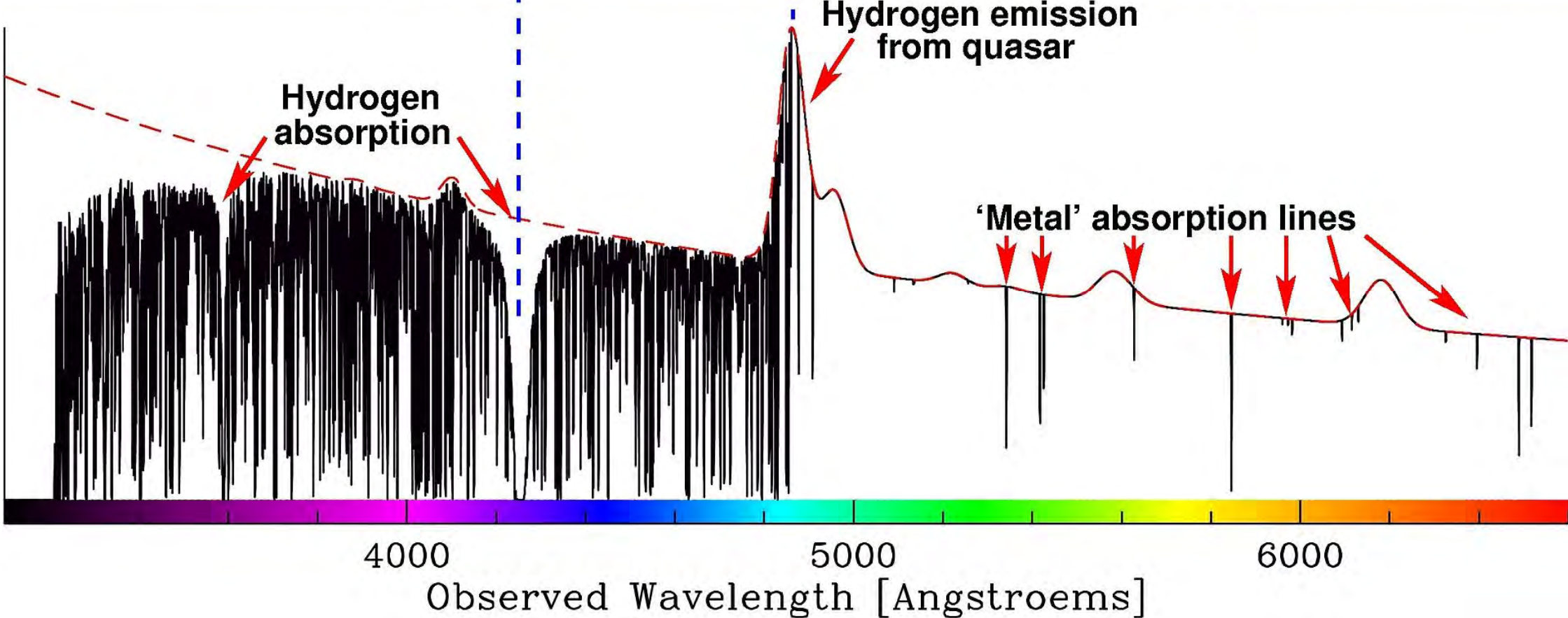
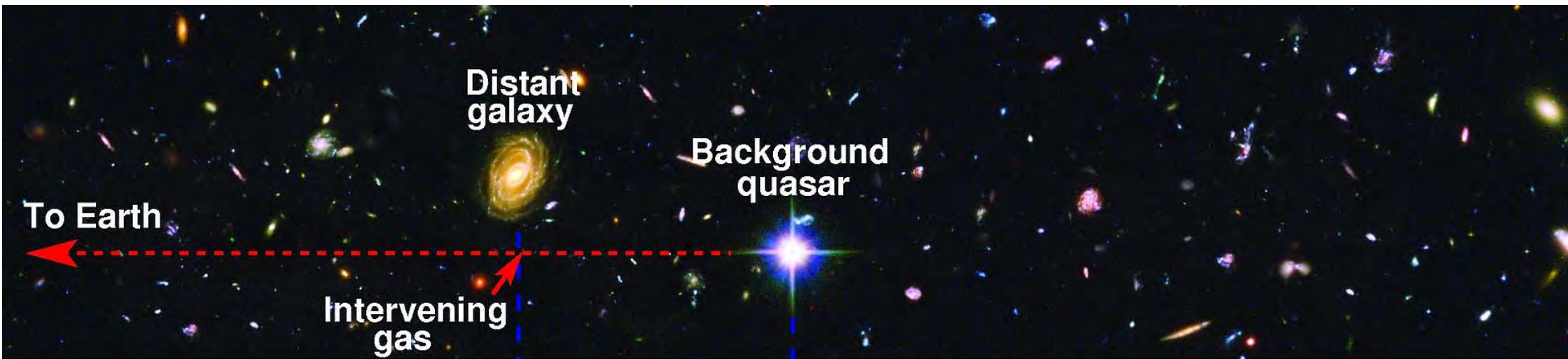
CSST/ LSST will be able to cover significantly larger area of sky than any current surveys (SDSS, GAMA...) in the local Universe, with better and deeper photometry, which will then provide better constraints on the stellar mass function and hence the estimate of Ω_\star .

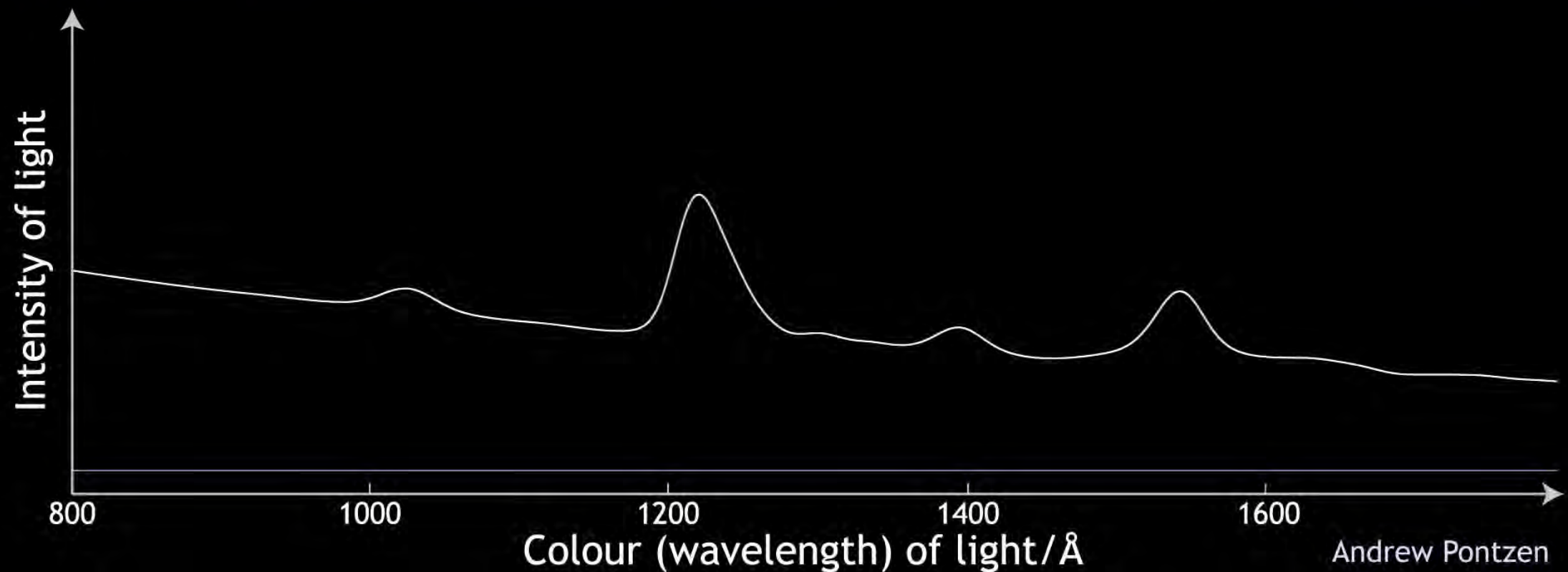


Abell 1689
 $z = 0.18$

X-ray (Chandra)
+ optical (HST)

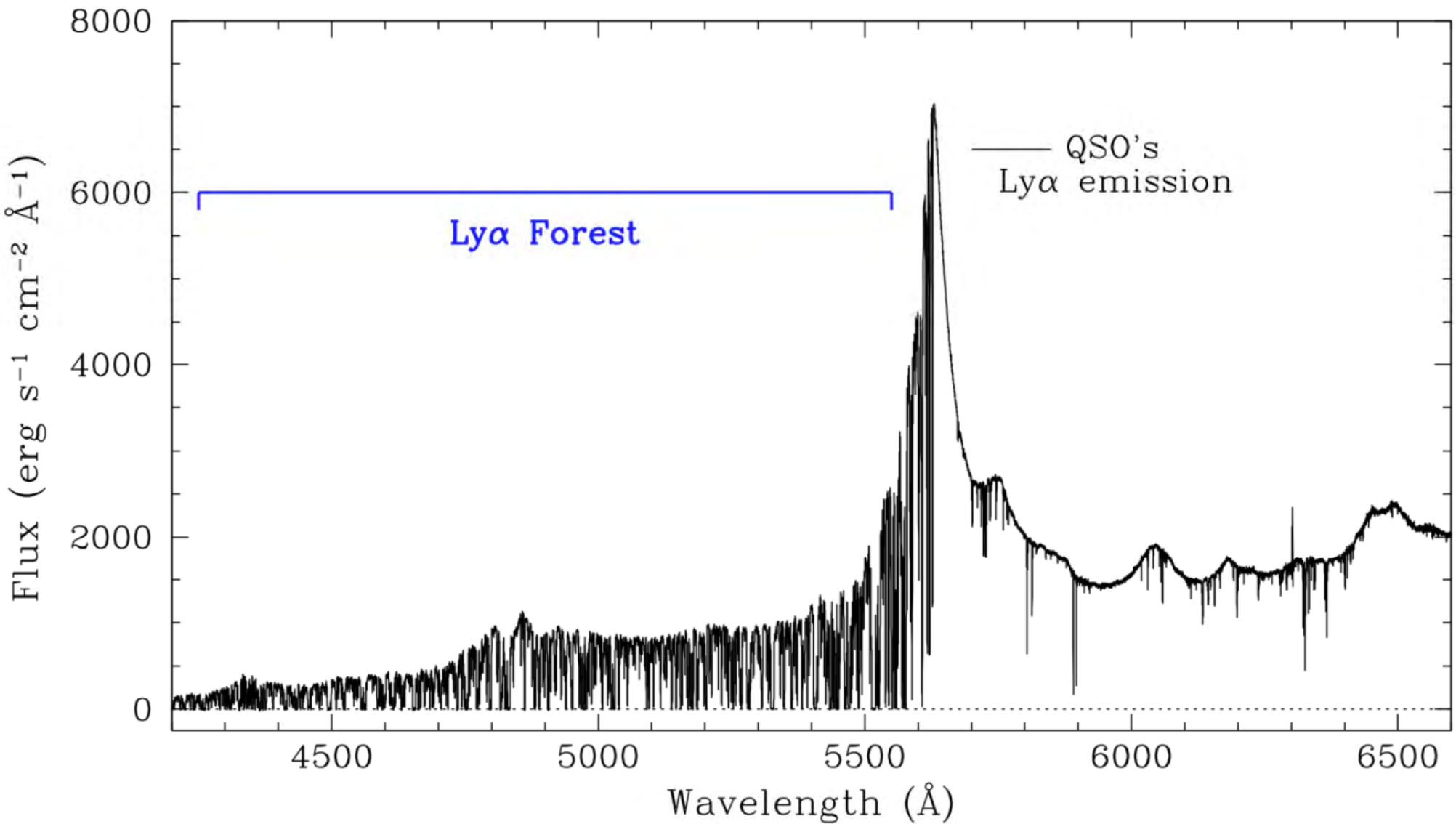




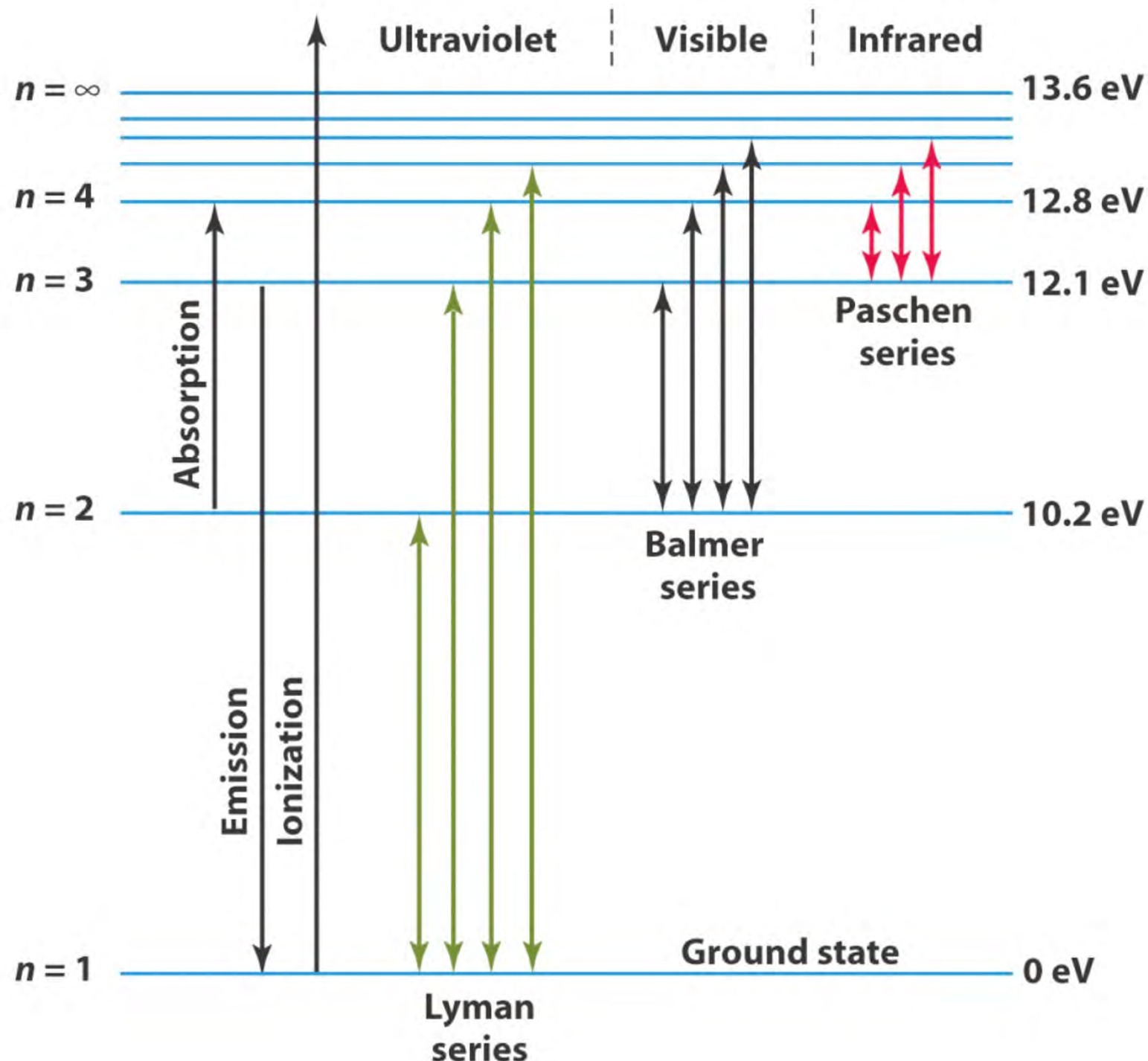


Andrew Pontzen

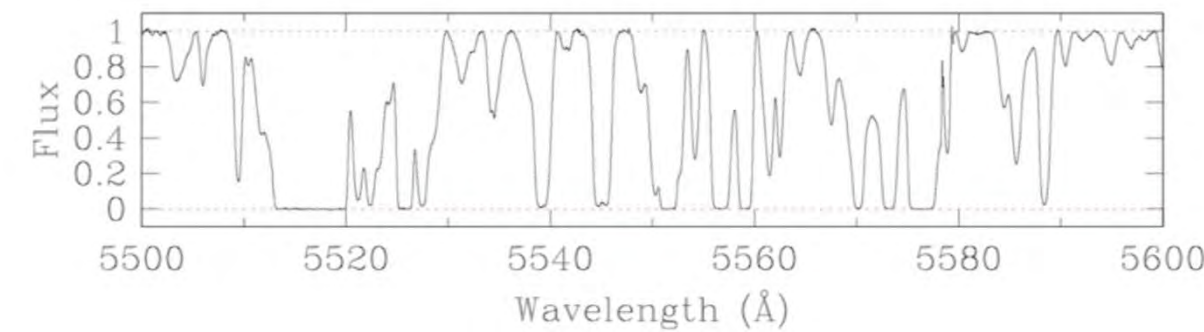
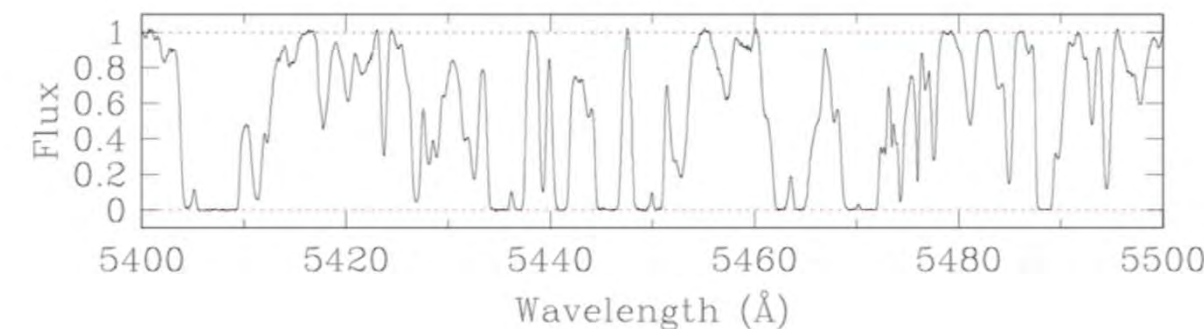
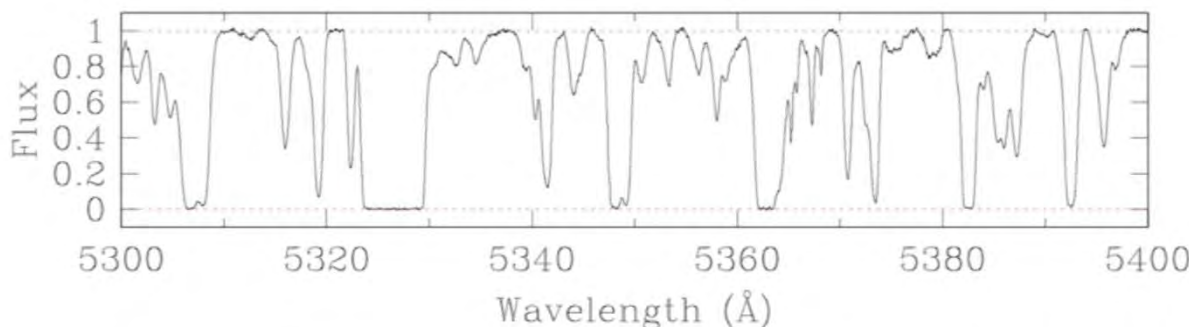
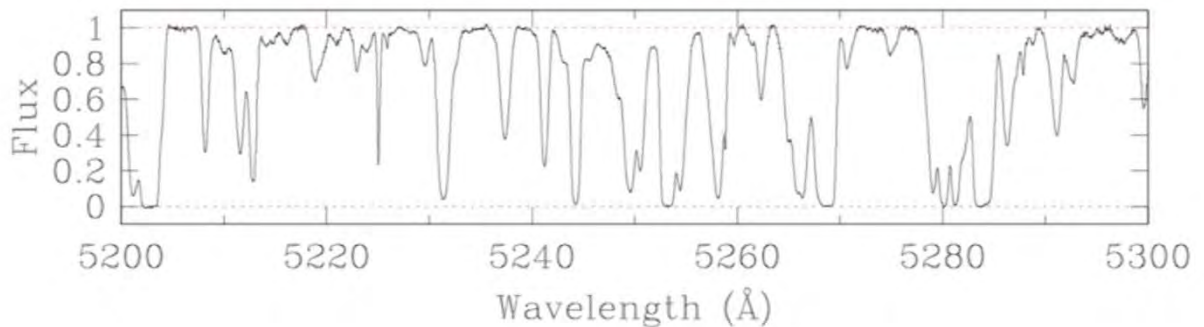
Q1422+231 $z_{\text{em}} = 3.625$



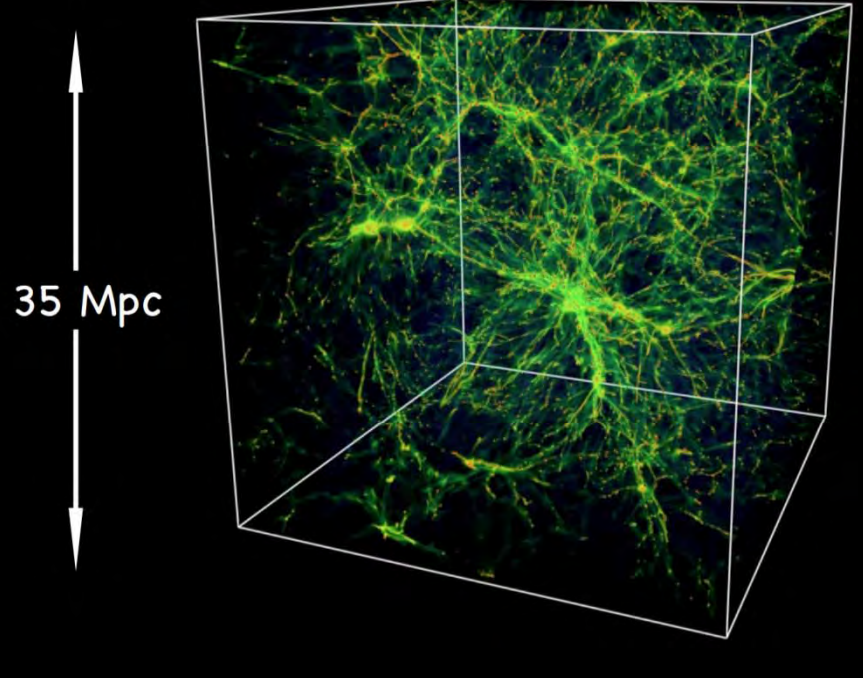
18.8 hours with HIRES (Keck I)



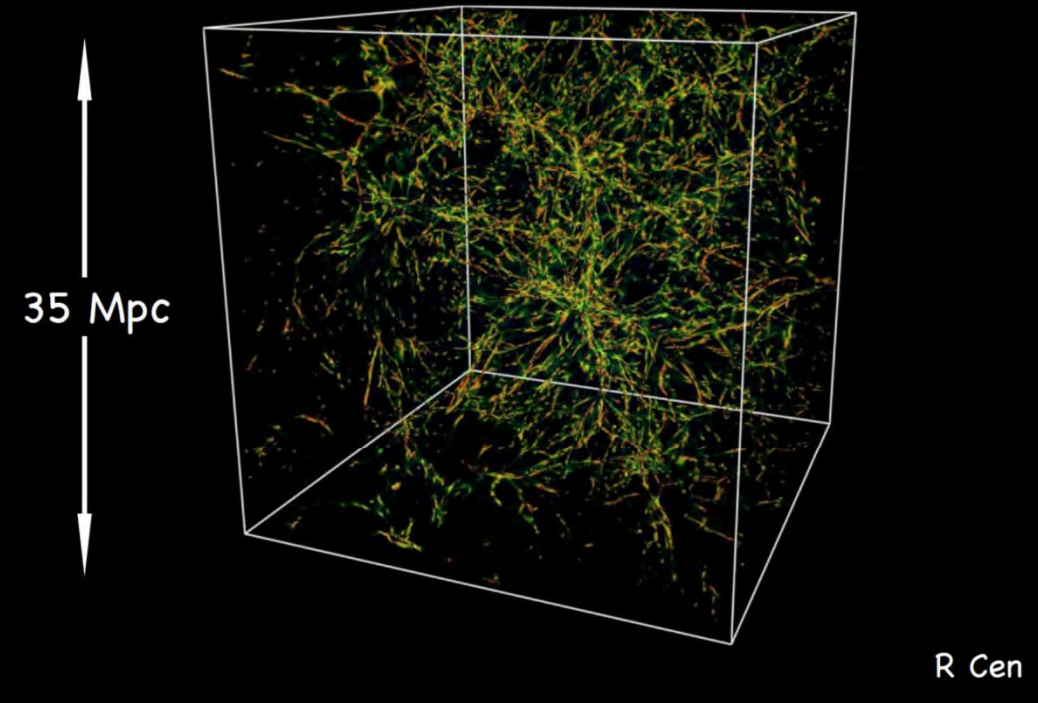
The Ly α forest at high spectral resolution

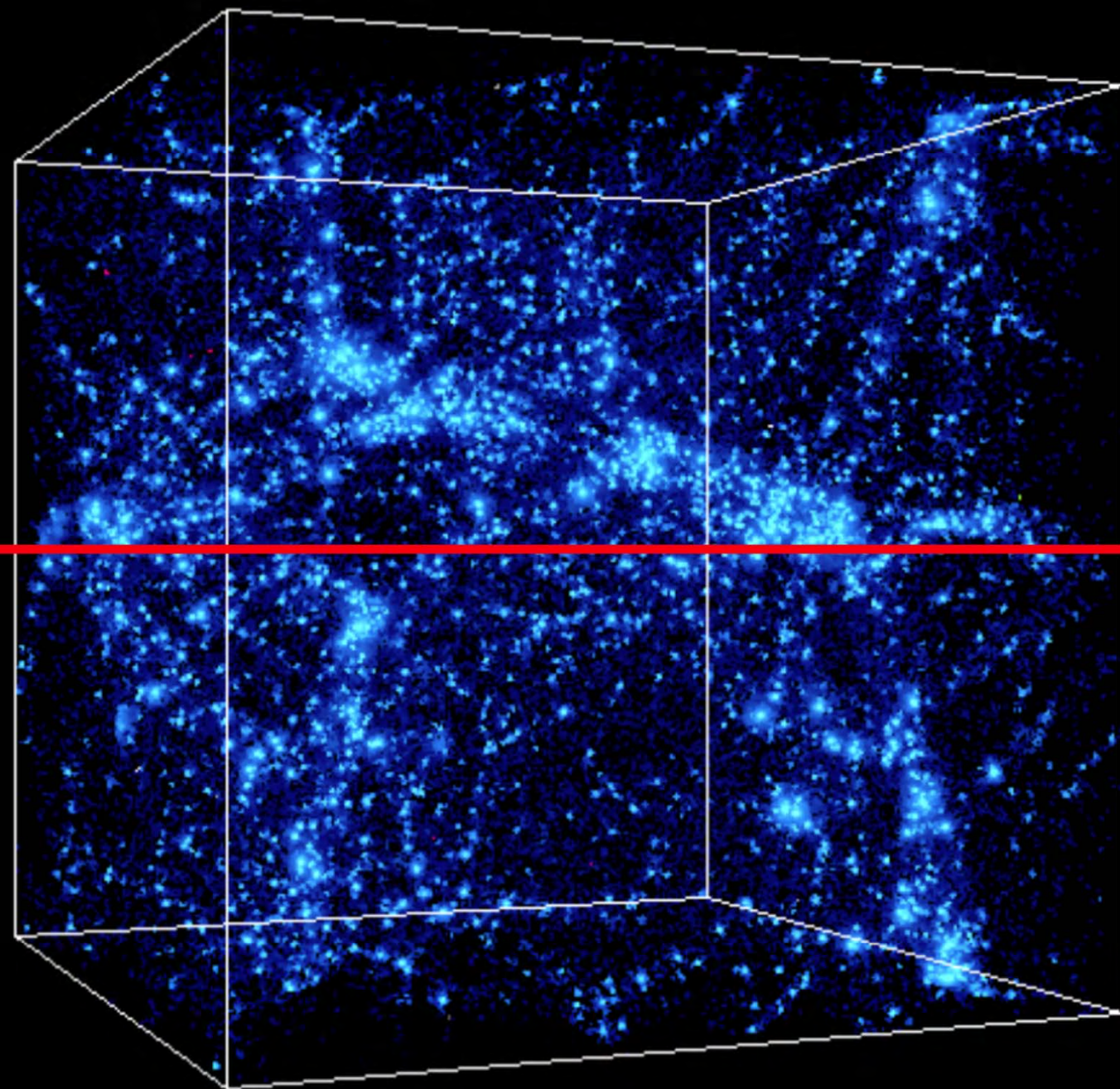


Distribution of gas at $z = 3$



Distribution of neutral gas at $z = 3$



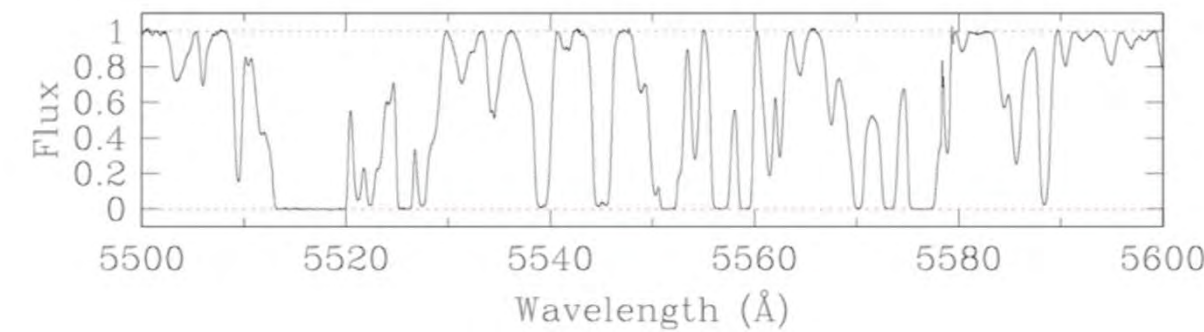
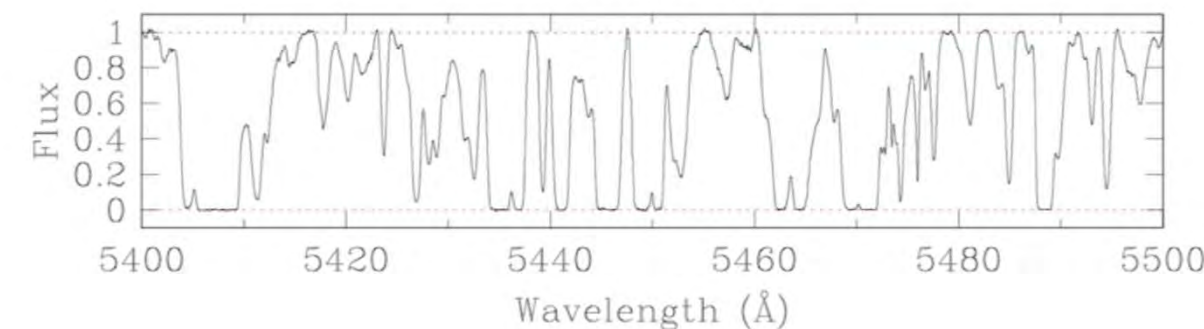
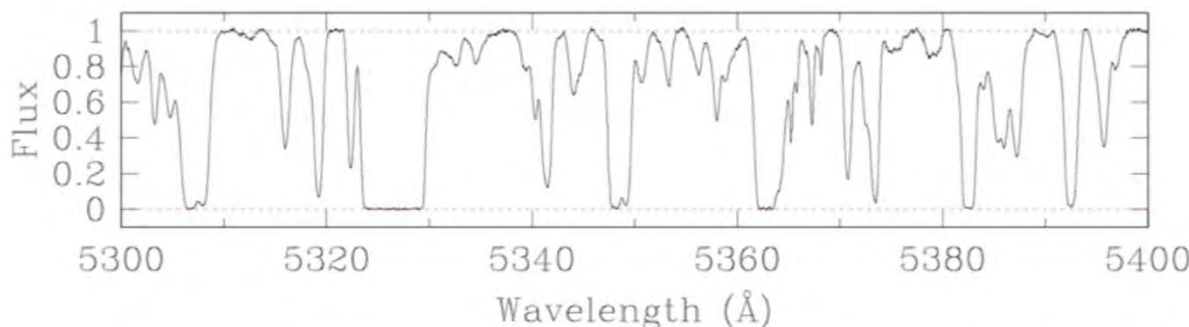
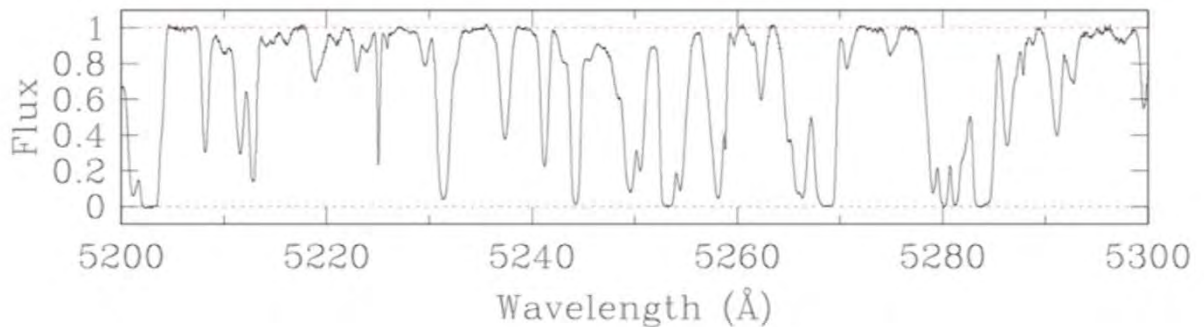


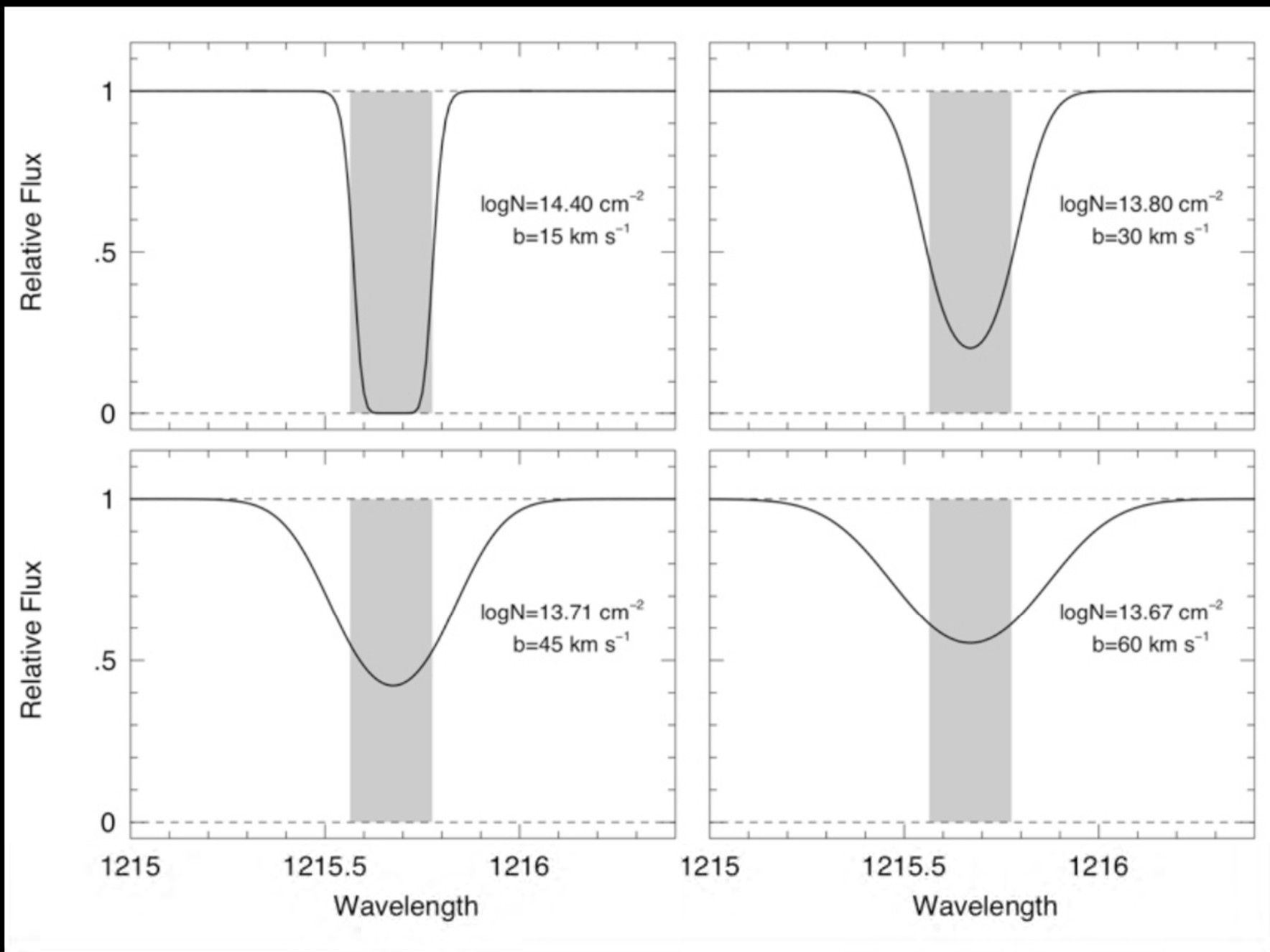
Galaxy Evolution

Playing God of the Universe

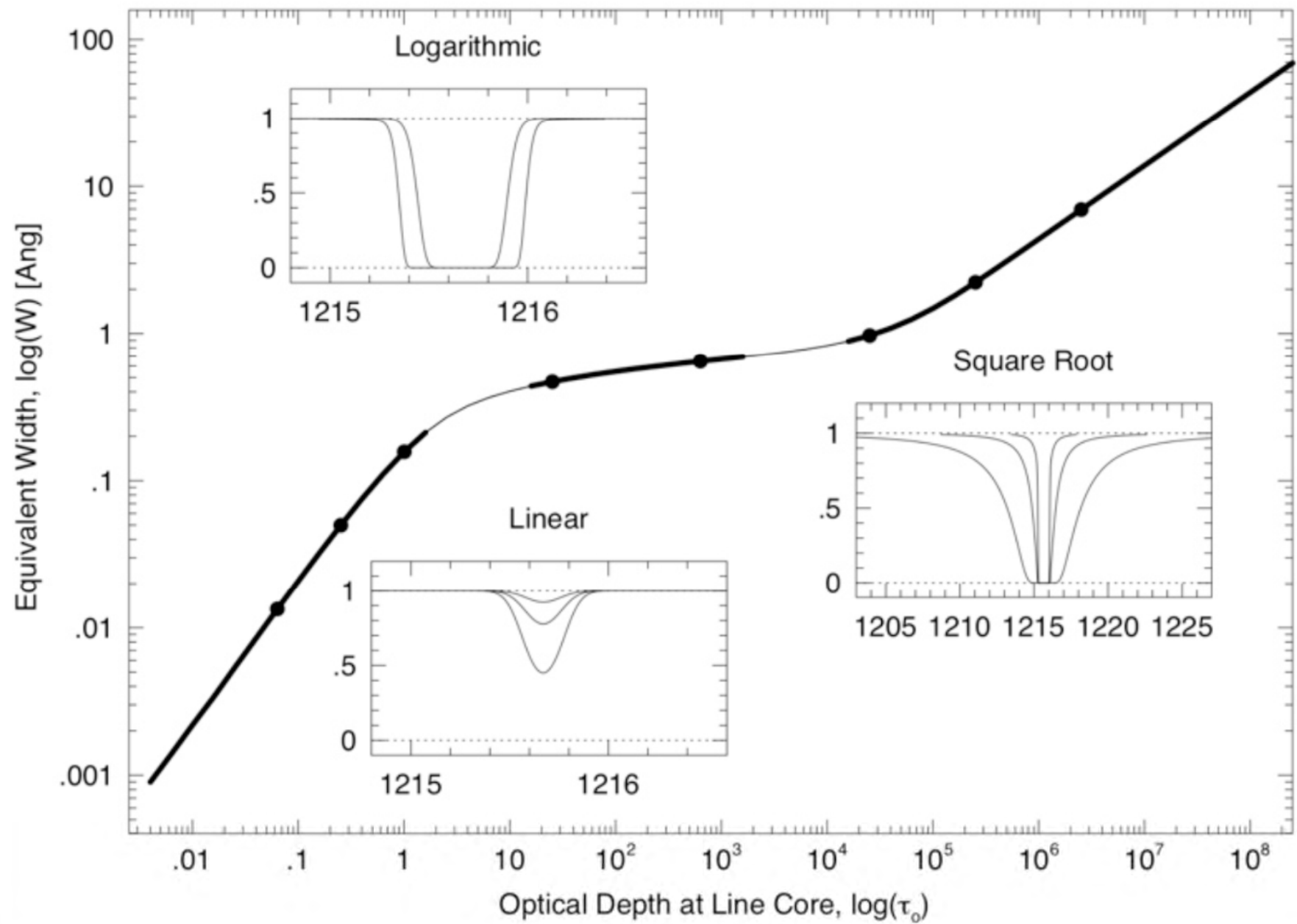
Illustris cosmological hydrodynamical simulation

The Ly α forest at high spectral resolution

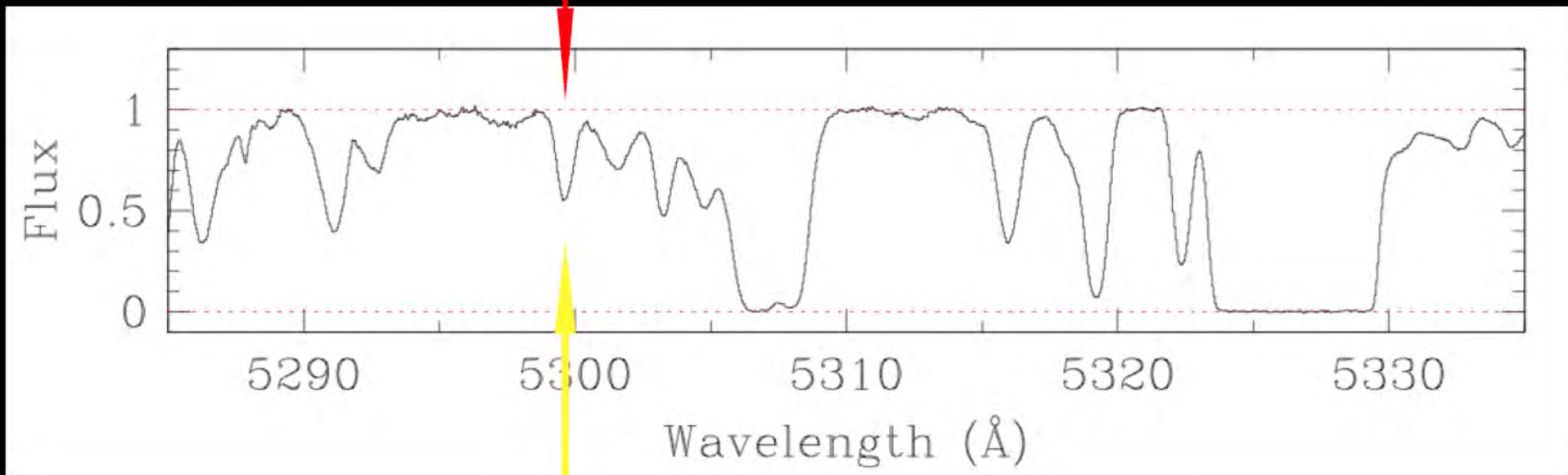




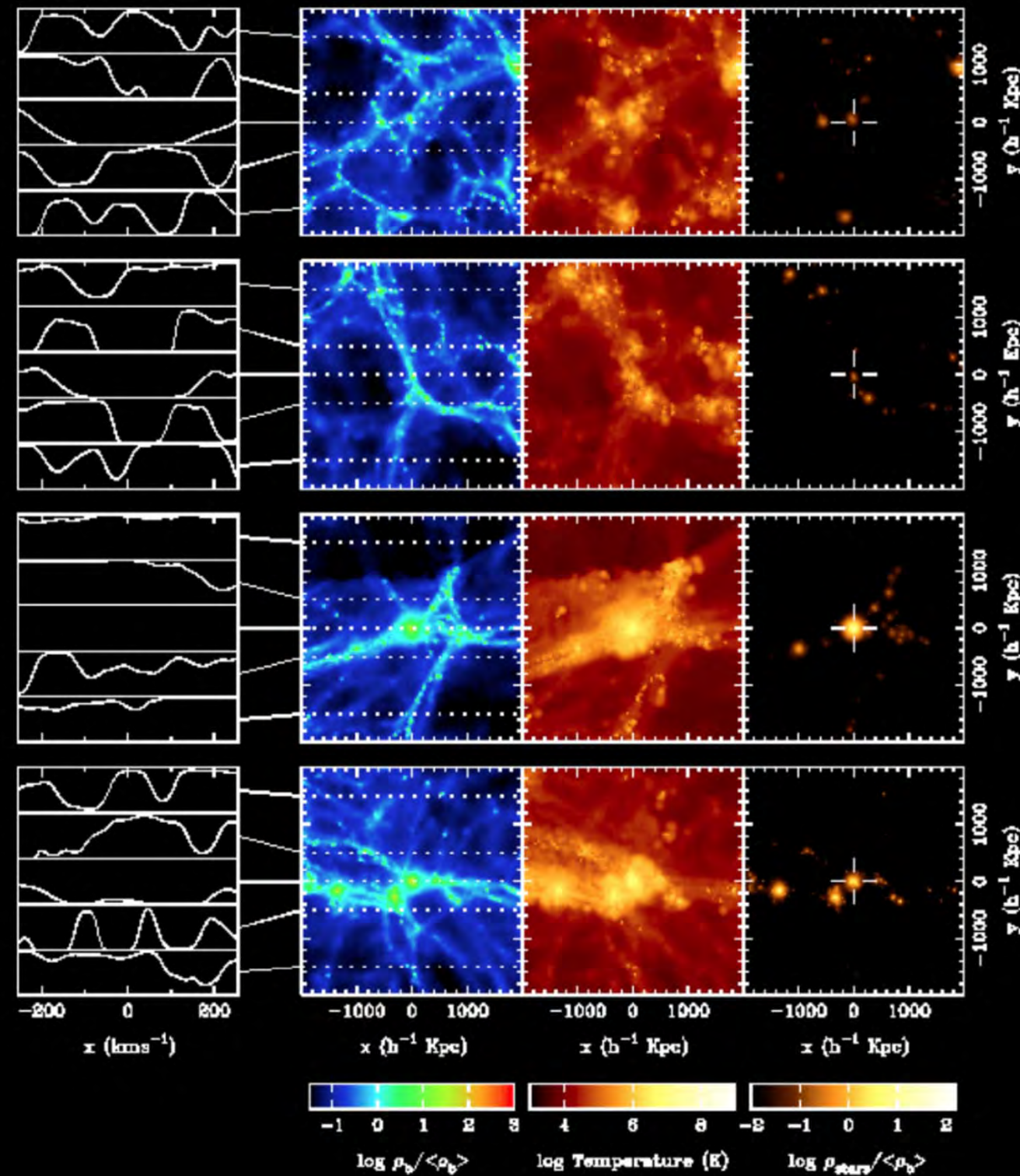
C. Churchill



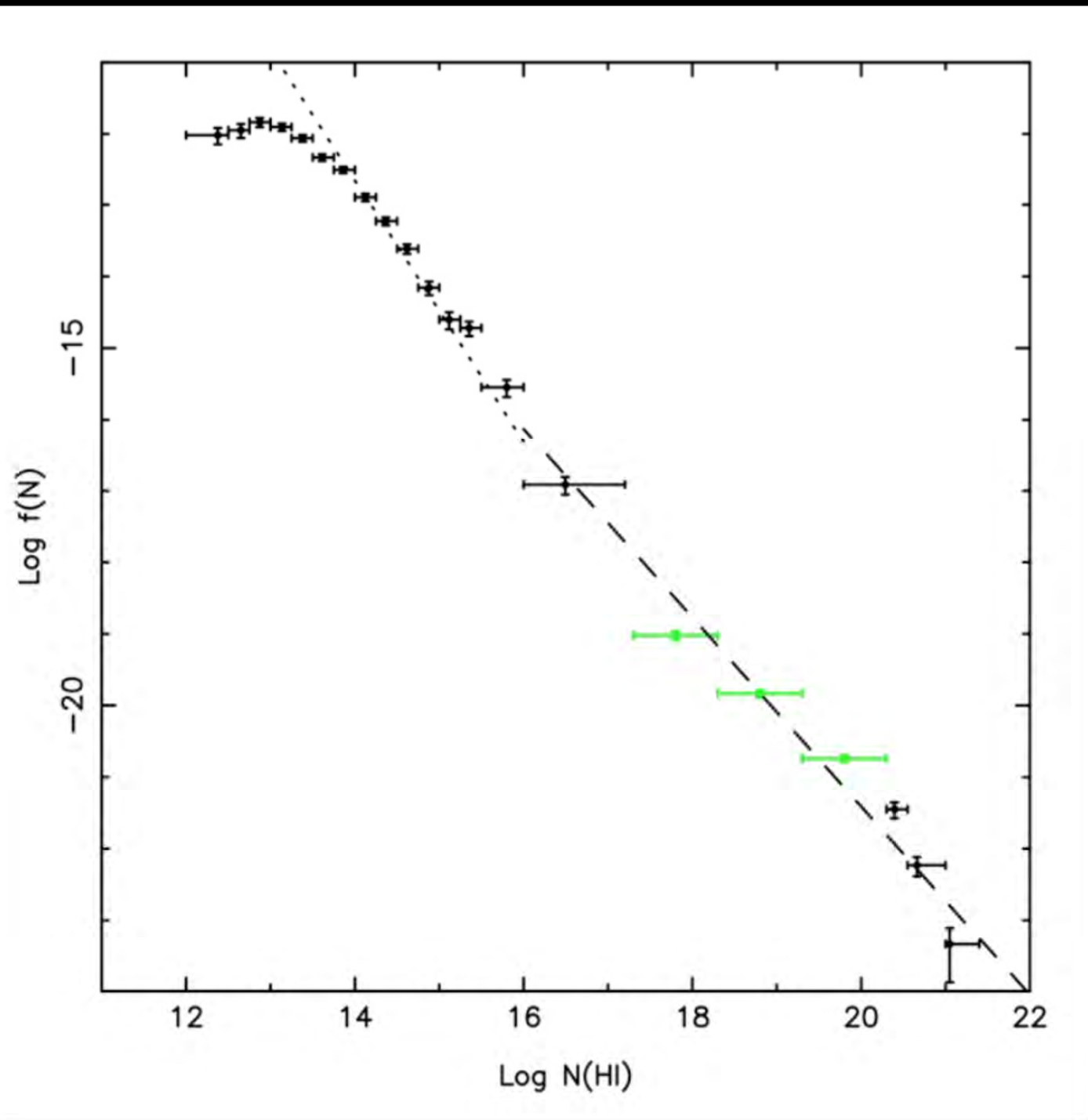
$$W_\lambda = 0.327 \text{ \AA} / (1 + z) = \frac{1}{\lambda_{\text{obs}}/\lambda_0} \rightarrow W_0 = 0.075 \text{ \AA}$$



$$N(\text{H I}) = 1.4 \times 10^{13} \text{ cm}^{-2}$$

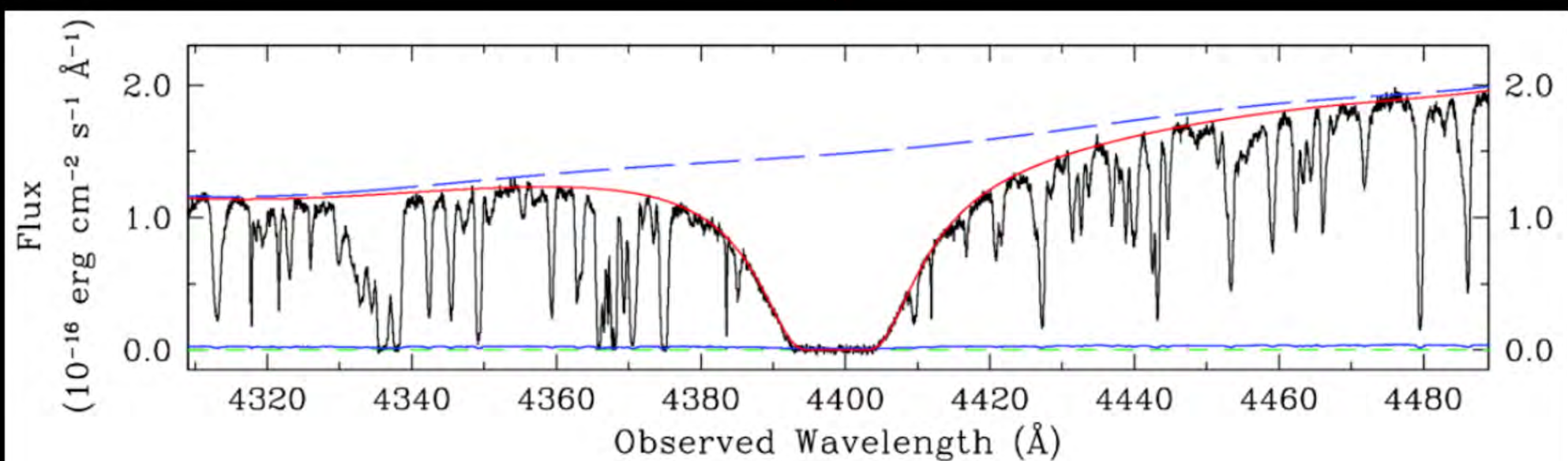


Croft+

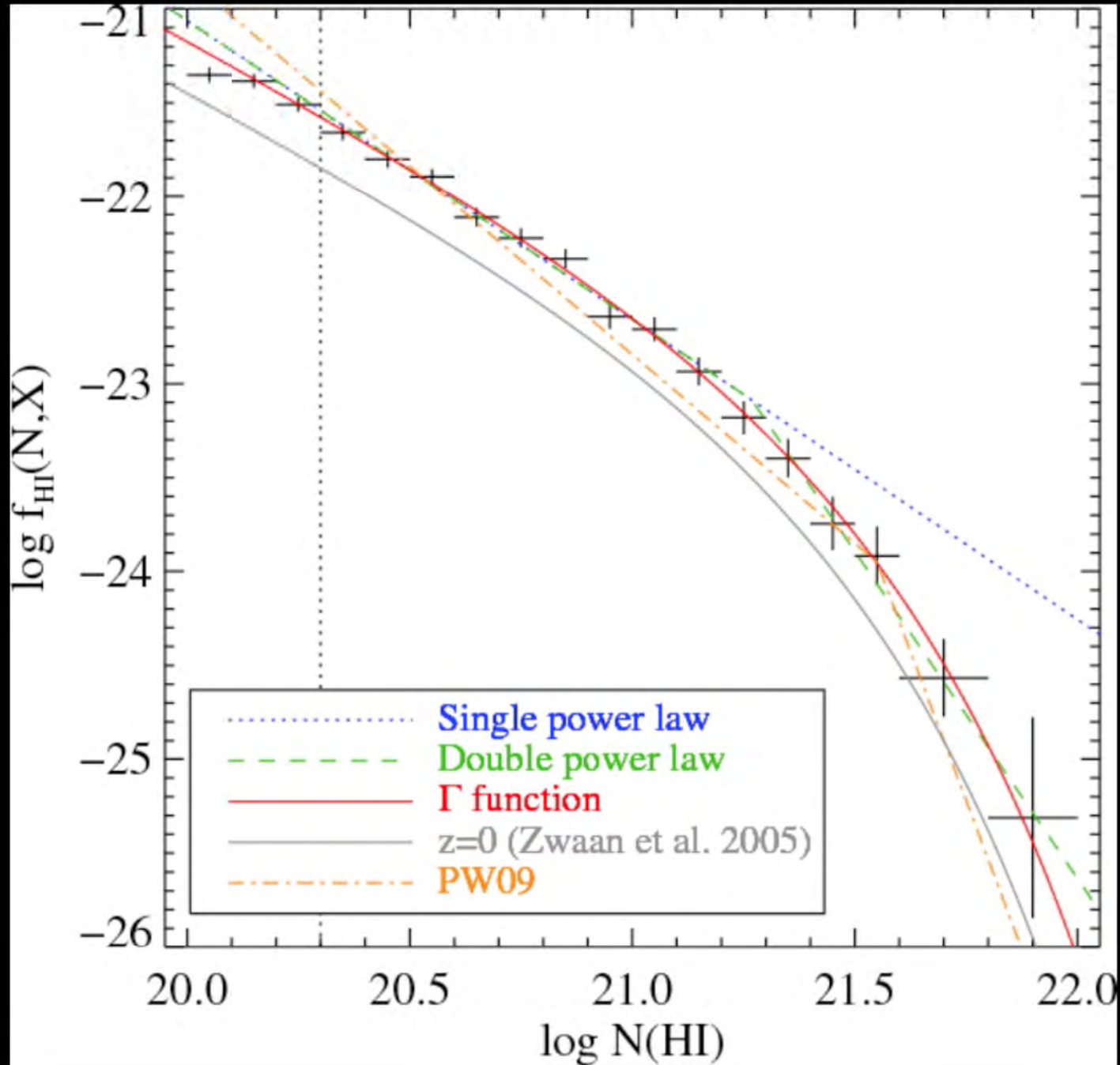


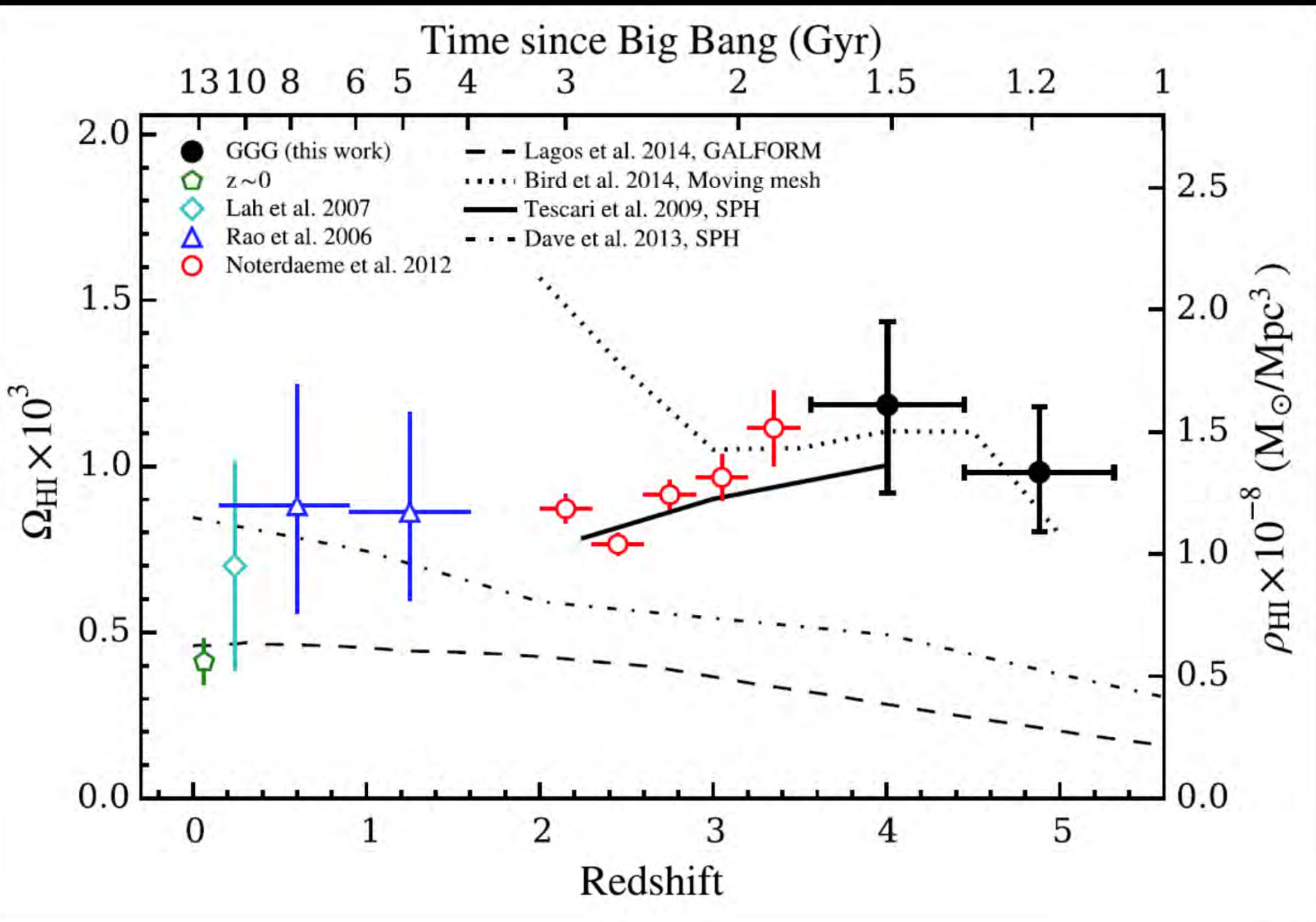
Péroux+ 2003

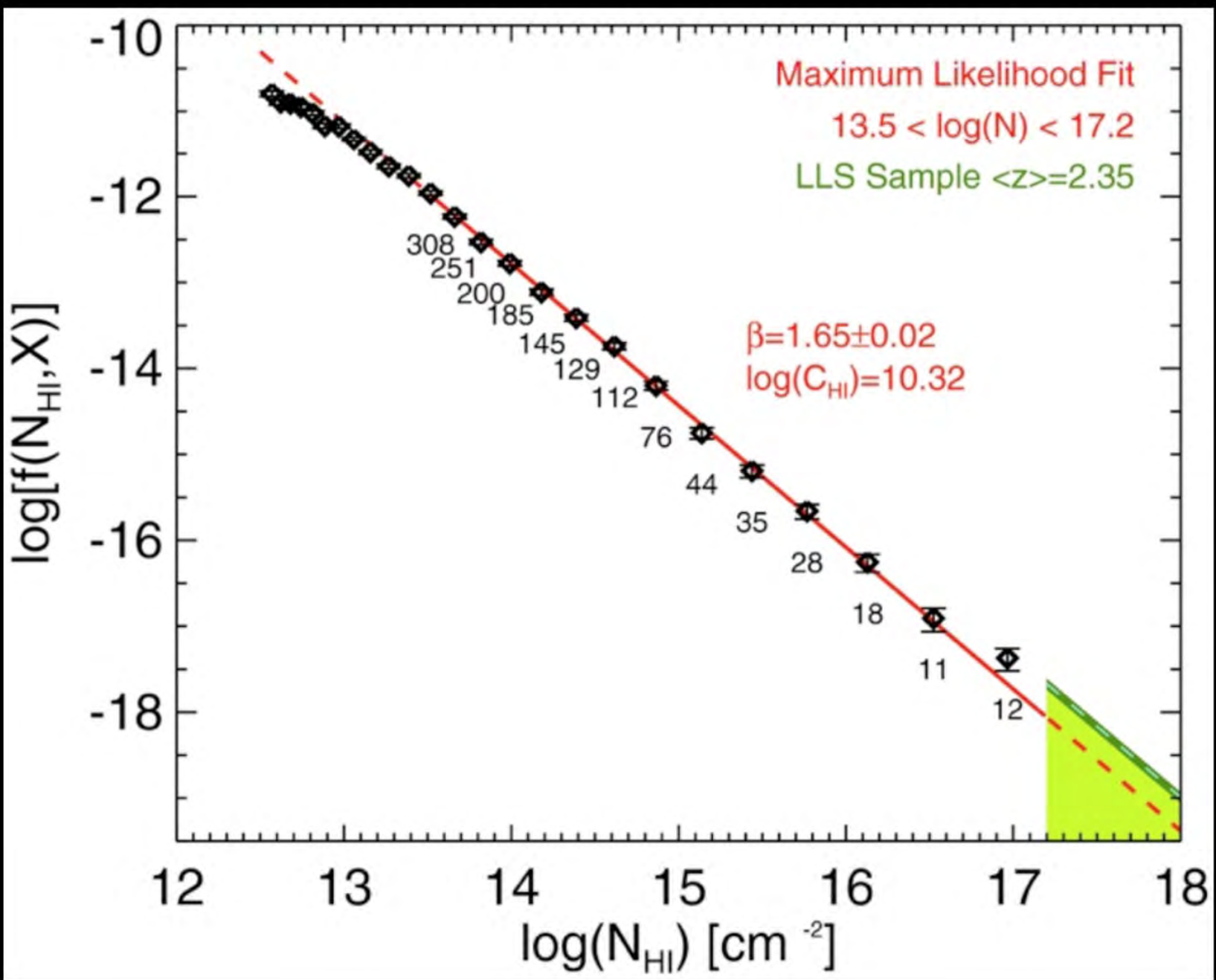
$$N(\text{H I}) = 2.2 \times 10^{20} \text{ cm}^{-2}$$



Cooke+ 2014





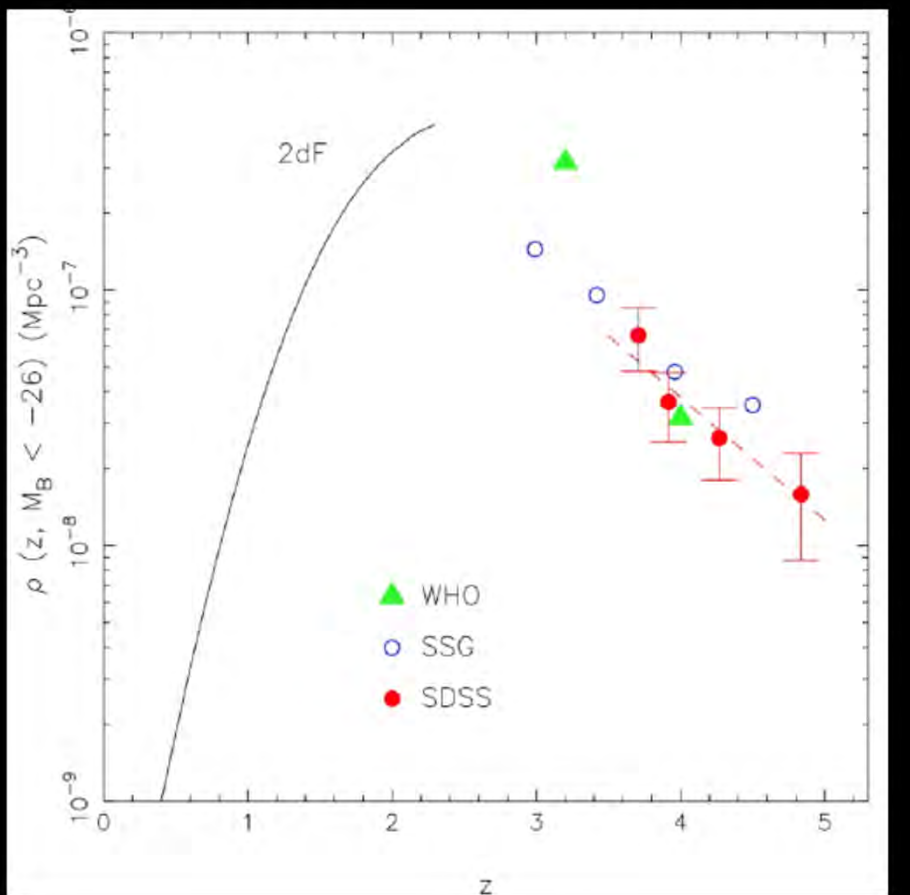


Rudie+ 2013

Cosmic Inventory

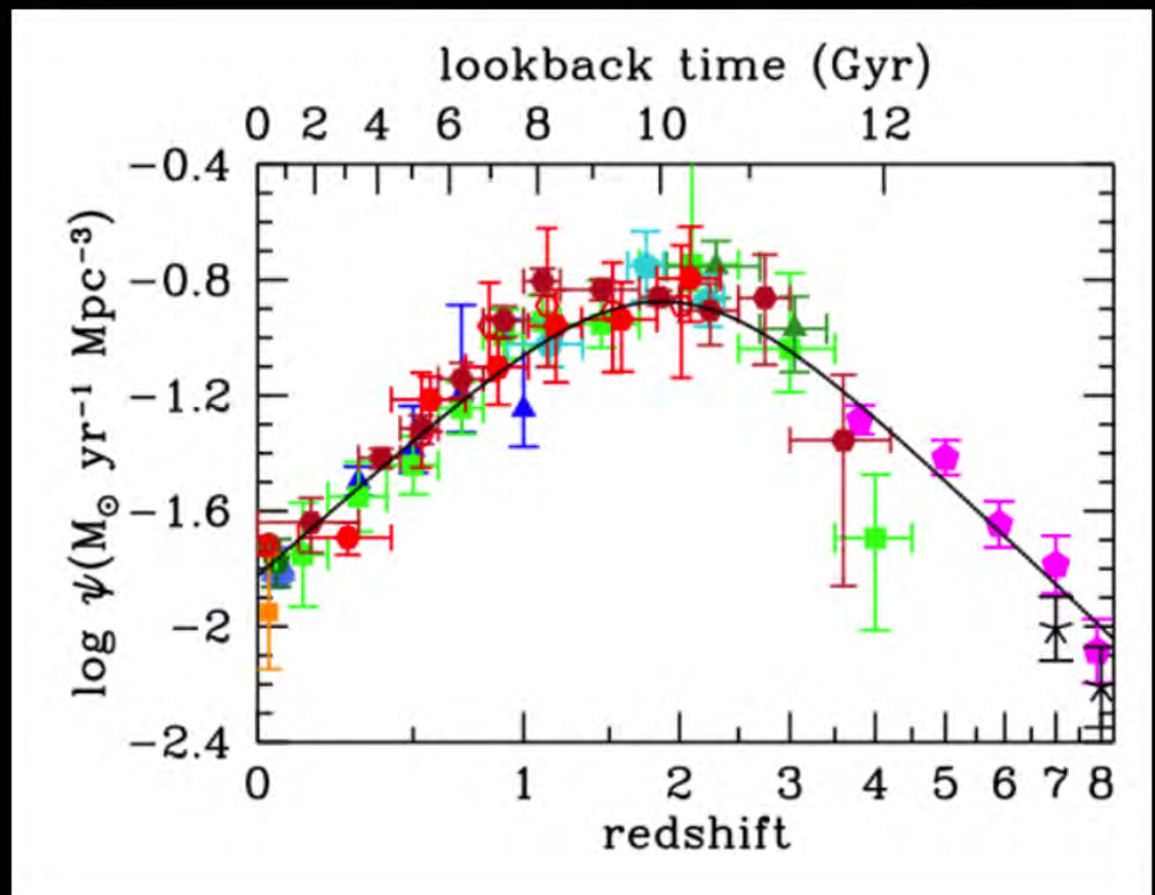
Component	Ω (ρ/ρ_c)
Dark Energy	0.691 ± 0.006
Matter (baryonic and non-baryonic)	0.312 ± 0.009
Baryons (Total)	0.0488 ± 0.0004
Baryons in stars and stellar remnants	~ 0.003
Neutrinos	~ 0.001
Photons (CMB)	5×10^{-5}

QUASARS



Fan+ 2001

STARS



Madau & Dickinson 2014

What is the Reionization Era?

A Schematic Outline of the Cosmic History

